JAGIELLONIAN UNIVERSITY
IN KRAKÓW

PHD THESIS

INTERPLAY BETWEEN TALIN AND β1-INTEGRIN IN CANCER CELLS MOTILITY

ZBIGNIEW BASTER

SUPERVISED BY: DR HAB. ZENON RAJFUR, PROF. UJ

FACULTY OF PHYSICS, ASTRONOMY AND
APPLIED COMPUTER SCIENCE
DEPARTMENT OF MOLECULAR AND INTERFACIAL BIOPHYSICS

KRAKÓW 2020

The main thing my thesis proved was how much I procrastinate

Jorge Cham, PhD Comics

Wydział Fizyki, Astronomii i Informatyki Stosowanej

Uniwersytet Jagielloński

OŚWIADCZENIE

Ja niżej podpisany *Zbigniew Baster* (nr indeksu: 1079731), doktorant Wydziału Fizyki, Astronomii i Informatyki Stosowanej Uniwersytetu Jagiellońskiego, oświadczam, że przedłożona przeze mnie rozprawa doktorska pt. „*Interplay between talin and β1-integrin in cancer cells motility*" jest oryginalna i przedstawia wyniki badań wykonanych przeze mnie osobiście, pod kierunkiem *dr hab. Zenona Rajfura, prof. UJ*. Pracę napisałem samodzielnie.

Oświadczam, że moja rozprawa doktorska została opracowana zgodnie z Ustawą o prawie autorskim i prawach pokrewnych z dnia 4 lutego 1994 r. (Dziennik Ustaw 1994 nr 24 poz. 83 wraz z późniejszymi zmianami).

Jestem świadom, że niezgodność niniejszego oświadczenia z prawdą ujawniona w dowolnym czasie, niezależnie od skutków prawnych wynikających z ww. ustawy, może spowodować unieważnienie stopnia nabytego na podstawie tej rozprawy.

Kraków, dnia …… ……

podpis doktorant

ACKNOWLEDGEMENTS

My PhD studies were an exciting journey with many ups and downs. I would not be able to accomplish that without help and support from many friends and colleagues, among whom some I would like to acknowledge especially.

First and foremost, I would like to express my deepest gratitude to my PhD advisor **Prof. Zenon Rajfur** for the continuous scientific guidance, new inspirations, and challenges. I especially acknowledge the opportunity to work in his group and for all the trust he put in me.

I would like to acknowledge my department's head **Prof. Andrzej Budkowski** and former department's head **Prof. Józef K. Mościcki** and for advices and support in my scientific and personal development. I would also like to thank my colleagues from **Mechanobiology Lab** for scientific discussions.

This research would not happen without a collaboration with **Prof. Cai Huang** from University of Kentucky, who was my research advisor during my fellowship there. I extremally grateful for the opportunity of working with him and for his guidance in the cancer biology field. I would also like to thank **Liqing Li** for all the scientific assistance during my stay abroad.

My sincere thanks also go to **Miranda Lin**, **Warren Rummage**, and **Leif Magnuson** for both being great friends and work colleagues, and for their support, especially during my first months in a foreign country.

I would like to thank **Prof. Francesco Difato** from Italiano Istituto di Tecnologia in Genova, **Prof. Louis Hodgson** from Albert Einstein College of Medicine, and **Dr. Vinay Swaminathan** from Lund University for hosting me in their groups and sharing their knowledge.

I am also grateful to **Dr. Clare Waterman**, **Dr. Hawa Racine Thiam**, and the whole **Waterman Lab** for their warm welcome, support during COVID-19 pandemic, exciting scientific discussions, and insightful comments on my studies.

I would like to thank **Dr. Sławomir Lasota** for showing me *how cell biology works* at the beginning of my PhD journey.

I would like to thank **Jorge Cham**, the cartoonist behind the PhD Comics, for showing that *grad school is a state of mind* and all of *that* is **kind-of** normal in PhD student life.

I would like to thank **my parents** for their love and support**.**

And last but not least, I thank my best friends **Magda** and **Jacek**, for their support, especially in the dark moments, and for all the late-night crazy scientific discussions.

The work presented in this thesis was supported by the following projects:

- *Talin2-mediated traction force drives MMP secretion and cell invasion* – financed by the National Institute of General Medical Sciences (NIGMS), USA, Research Project (R01) lead by prof. Cai Huang from University of Kentucky, KY, USA. R01 GM122994;
- *Aktywność białek związanych z migracją w komórkach eukariotycznych* – financed by the National Science Center, Poland, ETIUDA scheme scholarship to Zbigniew Baster. 2019/32/T/NZ3/00444.

The author is also a principal investigator in the National Science Center, Poland, PRELUDIUM scheme project: *Influence of culture substrate elasticity on talin recruitment to focal adhesion* (2018/31/N/NZ3/02031, supervised by dr hab. Zenon Rajfur, prof. UJ and a beneficiary of *Jagiellonian Interdisciplinary PhD Programme*, a part of *ZintegrUJ – Kompleksowy Program Rozwoju Uniwersytetu Jagiellońskiego*, a National Centre for Research and Development project and *Operational Programme Knowledge Education Development 2014 - 2020* co-financed from European Social Fund (POWR.03.05.00-00-Z309/17-00).

During the work included in this thesis, the Faculty of Physics Astronomy and Applied Computer Science of Jagiellonian University held *The Leading National Research Centre* status (*pl. Krajowy Naukowy Ośrodek Wiodący*, *KNOW*, 2012-2017) and Jagiellonian University held *Research University* status (*Excellence Initiative – Research University* programme, since 2020) supported by Polish Ministry of Science and Higher Education.

TABLE OF CONTENTS

ACRONYMS AND ABBREVIATIONS LIST

3D – 3-Dimentional;

ABD – Actin Binding Domain;

ADC – Analog-to-Digital Converter;

AMP – Amplifier;

Arp2/3 – Actin-related protein 2/3 complex;

ATCC – American Type Culture Collection;

BIG – Biomedical Imaging Group;

BRCA1 – Breast Cancer type 1 susceptibility protein;

BRCA2 – Breast Cancer type 2 susceptibility protein;

C3G – Cyanidin-3-O-Glucoside;

CCD – Charge-Coupled Device;

CLSM – Confocal Laser Scanning Microscope;

CMOS – Complementary Metal–Oxide–Semiconductor;

CVC – Charge-to-Voltage Converter;

DAPI – 4′,6-diamidino-2-phenylindole;

DNA – Deoxyribonucleic Acid;

ECM – Extracellular Matrix;

EGF – Epidermal Growth Factor;

EPFL – École Polytechnique Fédérale de Lausanne, Switzerland;

FA – Focal Adhesion;

Fluorescein – 3′,6′-dihydroxyspiro[isobenzofuran-1(3H),9′-[9H]xanthen]-3-one;

FWHM – Full Width at Half Maximum;

Ig – Immunoglobulin;

ITGB1 – β1 Integrin;

KO – Knock-Out;

MMP – Matrix Metallopeptidase / Matrix Metalloproteinase;

MT1-MMP – Membrane Type 1 Matrix Metalloproteinase;

N-WASp – Neural Wiskott-Aldrich Syndrome protein;

NA – Numerical Aperture;

NHE-1 – Sodium-Hydrogen Exchanger-1;

OUT – Output;

PDB – Protein Data Bank;

PSF – Point Spread Function;

TP53 – Tumor Protein p53 gene;

TIRF – Total Internal Reflection Fluorescence;

Tks5 – Tyrosine kinase substrate with 5 SH3 domains;

TIMP – Tissue Inhibitor of Metalloproteinases;

TLN – Talin;

WHO – World Health Organization;

WT – Wild-Type;

LIST OF PUBLICATIONS

This dissertation has been written based on the research previously reported in the following publications:

I. **Baster, Z.** & Rajfur, Z. BatchDeconvolution: a Fiji plugin for increasing deconvolution workflow. *Bio-Algorithms and Med-Systems* **16(3)**, (2020). https://doi.org/10.1515/bams-2020-0027.

II. **Baster, Z.**, Li, L., Rajfur, Z. & Huang, C. Talin2 mediates secretion and trafficking of matrix metallopeptidase 9 during invadopodium formation. *Biochim. Biophys. Acta - Mol. Cell Res.* **1867(7)**, 118693 (2020). https://doi.org/10.1016/j.bbamcr.2020.118693.

III. **Baster, Z.**, Li, L., Kukkurainen, S., Chen, J., Pentikäinen, O., Győrffy, B., Hytönen, V. P., Zhu, H., Rajfur, Z. & Huang, C. Cyanidin-3-glucoside binds to talin and modulates colon cancer cell adhesions and 3D growth. *FASEB J.* **34(2)**, 2227–2237 (2020). https://doi.org/10.1096/fj.201900945R.

Other publications not included in the dissertation:

IV. Adamczyk, O., **Baster, Z.**, Szczypior, M. & Rajfur, Z. Substrate Stiffness Mediates Formation of Novel Cytoskeletal Structures in Fibroblasts during Cell–Microspheres Interaction. Int. J. Mol. Sci. **22(2)**, 960 (2021). https://doi.org/10.3390/ijms22020960.

V. Witko, T., **Baster, Z.**, Rajfur, Z., Sofińska, K. & Barbasz, J. Increasing AFM colloidal probe accuracy by optical tweezers. Sci. Rep. **11(1)**, 509 (2021). https://doi.org/10.1038/s41598-020-79938-z.

VI. Bednarz, A., Lipiński, P., Starzyński, R. R., Tomczyk, M., Kraszewska, I., Herman, S., Kowalski, K., Gruca, E., Jończy, A., Mazgaj, R., Szudzik, M., Rajfur, Z., **Baster, Z.**, Józkowicz, A. & Lenartowicz, M. Exacerbation of neonatal hemolysis and impaired renal iron handling in heme oxygenase 1-deficient mice. *Int. J. Mol. Sci.* **21(20),** (2020). https://doi.org/10.3390/ijms21207754.

VII. Bartnicka, D., Karkowska-Kuleta, J., Zawrotniak, M., Satała, D., Michalik, K., Zielinska, G., Bochenska, O., Kozik, A., Ciaston, I., Koziel, J., Dutton, L. C., Nobbs, A. H., Potempa, B., **Baster, Z.**, Rajfur, Z., Potempa, J. & Rapala-Kozik, M. Adhesive protein-mediated cross-*talk* between Candida albicans and

Porphyromonas gingivalis in dual species biofilm protects the anaerobic bacterium in unfavorable oxic environment. *Sci. Rep.* **9(1),** 4376 (2019). https://doi.org/10.1038/s41598-019-40771-8.

VIII. Ogórek, M., Herman, S., Pierzchała, O., Bednarz, A., Rajfur, Z., **Baster, Z.**, Grzmil, P., Starzyński, R. R., Szudzik, M., Jończy, A., Lipiński, P. & Lenartowicz, M. Molecular machinery providing copper bioavailability for spermatozoa along the epididymial tubule in mouse. *Biol. Reprod.* **100(6),** 1505–1520 (2019). https://doi.org/10.1093/biolre/ioz028.

IX. Gadzała, M., Dułak, D., Kalinowska, B., **Baster, Z.**, Bryliński, M., Konieczny, L., Banach, M. & Roterman, I. The aqueous environment as an active participant in the protein folding process. *J. Mol. Graph. Model.* 87**,** 227–239 (2019). https://doi.org/10.1016/j.jmgm.2018.12.008.

X. Bednarz, A., Lipiński, P., Starzyński, R. R., Tomczyk, M., Nowak, W., Mucha, O., Ogórek, M., Pierzchała, O., Jończy, A., Staroń, R., Śmierzchalska, J., Rajfur, Z., **Baster, Z.**, Józkowicz, A., Lenartowicz, M. M., Jozkowicz, A. & Lenartowicz, M. M. Role of the kidneys in the redistribution of heme-derived iron during neonatal hemolysis in mice. *Sci. Rep.* **9(1),** 11102 (2019). https://doi.org/10.1038/s41598-019-47414-y.

XI. Durak-Kozica, M., **Baster, Z.**, Kubat, K. & Stępień, E. 3D visualization of extracellular vesicle uptake by endothelial cells. *Cell. Mol. Biol. Lett.* **23(1),** 57 (2018). https://doi.org/10.1186/s11658-018-0123-z.

XII. Szczepanski, A., Owczarek, K., Milewska, A., **Baster, Z.**, Rajfur, Z., Mitchell, J. A. & Pyrc, K. Canine respiratory coronavirus employs caveolin-1-mediated pathway for internalization to HRT-18G cells. *Vet. Res.* **49(1),** 55 (2018). https://doi.org/10.1186/s13567-018-0551-9.

XIII. Owczarek, K., Szczepanski, A., Milewska, A., **Baster, Z.**, Rajfur, Z., Sarna, M. & Pyrc, K. Early events during human coronavirus OC43 entry to the cell. *Sci. Rep.* **8(1),** 7124 (2018). https://doi.org/10.1038/s41598-018-25640-0.

XIV. Karkowska-Kuleta, J., Bartnicka, D., Zawrotniak, M., Zielinska, G., Kierońska, A., Bochenska, O., Ciaston, I., Koziel, J., Potempa, J., **Baster, Z.**, Rajfur, Z. & Rapala-Kozik, M. The activity of bacterial peptidylarginine deiminase is important during formation of dual-species biofilm by periodontal pathogen Porphyromonas gingivalis and opportunistic fungus Candida albicans. *Pathog. Dis.* **76(4),** fty033 (2018). https://doi.org/10.1093/femspd/fty033.

XV. Ogórek, M., Lenartowicz, M., Starzyński, R., Jończy, A., Staroń, R., Doniec, A., Krzeptowski, W., Bednarz, A., Pierzchała, O., Lipiński, P., Rajfur, Z., **Baster, Z.**, Gibas-Tybur, P. & Grzmil, P. Atp7a and Atp7b regulate copper homeostasis in developing male germ cells in mice. *Metallomics* **9(9),** 1288–1303 (2017). https://doi.org/10.1039/C7MT00134G.

XVI. Lenartowicz, M., Starzyński, R. R., Jończy, A., Staroń, R., Antoniuk, J., Krzeptowski, W., Grzmil, P., Bednarz, A., Pierzchała, O., Ogórek, M., Rajfur, Z., **Baster, Z.** & Lipiński, P. Copper therapy reduces intravascular hemolysis and derepresses ferroportin in mice with mosaic mutation (Atp7a mo-ms): An implication for copper-mediated regulation of the Slc40a1 gene expression. *Biochim. Biophys. Acta - Mol. Basis Dis.* **1863(6),** 1410–1421 (2017). https://doi.org/10.1016/j.bbadis.2017.02.020.

XVII. Milewska, A., Nowak, P., Owczarek, K., Szczepanski, A., Zarebski, M., Hoang, A., Berniak, K., Wojarski, J., Zeglen, S., **Baster, Z.**, Rajfur, Z. & Pyrc, K. Entry of Human Coronavirus NL63 into the Cell. *J. Virol.* **92(3),** e01933-17 (2017). https://doi.org/10.1128/JVI.01933-17.

XVIII. **Baster, Z.**, Lasota, S., Witko, T., Zimoląg, E., Sroka, J., Madeja, Z. & Rajfur, Z. Migration-related Protein Activity in Cell Electrotaxis. *Acta Phys. Pol. B* **48(10),** 1727 (2017). https://doi.org/10.5506/APhysPolB.48.1727.

XIX. Lasota, S., **Baster, Z.**, Witko, T., Zimoląg, E., Sroka, J., Rajfur, Z. & Madeja, Z. Zastosowanie biosensorów typu FRET w badaniach mikroskopowych procesu migracji komórkowej. *Postepy Biochem.* **63(1),** 16–33 (2017). https://pubmed.ncbi.nlm.nih.gov/28409572.

XX. Roterman, I., Konieczny, L., Banach, M., Marchewka, D., Kalinowska, B., **Baster, Z.**, Tomanek, M. & Piwowar, M. *Computational Methods to Study the Structure and Dynamics of Biomolecules and Biomolecular Processes*. *Comput. Methods to Study Struct. Dyn. Biomol. Biomol. Process.* 1**,** (Springer Berlin Heidelberg, 2014). https://doi.org/10.1007/978-3-642-28554-7.

XXI. Kalinowska, B., Alejster, P., Sałapa, K., **Baster, Z.** & Roterman, I. Hypothetical in silico model of the early-stage intermediate in protein folding. *J. Mol. Model.* **19(10),** 4259–4269 (2013). https://doi.org/10.1007/s00894-013-1909-6.

XXII. **Baster, Z.** The identification and the elimination of clashes in the structure of an early-stage intermediate in the protein folding process. *Bio-Algorithms and Med-Systems* **9(4),** 199–207 (2013). https://doi.org/10.1515/bams-2013-0113.

XXIII. Jurkowski, W., **Baster, Z.**, Dułak, D. & Roterman-Konieczna, I. The early-stage intermediate. in *Protein Fold. Silico* 1–20 (Elsevier, 2012). https://doi.org/10.1533/9781908818256.1.

Patent applications not included in the dissertation:

I. Barbasz J., Witko T. & **Baster Z.**, *Metoda wyznaczania stałej siłowej dźwigni typu "colloidal probe" dla mikroskopu sił atomowych*. Polish Patent no. P.422059 - pending (2017)

ABSTRACT

Cancer is the second most common cause of death after cardiovascular diseases. Although benign tumors have very high survival rate, cancer malignancy strongly increases mortality. The presented thesis concentrates on the interplay between talin and β1 integrin (adhesion related proteins, also strongly connected with cell migration and cancer development) in mediation of cancer cells physiology and motility, especially in regulating cell adhesion, positioning, and invasion.

For the purpose of the study, software capable to deconvolve multiple microscopy images in a single session was developed (**Publication I**); *BatchDeconvolution* is a *Fiji* plugin that bridges *PSF Generator* and *DeconvolutionLab2* (BIG, EPFL), programs serving for calculations of the Point Spread Function and performing image deconvolution, respectively. *BatchDeconvolution* expands functionalities of these software, providing an environment that allows to enhance multi-position, multi-channel time-lapse image files in a sequential, automated manner. This approach allowed to process a vast amount of microscopy images collected during *in vitro* studies presented in the following sections.

There are two isoforms of talin protein: talin1 and talin2. While talin1 has been extensively studied, there is still not much known about the biological role of talin2. It shares some functions with its sister variant, but the literature describes only a limited redundancy. The presented study concentrates on the molecular mechanism by which specifically talin2 mediates secretion and trafficking of matrix metallopeptidase 9 (MMP9), an enzyme important for extracellular matrix degradation and invadopodia maturation in initial stages of cancer invasion. The study was conducted in MDA-MB-231breast cancer cell line. The absence of talin2 caused inhibition of a process of MMP9 vesicles docking to the ventral membrane, consequently rerouting them towards lysosomal degradation. Furthermore, S339C mutation of talin2, specific for reducing talin2-β1 integrin interaction, gave similar results as the ablation of talin2. Due to a higher recycling rate, talin2-depleted cells started to exhibit enlarged vesicles containing MMP9, what suggests an overflow of the protein degradation process (**Publication II**).

Talin-β1 integrin interaction is also a factor in colon cancer tumorigenesis and colon cancer cells adhesion. In **Publication III,** included in the thesis, a role of cyanidino-3-O-glucoside (C3G) was examined in the context of mediating talin1- and talin2-β1 integrin interaction, tumor development, and colon cancer cells adhesion. C3G is a natural dye

found in many red and blue vegetables and fruits. It shows many health beneficial properties including anti-oxidative, anti-inflammation, and anti-diabetic ones. Moreover, several reports connect it with an anti-carcinogenic activity. The presented study shows that the C3G binding pocket is located at the interface between talin and integrin. The presence of the compound increases affinity between the two proteins, leading to stimulation of colon cancer cells adhesion. In result, it hinders tumorigenesis.

The new knowledge of the functions of talin1 and talin2 proteins allows a better understanding of the regulation of cancer metastasis. Furthermore, even though talin2 was discovered over 20 years ago, its role in cell biology and adhesion is still understudied. The presented research sheds some light on that aspect. Finally, the description of molecular mechanisms driving protein interactions in cancer development may help in designing new anti-cancer therapies.

STRESZCZENIE

Choroby nowotworowe są drugą, po chorobach układu krążenia, najczęstszą przyczyną zgonów na świecie. Chociaż łagodne zmiany nowotworowe cechują się wysoką przeżywalnością, złośliwe guzy często powiązane są z wysoką śmiertelnością pacjentów. Przedstawiona rozprawa koncentruje się badaniu jak oddziaływanie taliny z integryną β1 (białek związanych z adhezją, powiązanych również z migracją komórek oraz rozwojem nowotworów) wpływa na ruchliwość komórek nowotworowych, a w szczególności na ich adhezję, pozycjonowanie oraz inwazyjność.

Na potrzeby zaprezentowanych badań opracowano oprogramowanie umożliwiające dekonwolucję wielu obrazów mikroskopowych (**Publikacja I**); *BatchDeconvolution* to wtyczka do programu *Fiji*, która łączy ze sobą moduły *PSF Generator* oraz *DeconvolutionLab2* (BIG, EPFL), programy służące odpowiednio do wyznaczania Funkcji Rozmycia Punktu (*ang. Point Spread Function, PSF*) oraz dekonwolucji obrazów. BatchDeconvolution rozszerza w ten sposób funkcjonalność powyższego oprogramowania, zapewniając środowisko umożliwiające sekwencyjne, zautomatyzowane wyostrzenie wielopozycyjnych, wielokanałowych, poklatkowych plików graficznych. Takie podejście pozwoliło na przetworzenie dużej ilości obrazów mikroskopowych zebranych podczas badań *in vitro* przedstawionych w dalszych częściach pracy.

Istnieją dwie izoformy białka taliny: talina1 i talina2. Talina1 jest szeroko badana, natomiast niewiele wiadomo o biologicznej roli taliny2. Mimo tego, że posiada ona wiele funkcji wspólnych z jej siostrzanym białkiem, jednak literatura wskazuje, że białka te wykazują swoistą aktywność w komórkach i nie są względem siebie redundantne. Zaprezentowane badania skupiają się na mechanizmie molekularnym, za pomocą którego swoiście talina2 reguluje sekrecję i transport wewnątrzkomórkowy metalopeptydazy macierzowej 9 (MMP9), enzymu biorącego udział w degradacji macierzy zewnątrzkomórkowej i dojrzewania inwadopodiów w początkowych stadiach inwazji nowotworowej. Badania prowadzono na linii komórkowej raka piersi. Usunięcie taliny2 z komórek spowodowało zahamowanie dokowania pęcherzyków z MMP9 do błony podstawnej, a w konsekwencji skierowanie ich do degradacji w lizosomach. Co więcej, mutacja reszty aminokwasowej w talinie2 odpowiedzialnej za charakter oddziaływania talina2-integryna β1, dała podobne wyniki jak ablacja taliny2. Ze względu na wzmożony

recykling MMP9, komórki pozbawione taliny2 zaczęły gromadzić metalopeptydazę w przerośniętych pęcherzykach wewnątrzkomórkowych, co sugeruje przekroczenie maksymalnej wydajności procesu degradacji białek w komórce (**Publikacja II**).

Interakcja taliny z integryną β1 odgrywa rolę również w tworzeniu się guzów i adhezji nowotworów jelita grubego. **Publikacja III**, zawarta w tej rozprawie, opisuje rolę cyjanidyno-3-O-glukozydu (C3G) w kontekście regulacji oddziaływania taliny1 i taliny2 z integryną β1, procesu nowotworzenia oraz adhezji komórek raka jelita grubego. C3G jest naturalnym barwnikiem występującym w wielu czerwonych i niebieskich warzywach i owocach. Wykazuje on wiele korzystnych dla zdrowia właściwości, m.in. przeciwutleniające, przeciwzapalne czy przeciwcukrzycowe. Ponadto, kilka doniesień łączy C3G z działaniem przeciwnowotworowym. Z badań przedstawionych w niniejszej pracy wynika, że na granicy białek w kompleksie taliny i integryny tworzy się kieszeń wiążąca dla C3G. Obecność tego związku zwiększa powinowactwo między tymi białkami, prowadząc do zwiększenia adhezji w komórkach raka jelita grubego, co skutkuje w zahamowanie powstawania guzów.

Poszerzenie wiedzy na temat funkcji białek taliny1 i taliny2 umożliwia lepsze zrozumienie regulacji procesu powstawania i przerzutowania nowotworów. Co więcej, mimo że talina2 została odkryta ponad 20 lat temu, jej rola w biologii i adhezji komórek jest nadal słabo zbadana. Przedstawione badania pozwalają poszerzyć naszą wiedzę na ten temat. Ponadto, poznanie mechanizmów molekularnych odpowiedzialnych za interakcję białek biorących udział w rozwoju nowotworów może pomóc w opracowywaniu nowych terapii przeciwnowotworowych.

1. INTRODUCTION

1.1. CANCER

Cancer is a common name for a group of related diseases in which cells start to proliferate in an abnormal and uncontrolled manner, and gain a potential of invading neighboring tissues and organs [1,2], usually, as a result of an accumulation of mutations over time [3]. Cancer is usually classified based on two criteria: the primary anatomic site that it developed in and the histological tissue type that it developed from [4,5]. In the case of the latter criterium literature distinguishes several main histological types of cancer:

- carcinoma – originating from epithelial tissues such as skin;
- sarcoma – originating from connecting tissue such as muscles, bones, or cartilage;
- leukemia – originating from bone marrow;
- lymphoma – originating from lymphatic tissues;
- multiple myeloma, melanoma, brain and spinal cord cancer, and other [1,4,5]

There are also some mix-types cancers like carcinosarcoma [4]. The cancer type, together with the stage of its advancement are the main factors taken under consideration during an anti-cancer treatment [6].

1.1.1. Epidemiology

According to the World Health Organization (WHO), in 2018 cancer was the second most common cause of death in the World after cardiovascular diseases; over 1 in 6 deaths were caused by cancer [7]. Furthermore, statistically 1 in 8 men and 1 in 10 women will develop cancer during their lives [8]. The most common types of cancer are lung, breast, prostate, and colon cancers [8].

There are many factors influencing the risk of developing cancer, both genetic and environmental [9]. Many of the mutations that underlay carcinogenesis are present in germ cells, thus they are hereditary. The most common anomalies that are passed through generations are in tumor suppressor genes such as *BRCA1*, *BRCA2* and *TP53* [9,10].

In the case of environmental risk factors, one of the most prominent is tobacco smoking [7]. Approximately 4 % cancers in women and even 25 % in men are related to smoking [9]. Furthermore, studies show that smokers have 30-fold higher risk of developing lung cancer [11]. Another leading risk factor for cancer development is alcohol drinking [7]. It is estimated that around 5.5 % of all cancer cases can be attributed to alcohol [12]. The

risk of developing some kinds of cancer, such as neck or head, can be even 10 times higher in the case of heavy drinkers [9]. Moreover, alcohol may act as a solvent for other environmental carcinogens, like tobacco, leading to a synergistic effect in cancer morbidity [7,12,13].

Environmental pollution is another factor significantly increasing the risk of carcinogenesis [9]. Air can be contaminated with many carcinogens including asbestos, benzene, heavy metals, or ozone. People living near refineries and manufacturing plants are particularly exposed to higher local pollution [9]. Indoor air contamination is mostly connected with bad ventilation. Cooking residues, tobacco smoke or accumulation of radioactive radon significantly increases the risk of lung cancer [9,14,15]. There are many sources of water pollution including industrial discharges, soil leaching, agricultural wastes, atmospheric deposition, or water disinfection. They result in water contamination with carcinogens such as chlorination by-products or arsenic [9,16,17].

There are many other factors influencing the risk of developing cancer [7,9]. For example: high exposure to UV light or sunlight induces skin DNA damage and mutation, increasing probability of carcinogenesis [18]. Bad dietary habits can provide organism with carcinogens (e.g. trans-fats) [19]. On the other hand, a balanced diet and proper vitamin supplementation can reduce the cancer risk [20,21]. Also, some natural compounds, such as anthocyanins, found in blue and red fruits and vegetables, potentially have anti-cancer properties [22,23]. Another example of a cancer-preventive factor is increased physical activity, that reduces cancer risk through, among others, immune system stimulation [24].

1.1.2. Cellular hallmarks of cancer

The hallmarks are properties that are common to all cancers. Over the years, the number of hallmarks recognized by the scientific community has been changing, depending on new developments in the field and the level of specificity in their definition [25–30]. Currently, the most common model distinguishes ten hallmarks (**Fig. 1**) [30]:

- replicative immortality – normal cells have a limit of divisions that they can undergo, due to telomers shortening. In cancer cells, an enzyme called telomerase is activated from its dormant state, allowing cancer to elongate telomers [31,32];
- genome instability and mutation – cancer cells genome repair system is impaired due to the loss of tumor suppression genes or activation of oncogenes [32];

Fig. 1. The ten hallmarks of cancer. Based on [30,33].

- evasion of growth suppressors – cancer cells are insensitive to signals suppressing their entering to growth and division phases [29,34];
- resistance to apoptosis [35];
- sustained proliferation – tumors can provide themselves with pro-proliferation factors, such as Epidermal Growth Factor (EGF) [30,36];
- altered metabolism – due to increased growth, cancer cells require higher energy production. Instead of oxidative phosphorylation, they use an alternative process called *aerobic glycolysis* or *the Warburg Effect*. These cells convert pyruvate to lactate instead of oxidizing it in mitochondria, regardless of access to oxygen [37,38];
- avoiding immune destruction – cancer cells suppress the part of the immune system that is responsible for recognition and destruction of transformed cells [30,39];
- tumor-promoted inflammation – a tumor can mimic inflammatory conditions of normal tissues. Then, immune cells can provide it with factors promoting growth, motility and metastasis [40];

- induction of angiogenesis – tumor cells are able to induce formation of new blood vessels to provide themselves with oxygen and nutrients. As this is a pathological process, the new vessels are often of a low integrity, providing cancer cells an easier path for intravasation [41–43]; and;
- invasion and metastasis – creation of secondary tumors [44,45].

1.1.3. Tumorigenesis

Tumorigenesis is a process of producing a tumor [46]. It is often wrongly interchangeably used with *carcinogenesis*, which is a process of transformation of normal cells into cancer [46,47], and one of the pathways of creating a carcinogenic tumor [48]. Another pathway is *metastasis*, that results in a development of secondary tumors [49,50].

Carcinogenesis results from acquisition of multiple mutations over time [3]. In its *initial* stage, accumulated mutations cause deregulation of cell growth and differentiation, what leads to uncontrolled cell division and finally to *hyperplasia* [51,52]. Further DNA damage causes loss of cells classical morphology in a *dysplasia* stage [51,52]. Though dysplasia does not ascertains the development of cancer, in some cases altered cells may eventually occupy the entire cellular layer and create *carcinoma in situ* [51,53]. At this stage the tumor is localized to a single site, but its further growth leads to *malignancy* and *invasion* (**Fig. 2**) [51,54].

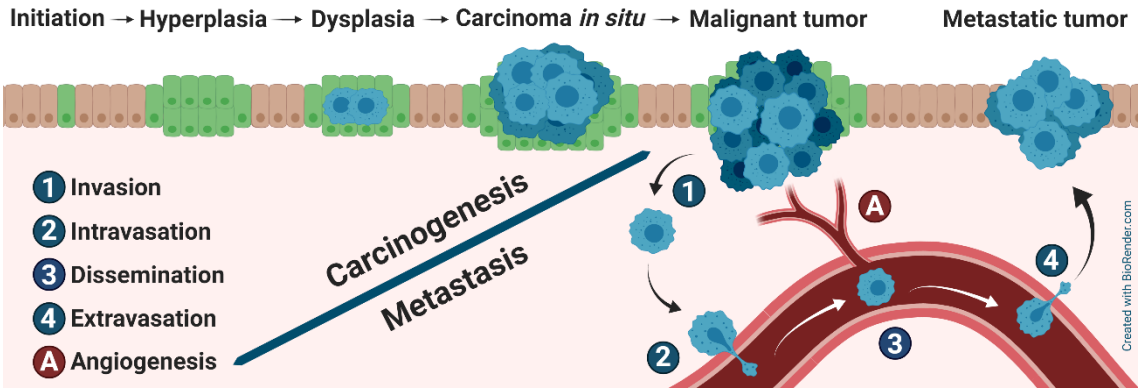

Fig. 2. Tumorigenesis in an epithelial layer: carcinogenesis and metastasis. Based on [44,45,48,50–52,54].

Invasion, the detachment of a cell from the primary tumor site, initiates the process of creation of secondary tumors called *metastasis* [55]. After penetrating the surrounding tissue, a cancer cell can enter the circulatory system through the process of *intravasation* [45,51]. Pathological *angiogenesis* supports this phenomenon further, making blood vessels more accessible [41,43]. Circulating tumor cells can *disseminate* at distant sites

of the body [54,56]. Then, through the process of *extravasation*, cells leave blood vessels and find new niches in remote tissues to develop *secondary (metastatic) tumors* (**Fig. 2**) [45,51,54].

1.1.4. Invasion

Invasion is the first step of metastasis, and also, the first step of spreading cancer cells into surrounding tissues and lymph nodes [30,43]. Literature usually divides it into three stages. In the first one, a cell positions itself on the extracellular matrix (ECM, see **Box 1. The Extracellular Matrix**). During this process, *cell-cell* interactions weaken, and *cell-ECM* interactions become stronger [59].

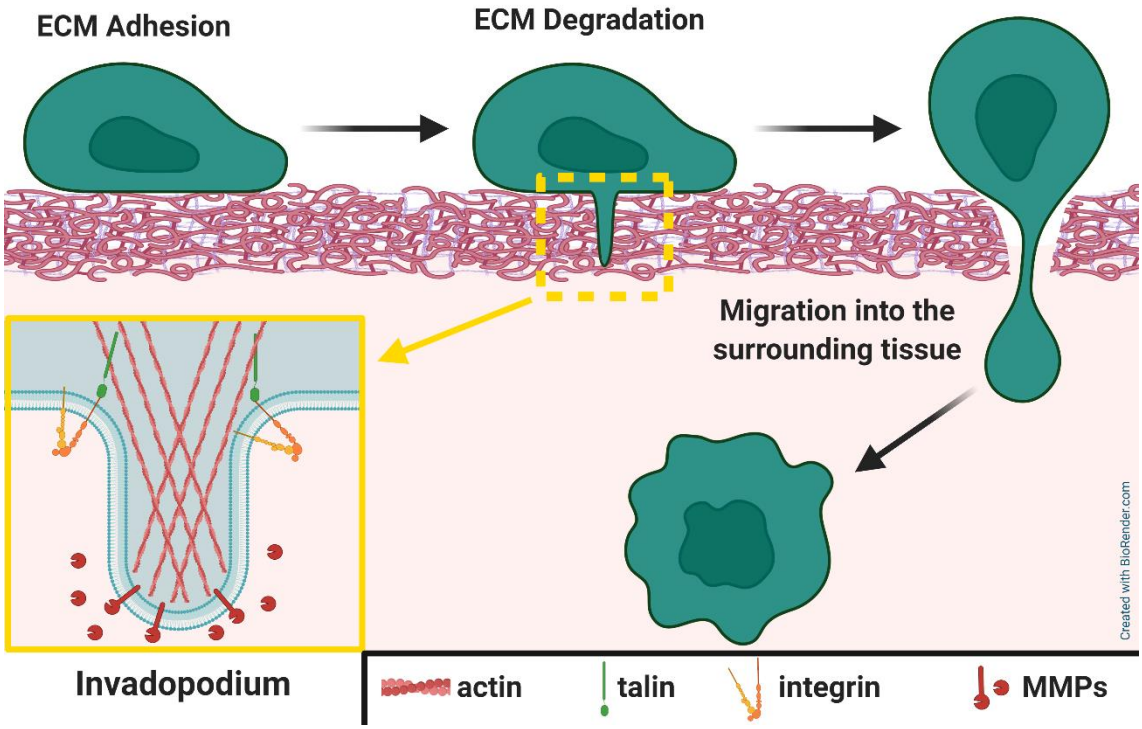

Fig. 3. Stages of cancer cell invasion from an epithelial tissue. Insert: a simplified scheme of an invadopodium. Based on [57–62].

In the second stage of invasion, in order to wade through the ECM, cancer cells form structures called *invadopodia* [57,58]. They are actin-rich thin long protrusions found on the ventral side of a cell. They are usually centrally localized [62]. Their main function is *degradation* of the ECM with various proteases mostly from matrix metallopeptidases (MMPs) family [60–63]. This allows cells to *penetrate* to the surrounding tissue in the last step of invasion [57,58].

1.1.5. Invadopodia

Invadopodia are actin-rich protrusions directed towards the ECM. Their main task is to degrade and penetrate the neighboring matrix, to allow cell invasion and metastasis [60]. The formation of a invadopodium starts with the assembly of precursors, such as cortactin, cofilin, Arp2/3, and N-WASp, that are later anchored to the plasma membrane by Tks5 protein [64,65]. In the next step, β1 integrin is recruited to the complex [60,66].

Independently from β1 integrin, talin1 binds to the invadopodium precursor complex [60,61]. Nonetheless, further interaction between these two proteins is critical for recruitment of moesin-NHE-1 complex, that leads to the initiation of degradation of the ECM by stimulating membrane type 1 matrix metalloproteinase (MT1-MMP) [60,61]. Simultaneously, activation of cofilin, promotes actin polymerization and growth of the invadopodium [60,61,66,67].

In the late maturation stages, invadopodium continues to elongate based on the further actin polymerization [60]. In these further stages, microtubule filaments are also to be found in these protrusions, presumably, serving as trafficking routes for proteases-containing vesicles (such as MMP2, MMP9 or MT1-MMP) [68,69].

Box 1. The Extracellular Matrix

The Extracellular Matrix (ECM) is a dense non-cellular 3-dimetional structure of entangled fibrous proteins (e.g. collagen, elastin, fibronectin) and proteoglycans (e.g. hyaluronan, perlecan) [336,337]. It provides scaffolding and support for cells, and contributes to strength and elasticity of tissues [338,339]. The ECM provides biochemical and mechanical cues regulating processes in cells, including adhesion and migration [340–342]. A healthy ECM creates an almost impenetrable barrier for cells [343,344].

1.2. ADHESION-RELATED PROTEINS IN CELL MOTILITY

Cell migration and motility underlie many biological processes, including physiological ones such as wound healing [70,71], immunological response [54,72], or embryonic and tissue development [73,74], and pathophysiological ones such as, mentioned earlier, invasion and metastasis in cancer development [75]. There are several different modes (strategies) of cell migration, that depend on several factors including cell adhesion level or environmental confinement/crowding [76]. In the case of cancer invasion, a single cell mesenchymal type of migration is the widest studied mode thus far, especially for research conducted in a high adhesion environment (**Fig. 4**) [77,78]. There are numerous proteins involved in coordination of cell migration [79,80], including scaffolding [81,82], cytoskeletal [83] and regulatory proteins [84,85], proteases responsible for ECM remodeling [68], or adhesion proteins such as talins and integrins [86–88]; thus, only selected proteins, most relevant to this work, will be discussed in more details.

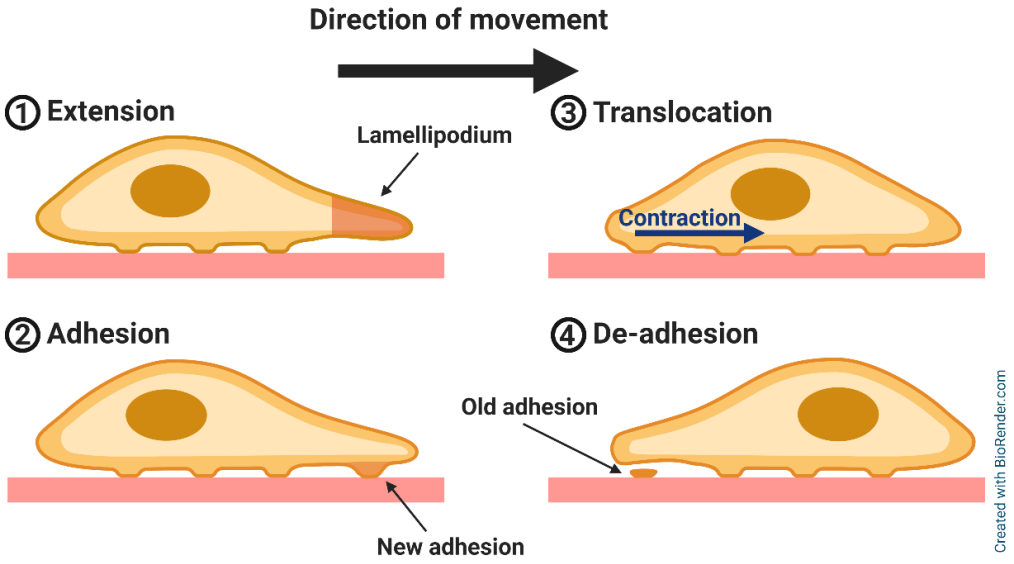

Fig. 4. The scheme of a single cell mesenchymal migration mode. **(1)** In the first step the cell protrudes a wide projection at the leading edge called *lamellipodium*. **(2)** At the interface between the lamellipodium and the substrate new adhesion structures are formed to stabilize the new position. **(3)** The contraction of the actomyosin cytoskeleton creates a force that propels the cell body towards the leading edge. **(4)** Adhesions in the back of the cell disassemble to allow retraction of the cell's tail. Then, the cell can repeat the cycle. Based on [89,90].

1.2.1. Talins

In vertebrates, there are two talin isoforms: talin1 and talin2. They are encoded by two separate genes: *TLN1* and *TLN2*, respectively [91]. Thus far, most of the scientific attention has been directed towards talin1 [87].

Talin1 is a large protein [92,93] primarily described by Keith Burridge and Laurie Connell in 1983 as a molecule playing a role in focal adhesion (FA, see **Box 2. Focal Adhesions**) dynamics and membrane ruffling [94]. Later, it was shown that it is crucial for initiation of cell adhesion by activating integrins [95], and through binding to both integrin and actin it creates a link between the cytoskeleton and the extracellular matrix [96]. In the following years several binding sites for adhesion and migration related proteins were found in talin, including multiple vinculin binding sites [97–101], a focal adhesion kinase (FAK) binding site [102,103] and a paxillin binding site [104] (**Fig. 5**).

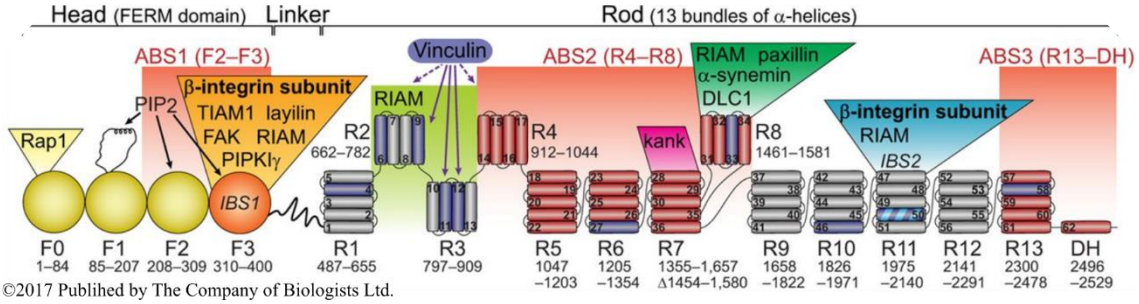

Fig. 5. The structure of talin1 protein. Domains, subdomains, and most important interaction sites are marked; vinculin binding regions are highlighted in purple. Reproduced from [88] with permission from The Company of Biologists Ltd.

Talin1 is composed of two main domains: an N-terminal head FERM (standing for **4**.1, **e**zrin, **r**adixin and **m**oesin proteins, where it was primarily described [105]) domain [106] and a C-terminal rod domain composed of 13 α-helix bundles [107]. The domains are connected by an unstructured linker [88,108]. FERM domains are associated with cytosolic plasma-membrane-targeted proteins [105]. Talin1's FERM domain has an atypical build with an additional F0 subdomain, being similar in its structure to F1 subdomain [106]. Thus far, this aberration was also found only in kindlins [106,109]. It is postulated that F0 domain is required for integrin activation and stabilization in its active state [110], as only talin1 and kindlins proteins were shown to activate integrins [111]. Beside interacting with the plasma membrane and integrins, the head domain has binding sites for several other proteins, including actin (ABS) [97,112]. Some of the sites overlap with one another leading to a complex regulation of talin1's activity (**Fig. 5**) [113,114].

The rod domain also contains multiple binding sites. It has a secondary integrin binding site within R11 bundle [115,116], though, the interaction mechanism and its role is still not defined well [87,88]. Also, all the talin1's vinculin binding sites are located in the rod [88,101]. Moreover, the rod has two actin binding sites [97,117]. It is postulated that they

play different roles in cell adhesion and migration, with one acting as a tension bearer, while the other as a force dependent trigger for vinculin binding [87]. A full length talin1 creates a homodimer through the last C-terminal dimerization helix (DH) [88,118]. Similarly to the head domain, some of the rod's binding sites overlap (**Fig. 5**) [87,107].

Talin1's activity can be regulated through the separation of the head and the rod domains [119,120]. A cleavage site for calpain protease is located in the talin1's linker region [87,121], thus, its conformational availability plays an important role in mediating cell migration and adhesion dynamics [108,121].

As mentioned before, talin1's functions are associated with regulation of integrins activity [88,95] and transduction of mechanical cues between the cytoskeleton and the cellular environment [96]. It is also engaged in cell migration [122] and focal adhesion dynamics [108,121–123]. Moreover, it mediates invasion [123], invadopodia formation [61] and metastasis [123,124] in cancer cells.

Talin2 was discovered in 1999 through a functional genomic analysis, as a result of a search for the third talin1 actin binding site motif in genomic databases [91,117,125]. Structurally talin2 is similar to talin1. Primary structures show 76 % of identity and 88 % of similarity [87,91]. Both proteins also share the same domain and subdomain organization including the localization of all of the interaction sites [87]. The main difference between these two isoforms is in their affinity towards some of the ligands. First of all, talin2's head shows much higher affinity towards integrin than the one of talin1 [126,127]. Nonetheless, thus far, it was not proven that talin2 is able to activate integrins. Moreover, several studies show that depletion of talin2 (in opposite to talin1) does not change the integrin activation level during cell spreading [124,126,128]. Furthermore, talin2 has also higher affinity towards actin [87]. These properties support the observation that talin1 is more abundant in young small peripheral adhesion structures, that are highly dynamic, whereas talin2 is rather associated with mature, stable centrally-localized large adhesions [126,129–132]. Although, dimerization helices between both talin isoforms are highly conserved, thus far heterodimers were not described in the literature [87]. Furthermore, the distribution of these two proteins differs among tissues; while talin1 is present in most of the cells in the human body (with an exception of a heart muscle), talin2 is to be found only in selected tissues, such as skeletal and heart muscles, the brain, and kidneys [87,133–136].

The biological role of talin2 is less understood than its sister isoform. As talins have similar structures and share many biological functions [128,137], it was initially presumed that talin2's functions are redundant in regard to talin1 [124,128]. However, closer studies showed that both, talin1 and talin2, play distinct roles, and often either of them is required in many cellular processes, including tumorigenesis, cancer invasion, and traction force generation [126,138]. Furthermore, due to its subcellular central localization, talin2 is believed to have stronger association with invadopodia maturation and extracellular matrix degradation than talin1 [126]. Moreover, talin2's muscle tissue specificity and stronger integrin and actin binding suggest, that one of its distinct role may be transduction of forces of a greater magnitude [132,139].

1.2.2. Integrins

Integrins are best recognized for being proteins anchoring cells to the ECM [140,141]. They are heterodimeric transmembrane receptors composed of α and β subunits. Most of the subunits have a large extracellular domain responsible for interacting with extracellular ligands, a single transmembrane helix, and a short intracellular domain responsible for interaction with cellular agents [142,143].

In mammals, there are 18 α and 8 β subunits, making 24 distinct heterodimer combinations (**Fig. 6A**) [86,140]. Different types of integrins show different affinity towards ECM ligands depending on their composition (**Fig. 6A**) [140]. In some cases, the binding site is located on the α subunit [144,145], in other, it is shared between both of the subunits [144,145].

There are three main integrins conformations, connected with integrins activation level; each of them shows a different affinity towards the ECM ligand [88,111]. There are several pathways leading to integrins activation. The most common one, mentioned earlier, is based on an initial interaction with talin1 [88,111]. Unbound integrin resides mostly in a thermodynamically preferable *bent closed* conformation [111,146], which has a very low affinity towards the ligand [146,147]. Upon interaction of a β subunit cytoplasmic tail with talin1's head domain, integrin unfolds taking an *extended closed* conformation, that still has a low-to-intermediate ligand binding capacity [146,147]. When interacting with the ligand, integrins are being stabilized in the third conformation called *extended open*, that may have even 5,000-fold stronger affinity towards the ligand than the two other states [147,148]. As the signaling comes from the inside of the cell this

kind of an activation pathway is called *inside-out* (**Fig. 6B**) [140]. The second kind of an activation pathway, called *outside-in*, is driven by ques from the extracellular environment [140]. Even though the bent closed state is thermodynamically optimal, due to thermal fluctuations, a small amount of unbound integrin is in the extended closed or open conformations (about 0.1 % and 0.15 %, respectively) [111,146,149]. Thus, in the extended open conformation, the ECM ligand can be bound simultaneously with talin on the other end, locking integrin in the open state [111]. Furthermore, integrins can be stabilized in the extended conformation by various extracellular (bio)chemical agents like manganese cations or conformation specific antibodies [147,150].

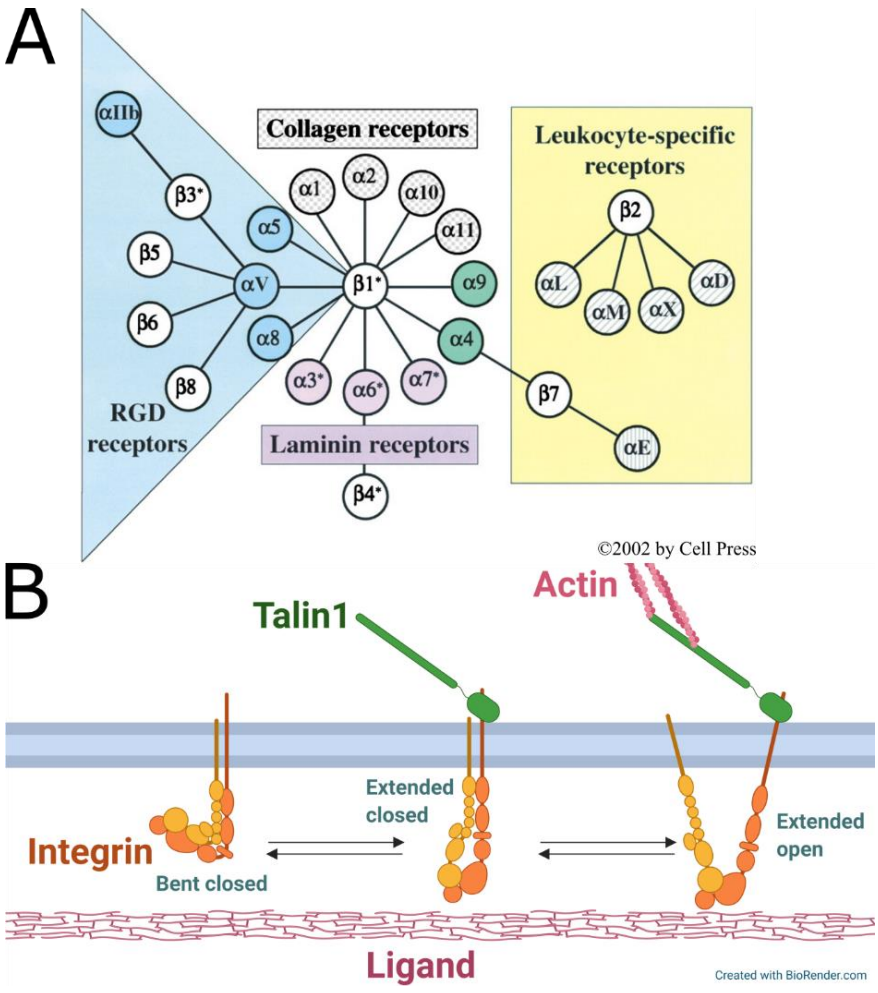

Fig. 6. Panel A. Integrin heterodimers with their most common ligands. Most of them recognize ECM ligands, such as RGD motif (present in e.g. fibronectin) or collagen; a small subgroup of leukocyte specific receptors recognizes Ig-superfamily cell surface counterreceptors. α4β1 and α9β1 integrins (in green) bind both ECM ligands and the counterreceptors [140]. Reprinted from [140] with permission from Elsevier. **Panel B.** A scheme of the *inside-out* activation of integrin by talin1. Based on [88,111].

Besides playing a key role in cellular adhesion, integrins are connected with many other biological phenomena. They mediate processes like immune response (mentioned earlier)

[151], cell cycle and proliferation [152,153], embryogenesis [154,155], or cancer invasion and metastasis [156–159]. Furthermore, misregulation of integrin signaling is associated with many pathological processes and diseases [160], such as severe muscular dystrophy (absence of integrin α7) [161], cardiac fibrosis (an overexpression of integrin α11) [162], the leukocyte adhesion deficiency I (a loss of expression of β2 integrin) [163], loss of platelet aggregation a (deletion of β3 integrin gene) [161], or cancer [164] (e.g. an overexpression of αVβ8 promotes growth and invasion of squamous cell carcinoma [165], an overexpression of integrin α11 promotes non-small-cell lung carcinoma [166]).

Box 2. Focal Adhesions

Focal adhesions are integrin-based structures that link cells to the ECM [345]. Beside cellular adhesion, they mediate the process of mechanotransduction, cell edge protrusion, and migration directionality and velocity [346–352]. They are composed of over 150 different types of proteins [79,80,353] organized in a composite multilaminar nano-architecture (**Fig. 7A**) [354]. The adhesion formation can be divided into several stages [355]. Initially, nascent adhesions are created at the leading edge. Most of them are quickly disassembled, but some grow into focal complexes and focal adhesions [129,356]. Further, these structures may also be disassembled or stabilized to create fibrillar adhesions in the central region of the cell. That, in result impedes migration (**Fig. 7B**) [355]. Colloquially, in many studies all integrin-based adhesion structures are often called focal adhesions, as the other names were adopted years after the discovery and naming of focal adhesions [345].

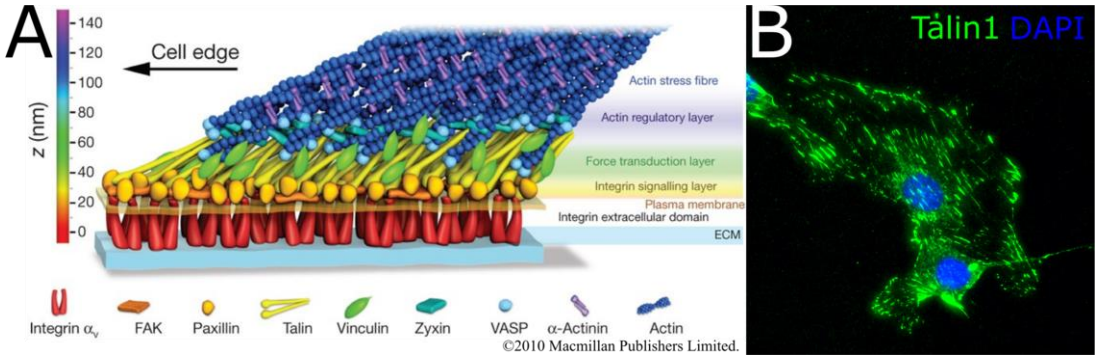

Fig. 7. Panel A. The nanoscale architecture of focal adhesions made of layers of different proteins. Reprinted from [354] with permission from Springer Nature. **Panel B.** The distribution of adhesion structures in 3T3/NIH mouse embryonic fibroblasts. Cells were stained for talin1 (green) – a focal adhesion marker and DAPI (blue) – a DNA marker. Young peripheral nascent and focal adhesions are small and numerous, after they mature, they can become fibrillar adhesions located in the center of the cell.

1.2.3. Talin-integrin-ECM interaction at the molecular level

In the previous section, the talin and integrin interaction during the inside-out signaling was briefly described. Even though the interplay between these two groups of proteins has been broadly studied, still, there are many aspects that need further investigation. One of the recent discoveries showed a nontrivial dependency between a pulling-force and an integrin-ligand interaction lifetime called a *catch-slip bond*, or more commonly, a *catch bond* [86,167].

In the standard model of molecules interaction, called a *slip bond*, the stability of the bond decreases with an exerted pulling-force [86,168]. In the case of a catch bond, at first, the attraction between molecules rises together with the force, and then, after reaching a threshold, it weakens [86,167]. Thus, binding integrin to talin and linking it with the actomyosin cytoskeleton provides additional tension that further stabilizes cellular adhesion [111,169]. The mechanism underlying the catch bond in integrins has not been thoroughly described yet [86]. One of the hypotheses presumes that the additional force provided into the interaction stabilizes the fluctuations between the open and closed states of the extended conformation, resulting in increasing lifetime of the open state (**Fig. 6B**) [86,170]. Moreover, studies show that upon tension, α5β1 integrin undergoes further conformation changes, leading to the formation of new hydrogen bonds at the interface between integrin and the ECM [170,171]. The catch bond behavior was observed for many integrins, including α5β1, αvβ3, αLβ2 or α4β1 [86,137,167,172,173].

The second worth-noting aspect is the molecular basis of the differences between talin1 and talin2 interaction with integrins (in this case, specifically with β1 integrin). Talins bind to integrin β subunits through its head F3 domain (**Fig. 5**, **Fig. 6B**) [88]. The differences in the molecular architecture of the binding sites in talins result in affinity differences between these proteins and integrins, as well as in differences in talin1- and talin2-integrin quaternary structures [126,127,174]. Recent studies show that a mutation of just a single residue (C336 or S339 in talin1 or talin2, respectively) is responsible for the majority of the differences [126,127]. Talin1^{C336S} has a higher affinity towards β1 integrin than the wild-type protein and it has the integrin binding geometry similar to talin2^{WT}. At the same time, talin2^{S339C} has a lower affinity towards its partner than talin2^{WT} [126,127]. Furthermore, studies made on talin2-knockout cells showed that the S339C mutant does not rescue the phenotype [126,138]. Therefore, it seems safe to

hypothesize that the aforementioned mutations result in the differences in the nature of the interaction between talin isoforms and β integrins [127].

1.2.4. Matrix metallopeptidases

Matrix metallopeptidases (MMPs), also known as *matrix metalloproteinases*, are a family of zinc depended proteins involved in degradation and remodeling of the ECM [175,176]. There are 23 different MMPs in humans, including 6 membrane-bound ones [177]. MMPs' activity is connected with several biological processes, including cell migration [178,179], apoptosis [180], synaptic plasticity [181], and embryogenesis [182]. They also play a key role in cancer invasion and metastasis [176,183].

In cancer invasion, MMP14, also called MT1-MMP, is the prominent ECM degradation enzyme that participates in the initiation of invadopodia formation [61,184]. Another two broadly studied proteases, strongly connected with tumor metastasis, are MMP2 and MMP9 [185–188]. The activities of these three MMPs are tightly connected [189,190]. First of all, in many cancers MMP2 and MMP9 are co-expressed [189]. They are secreted in a form of zymogens, proMMP2 and proMMP9, respectively. To gain their proteinase properties, they have to be cleaved first; MT1-MMP has catalytic properties towards proMMP2 [191], while MMP2 can cleave proMMP9 [189,190,192]. The pathway requires proximity to the plasma membrane and the presence of tissue inhibitor of metalloproteinases 2 (TIMP2) for high efficiency [189]. Some other proteinases also can activate MMP9 [193–195].

TIMPs are a family of four proteins that regulate activity of extracellular proteinases, including MMPs [196]. Even though their main function is inhibition of proteolytic processes, as mentioned before, the presence of TIMP2 provides the catalytic site for MMP2 activation [189,196]. TIMPs show poor specificity towards different proteases [197], although, TIMP1 has higher inhibition properties towards soluble MMPs [189,198,199], while TIMP2 is an efficient inhibitor of MT1-MMP [199]. Thus, in relatively low concentrations of TIMP2, it acts as a catalyzer for MMP2 activation (what consequently leads to MMP9 activation), while in high concentrations it inhibits the all three mentioned proteases, either directly, like MT1-MMP, or through blocking cleavage of the proenzymes [189].

Misregulation of MMPs and TIMPs is one of the markers of cancer [200]. Several recent studies showed that adjustment of their activity can reduce carcinogenesis and invasion

in cancer cells [187,188,190,201]. Therefore, these proteins might be promising targets for anti-cancer therapies.

1.3. FLUORESCENCE MICROSCOPY IN BIOLOGICAL STUDIES

Microscopy is one of the most popular techniques used in cell biology and biophysics research. It is used to magnify and manipulate microscopic size objects, thus it allows to observe, record, and elucidate cellular and sub-cellular mechanisms. Even though the optical properties of glass lenses were known to ancient Greeks and Romans [202], the first microscope, with an optical design corresponding to the ones that are currently in use, was invented around 1609. Yet, the original inventor is unknown and the design may be ascribed to several people, with Zacharias Janssen and Hans Lipperhey being the most probable ones [202,203].

1.3.1. Microscopy image formation

The general microscope setup employs two converging lenses to produce a magnified image. The first lens, the one closer to the object, is called an *objective lens*, the second one – an *eyepiece lens*. The first lens creates a real, magnified image. The second one forms a further magnified, virtual image based on the first one, that is then visible to an observers eye (**Fig. 8A**) [204].

In the case of an *electronic-detector* design, the final image has to be real and, in the case of widefield imaging, focused on the detection plane. Thus, in contrary to the *eye-detector* design, the simplest *electronic-detector* design does not require an eyepiece lens (**Fig. 8B**) [205]. Another possibility for this design is to use a three-lenses setup, with an additional lens between an eyepiece lens and camera's sensor matrix that mimics the lens of an eye [206].

In modern microscopes instead of a single objective and an eyepiece lenses, there are usually sets of several lenses designed and built as a single component. This allows for higher magnification and correction for some of optical aberrations [207–209]. Furthermore, there are often additional supporting lenses (e.g. tube lens), that are used for further minimalization of optical aberrations, manipulation the microscope's optical pathway or additional magnification (or reduction) of the image [210–212].

1.3.2. Image acquisition

There are two main modes of acquisition: widefield and scanning. In the widefield mode the signal from the whole imaging area is collected simultaneously using a camera with a matrix of photo-sensible semiconductors, capable of to accumulate charge proportional

to the light that illuminates them, called pixels (from *picture elements*) [213]. In the scanning mode, the image is created by collecting information from a specimen in a sequential pixel-by-pixel manner. It is usually executed through illumination of a single spot in a sample with a focused laser beam and then collection of the fluorescence signal (or transmitted light) with a single highly sensitive detector such as a photomultiplier or an avalanche photodiode [213,214]. There are also several hybrid techniques that benefit from both approaches. In example, *Image Scanning Microscopy* (ISM) uses laser scanning module for illumination, but instead of a single brightness value, a whole image is collected with a camera for each beam position. Then the set of images is analyzed and used to reconstruct the image of the whole specimen [215].

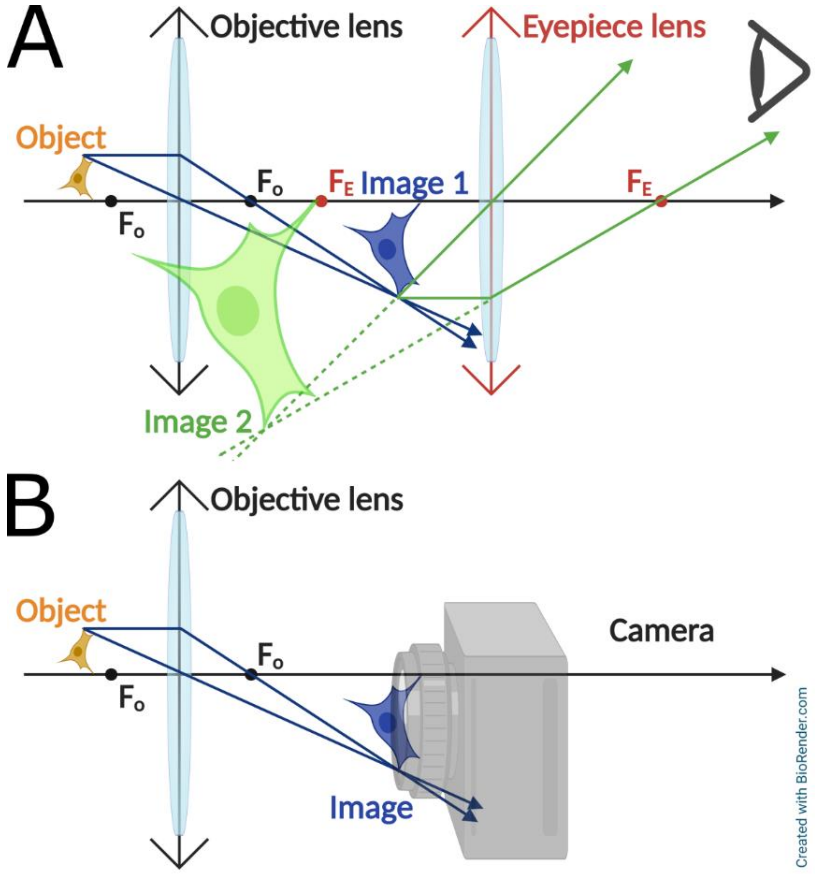

Fig. 8. Ray diagrams for image formation in a microscope. **Panel A.** The *eye-detector* design. An object must be positioned between the single and the doubled focal length distance (**F_O** – the **focal point** of the **objective lens**) of the **objective lens**. The first image created by the **objective lens** is *real, inverted, and magnified*. It is created between eyepiece lens and its focal point (F_E), thus the second image is *virtual*, *simple* (in relation to the first image), and further *magnified*. **Panel B.** In the case of the most simplified camera *electronic-detector* design, a *real* image has to be created at **the sensor**. In this setup, the image is built the same way as the first image in the *eye-detector* design, but then it is collected at this stage, without going through any subsequent lenses. Both presented panels are in scale in the relation to the object plane at the beginning of the rays.

Charge-Coupled Device (CCD) and Complementary Metal–Oxide–Semiconductor (CMOS) sensors are two classes of camera sensors the most widely used in microscopy. The basic CCD-type sensors work in two phases. During the exposure phase (also called the acquisition phase), the sensor matrix collects the signal from the specimen. In the readout phase, in first CCD cameras, the sensor was physically covered from light with a mechanical shutter. Charges accumulated in single pixels in the sensor matrix are transformed into the digital data stream. Each sensor line is transferred sequentially through the image array towards a register shift. In the register shift, information from each pixel is passed onto a *Charge-to-Voltage* converter, then the signal can be amplified, digitalized, and stored (**Fig. 9A**) [216,217].

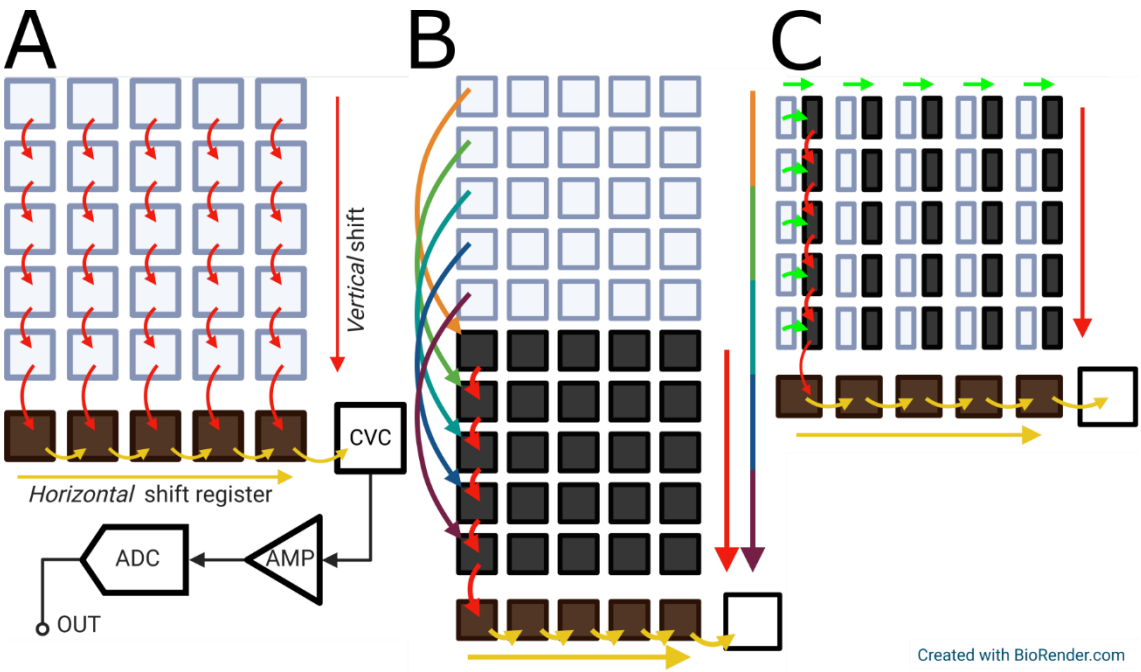

Fig. 9. A readout scheme of a CCD camera sensor. **Panel A.** During the exposure phase photons striking on the pixel's surface cause a charge build-up. In a readout phase, the sensor is covered from light. In this phase charges from all pixels are sequentially shifted line-by-line towards the *horizontal* shift register. Then, information is shifted pixel-by-pixel towards a *Charge-to-Voltage* Converter (**CVC**). Next, it can be amplified (**AMP**) and is digitized by an *Analog-to-Digital* Converter (**ADC**). Finally, data is transferred to an output device (**OUT**, e.g. a computer). Spaces between pixels are designed to be minimal to assure the most accurate imaging. Based on [218]. **Panel B.** A frame-transfer CCD scheme. Charges from the whole image section, after the exposure phase, are rapidly parallelly shifted into the second, masked storage region. Then data is read out as previously described. **Panel C.** An interline-transfer CCD scheme. Charges from all pixels are transferred to adjacent, covered pixels. Then, data is read out as previously described. In both cases the subsequent acquisition phase can begin right after shifting data to the covered part of the sensor. Based on [216].

The main caveat of this design is a relatively long readout phase (e.g. 50 ms for 1 megapixel sensor, 20 MHz readout), that is comparable in length to an acquisition phase. This results in a long sensor dead-time when data is not collected. There are several solutions addressing this problem that are currently in use, that allow to minimize time between subsequent acquisition phases and eliminate necessity of using a shutter. A *frame-transfer* CCD employs a second CCD matrix. After the exposure phase, data from the whole image array is shifted (still in a line-by-line manner) to the masked storage array. This process is fast enough that the subsequent exposure phase can be initiated almost immediately (< 0.5 ms), without the need of covering the sensor [219]. Next, the data that was shifted to the storage section can be read out the same way as described previously, simultaneously with a subsequent acquisition phase (**Fig. 9B**). The second most common solution is an *interline-transfer CCD*. Data from the image array is shifted to adjacent, covered pixels almost instantaneously (~1 μs) and then read out (**Fig. 9C**) [220]. This solution also does not require any shutter. Both architectures have their strengths and weaknesses (e.g. charge shifting time, sensor quantum efficiency, or price) that should be considered while choosing a CCD camera for a microscopy system.

The second class of camera sensors is CMOS. Their main difference from CCDs lays in their microarchitecture. Each CMOS's pixel has an internal circuit with a separate C*harge-to-Voltage* converter, amplifier, and *Analog-to-Digital* converter. The use of separate circuits allows to read each pixel separately and not as a part of a whole-sensor data stream like in CCD sensors [221]. Furthermore, CMOS-based cameras usually have a higher frame rate of the two classes. On the other hand, due to differences in performances of single semiconductors, a CMOS's *pixel-conversion-amplification* approach results in uneven *light-to-voltage* conversion rates between single pixels. Therefore, each sensor has to be calibrated and a specific amplification correction has to be applied to for each pixel [222]. Moreover, due to a more complex architecture, these kind of sensors usually show lower quantum efficiency than CCDs [223]. Nevertheless, modern CCD and CMOS cameras are characterized with very similar performances [213], thus not only a type of a sensor, but even a specific model of a camera should be considered while designing a microscopy system.

Laser scanning-based microscopy techniques show a different approach to image acquisition. Instead of simultaneous illumination of the whole object, only a single spot is illuminated with a focused laser beam, that scans a specimen, usually in a raster pattern

[224,225] (**Fig. 10A**). The signal from a sample is collected by a single-spot light sensitive detector. It is then used to reconstruct the image in a *pixel-by-pixel* manner. This approach, used with a confocal pinhole placed in the back focal plane before the detector, allows to almost completely eliminate *out-of-focus* light, thus, to optically section the sample in z-axis and to perform 3-dimensional (3D) imaging (**Fig. 10B**) [225,226]. This is advantageous especially for thicker samples [227]. The rejection of background light results also in an increase of contrast and the *signal-to-noise* ratio [214].

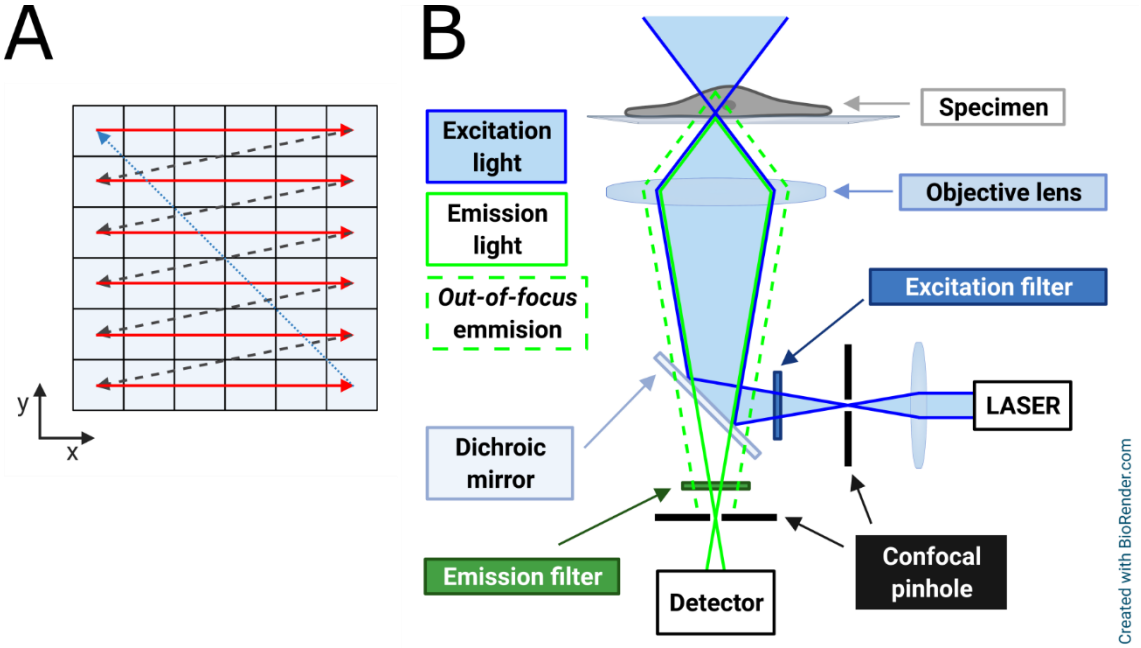

Fig. 10. Panel A. A scheme of a raster scanning pattern popularly used in laser scanning microscopy. The signal is collected while scanning from *left* to *right*. After finishing a line, the beam is shifted to the next line; data is not collected during the shift. After scanning the whole area, the beam is moved back to the beginning of the region of interest (ROI) for another scan of the area if planned. Based on [224]. **Panel B.** A scheme of a confocal laser scanning microscope optical design. The light beam generated by a laser (or other strong light source) is focused by a lens. It passes the **first confocal pinhole** to eliminate eventual reflexes of *out-of-focus* light. Then, it goes through the excitation filter, it is reflected from the dichroic mirror, and it is focused on the specimen by the objective lens, creating a single illumination spot at the focal plane. Fluorescent light emitted by the sample is focused by the objective and passes through the dichroic mirror. Then, it goes through the emission filter, to eliminate non-specific signal, and through the **second pinhole**, to eliminate *out-of-focus* emission, onto the surface of a detector. Based on [214,225].

Nonetheless, confocal laser scanning microscopy (CLSM) sectioning comes with several limitations. Together with *out-of-focus* light, a part of signal from imaging plane is also rejected. Therefore, CLSM requires higher total excitation light intensities than basic widefield techniques, what causes higher photodamage of a specimen. Furthermore, in 3D imaging the sample is scanned multiple times, what causes further damage [228]. A

low frame rate, being at a level of a single frame per second, is another caveat of laser scanning microscopy [214]. Nonetheless, currently there are several advancements to CLSM that increase acquisition rate to the levels comparable with camera-based widefield techniques [224,226,229,230].

1.3.3. Fluorescence

Fluorescence is a phenomenon in which molecule relaxation from the singlet excited state to the ground state is accompanied by an emission of a photon. (**Fig. 11A**) [231]. After either an excitation (usually due to a photon absorption) or a relaxation transition, a fluorescent molecule, called a fluorophore, can take any vibrational level (usually a higher one, than it was on, before the transition), but the excess of the energy is dissipated rapidly (**Fig. 11A**). This leads to two main properties of the fluorescence absorption-emission spectrum. The first one is called the Stokes shift. Due to a vibrational relaxation, the energy of the emission is usually smaller than that of the absorption (**Fig. 11A**). Thus, the wavelength of the emission will be longer than that of the absorption (**Fig. 11B**). The difference between spectra peaks is called the Stokes shift [231,232].

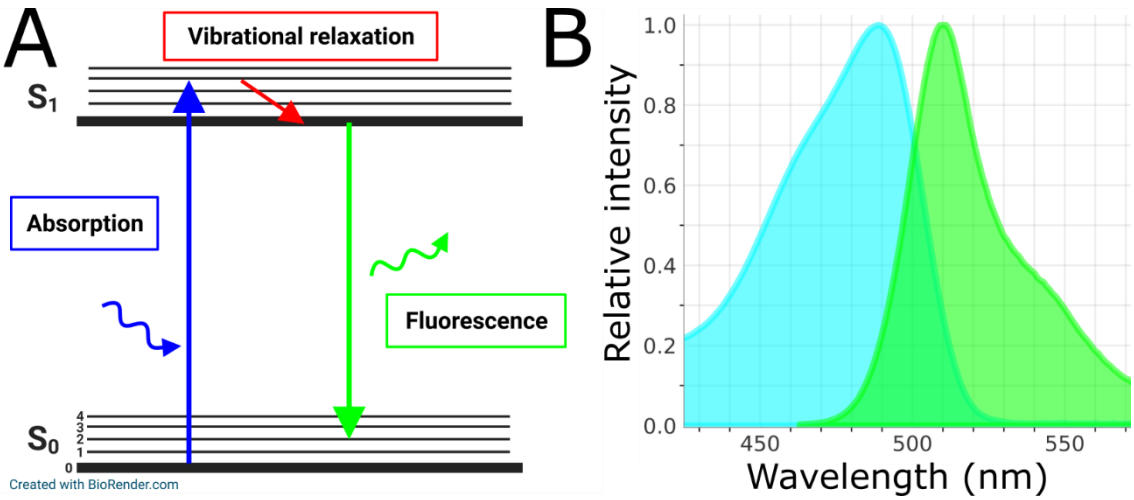

Fig. 11. Panel A. A simplified Jabłoński diagram for fluorescence phenomenon [233]. A fluorophore, after absorbing a photon, is excited into higher energy electronic (singlet) and vibrational states. In the case of the latter, the excess of the energy is dissipated rapidly. A fluorescent fluorophore relaxation is accompanied by an emission of a photon. There are several other excitation and relaxation phenomena that are not depicted in the figure [231]. **Panel B.** The absorption-emission spectrum of enhanced green fluorescence protein **(**EGFP) [234]. Generated with *FPbase* spectra viewer [235].

The second property is the mirror-image rule. According to the Franck-Condon principle, electronic transition does not cause any changes in the positions of atoms' nuclei. That leads to similar structures of vibrational energy levels in the ground and excited states

[236]. The second part of the principle says that the transitions have the highest probability to happen between vibrational levels of the highest wavefunctions overlap integral [237]. As most of the transitions happen from the lowest vibrational energy levels, regardless of the direction of an electronic transition, the distribution of vibrational levels taken by fluorophores after transition will be similar for both types of a transition. Therefore, absorption and emission spectra are typically mirroring each other to some extent (**Fig. 11B**) [231]. Nonetheless, there are several exceptions from these properties [231].

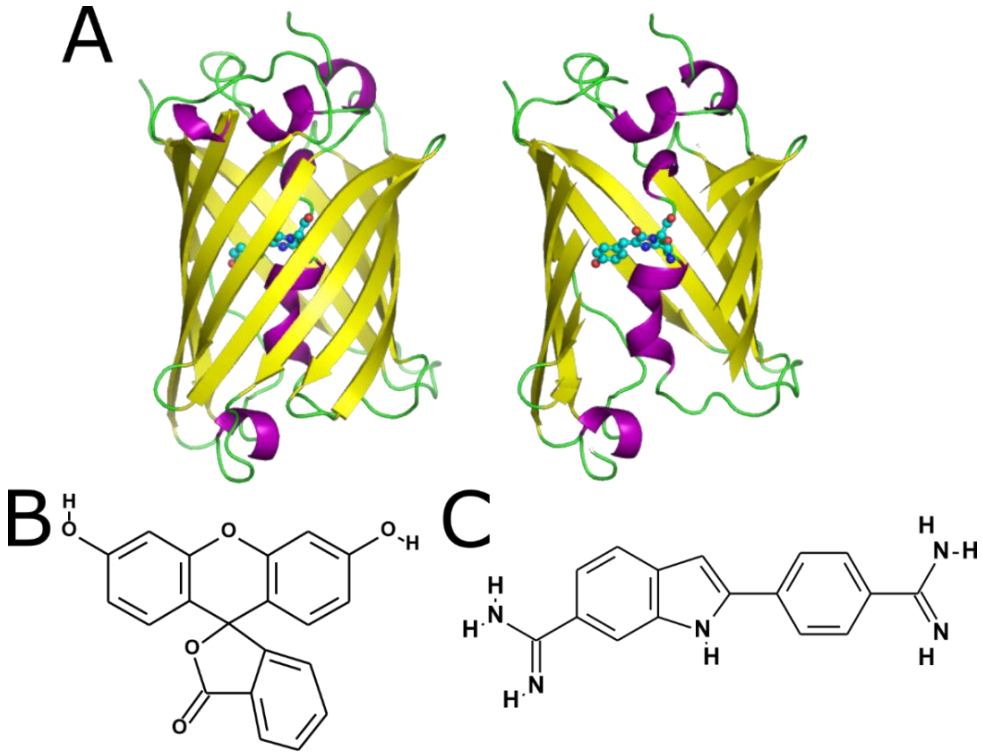

Fig. 12. Examples of florescent probes used in cellular research. **Panel A.** A structure of a green fluorescent protein (PDB entry code: 1GFL) [238] (**left**) with an exposed fluorophore (**right**). Created by [239]. **Panel B.** A structure of fluorescein. Based on PubChem [240,241], generated with PubChem Sketcher [242]. **Panel C.** A structure of DAPI. Based on PubChem [240,243], generated with PubChem Sketcher [242].

In bright-field microscopy, which employs light transmitted through a sample, most measurements depend on absorption or dispersion of the light by the sample. Thus, in the case of working with thin specimens like cells, where the absorption is minimal, the imaging contrast is low [244]. Limitations of bright-field microscopy can be overcome by using fluorescent probes bound to specific cellular structures or proteins. There are several kinds of probes including fluorescent proteins (**Fig. 12A**) [245,246], small-molecule fluorophores (**Fig. 12B-C**) [247,248], and quantum dots [249], with the two former being the most commonly used. In the case of small-molecule fluorophores they

either can bind themselves to specific structures (e.g. DAPI to DNA) [248] or are conjugated to another particle that recognizes the target (e.g. a fluorescein derivative bound to an antibody) [247]. Fluorescent proteins are usually being fused at the DNA level with a protein that is to be monitored. The construct is then introduced to cells in a form of a plasmid or incorporated into cells' genome. The fusion protein is synthesized by the cell protein expression machinery [250,251]. This way, it is possible to observe selected subcellular structures.

After staining a specimen, a fluorophore can be excited using a fluorescence microscope. Due to the Stokes shift, excitation and emission lights can be optically separated from each other based on their wavelengths. A basic filter set (often called a filter cube, as it is usually enclosed in a small cube) is composed of three chromatic filters: an excitation filter, a dichroic mirror, and an emission filter (**Fig. 10B**). The central element of the set, a dichroic mirror, is designed to reflect excitation light but to pass the emission light (**Fig. 10B**). The goal behind using excitation and emission filters is to further separate excitation and emission lights. The former is to increase selectivity of the fluorophore excitation, the latter to increase selectivity of fluorophore emission light and to eliminate eventual reflections of higher wavelengths of the excitation light that may pass through a dichroic mirror [213].

The application of fluorescent particles increases contrast and sensitivity through employment of a selective light emission with a dark background, instead of having darker spots on a bright background. Using probes that target particular structures increases specificity and selectivity, in comparison to bright-field microscopy [213]. Furthermore, by using fluorescence base super-resolution methods, it is possible to achieve significantly higher imaging resolution than the one of bright-field imaging methods [213]. Moreover, there are several microscopy techniques, that are based on various properties of fluorescent light other than intensity, such as polarization [252], anisotropy [253], or life-time of the excited state [254,255], that allow to perform more complex studies of biological systems at the molecular level.

1.3.4. Resolution of microscopy imaging

Resolution is described as the smallest distance between two objects at which they can be distinguished from each other [256]. In a microscope, an infinitely small point light source creates a distinct pattern with a bright *gaussian-like* peak [214] in the center and a low

intensity rings-like motif around it. This pattern is called the *Airy disc* (**Fig. 13A**) [257]. It results from a non-infinite observation setup and the phenomenon of diffraction; the objective lens acts like a wide slit, causing a *single slit*-based diffraction, with the rings being the successive fringes of the diffraction pattern [204]. Thus, by increasing the angular size of the *slit* by e.g. widening the lens or decreasing the distance between an objective and a sample, the peak will get narrower what leads to a better imaging resolution [204].

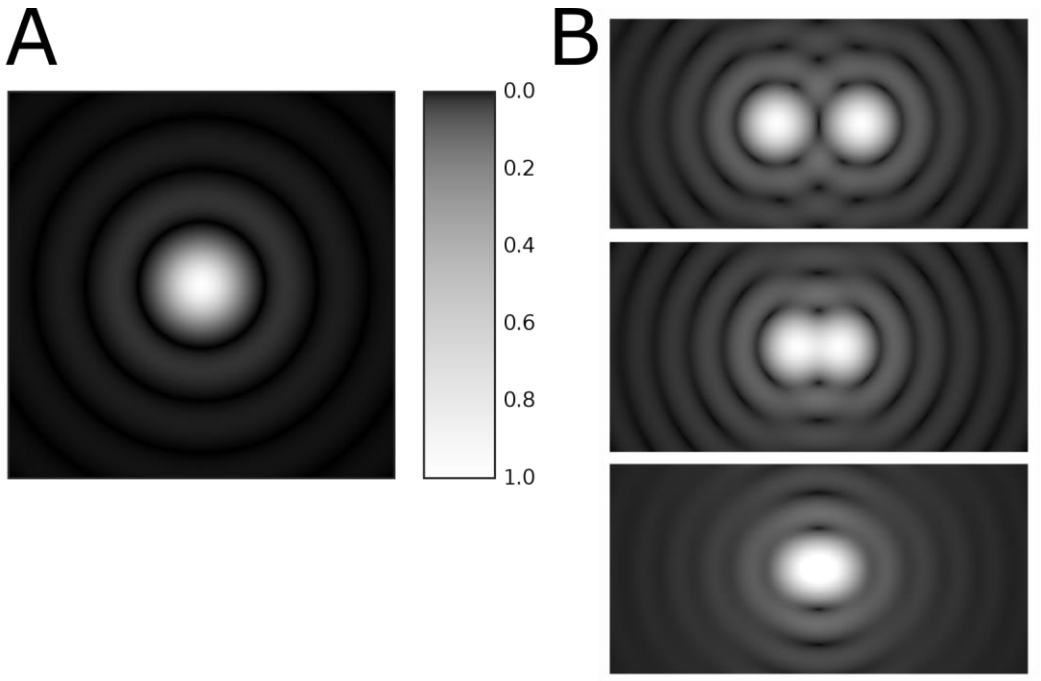

Fig. 13. Panel A. A generated image of a point light source. The Airy disc pattern is clearly visible. Generated by [258]. **Panel B.** Generated interference patterns of two separate point light sources. The **top image** shows the instance where one source is located at the first order maximum of the second source, the **middle** one – at the first minimum (the Rayleigh criterion), and the **bottom** one – at a distance closer than the criterion. In the top two images the objects can be easily distinguished from each other. Generated by [259].

There are several models to calculate the imaging resolution; the most common one used for fluorescence microscopy is Rayleigh's criterion [260,261]. By its definition, two bright points may be assumed resolvable if the maximum of the image of one point lays not closer than at the second point's image first minimum (**Fig. 13B**). For widefield epi-fluorescence microscopy, where the objective lens serves for both excitation and emission light paths, the theoretical lateral resolution d_R can be determined with:

$$d_R = \frac{0.61\,\lambda}{NA}, \qquad \textbf{Eq. (1)}$$

where λ is the wavelength of light and *NA* is the numerical aperture of the objective given by the equation:

$$NA = n \sin \alpha, \qquad \textbf{Eq. (2)}$$

with *n* standing for the refractive index of the imaging medium and α is the half of the angular aperture of the objective lens (the maximal angle of the rays emitted from the focal point and collected by the objective) [256]. A common alternative way to describe and compare resolutions between microscopes is to analyze the main peaks' FWHMs (Full Width at Half Maximum). The theoretical lateral FWHM-based resolution d_{FWHM} is given by the relation [214]:

$$d_{FWHM} = \frac{0.51\,\lambda}{NA}. \qquad \textbf{Eq. (3)}$$

This approach is especially useful while the Airy disk pattern is not clearly visible [262,263].

In widefield microscopy the *in-focus* image of a bright spot will be as presented in **Fig. 13A.** For laser scanning microscopy the physical and mathematical description is more complex. The excitation spot is not infinitely small, but the laser beam also diffracts, similarly to the way described above. Therefore, the gaussian shaped beam's FWHM is the same as describe with **Eq. (3)** [264] and the laser will be exciting specimen within a relatively large area at the focal plane. Moreover, in contrast to widefield microscopy, in laser scanning microscopy the excitation is uneven, thus the final image of a bright spot is an integral of the beam's excitation pattern and the emission pattern (the Airy pattern) [214]. Therefore, with a properly chosen pinhole diameter, in confocal microscopy it is possible to achieve an increment of resolution of 30 % or more [214].

While planning a microscopy experiment or an optical setup, it is worth to account for the resolution limit to avoid under- or oversampling. According to the Nyquist sampling theorem, the imaging sampling pixel size should be at least twice smaller than the intentional resolution [265–268]. Thus, in the case of widefield microscopy the system magnification must be chosen in relation to the camera pixel size [256].

It is important to underline that the considerations presented above relate to the theoretical diffraction-limited theory of optical resolution presented by Lord Rayleigh in 1879 [261]. They do not account for microscpy setup imperfections, imaging contrast, photon

detection sensitivity or imaging noise that may diminish the actual resolution of a microscope [214,260].

1.3.5. Point Spread Function

In the previous paragraph, the Airy disc was described as an *in-focus* image of a bright spot. Nevertheless, the Airy pattern describes only the image at the imaging plane. In the more general definition, the Point Spread Function (PSF) is used to characterize both 2D and 3D images of a point light source (**Fig. 14**) [256,269]. The same as for the Airy disc, the general brightness intensity distribution of the PSF originates from the diffraction and interference of light. The further details result from defects and imperfections present in the imaging system and the specimen [270]. As the image of a point source is represented by the PFS, an image of a whole physical object is a convolution of the object itself and the PSF [269]:

$$image = object * PSF. \qquad \textbf{Eq. (4)}$$

There are many algorithms that can be used to estimate a theoretical PSF [271–277]. They vary in mathematical approaches, complexities and numbers of parameters they account for [278]. Obtaining a PSF by calculating its intensity distribution is, usually, a relatively low time-consuming method, providing a noiseless good quality image. Though many of the models are capable to parametrize complex specimens, they usually are unable to account for defects in the optical setup [279]. Furthermore, some more complex algorithms require a high computing power to reach the solution [275].

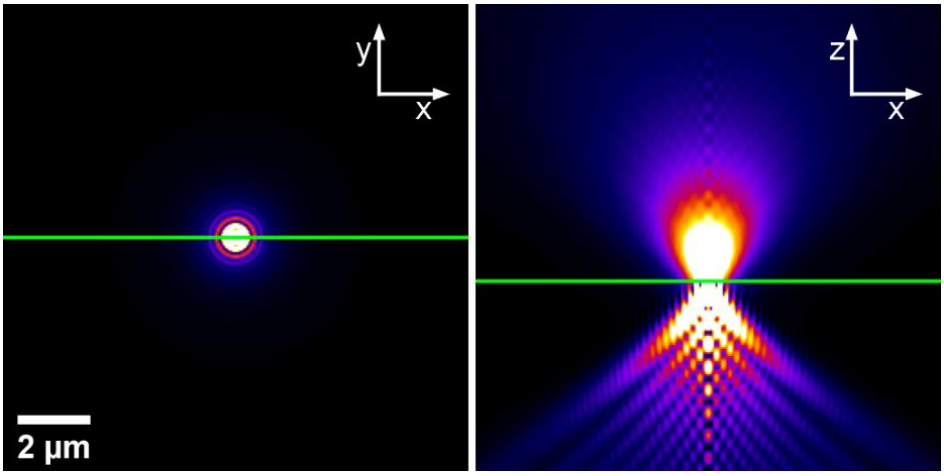

Fig. 14. An exemplary images of cross-sections of a PSF generated with *PSF Generator* software [278] using Gibson-Lanni algorithm [271]. The green lines show the orientations of the cross-sections. The image saturation level was set to 0.01 (high saturation). PSF generation parameters: NA = 1.4, n_i = 1.5, n_s = 1.33, λ = 488 nm, t_i = 170 µm, z_p = 1,000 nm. Fire LUT was applied (in *Fiji* software [280]). Based on [278].

The alternative to calculating a PSF is to measure the actual one on a microscope, using small fluorescent objects, such as nanometer-size beads [270]. This way all the aberrations, both connected with the sample and the optical pathway, can be accounted for, but the accuracy of the obtained PSF is limited by the system's *signal-to-noise* ratio. Furthermore, the procedure is complicated and time-consuming [270,278]. Therefore, whether to use an experimental or a theoretical PSF should be evaluated on a *case-by-case* basis [279].

1.3.6. Super-resolution microscopy

Without a sophisticated *high-end* microscopy setup, it is difficult to reach resolution below 200 nm [281,282]. This limit is several times bigger than most intracellular components (e.g. one of larger proteins: talin1 – size of about 50-60 nm [92,93]). Thus, it is impossible to approach this level of resolution even when using the best diffraction-limited microscope setups.

Super-resolution microscopy is a group of techniques allowing to image beyond the restrictions of diffraction. They are able to increase resolution even 10-fold [283]. The importance of these techniques was underlined through *the 2014 Nobel Prize in Chemistry* to Eric Betzig, Stefan W. Hell, and William E. Moerner for their contribution to the field [284].

In their works they took different approaches. Hell's method concentrated on building a microscopy system working in a confocal laser scanning mode. It employs a second, *doughnut shaped* laser beam that depletes fluorescence around the central point of the main beam, therefore, allowing registration of fluorescence from a more confined space. This method was named Stimulated Emission Depletion (STED) microscopy [284,285].

A different approach was presented by Betzig and Moerner. In traditional widefield microscopy all the fluorophore molecules are excited at the same time [286], thus their PSFs superimpose on one another. Single-molecule localization microscopy employs special photoswitchable fluorescent proteins [287] or small-molecule dyes [288]. This kind of fluorophores have, so called, *on* and *off,* or *bright* and *dark* states, when they can be excitable or irresponsive to light, respectively. The microscopy setup uses two lasers of different wavelengths to photoswitch and excite them. At the beginning of the experiment, all fluorophores are turned into the *dark* state, in the first step a small fraction is randomly switched *on* and imaged with a camera. Next, they are switched *off* or

photobleached and another batch of molecules is switched to the *bright* state and visualized in the next frame. The procedure is repeated until obtaining a satisfactory number of frames to reconstruct the image of the object [289,290]. Due to a sparse distribution of bright spots in each frame they can be considered as images of single light sources, thus, the position of each molecule can be determined and represented further as the center of a spot (with its location standard deviation as the new peak's width). Finally, all the new spots from all the frames can be rendered together to create a super-resolution image of the object [289]. This technique requires not only sophisticated microscopy setup but also image analysis and reconstruction after acquisition. The two most known single-molecule localization-based techniques are Photo-Activated Localization Microscopy (PALM) [289] and Stochastic Optical Reconstruction Microscopy (STORM) [290].

There are several other super-resolution microscopy techniques allowing to achieve different levels of resolution [291–295]. Unfortunately, their common caveats are usually relatively low frame rate, hindering live cell imaging, and high excitation intensity, resulting in excessive photobleaching and phototoxicity [296,297]. They are usually also expensive and often require a demanding sample preparation [298]. Fortunately, there are constantly new techniques and improvements under development that could reduce these negative properties [299–302]. Each super-resolution technique is characterized by different increment of resolution, frame rate, photobleaching level and other features, thus, a choice of the technique should base on an intended application [296].

1.3.7. Software-based image enhancement

There are two main branches of software-based image enhancement: deconvolution microscopy and deep learning-based methods [303]. Their main advantage is that they do not require sophisticated high-cost equipment. Nevertheless, some software may require a *high-end* computer station to improve calculation speed [279,304].

The goal of deconvolution microscopy is to reverse the process of integration of the PSF with the real image of the object (see **Section 1.3.5. Point Spread Function**) (**Fig. 15**). Image deconvolution can improve lateral and axial resolution even by 2-fold [305,306] and deblur images allowing 3D imaging for microscopy systems usually not suitable for that purpose [269]. There are several deconvolution algorithms [307–316] that employ different approaches and mathematical models, thus having different strengths and

limitations [269,317]. Most algorithms require to be provided with a PSF, but there are several *blind deconvolution* algorithms that are able to estimate it. Nonetheless, they require much more calculations than the other ones [318]. Usually the deconvolution process is carried out in the Fourier space [319].

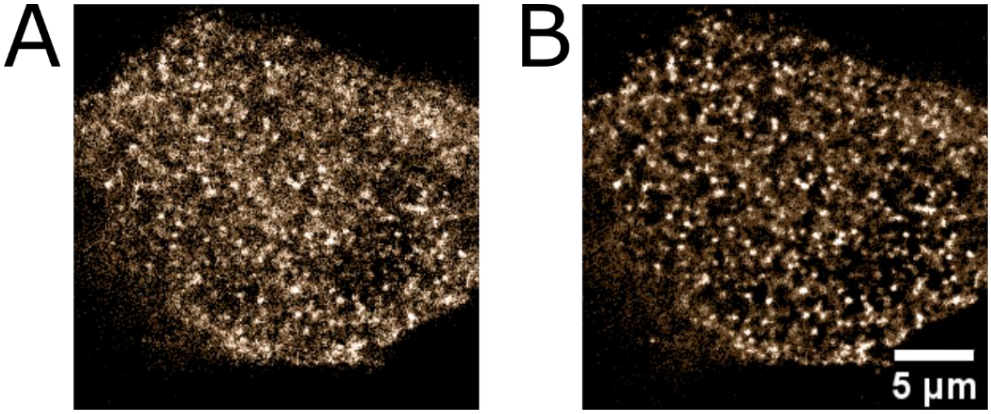

Fig. 15. An example of image deconvolution. **Panel A.** The original image of a immunofluorescence staining of proteasomes (PSMA2 marker) in MDA-MB-231 cells (for full description see [320]). The image was collected as a z-stack of 21 slices, one of the representative intermediate slices is presented. **Panel B.** The image after deconvolution with Richardson-Lucy algorithm (N = 10) [315,316] using *DeconvolutionLab2* software [317]. The brightness and contrast parameters were chosen to cover 50-99 % of the pixel brightness histogram, separately in the pre- and post-deconvolution images. Sepia LUT was applied (in *Fiji* software [280]).

Image deconvolution can be combined with most of microscopy techniques, both widefield and laser scanning [321,322]. It is often additionally included in super-resolution microscopy reconstruction algorithms [323,324]. There are several (usually expensive) programs, such as *Huygens* (Scientific Volume Imaging) or *AutoQuant X3* (Media Cybernetics), that are commercially available. On the other hand, programs like *DeconvolutionLab* and *DeconvolutionLab2* (Biomedical Imaging Group, EPFL) [317], *Iterative Deconvolve 3D* (OptiNav) [325], or *Parallel Iterative Deconvolution* (Piotr Wendykier) [326] represent freely available software, but they might be troublesome in use for an unexperienced user. Nonetheles, deconvolution microscopy presents a compelling approach to increase image resolution and *signal-to-noise* ratio, especially for groups that do not have access or can not afford expensive super-resolution systems.

Deep learning algorithms present a completely different functionality. Their goal is not to overcome the resolution limit of a microscope, but to restore low quality images to a level of high quality ones, that still, potentially, might be acquired with the same setup [303,327]. Therefore, they allow to reduce light exposure and increase imaging temporal

resolution; thus, they can increase imaging speed without a significant loss in the imaging quality [303,304,327]. They usually operate using artificial neural networks [328]. Furthermore, deep learning image restoration can be also used to aide deconvolution microscopy [304,329]. Nevertheless, this is still a new and developing approach in the image restoration field [330]. Users should be aware that there are still many caveats of the technique, such as relatively low robustness, causing creation of artifacts or not capturing small details of the specimen [328,331].

2. SCOPE OF THE STUDY

The goal of the study was to describe new aspects of the molecular mechanisms by which talins and β1 integrin mediate cancer cell adhesion and motility:

1) Characterization of the role of talin2 and talin2-β1 integrin interaction in invasion-related ECM degradation through regulation of secretion, vesicle trafficking and recycling of matrix metallopeptidase 9 in breast cancer cells.
2) Development of the molecular model of how cyanidin-3-O-glucoside influences talin1- and talin2-β1 integrin interaction, thus regulating adhesion and tumorigenesis of colon cancer cells.

3. SUMMARY OF THE RESULTS AND COMMENTS

The research presented in this thesis is divided into two main sections. The first one (**Publication I)** describes a tool that has been developed to support microscopy imaging employed in studies presented in the second part (**Publication II & Publication III**)

3.1. PUBLICATION I: *BATCHDECONVOLUTION*: A *FIJI* PLUGIN FOR INCREASING DECONVOLUTION WORKFLOW

Highlights

- There are several open access deconvolution microscopy programs.
- Most of them have a limited capability of processing multiple files in a single session.
- A *Fiji* plugin has been developed to process multi-position multi-channel time-lapse image files.
- It links functionalities of *PSF Generator* and *DeconvolutionLab2* programs from Biomedical Imaging Group at EPFL.
- The software is designed to work with most image file formats containing metadata, especially *raw* microscope images (e.g. czi, nd2, tif).

Microscopy imaging is often a tradeoff between the time of imaging, excitation light power and sample photodamage. However, even if the parameters would be chosen to collect the most qualitative image, low *signal-to-noise* ratio or high background images are still may be collected. Unfortunately, this kind of a situation often happens while trying to elucidate the finest details of the biological systems. One of the techniques attempting to challenge this problem is deconvolution microscopy.

The studies presented in the subsequent section required a vast amount of image acquisition and data analysis. In order to sharpen the collected images and facilitate the analysis, deconvolution microscopy technique was often applied. Unfortunately, most of freely available deconvolution programs do not allow multiple image processing or their capability in this area is strongly limited. Thus, they usually require a manual initiation of the process for each image. Often, they also need an additional, simple but time-consuming, preparation of input files. These processes can be easily automated, as after the initial establishment of the processing parameters, expert knowledge is not required to process subsequent files.

Publication I describes *BatchDeconvolution*, a *Fiji* plugin that has been developed to perform deconvolution on multi-position multi-channel time-lapse image files in a batch manner. It is also capable to automatically calculate a PSF if one is not provided. Thanks to an application of *Bio-Formats* library (Open Microscopy Environment) it reads most of the popular microscopy image formats in use. By linking highly rated programs for PSF calculation and image deconvolution, *PSF Generator* and *DeconvolutionLab2* (BIG, EPFL), it provides a pipeline for an automated image processing, that does not require any specialized knowledge in computer programing.

The software is open-source and available from https://github.com/Mechanobiology-Lab/BatchDeconvolution.

3.2. PUBLICATION II: TALIN2 MEDIATES SECRETION AND TRAFFICKING OF MATRIX METALLOPEPTIDASE 9 DURING INVADOPODIUM FORMATION

Highlights

- Blocking talin2 expression in breast cancer cells inhibits MMP2 and MMP9 secretion, therefore, inhibits ECM degradation.
- S339C mutation in talin2, that results in reduced affinity towards β1 integrin, also causes MMP9 secretion inhibition.
- Interaction between talin2 and β1 integrin is required for MMP9 vesicle docking.
- Inhibition of MMP9 secretion caused an accumulation of enlarged MMP9-containing vesicles in the lysosomal pathway.
- The accumulation of MMP9 suggests overflow in lysosome degradation process.

In their work, the group of prof. Cai Huang from University of Kentucky has been studying the role of talin2 in cancer development [126,138,332]. They showed the importance of this protein in ECM degradation, cancer invasion, tumorigenesis, and metastasis. Similar observations were made by other researchers [333,334].

The included publication concentrates on a molecular mechanism in which talin2 mediates invadopodia formation and matrix degradation through regulation of matrix metallopeptidase 9 (MMP9) secretion and trafficking. The study was carried out in MDA-MB-231 breast cancer cells: control and depleted of talin2.

MMP9 and talin2 colocalize at the sites of maturing invadopodia, showing that these two proteins may interact during cancer invasion. In the previous studies, knocking-out (KO) of talin2 led to inhibition of ECM degradation [126]. **Publication II** shows that the same KO cell lines have exocytosis of MMP2 and MMP9 inhibited, with their transcription levels preserved or even slightly elevated due to a possible feed-back loop.

The application of Total Internal Reflection Fluorescence (TIRF) microscopy imaging to visualize and analyze the quantity of MMP9 associated with the cell ventral membranes showed lower number of the protein in talin2-depleted cells. This suggests that the cause of the impaired secretion is connected with MMP9 vesicles docking process. A rescue experiment partially restored the levels of membrane associated MMP9. On the other

hand, an alternative rescue experiment using S339C talin2 mutant, a protein variant with a limited ability to bind β1 integrin (ITGB1), did not restore MMP9 membrane docking, showing that the interaction between talin2 and β1 integrin is specifically important for MMP9 secretion.

The analysis of MMP9 trafficking within both control and talin2-KO cells showed that talin2 depletion does not change MMP9 trafficking qualitatively; in both cases, recycled MMP9 vesicles were directed towards lysosomal degradation through early and late endosomes, and amphisomes. Nonetheless, much higher levels of the recycled MMP9 caused its accumulation in enlarged intracellular vesicles. This observation is presumed to be a result of an overflow in the protein degradation process. To support the hypothesis, lysosomal activity was inhibited with chloroquine or bafilomycin A_1 causing a similar effect in control cells.

In summary, the interaction between talin2 and β1 integrin is crucial for invadopodia maturation and extracellular matrix degradation. Talin2-ITGB1 complex regulates trafficking of MMP9 by directly providing or leading to a creation of a docking site for MMP9 vesicles, that can undergo exocytosis in the further steps of invadopodia formation. Unsecreted MMP9 is recycled towards lysosomes, which, in the case of the elevated level of the protein, may become overflowed, causing accumulation of MMP9 in enlarged intracellular vesicles.

3.3. PUBLICATION III: CYANIDIN-3-GLUCOSIDE BINDS TO TALIN AND MODULATES COLON CANCER CELL ADHESIONS AND 3D GROWTH

Highlights

- Increased expression of talin1 or β1 integrin correlates negatively with colon cancer patient survival rates.
- Depletion of talin1 inhibits growth of colon cancer mini-tumors (spheroids) in fibrin gels.
- Through binding to talin, cyanidin-3-glucoside (C3G) increases talin's affinity towards β1 integrin.
- C3G locates itself at the talin-integrin interface, influencing the complex's interaction mechanism.
- C3G stimulates adhesion of colon cancer cells plated on a fibronectin substrate but does not influence proliferation.
- C3G inhibits growth of colorectal cancer mini-tumors in fibrin gels.

Colon cancer is the fourth most common cancer type [8]. **Publication III** shows that elevated levels of either talin1 or β1 integrin result in a poor survival prognosis for patients suffering from this disease. Furthermore, the included *in vitro* studies on HT-29 and HCT116 colon cancer cell lines demonstrated that silencing talin1 leads to inhibition of spheroids growth.

Many natural products are likely to have anticancerogenic properties. In the presented study, natural products were analyzed for potential ability to influence talin-β1 integrin interaction and mediate colon cancer development. Cyanidin-3-O-glucoside (C3G), a natural dye found in many red-blue fruits and vegetables, showed to be the only pure compound tested, that influenced (increased) talin2-ITGB1 affinity, potentially stabilizing integrin in its active state. Further, it was shown that there is a similar phenomenon in the case of talin1-ITGB1 interaction.

A molecular docking experiment elucidated that C3G binds at the talin2-ITGB1 interface between their F3 domain and the cytoplasmic tail, respectively. The follow-up experiments using talin1 head domain mutants supported the bioinformatical model, indicating a similar binding molecular mechanism in the case of both talins.

Next, the influence of C3G on cancer cells was examined *in vitro*. The compound stimulated adhesion in colon cancer cells plated on fibronectin-coated substrates. Surprisingly, it had an opposite effect on breast cancer cells, suggesting a complex mechanism of C3G-mediation of integrin-based adhesion. Although the compound showed no or minimal influence on breast and colon cancer cell proliferation, it strongly inhibited mini-tumor (spheroid) creation in fibrin gels in a concentration dependent manner.

As the result of the study, a model of C3G-mediated tumor growth was proposed: cyanidino-3-O-glucoside locates at the interface between talin and integrin allosterically regulating integrin activation. The exact mechanism is yet to be determined, but it is presumed that enhanced talin-ITGB1 binding results in longer lifetime of the integrin active state. The increased cellular adhesion constrains cell positioning required for tumor growth, leading to an inhibition of the development of colon cancer.

4. FINAL REMARKS

The presented thesis concentrates on biophysical models describing cellular processes in cancer development at the molecular level. To reach the necessary imaging quality and resolution it was needed to apply deconvolution microscopy. To achieve a reasonable workflow efficiency, a software, *BatchDeconvolution Fiji* plugin, was developed, which allowed to almost fully automate the image enhancement process (**Publication I**). The further development in this area, that should be beneficial for the image enhancement, might be an application of deep learning networks. Many of the experiments were based on transient transfections with fusion proteins of a fluorescent protein and a protein in consideration. Depending on a cell line, it is often challenging to reach a satisfactory level of transfection. Thus, it is common either to get only a few cells transfected or to have a very week fluorescent signal. By applying deep learning algorithms, it should be possible to receive more data from fewer experiments, increasing overall workflow and reducing the cost of the experimental part of future studies [327,335]. This possibly might be improved by using cells that are easier to transfect to create the training image database.

The second section of this thesis describes interaction between talin and β1 integrin. Although it was shown that talin1 and talin2 play distinct roles in tumor invasion (**Publication II)**, however, in opposite to talin1 [61], the molecular model for the talin2 interactome during invadopodium formation has not been proposed yet. Furthermore, talin2-ITGB1 partners and the exact model for the MMPs-containing vesicles docking process is still to be elucidated.

Finally, the role of C3G in mediation of cancer motility and adhesion is not clear yet (**Publication III)**. Especially intriguing aspect is the varying effect of the compound on different types of cancer; for example: C3G induces colon cancer adhesion but inhibits it in breast cancer cells. Furthermore, the influence of C3G on talin-β1 integrin complex structure is unknown, as the presented data was from a molecular docking experiment without further energy minimalization. As mentioned earlier, a single mutation in both talins F3 domain drastically changes affinity and geometry of β1 integrin binding, and possibly ability of integrins activation by talin [126,127]. As C3G locates at the interface between the two proteins, its presence may inhibit the activation of integrin by increasing activation energy level required for the conformation transition, but at the same time stabilizes the activated talin-integrin complex. Based on American Type Culture

Collection (ATCC), colon cancer cells usually show lower spreading (thus also the ECM adhesion level) than breast cancer cells. Therefore, this might be the reason for the different responses of these cell types to C3G, as their motility might be driven by differently regulated molecular pathways. Alternatively, C3G may also affect other pathways, thus the observed phenomena might be a result of a cell-wide signaling, not restricted only to the adhesion interactome. Moreover, regardless of the influence of C3G on cancer progression, the knowledge of its impact on the talin-integrin complex, especially in the case of the complex's structure geometry shift, will shed more light on the molecular mechanisms of interaction between the two different talin variants and integrin.

5. REFERENCES

1. National Cancer Institute (NIH). What Is Cancer? *Underst. Cancer* at https://www.cancer.gov/about-cancer/understanding/what-is-cancer.
2. World Health Organisation. Cancer. at https://www.who.int/en/news-room/fact-sheets/detail/cancer.
3. Loeb, K. R. & Loeb, L. A. Significance of multiple mutations in cancer. *Carcinogenesis* **21(3),** 379–385 (2000). https://doi.org/10.1093/carcin/21.3.379.
4. National Cancer Institute (NIH). Cancer Classification. *SEER Train.* at https://training.seer.cancer.gov/disease/categories/classification.html.
5. World Health Organization. *International classification of diseases for oncology (ICD-O)*. (World Health Organization, 2013). at www.who.int.
6. National Cancer Institute (NIH). Types of Cancer Treatment. *Cancer Treat.* at https://www.cancer.gov/about-cancer/treatment/types.
7. Wild, C. P., Weiderpass, E. & Stewart, B. W. *World Cancer Report. Cancer research for cancer prevention* . (International Agency for Research on Cancer, World Health Organisation, 2020).
8. Bray, F., Ferlay, J., Soerjomataram, I., Siegel, R. L., Torre, L. A. & Jemal, A. Global cancer statistics 2018: GLOBOCAN estimates of incidence and mortality worldwide for 36 cancers in 185 countries. *CA. Cancer J. Clin.* **68(6),** 394–424 (2018). https://doi.org/10.3322/caac.21492.
9. Rahman, M. S., Suresh, S. & Waly, M. I. Risk Factors for Cancer: Genetic and Environment. in *Bioact. Components, Diet Med. Treat. Cancer Prev.* 1–23 (Springer International Publishing, 2018). https://doi.org/10.1007/978-3-319-75693-6_1.
10. Peng, L., Xu, T., Long, T. & Zuo, H. Association Between BRCA Status and P53 Status in Breast Cancer: A Meta-Analysis. *Med. Sci. Monit.* 22**,** 1939–1945 (2016). https://doi.org/10.12659/MSM.896260.
11. Dela Cruz, C. S., Tanoue, L. T. & Matthay, R. A. Lung Cancer: Epidemiology, Etiology, and Prevention. (2011). https://doi.org/10.1016/j.ccm.2011.09.001.
12. LoConte, N. K., Brewster, A. M., Kaur, J. S., Merrill, J. K. & Alberg, A. J. Alcohol and Cancer: A Statement of the American Society of Clinical Oncology. *J. Clin. Oncol.* **36(1),** 83–93 (2018). https://doi.org/10.1200/JCO.2017.76.1155.
13. World Cancer Research Fund & American Institute for Cancer Research. Alcoholic drinks and the risk of cancer. in *Diet, Nutr. Phys. Act. Cancer a Glob. Perspect.* (2018). at https://www.wcrf.org/dietandcancer.
14. Vogeltanz-Holm, N. & Schwartz, G. G. Radon and lung cancer: What does the public really know? *J. Environ. Radioact.* 192**,** 26–31 (2018). https://doi.org/10.1016/j.jenvrad.2018.05.017.
15. Kim, C., Gao, Y. T., Xiang, Y. B., Barone-Adesi, F., Zhang, Y., Hosgood, H. D., Ma, S., Shu, X. O., Ji, B. T., Chow, W. H., Seow, W. J., Bassig, B., Cai, Q., Zheng, W., Rothman, N. & Lan, Q. Home kitchen ventilation, cooking fuels, and lung cancer risk in a prospective cohort of never smoking women in Shanghai, China. *Int. J. Cancer* **136(3),** 632–638 (2015). https://doi.org/10.1002/ijc.29020.
16. Boffetta, P. & Nyberg, F. Contribution of environmental factors to cancer risk. *Br. Med. Bull.* **68(1),** 71–94 (2003). https://doi.org/10.1093/bmp/ldg023.
17. Khatri, N. & Tyagi, S. Influences of natural and anthropogenic factors on surface and groundwater quality in rural and urban areas. *Front. Life Sci.* **8(1),** 23–39 (2015). https://doi.org/10.1080/21553769.2014.933716.
18. Jhappan, C., Noonan, F. P. & Merlino, G. Ultraviolet radiation and cutaneous malignant melanoma. *Oncogene* **22(20),** 3099–3112 (2003). https://doi.org/10.1038/sj.onc.1206450.
19. Richman, E. L., Kenfield, S. A., Chavarro, J. E., Stampfer, M. J., Giovannucci, E. L., Willett, W. C. & Chan, J. M. Fat Intake After Diagnosis and Risk of Lethal Prostate Cancer and All-Cause Mortality. *JAMA Intern. Med.* **173(14),** 1318 (2013). https://doi.org/10.1001/jamainternmed.2013.6536.
20. Steck, S. E. & Murphy, E. A. Dietary patterns and cancer risk. *Nat. Rev. Cancer* **20(2),** 125–138 (2020). https://doi.org/10.1038/s41568-019-0227-4.
21. McCullough, M. L., Zoltick, E. S., Weinstein, S. J., Fedirko, V., Wang, M., Cook, N. R., Eliassen, A. H., Zeleniuch-Jacquotte, A., Agnoli, C., Albanes, D., Barnett, M. J., Buring, J. E., Campbell, P. T., Clendenen, T. V., Freedman, N. D., Gapstur, S. M., Giovannucci, E. L., Goodman, G. G., Haiman, C.

A., Ho, G. Y. F., Horst, R. L., Hou, T., Huang, W.-Y., Jenab, M., Jones, M. E., Joshu, C. E., Krogh, V., Lee, I.-M., Lee, J. E., Männistö, S., Le Marchand, L., Mondul, A. M., Neuhouser, M. L., Platz, E. A., Purdue, M. P., Riboli, E., Robsahm, T. E., Rohan, T. E., Sasazuki, S., Schoemaker, M. J., Sieri, S., Stampfer, M. J., Swerdlow, A. J., Thomson, C. A., Tretli, S., Tsugane, S., Ursin, G., Visvanathan, K., White, K. K., Wu, K., Yaun, S.-S., Zhang, X., Willett, W. C., Gail, M. H., Ziegler, R. G. & Smith-Warner, S. A. Circulating Vitamin D and Colorectal Cancer Risk: An International Pooling Project of 17 Cohorts. *JNCI J. Natl. Cancer Inst.* **111(2),** 158–169 (2019). https://doi.org/10.1093/jnci/djy087.

22. Liu, M., Du, Y., Li, H., Wang, L., Ponikwicka-Tyszko, D., Lebiedzinska, W., Pilaszewicz-Puza, A., Liu, H., Zhou, L., Fan, H., Wang, M., You, H., Wolczynnski, S., Rahman, N., Guo, Y.-D. & Li, X. Cyanidin-3-o-Glucoside Pharmacologically Inhibits Tumorigenesis via Estrogen Receptor β in Melanoma Mice. *Front. Oncol.* **9(OCT),** 1110 (2019). https://doi.org/10.3389/fonc.2019.01110.
23. Mazewski, C., Kim, M. S. & Gonzalez de Mejia, E. Anthocyanins, delphinidin-3-O-glucoside and cyanidin-3-O-glucoside, inhibit immune checkpoints in human colorectal cancer cells in vitro and in silico. *Sci. Rep.* **9(1),** 11560 (2019). https://doi.org/10.1038/s41598-019-47903-0.
24. de Boer, M. C., Wörner, E. A., Verlaan, D. & van Leeuwen, P. A. M. The Mechanisms and Effects of Physical Activity on Breast Cancer. *Clin. Breast Cancer* **17(4),** 272–278 (2017). https://doi.org/10.1016/j.clbc.2017.01.006.
25. Hanahan, D. & Weinberg, R. A. The hallmarks of cancer. *Cell* **100(1),** 57–70 (2000). https://doi.org/10.1016/S0092-8674(00)81683-9.
26. Zhong, Z., Yu, J., Virshup, D. M. & Madan, B. Wnts and the hallmarks of cancer. *Cancer Metastasis Rev.* (2020). https://doi.org/10.1007/s10555-020-09887-6.
27. Al-Bedeary, S., Getta, H. & Al-Sharafi, D. The hallmarks of cancer and their therapeutic targeting in current use and clinical trials. *Iraqi J. Hematol.* **9(1),** 1 (2020). https://doi.org/10.4103/ijh.ijh_24_19.
28. Fouad, Y. A. & Aanei, C. Revisiting the hallmarks of cancer. *Am. J. Cancer Res.* **7(5),** 1016–1036 (2017). https://pubmed.ncbi.nlm.nih.gov/28560055.
29. Gutschner, T. & Diederichs, S. The hallmarks of cancer. *RNA Biol.* **9(6),** 703–719 (2012). https://doi.org/10.4161/rna.20481.
30. Hanahan, D. & Weinberg, R. A. Hallmarks of cancer: The next generation. *Cell* **144(5),** 646–674 (2011). https://doi.org/10.1016/j.cell.2011.02.013.
31. Stratton, M. R., Campbell, P. J. & Futreal, P. A. The cancer genome. *Nature* **458(7239),** 719–24 (2009). https://doi.org/10.1038/nature07943.
32. Negrini, S., Gorgoulis, V. G. & Halazonetis, T. D. Genomic instability — an evolving hallmark of cancer. *Nat. Rev. Mol. Cell Biol.* **11(3),** 220–228 (2010). https://doi.org/10.1038/nrm2858.
33. Hanahan D & Weinberg RA. Next-generation Hallmarks of Cancer wheel with labels. *Wikipedia* (2011). at https://en.wikipedia.org/wiki/File:Next-generation_Hallmarks_of_Cancer_wheel_with_labels.svg.
34. Amin, A. R. M. R., Karpowicz, P. A., Carey, T. E., Arbiser, J., Nahta, R., Chen, Z. G., Dong, J.-T., Kucuk, O., Khan, G. N., Huang, G. S., Mi, S., Lee, H.-Y., Reichrath, J., Honoki, K., Georgakilas, A. G., Amedei, A., Amin, A., Helferich, B., Boosani, C. S., Ciriolo, M. R., Chen, S., Mohammed, S. I., Azmi, A. S., Keith, W. N., Bhakta, D., Halicka, D., Niccolai, E., Fujii, H., Aquilano, K., Ashraf, S. S., Nowsheen, S., Yang, X., Bilsland, A. & Shin, D. M. Evasion of anti-growth signaling: A key step in tumorigenesis and potential target for treatment and prophylaxis by natural compounds. *Semin. Cancer Biol.* 35**,** S55–S77 (2015). https://doi.org/10.1016/j.semcancer.2015.02.005.
35. Igney, F. H. & Krammer, P. H. Death and anti-death: tumour resistance to apoptosis. *Nat. Rev. Cancer* **2(4),** 277–288 (2002). https://doi.org/10.1038/nrc776.
36. Feitelson, M. A., Arzumanyan, A., Kulathinal, R. J., Blain, S. W., Holcombe, R. F., Mahajna, J., Marino, M., Martinez-Chantar, M. L., Nawroth, R., Sanchez-Garcia, I., Sharma, D., Saxena, N. K., Singh, N., Vlachostergios, P. J., Guo, S., Honoki, K., Fujii, H., Georgakilas, A. G., Bilsland, A., Amedei, A., Niccolai, E., Amin, A., Ashraf, S. S., Boosani, C. S., Guha, G., Ciriolo, M. R., Aquilano, K., Chen, S., Mohammed, S. I., Azmi, A. S., Bhakta, D., Halicka, D., Keith, W. N. & Nowsheen, S. Sustained proliferation in cancer: Mechanisms and novel therapeutic targets. *Semin. Cancer Biol.* 35**,** S25–S54 (2015). https://doi.org/10.1016/j.semcancer.2015.02.006.
37. Vander Heiden, M. G., Cantley, L. C. & Thompson, C. B. Understanding the Warburg Effect: The Metabolic Requirements of Cell Proliferation. *Science (80-.).* **324(5930),** 1029–1033 (2009). https://doi.org/10.1126/science.1160809.

38. Liberti, M. V. & Locasale, J. W. The Warburg Effect: How Does it Benefit Cancer Cells? *Trends Biochem. Sci.* **41(3),** 211–218 (2016). https://doi.org/10.1016/j.tibs.2015.12.001.
39. Yang, L., Pang, Y. & Moses, H. L. TGF-β and immune cells: an important regulatory axis in the tumor microenvironment and progression. *Trends Immunol.* **31(6),** 220–227 (2010). https://doi.org/10.1016/j.it.2010.04.002.
40. Qian, B.-Z. & Pollard, J. W. Macrophage Diversity Enhances Tumor Progression and Metastasis. *Cell* **141(1),** 39–51 (2010). https://doi.org/10.1016/j.cell.2010.03.014.
41. Deryugina, E. I. & Quigley, J. P. Tumor angiogenesis: MMP-mediated induction of intravasation- and metastasis-sustaining neovasculature. *Matrix Biol.* 44–46**,** 94–112 (2015). https://doi.org/10.1016/j.matbio.2015.04.004.
42. Nishida, N., Yano, H., Nishida, T., Kamura, T. & Kojiro, M. Angiogenesis in cancer. *Vasc. Health Risk Manag.* **2(3),** 213–219 (2006). https://doi.org/10.2147/vhrm.2006.2.3.213.
43. Chiang, S. P. H., Cabrera, R. M. & Segall, J. E. Tumor cell intravasation. *Am. J. Physiol. Physiol.* **311(1),** C1–C14 (2016). https://doi.org/10.1152/ajpcell.00238.2015.
44. Gupta, G. P., Minn, A. J., Kang, Y., Siegel, P. M., Serganova, I., Cordón-Cardo, C., Olshen, A. B., Gerald, W. L. & Massagué, J. Identifying site-specific metastasis genes and functions. in *Cold Spring Harb. Symp. Quant. Biol.* 70**,** 149–158 (Cold Spring Harbor Laboratory Press, 2005). https://doi.org/10.1101/sqb.2005.70.018.
45. Fares, J., Fares, M. Y., Khachfe, H. H., Salhab, H. A. & Fares, Y. Molecular principles of metastasis: a hallmark of cancer revisited. *Signal Transduct. Target. Ther.* **5(1),** 28 (2020). https://doi.org/10.1038/s41392-020-0134-x.
46. Iversen, O. H. Studies of the carcinogenesis and tumorigenesis of skin applications of dodecylbenzene on hairless mice. *Occup. Environ. Med.* **46(9),** 608–616 (1989). https://doi.org/10.1136/oem.46.9.608.
47. National Cancer Institute (NIH). Definition of carcinogenesis. *NCI Dict. Cancer Terms* at https://www.cancer.gov/publications/dictionaries/cancer-terms/def/carcinogenesis.
48. Ashkenazi, R., Gentry, S. N. & Jackson, T. L. Pathways to Tumorigenesis—Modeling Mutation Acquisition in Stem Cells and Their Progeny. *Neoplasia* **10(11),** 1170-IN6 (2008). https://doi.org/10.1593/neo.08572.
49. Yokota, J. Tumor progression and metastasis. *Carcinogenesis* **21(3),** 497–503 (2000). https://doi.org/10.1093/carcin/21.3.497.
50. Zefferino, Piccoli, Gioia, Capitanio & Conese. Gap Junction Intercellular Communication in the Carcinogenesis Hallmarks: Is This a Phenomenon or Epiphenomenon? *Cells* **8(8),** 896 (2019). https://doi.org/10.3390/cells8080896.
51. Li, X., He, S. & Ma, B. Autophagy and autophagy-related proteins in cancer. *Mol. Cancer* **19(1),** 12 (2020). https://doi.org/10.1186/s12943-020-1138-4.
52. Porcheri, C., Meisel, C. T. & Mitsiadis, T. Multifactorial Contribution of Notch Signaling in Head and Neck Squamous Cell Carcinoma. *Int. J. Mol. Sci.* **20(6),** 1520 (2019). https://doi.org/10.3390/ijms20061520.
53. Patel, K., Kademani, D. & Bagheri, S. C. Head and Neck Pathology. in *Clin. Rev. Oral Maxillofac. Surg.* 187–222 (Elsevier, 2014). https://doi.org/10.1016/B978-0-323-17126-7.00007-8.
54. Saxena, M. & Christofori, G. Rebuilding cancer metastasis in the mouse. *Mol. Oncol.* **7(2),** 283–296 (2013). https://doi.org/10.1016/j.molonc.2013.02.009.
55. van Zijl, F., Krupitza, G. & Mikulits, W. Initial steps of metastasis: Cell invasion and endothelial transmigration. *Mutat. Res. Mutat. Res.* **728(1–2),** 23–34 (2011). https://doi.org/10.1016/j.mrrev.2011.05.002.
56. Paget, S. The distribution of secondary growths in cancer of the breast. *Lancet* **133(3421),** 571–573 (1889). https://doi.org/10.1016/S0140-6736(00)49915-0.
57. Liotta, L. A. Adhere, Degrade, and Move: The Three-Step Model of Invasion. *Cancer Res.* **76(11),** 3115–3117 (2016). https://doi.org/10.1158/0008-5472.CAN-16-1297.
58. Liotta, L. A. Tumor invasion and metastases--role of the extracellular matrix: Rhoads Memorial Award lecture. *Cancer Res.* **46(1),** 1–7 (1986). https://pubmed.ncbi.nlm.nih.gov/2998604.
59. Andasari, V. & Chaplain, M. A. J. Intracellular Modelling of Cell-Matrix Adhesion during Cancer Cell Invasion. *Math. Model. Nat. Phenom.* **7(1),** 29–48 (2012). https://doi.org/10.1051/mmnp/20127103.

60. Beaty, B. T. & Condeelis, J. Digging a little deeper: The stages of invadopodium formation and maturation. *Eur. J. Cell Biol.* **93(10–12),** 438–444 (2014). https://doi.org/10.1016/j.ejcb.2014.07.003.
61. Beaty, B. T., Wang, Y., Bravo-Cordero, J. J., Sharma, V. P., Miskolci, V., Hodgson, L. & Condeelis, J. Talin regulates moesin–NHE-1 recruitment to invadopodia and promotes mammary tumor metastasis. *J. Cell Biol.* **205(5),** 737–751 (2014). https://doi.org/10.1083/jcb.201312046.
62. Murphy, D. A. & Courtneidge, S. A. The 'ins' and 'outs' of podosomes and invadopodia: characteristics, formation and function. *Nat. Rev. Mol. Cell Biol.* **12(7),** 413–426 (2011). https://doi.org/10.1038/nrm3141.
63. Paterson, E. K. & Courtneidge, S. A. Invadosomes are coming: new insights into function and disease relevance. *FEBS J.* **285(1),** 8–27 (2018). https://doi.org/10.1111/febs.14123.
64. Sharma, V. P., Eddy, R., Entenberg, D., Kai, M., Gertler, F. B. & Condeelis, J. Tks5 and SHIP2 regulate invadopodium maturation, but not initiation, in breast carcinoma cells. *Curr. Biol.* **23(21),** 2079–2089 (2013). https://doi.org/10.1016/j.cub.2013.08.044.
65. Eddy, R. J., Weidmann, M. D., Sharma, V. P. & Condeelis, J. S. Tumor Cell Invadopodia: Invasive Protrusions that Orchestrate Metastasis. *Trends Cell Biol.* **27(8),** 595–607 (2017). https://doi.org/10.1016/j.tcb.2017.03.003.
66. Beaty, B. T., Sharma, V. P., Bravo-Cordero, J. J., Simpson, M. A., Eddy, R. J., Koleske, A. J. & Condeelis, J. β1 integrin regulates Arg to promote invadopodial maturation and matrix degradation. *Mol. Biol. Cell* **24(11),** 1661–1675 (2013). https://doi.org/10.1091/mbc.E12-12-0908.
67. Bravo-Cordero, J. J., Magalhaes, M. A. O., Eddy, R. J., Hodgson, L. & Condeelis, J. Functions of cofilin in cell locomotion and invasion. *Nat. Rev. Mol. Cell Biol.* **14(7),** 405–417 (2013). https://doi.org/10.1038/nrm3609.
68. Jacob, A. & Prekeris, R. The regulation of MMP targeting to invadopodia during cancer metastasis. *Front. cell Dev. Biol.* 3**,** 4 (2015). https://doi.org/10.3389/fcell.2015.00004.
69. Schoumacher, M., Goldman, R. D., Louvard, D. & Vignjevic, D. M. Actin, microtubules, and vimentin intermediate filaments cooperate for elongation of invadopodia. *J. Cell Biol.* **189(3),** 541–556 (2010). https://doi.org/10.1083/jcb.200909113.
70. Liang, C. C., Park, A. Y. & Guan, J. L. In vitro scratch assay: A convenient and inexpensive method for analysis of cell migration in vitro. *Nat. Protoc.* **2(2),** 329–333 (2007). https://doi.org/10.1038/nprot.2007.30.
71. Xiao, Y., Riahi, R., Torab, P., Zhang, D. D. & Wong, P. K. Collective Cell Migration in 3D Epithelial Wound Healing. *ACS Nano* (2019). https://doi.org/10.1021/acsnano.8b06305.
72. Hons, M., Kopf, A., Hauschild, R., Leithner, A., Gaertner, F., Abe, J., Renkawitz, J., Stein, J. V. & Sixt, M. Chemokines and integrins independently tune actin flow and substrate friction during intranodal migration of T cells. *Nat. Immunol.* **19(6),** 606–616 (2018). https://doi.org/10.1038/s41590-018-0109-z.
73. Scarpa, E. & Mayor, R. Collective cell migration in development. *J. Cell Biol.* **212(2),** 143–155 (2016). https://doi.org/10.1083/jcb.201508047.
74. Reig, G., Pulgar, E. & Concha, M. L. Cell migration: From tissue culture to embryos. *Dev.* **141(10),** 1999–2013 (2014). https://doi.org/10.1242/dev.101451.
75. Devreotes, P. & Horwitz, A. R. Signaling Networks that Regulate Cell Migration. *Cold Spring Harb. Perspect. Biol.* **7(8),** a005959 (2015). https://doi.org/10.1101/cshperspect.a005959.
76. Liu, Y. J., Le Berre, M., Lautenschlaeger, F., Maiuri, P., Callan-Jones, A., Heuzé, M., Takaki, T., Voituriez, R. & Piel, M. Confinement and low adhesion induce fast amoeboid migration of slow mesenchymal cells. *Cell* **160(4),** 659–672 (2015). https://doi.org/10.1016/j.cell.2015.01.007.
77. Paňková, K., Rösel, D., Novotný, M. & Brábek, J. The molecular mechanisms of transition between mesenchymal and amoeboid invasiveness in tumor cells. *Cell. Mol. Life Sci.* **67(1),** 63–71 (2010). https://doi.org/10.1007/s00018-009-0132-1.
78. Clark, A. G. & Vignjevic, D. M. Modes of cancer cell invasion and the role of the microenvironment. *Curr. Opin. Cell Biol.* 36**,** 13–22 (2015). https://doi.org/10.1016/j.ceb.2015.06.004.
79. Collins, K. L., Gates, E. M., Gilchrist, C. L. & Hoffman, B. D. Bio-Instructive Cues in Scaffolds for Musculoskeletal Tissue Engineering and Regenerative Medicine. in *Bio-Instructive Scaffolds Musculoskelet. Tissue Eng. Regen. Med.* 3–35 (Elsevier Inc., 2017). https://doi.org/10.1016/B978-0-12-803394-4.00001-X.

80. Trepat, X., Chen, Z. & Jacobson, K. Cell migration. *Compr. Physiol.* **2(4),** 2369–2392 (2012). https://doi.org/10.1002/cphy.c110012.

81. Yin, M., Ma, W. & An, L. Cortactin in cancer cell migration and invasion. *Oncotarget* **8(50),** 88232–88243 (2017). https://doi.org/10.18632/oncotarget.21088.

82. Nammalwar, R. C., Heil, A. & Gerke, V. Ezrin interacts with the scaffold protein IQGAP1 and affects its cortical localization. *Biochim. Biophys. Acta - Mol. Cell Res.* **1853(9),** 2086–2094 (2014). https://doi.org/10.1016/j.bbamcr.2014.12.026.

83. Etienne-Manneville, S. Actin and Microtubules in Cell Motility: Which One is in Control? *Traffic* **5(7),** 470–477 (2004). https://doi.org/10.1111/j.1600-0854.2004.00196.x.

84. Moshfegh, Y., Bravo-Cordero, J. J., Miskolci, V., Condeelis, J. & Hodgson, L. A Trio-Rac1-Pak1 signalling axis drives invadopodia disassembly. *Nat. Cell Biol.* **16(6),** 574–86 (2014). https://doi.org/10.1038/ncb2972.

85. Machacek, M., Hodgson, L., Welch, C., Elliott, H., Pertz, O., Nalbant, P., Abell, A., Johnson, G. L., Hahn, K. M. & Danuser, G. Coordination of Rho GTPase activities during cell protrusion. *Nature* **461(7260),** 99–103 (2009). https://doi.org/10.1038/nature08242.

86. Kechagia, J. Z., Ivaska, J. & Roca-Cusachs, P. *Integrins as biomechanical sensors of the microenvironment*. *Nat. Rev. Mol. Cell Biol.* **20(8),** 457–473 (Nature Publishing Group, 2019). https://doi.org/10.1038/s41580-019-0134-2.

87. Gough, R. E. & Goult, B. T. The tale of two talins - two isoforms to fine-tune integrin signalling. *FEBS Lett.* **592(12),** 2108–2125 (2018). https://doi.org/10.1002/1873-3468.13081.

88. Klapholz, B. & Brown, N. H. Talin – the master of integrin adhesions. *J. Cell Sci.* **130(15),** 2435–2446 (2017). https://doi.org/10.1242/jcs.190991.

89. Tschumperlin, D. J. Fibroblasts and the Ground They Walk On. *Physiology* **28(6),** 380–390 (2013). https://doi.org/10.1152/physiol.00024.2013.

90. Ladoux, B. & Nicolas, A. Physically based principles of cell adhesion mechanosensitivity in tissues. *Reports Prog. Phys.* **75(11),** (2012). https://doi.org/10.1088/0034-4885/75/11/116601.

91. Monkley, S. J., Pritchard, C. A. & Critchley, D. R. Analysis of the mammalian talin2 gene TLN2. *Biochem. Biophys. Res. Commun.* **286(5),** 880–885 (2001). https://doi.org/10.1006/bbrc.2001.5497.

92. Molony, L., McCaslin, D., Abernethy, J., Paschal, B. & Burridge, K. Properties of talin from chicken gizzard smooth muscle. *J. Biol. Chem.* **262(16),** 7790–5 (1987). https://pubmed.ncbi.nlm.nih.gov/3108258.

93. Goldmann, W. H., Bremer, A., Häner, M., Aebi, U. & Isenberg, G. Native Talin Is a Dumbbell-Shaped Homodimer When It Interacts with Actin. *J. Struct. Biol.* **112(1),** 3–10 (1994). https://doi.org/10.1006/jsbi.1994.1002.

94. Burridge, K. & Connell, L. A new protein of adhesion plaques and ruffling membranes. *J. Cell Biol.* **97(2),** 359–67 (1983). https://pubmed.ncbi.nlm.nih.gov/6684120.

95. Horwitz, A., Duggan, K., Buck, C., Beckerle, M. C. & Burridge, K. Interaction of plasma membrane fibronectin receptor with talin—a transmembrane linkage. *Nature* **320(6062),** 531–533 (1986). https://doi.org/10.1038/320531a0.

96. Muguruma, M., Matsumura, S. & Fukazawa, T. Direct interactions between talin and actin. *Biochem. Biophys. Res. Commun.* **171(3),** 1217–1223 (1990). https://doi.org/10.1016/0006-291X(90)90815-5.

97. Hemmings, L., Rees, D. J., Ohanian, V., Bolton, S. J., Gilmore, A. P., Patel, B., Priddle, H., Trevithick, J. E., Hynes, R. O. & Critchley, D. R. Talin contains three actin-binding sites each of which is adjacent to a vinculin-binding site. *J. Cell Sci.* 109 (Pt 1**,** 2715–26 (1996). https://pubmed.ncbi.nlm.nih.gov/8937989.

98. Gilmore, A., Wood, C., Ohanian, V., Jackson, P., Patel, B., Rees, D., Hynes, R. & Critchley, D. The cytoskeletal protein talin contains at least two distinct vinculin binding domains. *J. Cell Biol.* **122(2),** 337–347 (1993). https://doi.org/10.1083/jcb.122.2.337.

99. Lee, S. W., Wulfkuhle, J. D. & Otto, J. J. Vinculin binding site mapped on talin with an anti-idiotypic antibody. *J. Biol. Chem.* **267(23),** 16355–8 (1992). https://pubmed.ncbi.nlm.nih.gov/1379597.

100. Burridge, K. & Mangeat, P. An interaction between vinculin and talin. *Nature* **308(5961),** 744–746 (1984). https://doi.org/10.1038/308744a0.

101. Gingras, A. R., Ziegler, W. H., Frank, R., Barsukov, I. L., Roberts, G. C. K., Critchley, D. R. & Emsley, J. Mapping and Consensus Sequence Identification for Multiple Vinculin Binding Sites

within the Talin Rod. *J. Biol. Chem.* **280(44),** 37217–37224 (2005). https://doi.org/10.1074/jbc.M508060200.

102. Chen, H. C., Appeddu, P. A., Parsons, J. T., Hildebrand, J. D., Schaller, M. D. & Guan, J. L. Interaction of focal adhesion kinase with cytoskeletal protein talin. *J. Biol. Chem.* **270(28),** 16995–16999 (1995). https://doi.org/10.1074/jbc.270.28.16995.
103. Borowsky, M. L. & Hynes, R. O. Layilin, a novel talin-binding transmembrane protein homologous with C- type lectins, is localized in membrane ruffles. *J. Cell Biol.* **143(2),** 429–442 (1998). https://doi.org/10.1083/jcb.143.2.429.
104. Zacharchenko, T., Qian, X., Goult, B. T., Jethwa, D., Almeida, T. B., Ballestrem, C., Critchley, D. R., Lowy, D. R. & Barsukov, I. L. LD Motif Recognition by Talin: Structure of the Talin-DLC1 Complex. *Structure* **24(7),** 1130–1141 (2016). https://doi.org/10.1016/j.str.2016.04.016.
105. Chishti, A. H., Kim, A. C., Marfatia, S. M., Lutchman, M., Hanspal, M., Jindal, H., Liu, S.-C., Low, P. S., Rouleau, G. A., Mohandas, N., Chasis, J. A., Conboy, J. G., Gascard, P., Takakuwa, Y., Huang, S.-C., Benz Jr, E. J., Bretscher, A., Fehon, R. G., Gusella, J. F., Ramesh, V., Solomon, F., Marchesi, V. T., Tsukita, S., Tsukita, S., Arpin, M., Louvard, D., Tonks, N. K., Anderson, J. M., Fanning, A. S., Bryant, P. J., Woods, D. F. & Hoover, K. B. The FERM domain: a unique module involved in the linkage of cytoplasmic proteins to the membrane. *Trends Biochem. Sci.* **23(8),** 281–282 (1998). https://doi.org/10.1016/S0968-0004(98)01237-7.
106. Goult, B. T., Bouaouina, M., Elliott, P. R., Bate, N., Patel, B., Gingras, A. R., Grossmann, J. G., Roberts, G. C. K., Calderwood, D. A., Critchley, D. R. & Barsukov, I. L. Structure of a double ubiquitin-like domain in the talin head: a role in integrin activation. *EMBO J.* **29(6),** 1069–1080 (2010). https://doi.org/10.1038/emboj.2010.4.
107. Goult, B. T., Zacharchenko, T., Bate, N., Tsang, R., Hey, F., Gingras, A. R., Elliott, P. R., Roberts, G. C. K., Ballestrem, C., Critchley, D. R. & Barsukov, I. L. RIAM and vinculin binding to talin are mutually exclusive and regulate adhesion assembly and turnover. *J. Biol. Chem.* **288(12),** 8238–8249 (2013). https://doi.org/10.1074/jbc.M112.438119.
108. Bate, N., Gingras, A. R., Bachir, A., Horwitz, R., Ye, F., Patel, B., Goult, B. T. & Critchley, D. R. Talin Contains A C-Terminal Calpain2 Cleavage Site Important In Focal Adhesion Dynamics. *PLoS One* **7(4),** e34461 (2012). https://doi.org/10.1371/journal.pone.0034461.
109. Goult, B. T., Bouaouina, M., Harburger, D. S., Bate, N., Patel, B., Anthis, N. J., Campbell, I. D., Calderwood, D. A., Barsukov, I. L., Roberts, G. C. & Critchley, D. R. The Structure of the N-Terminus of Kindlin-1: A Domain Important for αIIbβ3 Integrin Activation. *J. Mol. Biol.* **394(5),** 944–956 (2009). https://doi.org/10.1016/j.jmb.2009.09.061.
110. Elliott, P. R., Goult, B. T., Kopp, P. M., Bate, N., Grossmann, J. G., Roberts, G. C. K., Critchley, D. R. & Barsukov, I. L. The Structure of the Talin Head Reveals a Novel Extended Conformation of the FERM Domain. *Structure* **18(10),** 1289–1299 (2010). https://doi.org/10.1016/j.str.2010.07.011.
111. Sun, Z., Costell, M. & Fässler, R. Integrin activation by talin, kindlin and mechanical forces. *Nat. Cell Biol.* **21(1),** 25–31 (2019). https://doi.org/10.1038/s41556-018-0234-9.
112. Lee, H. S., Bellin, R. M., Walker, D. L., Patel, B., Powers, P., Liu, H., Garcia-Alvarez, B., De Pereda, J. M., Liddington, R. C., Volkmann, N., Hanein, D., Critchley, D. R. & Robson, R. M. Characterization of an actin-binding site within the talin FERM domain. *J. Mol. Biol.* **343(3),** 771–784 (2004). https://doi.org/10.1016/j.jmb.2004.08.069.
113. De Pereda, J. M., Wegener, K. L., Santelli, E., Bate, N., Ginsberg, M. H., Critchley, D. R., Campbell, I. D. & Liddington, R. C. Structural basis for phosphatidylinositol phosphate kinase type Iγ binding to talin at focal adhesions. *J. Biol. Chem.* **280(9),** 8381–8386 (2005). https://doi.org/10.1074/jbc.M413180200.
114. Barsukov, I. L., Prescot, A., Bate, N., Patel, B., Floyd, D. N., Bhanji, N., Bagshaw, C. R., Letinic, K., Di Paolo, G., De Camilli, P., Roberts, G. C. K. & Critchley, D. R. Phosphatidylinositol phosphate kinase type 1γ and β 1-integrin cytoplasmic domain bind to the same region in the talin FERM domain. *J. Biol. Chem.* **278(33),** 31202–31209 (2003). https://doi.org/10.1074/jbc.M303850200.
115. Gingras, A. R., Ziegler, W. H., Bobkov, A. A., Joyce, M. G., Fasci, D., Himmel, M., Rothemund, S., Ritter, A., Grossmann, J. G., Patel, B., Bate, N., Goult, B. T., Emsley, J., Barsukov, I. L., Roberts, G. C. K., Liddington, R. C., Ginsberg, M. H. & Critchley, D. R. Structural determinants of integrin binding to the talin rod. *J. Biol. Chem.* **284(13),** 8866–8876 (2009). https://doi.org/10.1074/jbc.M805937200.
116. Rodius, S., Chaloin, O., Moes, M., Schaffner-Reckinger, E., Landrieu, I., Lippens, G., Lin, M., Zhang,

J. & Kieffer, N. The talin rod IBS2 α-helix interacts with the β3 integrin cytoplasmic tail membrane-proximal helix by establishing charge complementary salt bridges. *J. Biol. Chem.* **283(35),** 24212–24223 (2008). https://doi.org/10.1074/jbc.M709704200.

117. Mccann, R. O. & Craig, S. W. *The ILWEQ module: a conserved sequence that signifies F-actin binding in functionally diverse proteins from yeast to mammals*. *Cell Biol.* 94**,** (1997). at www.pnas.org.
118. Gingras, A. R., Bate, N., Goult, B. T., Hazelwood, L., Canestrelli, I., Grossmann, J. G., Liu, H., Putz, N. S. M., Roberts, G. C. K., Volkmann, N., Hanein, D., Barsukov, I. L. & Critchley, D. R. The structure of the C-terminal actin-binding domain of talin. *EMBO J.* **27(2),** 458–469 (2008). https://doi.org/10.1038/sj.emboj.7601965.
119. Saxena, M., Changede, R., Hone, J., Wolfenson, H. & Sheetz, M. P. Force-Induced Calpain Cleavage of Talin Is Critical for Growth, Adhesion Development, and Rigidity Sensing. *Nano Lett.* **17(12),** 7242–7251 (2017). https://doi.org/10.1021/acs.nanolett.7b02476.
120. O'halloran, T., Beckerle, M. C. & Burridge, K. Identification of talin as a major cytoplasmic protein implicated in platelet activation. *Nature* **317(6036),** 449–451 (1985). https://doi.org/10.1038/317449a0.
121. Franco, S. J., Rodgers, M. A., Perrin, B. J., Han, J., Bennin, D. A., Critchley, D. R. & Huttenlocher, A. Calpain-mediated proteolysis of talin regulates adhesion dynamics. *Nat. Cell Biol.* **6(10),** 977–983 (2004). https://doi.org/10.1038/ncb1175.
122. Huang, C., Rajfur, Z., Yousefi, N., Chen, Z., Jacobson, K. & Ginsberg, M. H. Talin phosphorylation by Cdk5 regulates Smurf1-mediated talin head ubiquitylation and cell migration. *Nat. Cell Biol.* **11(5),** 624–630 (2009). https://doi.org/10.1038/ncb1868.
123. Sakamoto, S., McCann, R. O., Dhir, R. & Kyprianou, N. Talin1 Promotes Tumor Invasion and Metastasis via Focal Adhesion Signaling and Anoikis Resistance. *Cancer Res.* **70(5),** 1885–1895 (2010). https://doi.org/10.1158/0008-5472.CAN-09-2833.
124. Jin, J.-K., Tien, P.-C., Cheng, C.-J., Song, J. H., Huang, C., Lin, S.-H. & Gallick, G. E. Talin1 phosphorylation activates β1 integrins: a novel mechanism to promote prostate cancer bone metastasis. *Oncogene* **34(14),** 1811–1821 (2015). https://doi.org/10.1038/onc.2014.116.
125. McCann, R. O. & Craig, S. W. Functional genomic analysis reveals the utility of the I/LWEQ module as a predictor of protein:actin interaction. *Biochem. Biophys. Res. Commun.* **266(1),** 135–140 (1999). https://doi.org/10.1006/bbrc.1999.1776.
126. Qi, L., Jafari, N., Li, X., Chen, Z., Li, L., Hytönen, V. P., Goult, B. T., Zhan, C.-G. & Huang, C. Talin2-mediated traction force drives matrix degradation and cell invasion. *J. Cell Sci.* **129(19),** 3661–3674 (2016). https://doi.org/10.1242/jcs.185959.
127. Yuan, Y., Li, L., Zhu, Y., Qi, L., Azizi, L., Hytönen, V. P., Zhan, C.-G. & Huang, C. The molecular basis of talin2's high affinity toward β1-integrin. *Sci. Rep.* **7(1),** 41989 (2017). https://doi.org/10.1038/srep41989.
128. Zhang, X., Jiang, G., Cai, Y., Monkley, S. J., Critchley, D. R. & Sheetz, M. P. Talin depletion reveals independence of initial cell spreading from integrin activation and traction. *Nat. Cell Biol.* **10(9),** 1062–1068 (2008). https://doi.org/10.1038/ncb1765.
129. Zaidel-Bar, R., Ballestrem, C., Kam, Z. & Geiger, B. Early molecular events in the assembly of matrix adhesions at the leading edge of migrating cells. *J. Cell Sci.* **116(Pt 22),** 4605–13 (2003). https://doi.org/10.1242/jcs.00792.
130. Lawson, C., Lim, S.-T., Uryu, S., Chen, X. L., Calderwood, D. A. & Schlaepfer, D. D. FAK promotes recruitment of talin to nascent adhesions to control cell motility. *J. Cell Biol.* **196(2),** 223–32 (2012). https://doi.org/10.1083/jcb.201108078.
131. Praekelt, U., Kopp, P. M., Rehm, K., Linder, S., Bate, N., Patel, B., Debrand, E., Manso, A. M., Ross, R. S., Conti, F., Zhang, M.-Z., Harris, R. C., Zent, R., Critchley, D. R. & Monkley, S. J. New isoform-specific monoclonal antibodies reveal different sub-cellular localisations for talin1 and talin2. *Eur. J. Cell Biol.* **91(3),** 180–191 (2012). https://doi.org/10.1016/j.ejcb.2011.12.003.
132. Senetar, M. A., Moncman, C. L. & McCann, R. O. Talin2 is induced during striated muscle differentiation and is targeted to stable adhesion complexes in mature muscle. *Cell Motil. Cytoskeleton* **64(3),** 157–173 (2007). https://doi.org/10.1002/cm.20173.
133. Tissue expression of TLN2. *Hum. Protein Atlas* at https://www.proteinatlas.org/ENSG00000171914-TLN2/tissue.

134. Tissue expression of TLN1. *Hum. Protein Atlas* at https://www.proteinatlas.org/ENSG00000137076-TLN1/tissue.

135. The Human Protein Atlas. at https://www.proteinatlas.org/.

136. Uhlen, M., Fagerberg, L., Hallstrom, B. M., Lindskog, C., Oksvold, P., Mardinoglu, A., Sivertsson, A., Kampf, C., Sjostedt, E., Asplund, A., Olsson, I., Edlund, K., Lundberg, E., Navani, S., Szigyarto, C. A.-K., Odeberg, J., Djureinovic, D., Takanen, J. O., Hober, S., Alm, T., Edqvist, P.-H., Berling, H., Tegel, H., Mulder, J., Rockberg, J., Nilsson, P., Schwenk, J. M., Hamsten, M., von Feilitzen, K., Forsberg, M., Persson, L., Johansson, F., Zwahlen, M., von Heijne, G., Nielsen, J. & Ponten, F. Tissue-based map of the human proteome. *Science (80-.).* **347(6220),** 1260419–1260419 (2015). https://doi.org/10.1126/science.1260419.

137. Elosegui-Artola, A., Oria, R., Chen, Y., Kosmalska, A., Pérez-González, C., Castro, N., Zhu, C., Trepat, X. & Roca-Cusachs, P. Mechanical regulation of a molecular clutch defines force transmission and transduction in response to matrix rigidity. *Nat. Cell Biol.* **18(5),** 540–548 (2016). https://doi.org/10.1038/ncb3336.

138. Li, L., Li, X., Qi, L., Rychahou, P., Jafari, N. & Huang, C. The role of talin2 in breast cancer tumorigenesis and metastasis. *Oncotarget* **8(63),** 106876–106887 (2017). https://doi.org/10.18632/oncotarget.22449.

139. Senetar, M. A., Foster, S. J. & McCann, R. O. Intrasteric inhibition mediates the interaction of the I/LWEQ module proteins Talin1, Talin2, Hip1, and Hip12 with actin. *Biochemistry* **43(49),** 15418–15428 (2004). https://doi.org/10.1021/bi0487239.

140. Hynes, R. O. Integrins: Bidirectional, allosteric signaling machines. *Cell* **110(6),** 673–687 (2002). https://doi.org/10.1016/S0092-8674(02)00971-6.

141. Hynes, R. O. Integrins: A family of cell surface receptors. *Cell* **48(4),** 549–554 (1987). https://doi.org/10.1016/0092-8674(87)90233-9.

142. Xia, T., Takagi, J., Coller, B. S., Wang, J. H. & Springer, T. A. Structural basis for allostery in integrins and binding to fibrinogen-mimetic therapeutics. *Nature* **432(7013),** 59–67 (2004). https://doi.org/10.1038/nature02976.

143. Anderson, L. R., Owens, T. W. & Naylor, M. J. Structural and mechanical functions of integrins. *Biophys. Rev.* **6(2),** 203–213 (2014). https://doi.org/10.1007/s12551-013-0124-0.

144. Lee, J.-O., Rieu, P., Amin Arnaout, M. & Liddington, R. *Crystal Structure of the A Domain from the a Subunit of Integrin CR3 (CD11b/CD18)*. *Cell* 80**,** (1995).

145. Humphries, J. D., Byron, A. & Humphries, M. J. Integrin ligands at a glance. *J. Cell Sci.* **119(19),** 3901–3903 (2006). https://doi.org/10.1242/jcs.03098.

146. Li, J., Su, Y., Xia, W., Qin, Y., Humphries, M. J., Vestweber, D., Cabañas, C., Lu, C. & Springer, T. A. Conformational equilibria and intrinsic affinities define integrin activation. *EMBO J.* **36(5),** 629–645 (2017). https://doi.org/10.15252/embj.201695803.

147. Takagi, J., Petre, B. M., Walz, T. & Springer, T. A. Global conformational earrangements in integrin extracellular domains in outside-in and inside-out signaling. *Cell* **110(5),** 599–611 (2002). https://doi.org/10.1016/S0092-8674(02)00935-2.

148. Wang, J., Su, Y., Iacob, R. E., Engen, J. R. & Springer, T. A. General structural features that regulate integrin affinity revealed by atypical αVβ8. *Nat. Commun.* **10(1),** 1–13 (2019). https://doi.org/10.1038/s41467-019-13248-5.

149. Li, J. & Springer, T. A. Integrin extension enables ultrasensitive regulation by cytoskeletal force. *Proc. Natl. Acad. Sci. U. S. A.* **114(18),** 4685–4690 (2017). https://doi.org/10.1073/pnas.1704171114.

150. Byron, A., Humphries, J. D., Askari, J. A., Craig, S. E., Mould, A. P. & Humphries, M. J. Anti-integrin monoclonal antibodies. *J. Cell Sci.* **122(22),** 4009–4011 (2009). https://doi.org/10.1242/jcs.056770.

151. Evans, R., Patzak, I., Svensson, L., De Filippo, K., Jones, K., McDowall, A. & Hogg, N. Integrins in immunity. *J. Cell Sci.* **122(2),** 215–225 (2009). https://doi.org/10.1242/jcs.019117.

152. Schwartz, M. A. & Assoian, R. K. Integrins and cell proliferation: regulation of cyclin-dependent kinases via cytoplasmic signaling pathways. *J. Cell Sci.* **114(Pt 14),** 2553–60 (2001). https://pubmed.ncbi.nlm.nih.gov/11683383.

153. Moreno-Layseca, P. & Streuli, C. H. Signalling pathways linking integrins with cell cycle progression. *Matrix Biol.* 34**,** 144–153 (2014). https://doi.org/10.1016/j.matbio.2013.10.011.

154. Brown, K. E. & Yamada, K. M. The role of integrins during vertebrate development. *Semin. Dev.*

Biol. **6(2),** 69–77 (1995). https://doi.org/10.1016/S1044-5781(06)80016-2.

155. Darribére, T., Skalski, M., Cousin, H., Gaultier, A., Montmory, C. & Alfandari, D. Integrins: Regulators of embryogenesis. *Biol. Cell* **92(1),** 5–25 (2000). https://doi.org/10.1016/S0248-4900(00)88760-2.
156. Hood, J. D. & Cheresh, D. A. Role of integrins in cell invasion and migration. *Nat. Rev. Cancer* **2(2),** 91–100 (2002). https://doi.org/10.1038/nrc727.
157. Haeger, A., Alexander, S., Vullings, M., Kaiser, F. M. P., Veelken, C., Flucke, U., Koehl, G. E., Hirschberg, M., Flentje, M., Hoffman, R. M., Geissler, E. K., Kissler, S. & Friedl, P. Collective cancer invasion forms an integrin-dependent radioresistant niche. *J. Exp. Med.* **217(1),** (2020). https://doi.org/10.1084/jem.20181184.
158. Mierke, C. T., Frey, B., Fellner, M., Herrmann, M. & Fabry, B. Integrin α5β1 facilitates cancer cell invasion through enhanced contractile forces. *J. Cell Sci.* **124(3),** 369–383 (2011). https://doi.org/10.1242/jcs.071985.
159. Akiyama, S. K., Olden, K. & Yamada, K. M. Fibronectin and integrins in invasion and metastasis. *Cancer Metastasis Rev.* **14(3),** 173–189 (1995). https://doi.org/10.1007/BF00690290.
160. Bouvard, D., Brakebusch, C., Gustafsson, E., Aszódi, A., Bengtsson, T., Berna, A. & Fässler, R. Functional Consequences of Integrin Gene Mutations in Mice. *Circ. Res.* **89(3),** 211–223 (2001). https://doi.org/10.1161/hh1501.094874.
161. Mayer, U., Saher, G., Fässler, R., Bornemann, A., Echtermeyer, F., Mark, H. von der, Miosge, N., Pösch, E. & Mark, K. von der. Absence of integrin α7 causes a novel form of muscular dystrophy. *Nat. Genet.* **17(3),** 318–323 (1997). https://doi.org/10.1038/ng1197-318.
162. Romaine, A., Sørensen, I. W., Zeltz, C., Lu, N., Erusappan, P. M., Melleby, A. O., Zhang, L., Bendiksen, B., Robinson, E. L., Aronsen, J. M., Herum, K. M., Danielsen, H. E., Sjaastad, I., Christensen, G. & Gullberg, D. Overexpression of integrin α11 induces cardiac fibrosis in mice. *Acta Physiol.* **222(2),** e12932 (2018). https://doi.org/10.1111/apha.12932.
163. Wickström, S. A., Radovanac, K. & Fässler, R. Genetic analyses of integrin signaling. *Cold Spring Harb. Perspect. Biol.* **3(2),** 1–22 (2011). https://doi.org/10.1101/cshperspect.a005116.
164. Desgrosellier, J. S. & Cheresh, D. A. Integrins in cancer: Biological implications and therapeutic opportunities. *Nat. Rev. Cancer* **10(1),** 9–22 (2010). https://doi.org/10.1038/nrc2748.
165. Hayashido, Y., Kitano, H., Sakaue, T., Fujii, T., Suematsu, M., Sakurai, S. & Okamoto, T. Overexpression of integrin αv facilitates proliferation and invasion of oral squamous cell carcinoma cells via mek/erk signaling pathway that is activated by interaction of integrin αvβ8 with type I collagen. *Int. J. Oncol.* **45(5),** 1875–1882 (2014). https://doi.org/10.3892/ijo.2014.2642.
166. Zhu, C. Q., Popova, S. N., Brown, E. R. S., Barsyte-Lovejoy, D., Navab, R., Shih, W., Li, M., Lu, M., Jurisica, I., Penn, L. Z., Gullberg, D. & Tsao, M. S. Integrin α11 regulates IGF2 expression in fibroblasts to enhance tumorigenicity of human non-small-cell lung cancer cells. *Proc. Natl. Acad. Sci. U. S. A.* **104(28),** 11754–11759 (2007). https://doi.org/10.1073/pnas.0703040104.
167. Kong, F., García, A. J., Mould, A. P., Humphries, M. J. & Zhu, C. Demonstration of catch bonds between an integrin and its ligand. *J. Cell Biol.* **185(7),** 1275–1284 (2009). https://doi.org/10.1083/jcb.200810002.
168. Bell, G. I. Models for the specific adhesion of cells to cells. *Science (80-.).* **200(4342),** 618–627 (1978). https://doi.org/10.1126/science.347575.
169. Swaminathan, V., Alushin, G. M. & Waterman, C. M. Mechanosensation: A Catch Bond That Only Hooks One Way. *Curr. Biol.* **27(21),** R1158–R1160 (2017). https://doi.org/10.1016/j.cub.2017.09.023.
170. Chakrabarti, S., Hinczewski, M. & Thirumalai, D. Plasticity of hydrogen bond networks regulates mechanochemistry of cell adhesion complexes. *Proc. Natl. Acad. Sci. U. S. A.* **111(25),** 9048–9053 (2014). https://doi.org/10.1073/pnas.1405384111.
171. Benito-Jardón, M., Klapproth, S., Gimeno-Lluch, I., Petzold, T., Bharadwaj, M., Müller, D. J., Zuchtriegel, G., Reichel, C. A. & Costell, M. The fibronectin synergy site re-enforces cell adhesion and mediates a crosstalk between integrin classes. *Elife* 6**,** (2017). https://doi.org/10.7554/eLife.22264.001.
172. Chen, W., Lou, J. & Zhu, C. Forcing switch from short- to intermediate- and long-lived states of the αA domain generates LFA-1/ICAM-1 catch bonds. *J. Biol. Chem.* **285(46),** 35967–35978 (2010). https://doi.org/10.1074/jbc.M110.155770.

173. Choi, Y. I., Duke-Cohan, J. S., Chen, W., Liu, B., Rossy, J., Tabarin, T., Ju, L., Gui, J., Gaus, K., Zhu, C. & Reinherz, E. L. Dynamic control of β1 integrin adhesion by the plexinD1-sema3E axis. *Proc. Natl. Acad. Sci. U. S. A.* **111(1),** 379–384 (2014). https://doi.org/10.1073/pnas.1314209111.

174. Anthis, N. J., Wegener, K. L., Ye, F., Kim, C., Goult, B. T., Lowe, E. D., Vakonakis, I., Bate, N., Critchley, D. R., Ginsberg, M. H. & Campbell, I. D. The structure of an integrin/talin complex reveals the basis of inside-out signal transduction. *EMBO J.* **28(22),** 3623–3632 (2009). https://doi.org/10.1038/emboj.2009.287.

175. McCawley, L. J. & Matrisian, L. M. Matrix metalloproteinases: They're not just for matrix anymore! *Curr. Opin. Cell Biol.* **13(5),** 534–540 (2001). https://doi.org/10.1016/S0955-0674(00)00248-9.

176. Kessenbrock, K., Plaks, V. & Werb, Z. Matrix Metalloproteinases: Regulators of the Tumor Microenvironment. *Cell* **141(1),** 52–67 (2010). https://doi.org/10.1016/j.cell.2010.03.015.

177. Nagase, H., Visse, R. & Murphy, G. Structure and function of matrix metalloproteinases and TIMPs. *Cardiovasc. Res.* **69(3),** 562–573 (2006). https://doi.org/10.1016/j.cardiores.2005.12.002.

178. Gifford, V. & Itoh, Y. MT1-MMP-dependent cell migration: Proteolytic and non-proteolytic mechanisms. *Biochem. Soc. Trans.* **47(3),** 811–826 (2019). https://doi.org/10.1042/BST20180363.

179. Newby, A. C. Matrix metalloproteinases regulate migration, proliferation, and death of vascular smooth muscle cells by degrading matrix and non-matrix substrates. *Cardiovasc. Res.* **69(3),** 614–624 (2006). https://doi.org/10.1016/j.cardiores.2005.08.002.

180. Pirici, D., Pirici, I., Mogoanta, L., Margaritescu, O., Tudorica, V., Margaritescu, C., Ion, D. A., Simionescu, C. & Coconu, M. Matrix metalloproteinase-9 expression in the nuclear compartment of neurons and glial cells in aging and stroke. *Neuropathology* **32(5),** 492–504 (2012). https://doi.org/10.1111/j.1440-1789.2011.01279.x.

181. Vafadari, B., Salamian, A. & Kaczmarek, L. MMP-9 in translation: from molecule to brain physiology, pathology, and therapy. *J. Neurochem.* 139**,** 91–114 (2016). https://doi.org/10.1111/jnc.13415.

182. Kyprianou, C., Christodoulou, N., Hamilton, R. S., Nahaboo, W., Boomgaard, D. S., Amadei, G., Migeotte, I. & Zernicka-Goetz, M. Basement membrane remodelling regulates mouse embryogenesis. *Nature* **582(7811),** 253–258 (2020). https://doi.org/10.1038/s41586-020-2264-2.

183. Stamenkovic, I. Matrix metalloproteinases in tumor invasion and metastasis. *Semin. Cancer Biol.* **10(6),** 415–433 (2000). https://doi.org/10.1006/scbi.2000.0379.

184. Poincioux, R., Lizárraga, F. & Chavrier, P. Matrix invasion by tumour cells: A focus on MT1-MMP trafficking to invadopodia. *J. Cell Sci.* **122(17),** 3015–3024 (2009). https://doi.org/10.1242/jcs.034561.

185. Wieczorek, E., Jablonska, E., Wasowicz, W. & Reszka, E. Matrix metalloproteinases and genetic mouse models in cancer research: a mini-review. *Tumor Biol.* **36(1),** 163–175 (2014). https://doi.org/10.1007/s13277-014-2747-6.

186. Foda, H. D. & Zucker, S. Matrix metalloproteinases in cancer invasion, metastasis and angiogenesis. *Drug Discov. Today* **6(9),** 478–482 (2001). https://doi.org/10.1016/S1359-6446(01)01752-4.

187. Webb, A. H., Gao, B. T., Goldsmith, Z. K., Irvine, A. S., Saleh, N., Lee, R. P., Lendermon, J. B., Bheemreddy, R., Zhang, Q., Brennan, R. C., Johnson, D., Steinle, J. J., Wilson, M. W. & Morales-Tirado, V. M. Inhibition of MMP-2 and MMP-9 decreases cellular migration, and angiogenesis in in vitro models of retinoblastoma. *BMC Cancer* **17(1),** 434 (2017). https://doi.org/10.1186/s12885-017-3418-y.

188. Jacob, A., Jing, J., Lee, J., Schedin, P., Gilbert, S. M., Peden, A. A., Junutula, J. R. & Prekeris, R. Rab40b regulates trafficking of MMP2 and MMP9 during invadopodia formation and invasion of breast cancer cells. *J. Cell Sci.* **126(20),** 4647–4658 (2013). https://doi.org/10.1242/jcs.126573.

189. Toth, M., Chvyrkova, I., Bernardo, M. M., Hernandez-Barrantes, S. & Fridman, R. Pro-MMP-9 activation by the MT1-MMP/MMP-2 axis and MMP-3: Role of TIMP-2 and plasma membranes. *Biochem. Biophys. Res. Commun.* **308(2),** 386–395 (2003). https://doi.org/10.1016/S0006-291X(03)01405-0.

190. Li, Z., Takino, T., Endo, Y. & Sato, H. Activation of MMP-9 by membrane type-1 MMP/MMP-2 axis stimulates tumor metastasis. *Cancer Sci.* **108(3),** 347–353 (2017). https://doi.org/10.1111/cas.13134.

191. Hernandez-Barrantes, S., Toth, M., Bernardo, M. M., Yurkova, M., Gervasi, D. C., Raz, Y., Sang, Q. X. A. & Fridman, R. Binding of active (57 kDa) membrane type 1-matrix metalloproteinase (MT1-MMP) to tissue inhibitor of metalloproteinase (TIMP)-2 regulates MT1-MMP processing and pro-

MMP-2 activation. *J. Biol. Chem.* **275(16),** 12080–12089 (2000). https://doi.org/10.1074/jbc.275.16.12080.

192. Fridman, R., Toth, M., Peña, D. & Mobashery, S. Activation of Progelatinase B (MMP-9) by Gelatinase A (MMP-2). *Cancer Res.* **55(12),** 2548–2555 (1995). https://pubmed.ncbi.nlm.nih.gov/7780967.
193. Ogata, Y., Enghild, J. J. & Nagase, H. Matrix metalloproteinase 3 (stromelysin) activates the precursor for the human matrix metalloproteinase 9. *J. Biol. Chem.* **267(6),** 3581–4 (1992). https://pubmed.ncbi.nlm.nih.gov/1371271.
194. Uría, J. A. & López-Otín, C. Matrilysin-2, a new matrix metalloproteinase expressed in human tumors and showing the minimal domain organization required for secretion, latency, and activity. *Cancer Res.* **60(17),** 4745–51 (2000). https://pubmed.ncbi.nlm.nih.gov/10987280.
195. Knäuper, V., Smith, B., López-Otin, C. & Murphy, G. Activation of progelatinase B (proMMP-9) by active collagenase-3 (MMP-13). *Eur. J. Biochem.* **248(2),** 369–373 (1997). https://doi.org/10.1111/j.1432-1033.1997.00369.x.
196. Arpino, V., Brock, M. & Gill, S. E. The role of TIMPs in regulation of extracellular matrix proteolysis. *Matrix Biol.* 44**–**46**,** 247–254 (2015). https://doi.org/10.1016/j.matbio.2015.03.005.
197. Cui, N., Hu, M. & Khalil, R. A. Biochemical and Biological Attributes of Matrix Metalloproteinases. in *Prog. Mol. Biol. Transl. Sci.* 147**,** 1–73 (Elsevier B.V., 2017). https://doi.org/10.1016/bs.pmbts.2017.02.005.
198. Brew, K. & Nagase, H. The tissue inhibitors of metalloproteinases (TIMPs): An ancient family with structural and functional diversity. *Biochim. Biophys. Acta - Mol. Cell Res.* **1803(1),** 55–71 (2010). https://doi.org/10.1016/j.bbamcr.2010.01.003.
199. Nagase, H. & Murphy, G. Tailoring TIMPs for selective metalloproteinase inhibition. in *Cancer Degrad. Proteases Cancer Biol.* 787–810 (Springer New York, 2008). https://doi.org/10.1007/978-0-387-69057-5_37.
200. Jackson, H. W., Defamie, V., Waterhouse, P. & Khokha, R. TIMPs: Versatile extracellular regulators in cancer. *Nat. Rev. Cancer* **17(1),** 38–53 (2017). https://doi.org/10.1038/nrc.2016.115.
201. Peeney, D., Jensen, S. M., Castro, N. P., Kumar, S., Noonan, S., Handler, C., Kuznetsov, A., Shih, J., Tran, A. D., Salomon, D. S. & Stetler-Stevenson, W. G. TIMP-2 suppresses tumor growth and metastasis in murine model of triple-negative breast cancer. *Carcinogenesis* **41(3),** 313–325 (2020). https://doi.org/10.1093/carcin/bgz172.
202. Bardell, D. The Biologists' Forum: The invention of the microscope. *Bios* **75(2),** 78–84 (2004). https://doi.org/10.1893/0005-3155(2004)75<78:TIOTM>2.0.CO;2.
203. Zuidervaart, H. J. The 'true inventor' of the telescope. A survey of 400 years of debate. in *Orig. Telesc.* (eds. Van Helden, A., Dupré, S., van Gent, R. & Zuidervaart, H.) 5–44 (KNAW Press, 2010).
204. Vangindertael, J., Camacho, R., Sempels, W., Mizuno, H., Dedecker, P. & Janssen, K. P. F. An introduction to optical super-resolution microscopy for the adventurous biologist. *Methods Appl. Fluoresc.* **6(2),** 022003 (2018). https://doi.org/10.1088/2050-6120/aaae0c.
205. Pechprasarn, S., Sukkasem, C., Suvarnaphaet, P., Thongchoom, R., Chuwittaya, S. & Janyasupab, M. Low-cost instrumentation of Automated Whole - Slide Microscope for Biomedical Imaging. in *BMEiCON 2018 - 11th Biomed. Eng. Int. Conf.* (Institute of Electrical and Electronics Engineers Inc., 2019). https://doi.org/10.1109/BMEiCON.2018.8609942.
206. Skandarajah, A., Reber, C. D., Switz, N. A. & Fletcher, D. A. Quantitative Imaging with a Mobile Phone Microscope. *PLoS One* **9(5),** e96906 (2014). https://doi.org/10.1371/journal.pone.0096906.
207. Zhang, Y. & Gross, H. Systematic design of microscope objectives. Part I: System review and analysis. *Adv. Opt. Technol.* **8(5),** 313–347 (2019). https://doi.org/10.1515/aot-2019-0002.
208. Zhang, Y. & Gross, H. Systematic design of microscope objectives. Part II: Lens modules and design principles. *Adv. Opt. Technol.* **8(5),** 349–384 (2019). https://doi.org/10.1515/aot-2019-0013.
209. Zhang, Y. & Gross, H. Systematic design of microscope objectives. Part III: Miscellaneous design principles and system synthesis: Systematic design of microscope objectives. *Adv. Opt. Technol.* **8(5),** 385–402 (2019). https://doi.org/10.1515/aot-2019-0014.
210. Sanderson, J. Microscope Anatomy and Design. in *Underst. Light Microsc.* 75–90 (John Wiley & Sons, Ltd, 2019). https://doi.org/10.1002/9781118696736.ch4.
211. Reihani, S. N. S., Charsooghi, M. A., Khalesifard, H. R. & Golestanian, R. Efficient in-depth trapping

with an oil-immersion objective lens. *Opt. Lett.* **31(6),** 766 (2006). https://doi.org/10.1364/OL.31.000766.

212. Sheppard, C. J. R. & Cogswell, C. J. Effects of aberrating layers and tube length on con focal imaging properties. *Optik (Stuttg).* **87(1),** 34–38 (1991).
213. Dobrucki, J. W. & Kubitscheck, U. Fluorescence Microscopy. in *Fluoresc. Microsc.* 85–132 (Wiley-VCH Verlag GmbH & Co. KGaA, 2017). https://doi.org/10.1002/9783527687732.ch3.
214. Naredi-Rainer, N., Prescher, J., Hartschuh, A. & Lamb, D. C. Confocal Microscopy. in *Fluoresc. Microsc.* 165–202 (Wiley-VCH Verlag GmbH & Co. KGaA, 2017). https://doi.org/10.1002/9783527687732.ch5.
215. Müller, C. B. & Enderlein, J. Image Scanning Microscopy. *Phys. Rev. Lett.* **104(19),** 198101 (2010). https://doi.org/10.1103/PhysRevLett.104.198101.
216. Ng, K. K. Charge-Coupled Device. in *Complet. Guid. to Semicond. Devices* 164–174 (John Wiley & Sons, Inc., 2010). https://doi.org/10.1002/9781118014769.ch21.
217. Spring, K. R., Fellers, T. J. & Davidson, M. W. Introduction to Charge-Coupled Devices (CCDs) | MicroscopyU, Nikon's. at https://www.microscopyu.com/digital-imaging/introduction-to-charge-coupled-devices-ccds.
218. Hamamatsu Photonics. A visual guide to CCD vs. EM-CCD vs. CMOS:Technical guides. at https://camera.hamamatsu.com/jp/en/technical_guides/visual_guide/index.html.
219. Abramowitz, M. & Davidson, M. W. Hamamatsu Learning Center: Frame-Transfer CCD Architecture. at https://hamamatsu.magnet.fsu.edu/articles/frametransfer.html.
220. Abramowitz, M. & Davidson, M. W. Hamamatsu Learning Center: Interline Transfer CCD Architecture. at https://hamamatsu.magnet.fsu.edu/articles/interline.html.
221. Theuwissen, A. J. P., Snoeij, M. F., Wang, X., Rao, P. R. & Bodegom, E. CMOS Image Sensors for Ambient Intelligence. in *AmIware Hardw. Technol. Drivers Ambient Intell.* 125–150 (Kluwer Academic Publishers, 2006). https://doi.org/10.1007/1-4020-4198-5_8.
222. Bao, J., Xing, F., Sun, T. & You, Z. CMOS imager non-uniformity response correction-based high-accuracy spot target localization. *Appl. Opt.* **58(16),** 4560 (2019). https://doi.org/10.1364/AO.58.004560.
223. Bigas, M., Cabruja, E., Forest, J. & Salvi, J. Review of CMOS image sensors. *Microelectronics J.* **37(5),** 433–451 (2006). https://doi.org/10.1016/j.mejo.2005.07.002.
224. Yoo, H. W., Ito, S. & Schitter, G. High speed laser scanning microscopy by iterative learning control of a galvanometer scanner. *Control Eng. Pract.* 50**,** 12–21 (2016). https://doi.org/10.1016/j.conengprac.2016.02.007.
225. Maddox, A. S. & Maddox, P. S. High-Resolution Imaging of Cellular Processes in Caenorhabditis elegans. in *Methods Cell Biol.* 107**,** 1–34 (Academic Press Inc., 2012). https://doi.org/10.1016/B978-0-12-394620-1.00001-1.
226. Xi, P., Liu, Y. & Re, Q. Scanning and Image Reconstruction Techniques in Confocal Laser Scanning Microscopy. in *Laser Scanning, Theory Appl.* (ed. Wang, C.-C.) (InTech, 2011). https://doi.org/10.5772/14545.
227. Reihani, S. N. S. & Oddershede, L. B. Confocal microscopy of thick specimens. *J. Biomed. Opt.* **14(3),** 030513 (2009). https://doi.org/10.1117/1.3156813.
228. St. Croix, C. M., Shand, S. H. & Watkins, S. C. Confocal microscopy: comparisons, applications, and problems. *Biotechniques* **39(6S),** S2–S5 (2005). https://doi.org/10.2144/000112089.
229. Straub, B. B., Lah, D. C., Schmidt, H., Roth, M., Gilson, L., Butt, H.-J. & Auernhammer, G. K. Versatile high-speed confocal microscopy using a single laser beam. *Rev. Sci. Instrum.* **91(3),** 033706 (2020). https://doi.org/10.1063/1.5122311.
230. Choi, S., Kim, P., Boutilier, R., Kim, M. Y., Lee, Y. J. & Lee, H. Development of a high speed laser scanning confocal microscope with an acquisition rate up to 200 frames per second. *Opt. Express* **21(20),** 23611 (2013). https://doi.org/10.1364/OE.21.023611.
231. Lakowicz, J. R. *Principles of Fluorescence Spectroscopy*. *Princ. Fluoresc. Spectrosc.* (Springer US, 2006). https://doi.org/10.1007/978-0-387-46312-4.
232. Stokes, G. G. XXX. On the change of refrangibility of light. *Philos. Trans. R. Soc. London* 142**,** 463–562 (1852). https://doi.org/10.1098/rstl.1852.0022.

233. Jablonski, A. Efficiency of Anti-Stokes Fluorescence in Dyes. *Nature* **131(3319),** 839–840 (1933). https://doi.org/10.1038/131839b0.

234. Cormack, B. P., Valdivia, R. H. & Falkow, S. FACS-optimized mutants of the green fluorescent protein (GFP). *Gene* **173(1),** 33–38 (1996). https://doi.org/10.1016/0378-1119(95)00685-0.

235. Lambert, T. J. FPbase: a community-editable fluorescent protein database. *Nat. Methods* **16(4),** 277–278 (2019). https://doi.org/10.1038/s41592-019-0352-8.

236. Franck, J. & Dymond, E. G. Elementary processes of photochemical reactions. *Trans. Faraday Soc.* **21(February),** 536 (1926). https://doi.org/10.1039/tf9262100536.

237. Condon, E. A Theory of Intensity Distribution in Band Systems. *Phys. Rev.* **28(6),** 1182–1201 (1926). https://doi.org/10.1103/PhysRev.28.1182.

238. Yang, F., Moss, L. G. & Phillips, G. N. The molecular structure of green fluorescent protein. *Nat. Biotechnol.* **14(10),** 1246–1251 (1996). https://doi.org/10.1038/nbt1096-1246.

239. Keller, R. GFP and fluorophore. *Wikipedia* (2008). at https://en.wikipedia.org/wiki/File:Gfp_and_fluorophore.png.

240. Kim, S., Chen, J., Cheng, T., Gindulyte, A., He, J., He, S., Li, Q., Shoemaker, B. A., Thiessen, P. A., Yu, B., Zaslavsky, L., Zhang, J. & Bolton, E. E. PubChem 2019 update: Improved access to chemical data. *Nucleic Acids Res.* **47(D1),** D1102–D1109 (2019). https://doi.org/10.1093/nar/gky1033.

241. National Center for Biotechnology Information. PubChem Compound Summary for CID 16850, Fluorescein. *PubChem* at https://pubchem.ncbi.nlm.nih.gov/compound/Fluorescein.

242. Ihlenfeldt, W. D., Bolton, E. E. & Bryant, S. H. The PubChem chemical structure sketcher. *J. Cheminform.* **1(1),** 20 (2009). https://doi.org/10.1186/1758-2946-1-20.

243. National Center for Biotechnology Information. PubChem Compound Summary for CID 2954, 4',6-Diamidino-2-phenylindole. *PubChem* at https://pubchem.ncbi.nlm.nih.gov/compound/4_6-Diamidino-2-phenylindole.

244. Mualla, F., Aubreville, M. & Maier, A. Microscopy. in *Lect. Notes Comput. Sci. (including Subser. Lect. Notes Artif. Intell. Lect. Notes Bioinformatics)* 11111 LNCS**,** 69–90 (Springer Verlag, 2018). https://doi.org/10.1007/978-3-319-96520-8_5.

245. Shimomura, O., Johnson, F. H. & Saiga, Y. Extraction, Purification and Properties of Aequorin, a Bioluminescent Protein from the Luminous Hydromedusan,Aequorea. *J. Cell. Comp. Physiol.* **59(3),** 223–239 (1962). https://doi.org/10.1002/jcp.1030590302.

246. Tsien, R. Y. THE GREEN FLUORESCENT PROTEIN. *Annu. Rev. Biochem.* **67(1),** 509–544 (1998). https://doi.org/10.1146/annurev.biochem.67.1.509.

247. The, T. H. & Feltkamp, T. E. Conjugation of fluorescein isothiocyanate to antibodies. II. A reproducible method. *Immunology* **18(6),** 875–81 (1970). https://pubmed.ncbi.nlm.nih.gov/4913804.

248. Kapuscinski, J. DAPI: a DNA-Specific Fluorescent Probe. *Biotech. Histochem.* **70(5),** 220–233 (1995). https://doi.org/10.3109/10520299509108199.

249. Rosenthal, S. J., Chang, J. C., Kovtun, O., McBride, J. R. & Tomlinson, I. D. Biocompatible Quantum Dots for Biological Applications. *Chem. Biol.* **18(1),** 10–24 (2011). https://doi.org/10.1016/j.chembiol.2010.11.013.

250. Doudna, J. A. & Charpentier, E. The new frontier of genome engineering with CRISPR-Cas9. *Science (80-.).* **346(6213),** 1258096 (2014). https://doi.org/10.1126/science.1258096.

251. Chalfie, M., Tu, Y., Euskirchen, G., Ward, W. W. & Prasher, D. C. Green fluorescent protein as a marker for gene expression. *Science (80-.).* **263(5148),** 802–805 (1994). https://doi.org/10.1126/science.8303295.

252. Camacho, R., Täuber, D., Hansen, C., Shi, J., Bousset, L., Melki, R., Li, J.-Y. & Scheblykin, I. G. 2D polarization imaging as a low-cost fluorescence method to detect α-synuclein aggregation ex vivo in models of Parkinson's disease. *Commun. Biol.* **1(1),** 157 (2018). https://doi.org/10.1038/s42003-018-0156-x.

253. Clayton, A. H. A., Hanley, Q. S., Arndt-Jovin, D. J., Subramaniam, V. & Jovin, T. M. Dynamic Fluorescence Anisotropy Imaging Microscopy inthe Frequency Domain (rFLIM). *Biophys. J.* **83(3),** 1631–1649 (2002). https://doi.org/10.1016/S0006-3495(02)73932-5.

254. Wang, X. F., Uchida, T., Coleman, D. M. & Minami, S. A Two-Dimensional Fluorescence Lifetime Imaging System Using a Gated Image Intensifier. *Appl. Spectrosc.* **45(3),** 360–366 (1991). https://doi.org/10.1366/0003702914337182.

255. Marriott, G., Clegg, R. M., Arndt-Jovin, D. J. & Jovin, T. M. Time resolved imaging microscopy. Phosphorescence and delayed fluorescence imaging. *Biophys. J.* **60(6),** 1374–1387 (1991). https://doi.org/10.1016/S0006-3495(91)82175-0.

256. Kubitscheck, U. Principles of Light Microscopy. in *Fluoresc. Microsc.* 23–83 (Wiley-VCH Verlag GmbH & Co. KGaA, 2017). https://doi.org/10.1002/9783527687732.ch2.

257. Airy, G. B. & B., G. On the Diffraction of an Object-glass with Circular Aperture. *TCaPS* 5**,** 283 (1835). at https://ui.adsabs.harvard.edu/abs/1835TCaPS...5..283A/abstract.

258. Sakurambo. Airy-pattern. *Wikipedia* (2007). at https://en.wikipedia.org/wiki/File:Airy-pattern.svg.

259. Bliven, S. Airy disk spacing near Rayleigh criterion. *Wikipedia* (2014). at https://en.wikipedia.org/wiki/File:Airy_disk_spacing_near_Rayleigh_criterion.png.

260. Ram, S., Ward, E. S. & Ober, R. J. Beyond Rayleigh's criterion: A resolution measure with application to single-molecule microscopy. *Proc. Natl. Acad. Sci.* **103(12),** 4457–4462 (2006). https://doi.org/10.1073/pnas.0508047103.

261. Rayleigh. XXXI. Investigations in optics, with special reference to the spectroscope. *London, Edinburgh, Dublin Philos. Mag. J. Sci.* **8(49),** 261–274 (1879). https://doi.org/10.1080/14786447908639684.

262. Thorley, J. A., Pike, J. & Rappoport, J. Z. Super-resolution Microscopy. in *Fluoresc. Microsc.* 199–212 (Elsevier, 2014). https://doi.org/10.1016/B978-0-12-409513-7.00014-2.

263. Wegel, E., Göhler, A., Lagerholm, B. C., Wainman, A., Uphoff, S., Kaufmann, R. & Dobbie, I. M. Imaging cellular structures in super-resolution with SIM, STED and Localisation Microscopy: A practical comparison. *Sci. Rep.* **6(1),** 1–13 (2016). https://doi.org/10.1038/srep27290.

264. Cogswell, C. J. & Larkin, K. G. The Specimen Illumination Path and Its Effect on Image Quality. in *Handb. Biol. Confocal Microsc.* 127–137 (Springer US, 1995). https://doi.org/10.1007/978-1-4757-5348-6_8.

265. Pawley, J. Fundamental Limits in Confocal Microscopy. in *Handb. Biol. Confocal Microsc.* 15–26 (Springer US, 1990). https://doi.org/10.1007/978-1-4615-7133-9_2.

266. Sauer, M. & Heilemann, M. Localization-Based Super-Resolution Microscopy. in *Fluoresc. Microsc.* 267–289 (Wiley-VCH Verlag GmbH & Co. KGaA, 2017). https://doi.org/10.1002/9783527687732.ch8.

267. Nyquist, H. Certain Topics in Telegraph Transmission Theory. *Trans. Am. Inst. Electr. Eng.* **47(2),** 617–644 (1928). https://doi.org/10.1109/T-AIEE.1928.5055024.

268. Shannon, C. E. Communication in the Presence of Noise. *Proc. IRE* **37(1),** 10–21 (1949). https://doi.org/10.1109/JRPROC.1949.232969.

269. Sibarita, J. B. Deconvolution microscopy. *Adv. Biochem. Eng. Biotechnol.* 95**,** 201–243 (2005). https://doi.org/10.1007/b102215.

270. Cole, R. W., Jinadasa, T. & Brown, C. M. Measuring and interpreting point spread functions to determine confocal microscope resolution and ensure quality control. *Nat. Protoc.* **6(12),** 1929–1941 (2011). https://doi.org/10.1038/nprot.2011.407.

271. Gibson, S. F. & Lanni, F. Experimental test of an analytical model of aberration in an oil-immersion objective lens used in three-dimensional light microscopy. *J. Opt. Soc. Am. A* **9(1),** 154 (1992). https://doi.org/10.1364/JOSAA.9.000154.

272. Born, M., Wolf, E., Bhatia, A. B., Clemmow, P. C., Gabor, D., Stokes, A. R., Taylor, A. M., Wayman, P. A. & Wilcock, W. L. Elements of the theory of diffraction. in *Princ. Opt.* 412–516 (Cambridge University Press, 1999). https://doi.org/10.1017/CBO9781139644181.017.

273. Richardst, B. & Wolfs, E. Electromagnetic diffraction in optical systems, II. Structure of the image field in an aplanatic system. *Proc. R. Soc. London. Ser. A. Math. Phys. Sci.* **253(1274),** 358–379 (1959). https://doi.org/10.1098/rspa.1959.0200.

274. Hiware, S., Porwal, P., Velmurugan, R. & Chaudhuri, S. Modeling of PSF for refractive index variation in fluorescence microscopy. in *2011 18th IEEE Int. Conf. Image Process.* 2037–2040 (IEEE, 2011). https://doi.org/10.1109/ICIP.2011.6115879.

275. Li, J., Xue, F. & Blu, T. Fast and accurate three-dimensional point spread function computation for fluorescence microscopy. *J. Opt. Soc. Am. A* **34(6),** 1029 (2017). https://doi.org/10.1364/JOSAA.34.001029.

276. Török, P. & Varga, P. Electromagnetic diffraction of light focused through a stratified medium. *Appl.*

Opt. **36(11),** 2305 (1997). https://doi.org/10.1364/AO.36.002305.

277. Hell, S., Reiner, G., Cramer, C. & Stelzer, E. H. K. Aberrations in confocal fluorescence microscopy induced by mismatches in refractive index. *J. Microsc.* **169(3),** 391–405 (1993). https://doi.org/10.1111/j.1365-2818.1993.tb03315.x.
278. Kirshner, H., Aguet, F., Sage, D. & Unser, M. 3-D PSF fitting for fluorescence microscopy: Implementation and localization application. *J. Microsc.* **249(1),** 13–25 (2013). https://doi.org/10.1111/j.1365-2818.2012.03675.x.
279. McNally, J. G., Karpova, T., Cooper, J. & Conchello, J. A. Three-Dimensional Imaging by Deconvolution Microscopy. *Methods* **19(3),** 373–385 (1999). https://doi.org/10.1006/meth.1999.0873.
280. Schindelin, J., Arganda-Carreras, I., Frise, E., Kaynig, V., Longair, M., Pietzsch, T., Preibisch, S., Rueden, C., Saalfeld, S., Schmid, B., Tinevez, J.-Y., White, D. J., Hartenstein, V., Eliceiri, K., Tomancak, P. & Cardona, A. Fiji: an open-source platform for biological-image analysis. *Nat. Methods* **9(7),** 676–682 (2012). https://doi.org/10.1038/nmeth.2019.
281. Huang, B., Bates, M. & Zhuang, X. Super-resolution fluorescence microscopy. *Annu. Rev. Biochem.* 78**,** 993–1016 (2009). https://doi.org/10.1146/annurev.biochem.77.061906.092014.
282. Zelger, P., Kaser, K., Rossboth, B., Velas, L., Schütz, G. J. & Jesacher, A. Three-dimensional localization microscopy using deep learning. *Opt. Express* **26(25),** 33166 (2018). https://doi.org/10.1364/OE.26.033166.
283. Fischer, R. S., Wu, Y., Kanchanawong, P., Shroff, H. & Waterman, C. M. Microscopy in 3D: a biologist's toolbox. *Trends Cell Biol.* **21(12),** 682–691 (2011). https://doi.org/10.1016/j.tcb.2011.09.008.
284. Hell, S. W. & Wichmann, J. Breaking the diffraction resolution limit by stimulated emission: stimulated-emission-depletion fluorescence microscopy. *Opt. Lett.* **19(11),** 780 (1994). https://doi.org/10.1364/OL.19.000780.
285. Klar, T. A., Jakobs, S., Dyba, M., Egner, A. & Hell, S. W. Fluorescence microscopy with diffraction resolution barrier broken by stimulated emission. *Proc. Natl. Acad. Sci.* **97(15),** 8206–8210 (2000). https://doi.org/10.1073/pnas.97.15.8206.
286. Tam, J. & Merino, D. Stochastic optical reconstruction microscopy (STORM) in comparison with stimulated emission depletion (STED) and other imaging methods. *J. Neurochem.* **135(4),** 643–658 (2015). https://doi.org/10.1111/jnc.13257.
287. Dickson, R. M., Cubitt, A. B., Tsien, R. Y. & Moerner, W. E. On/off blinking and switching behaviour of single molecules of green fluorescent protein. *Nature* **388(6640),** 355–358 (1997). https://doi.org/10.1038/41048.
288. Bates, M., Blosser, T. R. & Zhuang, X. Short-Range Spectroscopic Ruler Based on a Single-Molecule Optical Switch. *Phys. Rev. Lett.* **94(10),** 108101 (2005). https://doi.org/10.1103/PhysRevLett.94.108101.
289. Betzig, E., Patterson, G. H., Sougrat, R., Lindwasser, O. W., Olenych, S., Bonifacino, J. S., Davidson, M. W., Lippincott-Schwartz, J. & Hess, H. F. Imaging intracellular fluorescent proteins at nanometer resolution. *Science (80-.).* **313(5793),** 1642–1645 (2006). https://doi.org/10.1126/science.1127344.
290. Rust, M. J., Bates, M. & Zhuang, X. Sub-diffraction-limit imaging by stochastic optical reconstruction microscopy (STORM). *Nat. Methods* **3(10),** 793–795 (2006). https://doi.org/10.1038/nmeth929.
291. Paszek, M. J., DuFort, C. C., Rubashkin, M. G., Davidson, M. W., Thorn, K. S., Liphardt, J. T. & Weaver, V. M. Scanning angle interference microscopy reveals cell dynamics at the nanoscale. *Nat. Methods* **9(8),** 825–827 (2012). https://doi.org/10.1038/nmeth.2077.
292. Hell, S. & Stelzer, E. H. K. Properties of a 4Pi confocal fluorescence microscope. *J. Opt. Soc. Am. A* **9(12),** 2159 (1992). https://doi.org/10.1364/JOSAA.9.002159.
293. Albrecht, B., Failla, A. V., Heintzmann, R. & Cremer, C. Spatially modulated illumination microscopy: online visualization of intensity distribution and prediction of nanometer precision of axial distance measurements by computer simulations. *J. Biomed. Opt.* **6(3),** 292 (2001). https://doi.org/10.1117/1.1383293.
294. Chen, F., Tillberg, P. W. & Boyden, E. S. Expansion microscopy. *Science (80-.).* **347(6221),** 543–548 (2015). https://doi.org/10.1126/science.1260088.
295. Gustafsson, M. G. L. Surpassing the lateral resolution limit by a factor of two using structured

illumination microscopy. SHORT COMMUNICATION. *J. Microsc.* **198(2),** 82–87 (2000). https://doi.org/10.1046/j.1365-2818.2000.00710.x.

296. Schermelleh, L., Ferrand, A., Huser, T., Eggeling, C., Sauer, M., Biehlmaier, O. & Drummen, G. P. C. Super-resolution microscopy demystified. *Nat. Cell Biol.* **21(1),** 72–84 (2019). https://doi.org/10.1038/s41556-018-0251-8.
297. Waldchen, S., Lehmann, J., Klein, T., Van De Linde, S. & Sauer, M. Light-induced cell damage in live-cell super-resolution microscopy. *Sci. Rep.* 5**,** (2015). https://doi.org/10.1038/srep15348.
298. Galbraith, C. G. & Galbraith, J. A. Super-resolution microscopy at a glance. *J. Cell Sci.* **124(10),** 1607–1611 (2011). https://doi.org/10.1242/jcs.080085.
299. Wombacher, R., Heidbreder, M., van de Linde, S., Sheetz, M. P., Heilemann, M., Cornish, V. W. & Sauer, M. Live-cell super-resolution imaging with trimethoprim conjugates. *Nat. Methods* **7(9),** 717–719 (2010). https://doi.org/10.1038/nmeth.1489.
300. Takasaki, K. T., Ding, J. B. & Sabatini, B. L. Live-Cell Superresolution Imaging by Pulsed STED Two-Photon Excitation Microscopy. *Biophys. J.* **104(4),** 770–777 (2013). https://doi.org/10.1016/j.bpj.2012.12.053.
301. Guo, M., Chandris, P., Giannini, J. P., Trexler, A. J., Fischer, R., Chen, J., Vishwasrao, H. D., Rey-Suarez, I., Wu, Y., Wu, X., Waterman, C. M., Patterson, G. H., Upadhyaya, A., Taraska, J. W. & Shroff, H. Single-shot super-resolution total internal reflection fluorescence microscopy. *Nat. Methods* **15(6),** 425–428 (2018). https://doi.org/10.1038/s41592-018-0004-4.
302. York, A. G., Parekh, S. H., Nogare, D. D., Fischer, R. S., Temprine, K., Mione, M., Chitnis, A. B., Combs, C. A. & Shroff, H. Resolution doubling in live, multicellular organisms via multifocal structured illumination microscopy. *Nat. Methods* **9(7),** 749–754 (2012). https://doi.org/10.1038/nmeth.2025.
303. Weigert, M., Schmidt, U., Boothe, T., Müller, A., Dibrov, A., Jain, A., Wilhelm, B., Schmidt, D., Broaddus, C., Culley, S., Rocha-Martins, M., Segovia-Miranda, F., Norden, C., Henriques, R., Zerial, M., Solimena, M., Rink, J., Tomancak, P., Royer, L., Jug, F. & Myers, E. W. Content-aware image restoration: pushing the limits of fluorescence microscopy. *Nat. Methods* **15(12),** 1090–1097 (2018). https://doi.org/10.1038/s41592-018-0216-7.
304. Belthangady, C. & Royer, L. A. Applications, promises, and pitfalls of deep learning for fluorescence image reconstruction. *Nat. Methods* **16(12),** 1215–1225 (2019). https://doi.org/10.1038/s41592-019-0458-z.
305. Lam, F., Cladière, D., Guillaume, C., Wassmann, K. & Bolte, S. Super-resolution for everybody: An image processing workflow to obtain high-resolution images with a standard confocal microscope. *Methods* 115**,** 17–27 (2017). https://doi.org/10.1016/j.ymeth.2016.11.003.
306. Chen, L., Wang, Y. & Song, W. Super-Resolution Confocal Microscopy Through Pixel Reassignment. in *Microsc. Anal.* (InTech, 2016). https://doi.org/10.5772/63192.
307. Hom, E. F. Y., Marchis, F., Lee, T. K., Haase, S., Agard, D. A. & Sedat, J. W. AIDA: an adaptive image deconvolution algorithm with application to multi-frame and three-dimensional data. *J. Opt. Soc. Am. A* **24(6),** 1580 (2007). https://doi.org/10.1364/JOSAA.24.001580.
308. Levin, A., Weiss, Y., Durand, F. & Freeman, W. T. Understanding Blind Deconvolution Algorithms. *IEEE Trans. Pattern Anal. Mach. Intell.* **33(12),** 2354–2367 (2011). https://doi.org/10.1109/TPAMI.2011.148.
309. Ikoma, H., Broxton, M., Kudo, T. & Wetzstein, G. A convex 3D deconvolution algorithm for low photon count fluorescence imaging. *Sci. Rep.* **8(1),** 11489 (2018). https://doi.org/10.1038/s41598-018-29768-x.
310. Beck, A. & Teboulle, M. A Fast Iterative Shrinkage-Thresholding Algorithm for Linear Inverse Problems. *SIAM J. Imaging Sci.* **2(1),** 183–202 (2009). https://doi.org/10.1137/080716542.
311. Tikhonov, A. N. Solution of Incorrectly Formulated Problems and the Regularization Method. *Sov. Math. Dokl.* 4**,** 1035–1038 (1963).
312. Wiener, N. *Extrapolation, Interpolation, and Smoothing of Stationary Time Series: With Engineering Applications.* (MIT Press, 1949).
313. Dey, N., Blanc-Feraud, L., Zimmer, C., Roux, P., Kam, Z., Olivo-Marin, J.-C. & Zerubia, J. Richardson–Lucy algorithm with total variation regularization for 3D confocal microscope deconvolution. *Microsc. Res. Tech.* **69(4),** 260–266 (2006). https://doi.org/10.1002/jemt.20294.

314. Landweber, L. An Iteration Formula for Fredholm Integral Equations of the First Kind. *Am. J. Math.* **73(3),** 615 (1951). https://doi.org/10.2307/2372313.

315. Richardson, W. H. Bayesian-Based Iterative Method of Image Restoration*. *J. Opt. Soc. Am.* **62(1),** 55 (1972). https://doi.org/10.1364/JOSA.62.000055.

316. Lucy, L. B. & B., L. An iterative technique for the rectification of observed distributions. *Astron. J.* **79(6),** 745 (1974). https://doi.org/10.1086/111605.

317. Sage, D., Donati, L., Soulez, F., Fortun, D., Schmit, G., Seitz, A., Guiet, R., Vonesch, C. & Unser, M. DeconvolutionLab2: An open-source software for deconvolution microscopy. *Methods* 115**,** 28–41 (2017). https://doi.org/10.1016/j.ymeth.2016.12.015.

318. Lim, S. & Ye, J. C. Blind Deconvolution Microscopy Using Cycle Consistent CNN with Explicit PSF Layer. in *Lect. Notes Comput. Sci. (including Subser. Lect. Notes Artif. Intell. Lect. Notes Bioinformatics)* 11905 LNCS**,** 173–180 (Springer, 2019). https://doi.org/10.1007/978-3-030-33843-5_16.

319. Swedlow, J. R. Quantitative Fluorescence Microscopy and Image Deconvolution. in *Methods Cell Biol.* 407–426 (2013). https://doi.org/10.1016/B978-0-12-407761-4.00017-8.

320. Baster, Z., Li, L., Rajfur, Z. & Huang, C. Talin2 mediates secretion and trafficking of matrix metallopeptidase 9 during invadopodium formation. *Biochim. Biophys. Acta - Mol. Cell Res.* **1867(7),** 118693 (2020). https://doi.org/10.1016/j.bbamcr.2020.118693.

321. Boutet de Monvel, J., Le Calvez, S. & Ulfendahl, M. Image Restoration for Confocal Microscopy: Improving the Limits of Deconvolution, with Application to the Visualization of the Mammalian Hearing Organ. *Biophys. J.* **80(5),** 2455–2470 (2001). https://doi.org/10.1016/S0006-3495(01)76214-5.

322. Day, K. J., La Rivière, P. J., Chandler, T., Bindokas, V. P., Ferrier, N. J. & Glick, B. S. Improved deconvolution of very weak confocal signals. *F1000Research* 6**,** 787 (2017). https://doi.org/10.12688/f1000research.11773.1.

323. Mukamel, E. A., Babcock, H. & Zhuang, X. Statistical Deconvolution for Superresolution Fluorescence Microscopy. *Biophys. J.* **102(10),** 2391–2400 (2012). https://doi.org/10.1016/j.bpj.2012.03.070.

324. Müller, M., Mönkemöller, V., Hennig, S., Hübner, W. & Huser, T. Open-source image reconstruction of super-resolution structured illumination microscopy data in ImageJ. *Nat. Commun.* **7(1),** 10980 (2016). https://doi.org/10.1038/ncomms10980.

325. Dougherty, R. Extensions of DAMAS and Benefits and Limitations of Deconvolution in Beamforming. in *11th AIAA/CEAS Aeroacoustics Conf.* (American Institute of Aeronautics and Astronautics, 2005). https://doi.org/10.2514/6.2005-2961.

326. Wendykier, P. High Performance Java Software for Image Processing. (2009).

327. Jin, L., Liu, B., Zhao, F., Hahn, S., Dong, B., Song, R., Elston, T. C., Xu, Y. & Hahn, K. M. Deep learning enables structured illumination microscopy with low light levels and enhanced speed. *Nat. Commun.* **11(1),** (2020). https://doi.org/10.1038/s41467-020-15784-x.

328. Möckl, L., Roy, A. R. & Moerner, W. E. Deep learning in single-molecule microscopy: fundamentals, caveats, and recent developments [Invited]. *Biomed. Opt. Express* **11(3),** 1633 (2020). https://doi.org/10.1364/BOE.386361.

329. de Haan, K., Rivenson, Y., Wu, Y. & Ozcan, A. Deep-Learning-Based Image Reconstruction and Enhancement in Optical Microscopy. *Proc. IEEE* **108(1),** 30–50 (2020). https://doi.org/10.1109/JPROC.2019.2949575.

330. Rivenson, Y., Göröcs, Z., Günaydin, H., Zhang, Y., Wang, H. & Ozcan, A. Deep learning microscopy. *Optica* **4(11),** 1437 (2017). https://doi.org/10.1364/OPTICA.4.001437.

331. Antun, V., Renna, F., Poon, C., Adcock, B. & Hansen, A. C. On instabilities of deep learning in image reconstruction and the potential costs of AI. *Proc. Natl. Acad. Sci.* 201907377 (2020). https://doi.org/10.1073/pnas.1907377117.

332. Qi, L., Kolodziej, T., Rajfur, Z. & Huang, C. Roles of Talin2 in Traction Force Generation, Tumor Metastasis and Cardiovascular Integrity. *Curr. Protein Pept. Sci.* **19(11),** 1071–1078 (2018). https://doi.org/10.2174/1389203719666180809094731.

333. Wen, Z., Liang, Y., Deng, S., Zou, L., Xie, X., Yang, J. & Wu, Y. Talin2 regulates invasion of human breast cancer MDA-MB-231 cells via alteration of the tumor microenvironment. *Oncol. Lett.* **17(6),**

4835–4842 (2019). https://doi.org/10.3892/ol.2019.10175.

334. Liang, Y., Chen, H., Ji, L., Du, J., Xie, X., Li, X. & Lou, Y. Talin2 regulates breast cancer cell migration and invasion by apoptosis. *Oncol. Lett.* **16(1),** 285–293 (2018). https://doi.org/10.3892/ol.2018.8641.

335. Ouyang, W., Aristov, A., Lelek, M., Hao, X. & Zimmer, C. Deep learning massively accelerates super-resolution localization microscopy. *Nat. Biotechnol.* **36(5),** 460–468 (2018). https://doi.org/10.1038/nbt.4106.

336. Järveläinen, H., Sainio, A., Koulu, M., Wight, T. N. & Penttinen, R. Extracellular matrix molecules: Potential targets in pharmacotherapy. *Pharmacol. Rev.* **61(2),** 198–223 (2009). https://doi.org/10.1124/pr.109.001289.

337. Frantz, C., Stewart, K. M. & Weaver, V. M. The extracellular matrix at a glance. *J. Cell Sci.* **123(24),** 4195–4200 (2010). https://doi.org/10.1242/jcs.023820.

338. Bonnans, C., Chou, J. & Werb, Z. Remodelling the extracellular matrix in development and disease. *Nat. Rev. Mol. Cell Biol.* **15(12),** 786–801 (2014). https://doi.org/10.1038/nrm3904.

339. Tanzer, M. L. Current concepts of extracellular matrix. *J. Orthop. Sci.* **11(3),** 326–331 (2006). https://doi.org/10.1007/s00776-006-1012-2.

340. Nallanthighal, S., Heiserman, J. P. & Cheon, D.-J. The Role of the Extracellular Matrix in Cancer Stemness. *Front. Cell Dev. Biol.* 7**,** 86 (2019). https://doi.org/10.3389/fcell.2019.00086.

341. Yamada, K. M., Collins, J. W., Cruz Walma, D. A., Doyle, A. D., Morales, S. G., Lu, J., Matsumoto, K., Nazari, S. S., Sekiguchi, R., Shinsato, Y. & Wang, S. Extracellular matrix dynamics in cell migration, invasion and tissue morphogenesis. *Int. J. Exp. Pathol.* **100(3),** 144–152 (2019). https://doi.org/10.1111/iep.12329.

342. Hartman, C. D., Isenberg, B. C., Chua, S. G. & Wong, J. Y. Extracellular matrix type modulates cell migration on mechanical gradients. *Exp. Cell Res.* **359(2),** 361–366 (2017). https://doi.org/10.1016/j.yexcr.2017.08.018.

343. van Helvert, S., Storm, C. & Friedl, P. Mechanoreciprocity in cell migration. *Nat. Cell Biol.* **20(1),** 8–20 (2018). https://doi.org/10.1038/s41556-017-0012-0.

344. Yamada, K. M. & Sixt, M. Mechanisms of 3D cell migration. *Nat. Rev. Mol. Cell Biol.* **20(12),** 738–752 (2019). https://doi.org/10.1038/s41580-019-0172-9.

345. Burridge, K. Focal adhesions: a personal perspective on a half century of progress. *FEBS J.* **284(20),** 3355–3361 (2017). https://doi.org/10.1111/febs.14195.

346. Wozniak, M. A., Modzelewska, K., Kwong, L. & Keely, P. J. Focal adhesion regulation of cell behavior. *Biochim. Biophys. Acta - Mol. Cell Res.* **1692(2–3),** 103–119 (2004). https://doi.org/10.1016/j.bbamcr.2004.04.007.

347. Hennig, K., Wang, I., Moreau, P., Valon, L., DeBeco, S., Coppey, M., Miroshnikova, Y. A., Albiges-Rizo, C., Favard, C., Voituriez, R. & Balland, M. Stick-slip dynamics of cell adhesion triggers spontaneous symmetry breaking and directional migration of mesenchymal cells on one-dimensional lines. *Sci. Adv.* **6(1),** eaau5670 (2020). https://doi.org/10.1126/sciadv.aau5670.

348. Gupton, S. L. & Waterman-Storer, C. M. Spatiotemporal Feedback between Actomyosin and Focal-Adhesion Systems Optimizes Rapid Cell Migration. *Cell* **125(7),** 1361–1374 (2006). https://doi.org/10.1016/j.cell.2006.05.029.

349. Kim, D. H. & Wirtz, D. Focal adhesion size uniquely predicts cell migration. *FASEB J.* **27(4),** 1351–1361 (2013). https://doi.org/10.1096/fj.12-220160.

350. Shemesh, T., Geiger, B., Bershadsky, A. D. & Kozlov, M. M. Focal adhesions as mechanosensors: A physical mechanism. *Proc. Natl. Acad. Sci. U. S. A.* **102(35),** 12383–12388 (2005). https://doi.org/10.1073/pnas.0500254102.

351. Geiger, B., Spatz, J. P. & Bershadsky, A. D. Environmental sensing through focal adhesions. *Nat. Rev. Mol. Cell Biol.* **10(1),** 21–33 (2009). https://doi.org/10.1038/nrm2593.

352. Morgan, M. R., Humphries, M. J. & Bass, M. D. Synergistic control of cell adhesion by integrins and syndecans. *Nat. Rev. Mol. Cell Biol.* **8(12),** 957–969 (2007). https://doi.org/10.1038/nrm2289.

353. Zaidel-Bar, R., Itzkovitz, S., Ma'ayan, A., Iyengar, R. & Geiger, B. Functional atlas of the integrin adhesome. *Nat. Cell Biol.* **9(8),** 858–867 (2007). https://doi.org/10.1038/ncb0807-858.

354. Kanchanawong, P., Shtengel, G., Pasapera, A. M., Ramko, E. B., Davidson, M. W., Hess, H. F. & Waterman, C. M. Nanoscale architecture of integrin-based cell adhesions. *Nature* **468(7323),** 580–

584 (2010). https://doi.org/10.1038/nature09621.

355. Gardel, M. L., Schneider, I. C., Aratyn-Schaus, Y. & Waterman, C. M. Mechanical integration of actin and adhesion dynamics in cell migration. *Annu. Rev. Cell Dev. Biol.* 26**,** 315–33 (2010). https://doi.org/10.1146/annurev.cellbio.011209.122036.

356. Choi, C. K., Vicente-Manzanares, M., Zareno, J., Whitmore, L. A., Mogilner, A. & Horwitz, A. R. Actin and α-actinin orchestrate the assembly and maturation of nascent adhesions in a myosin II motor-independent manner. *Nat. Cell Biol.* **10(9),** 1039–1050 (2008). https://doi.org/10.1038/ncb1763.

APPENDIX – PUBLICATION I

BatchDeconvolution: a Fiji plugin for increasing deconvolution workflow

Zbigniew Baster, Zenon Rajfur

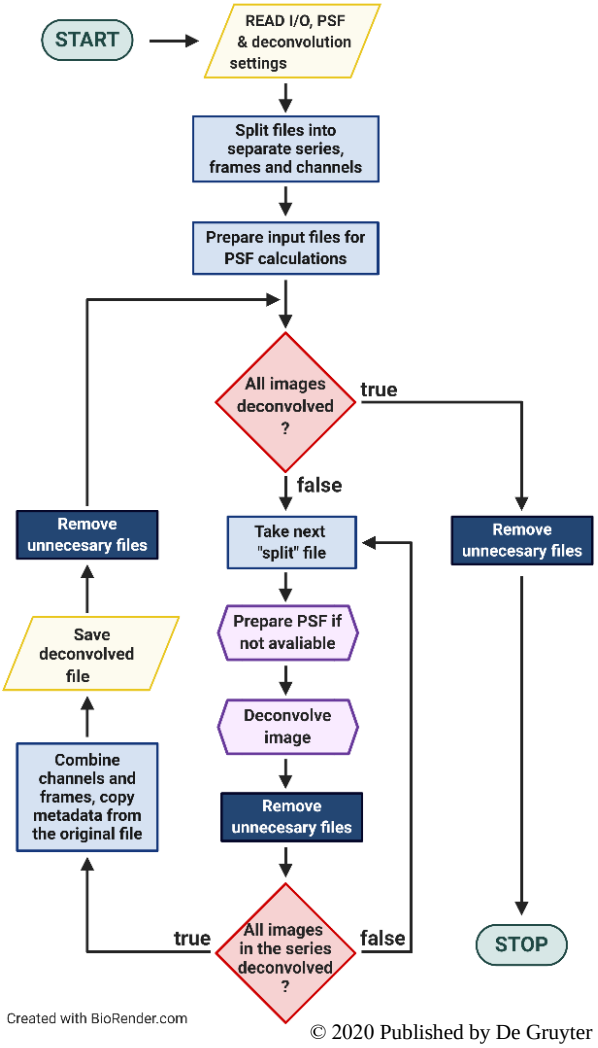

Highlights

- There are several open access deconvolution microscopy programs.
- Most of them have a limited capability of processing multiple files in a single session.
- A *Fiji* plugin has been developed to process multi-position multi-channel time-lapse image files.
- It links functionalities of *PSF Generator* and *DeconvolutionLab2* programs from Biomedical Imaging Group at EPFL.
- The software is designed to work with most image file formats containing metadata, especially *raw* microscope images (e.g. czi, nd2, tif).

Zbigniew Baster* and Zenon Rajfur

BatchDeconvolution: a *Fiji* plugin for increasing deconvolution workflow

https://doi.org/10.1515/bams-2020-0027
Received May 7, 2020; accepted August 17, 2020; published online September 9, 2020

Abstract: Deconvolution microscopy is a very useful, software-based technique allowing to deblur microscopy images and increase both lateral and axial resolutions. It can be used along with many of fluorescence microscopy imaging techniques. By increasing axial resolution, it also enables three-dimensional imaging using a basic wide-field fluorescence microscope. Unfortunately, commercially available deconvolution software is expensive, while freely available programs have limited capabilities of a batch file processing. In this work we present *BatchDeconvolution*, a *Fiji* plugin that bridges two programs that we used subsequently in an image deconvolution pipeline: *PSF Generator* and *DeconvolutionLab2*, both from Biomedical Imaging Group, EPFL. Our software provides a simple way to perform a batch processing of multiple microscopy files with minimal working time required from the user.

Keywords: deconvolution microscopy; *Fiji*; image deconvolution; *ImageJ*; point spread function.

Introduction

Fluorescence microscopy is one of the most commonly used techniques in life sciences. The use of fluorescent probes allowed to tag specific proteins and structures within live or fixed cells and image them with high contrast and resolution [1]. Using a relatively low-cost fluorescence microscope, it is possible to achieve the lateral resolution as low as 200 nm [2]. Unfortunately, it is much harder to reach high resolution along the *Z* optical axis, therefore three-dimensional (3D) imaging is much more challenging [2]. There is a number of microscopy techniques allowing 3D imaging, such as confocal microscopy, 3D structured illumination microscopy, 3D stochastic optical reconstruction microscopy/photo-activated localization microscopy or light sheet microscopy, but most of them require additional, usually expensive, modules, which have to be mounted on a microscope [3].

Deconvolution microscopy is one of a few techniques that do not require any additional hardware. Based on a computational image reconstruction, it can improve both lateral and axial resolutions, allowing 3D imaging without any additional equipment cost [4]. Nevertheless, one of the main drawbacks of this technique is the requirement of vast amount of calculations, what significantly extends image preparation time [5]. Secondly, in comparison to other techniques, the intensity-based quantitative analysis on deconvolved images is much more challenging due to nonlinear operations required for image reconstruction [6].

An image of a single bright point is visible as a characteristic diffraction-based pattern called point spread function (PSF) (Figure 1A) which is specific for every optical set-up [4]. It is shaped due to physical limitation of light, physical limitations of imaging environment, and also defects and imperfections present in the imaging system. An image of a physical object (e.g. a cytoskeleton or an organelle) is a superposition of many single bright points convolved with the PSF [4]:

[1] $image = object * PSF$.

The goal of deconvolution algorithms is to reverse this process. There are two ways of obtaining a PSF. First is to measure the actual PSF on a microscope using, for example, nanometre-sized fluorescent beads [7]. This solution accounts for many of the deviations in the experimental set-up (such as flaws in the optical pathway), but the resolution of the PSF is limited by a signal-to-noise ratio, and it requires a demanding experimental procedure [7, 8]. The second approach is to calculate a theoretical PSF using one of the models approximating the optical set-up [8]. It is not restricted by the resolution limitations and it is noise free but usually cannot imitate defects of the optical set-up, as well as the experimental one [5]. Moreover, depending on the complexity of the model and its accuracy, the calculations

***Corresponding author: Zbigniew Baster**, Department of Molecular and Interfacial Biophysics, Faculty of Physics, Astronomy and Applied Computer Science, Jagiellonian University, Krakow, Poland; and Institute of Physics, Faculty of Physics, Astronomy and Applied Computer Science, Jagiellonian University, 11 Lojasiewicza Street, 30-348 Krakow, Poland. Phone: +48 12 664 48 19, E-mail: zbigniew.baster@doctoral.uj.edu.pl. https://orcid.org/0000-0002-5987-5712
Zenon Rajfur, Department of Molecular and Interfacial Biophysics, Faculty of Physics, Astronomy and Applied Computer Science, Jagiellonian University, Krakow, Poland

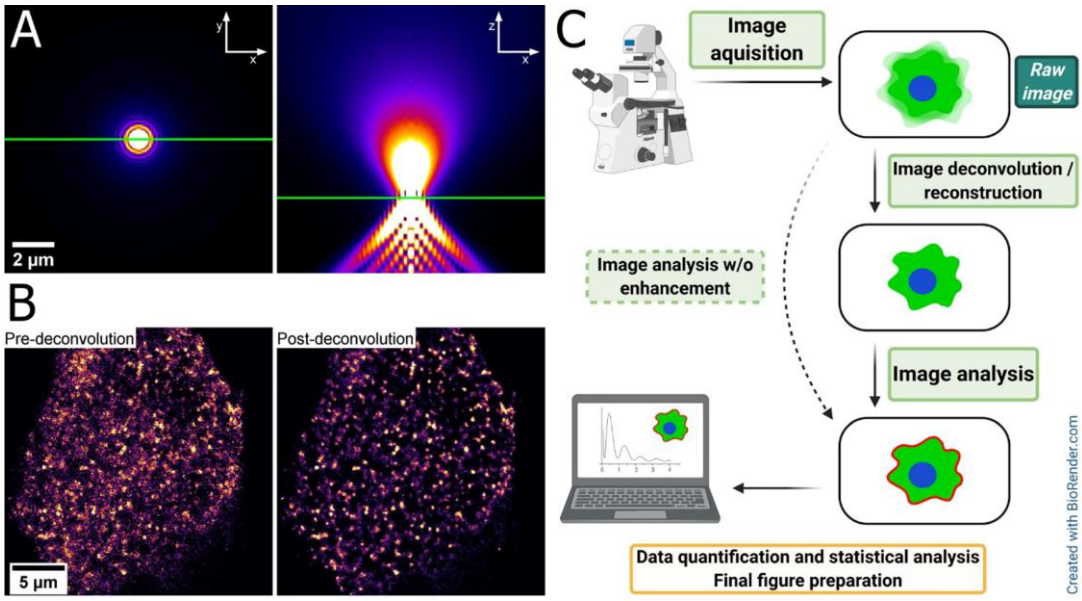

Figure 1: **Panel A** shows exemplary cross-section images of a point spread function (PSF) generated with PSF Generator using Gibson-Lanni algorithm [22]. The green lines show the orientations of the cross-sections. Image saturation level was set to 0.01 (high saturation). PSF generation parameters: $NA = 1.4$, $n_i = 1.518$, n_s=1.33, $\lambda = 561$ nm, $t_i = 170$ µm, $z_p = 2{,}000$ nm. Based on a study by Kirshner et al. [8]. **Panel B** shows an example of a deconvolved image of immunofluorescence staining of proteasomes (PSMA2 marker) in MDA-MB-231 cells (full description in a study by Baster et al. [20]). The image was collected as a z-stack of 21 slices, one of the representative intermediate slices is presented. The brightness and contrast parameter was chosen to cover 50–99% of the pixel brightness histogram, separately in the predeconvolution and postdeconvolution images. Mpl-inferno LUT was used. **Panel C** shows the microscopy image acquisition-analysis pipeline. After acquisition, depending on a type of microscopy and analysis required, image may be enhanced (e.g. reconstructed or deconvolved) and then subjected to image analysis, or analysed without any additional intermediate steps. The final step is the data extraction, statistical analysis (if applicable), and preparation of a figure for presentation. Each of the steps can be automated to some extent.

can be highly time consuming. Whether it is better to use an experimental or a theoretical PSF it needs to be evaluated on a case-by-case basis [5].

There are several deconvolution algorithms that depend on different approaches and mathematical models and have different strengths and limitations [4, 9]. Most of them (if not all) carry out calculations in Fourier space to simplify operations [10]. Deconvolution can be applied to regular widefield microscopy and also to standard 3D techniques, such as confocal microscopy, in order to further increase contrast and resolution (Figure 1B) [11, 12]. Beside reducing out of focus light, deconvolution can also be used for deblurring single-slice images.

There are several commercially available deconvolution software such as *Huygens* (Scientific Volume Imaging) or *AutoQuant X3* (Media Cybernetics) allowing batch processing of many images. Their main drawback is their high cost. There are several free, usually open-source, alternatives, such as *DeconvolutionLab* and *DeconvolutionLab2* (Biomedical Imaging Group, EPFL) [9], *Iterative Deconvolve 3D* (OptiNav) [13], or *Parallel Iterative Deconvolution* (Piotr Wendykier) [14]. They are in general less user-friendly than commercial ones and they have limited batch processing capabilities, especially in cases requiring more than one PSF such as multichannel images.

The microscopy image acquisition-analysis pipeline can be separated into several stages, that, to some extent, might be automated (Figure 1C). One of the facts advocating for automatization, is that it increases data processing reproducibility. Furthermore, it also serves as an additional pair (or rather many pairs) of hands allowing one to address one's attention to other matters, after starting calculations.

In this work, we present *BatchDeconvolution* a bridging *Fiji* plugin, allowing a batch processing of multiple optical microscopy images. The software employs currently available programs and plugins for PSF generation and deconvolution, binding them together, providing a user-friendly deconvolution platform of multiposition, time-lapse, multichannel, z-stack raw ("straight from a microscope") image files.

Material and methods

PSF Generator [8] v. 18.12.2017 was downloaded from http://bigwww.epfl.ch/algorithms/psfgenerator/, and its source code was obtained from https://github.com/Biomedical-Imaging-Group/PSFGenerator. *DeconvolutionLab2* [9], version 2.1.2 was downloaded from http://bigwww.epfl.ch/deconvolution/deconvolutionlab2/, and its source code was obtained from https://github.com/Biomedical-Imaging-Group/DeconvolutionLab2. FFTW2 dynamic libraries for *DeconvolutionLab2* were downloaded from http://bigwww.epfl.ch/deconvolution/deconvolutionlab2/.

The software was developed using *Java 1.8* (Oracle) in NetBeans IDE 8.2 environment (Oracle). It was tested using *Fiji* [15] and *ImageJ* [16].

Results and discussion

During our research in the field of cell migration and mechanotransduction, we have found that using elastic polyacrylamide gels [17] to mimic tissue stiffness causes blurring and distortion of microscopy images. It is a result of a more complex optical set-up than in a case of cells plated directly on a glass or a plastic substrate. This phenomenon impedes the analysis of obtained images. By applying image deconvolution, we were able to improve quality of these images. Unfortunately, at that point none of the freely available software allowed us a batch files processing to the satisfactory extent. Furthermore, because we were often collecting confocal images of different image and voxel sizes, we needed to calculate a PSF matching every of our images. To address this problem, we checked several *ImageJ/Fiji* plugins allowing to calculate a theoretical PSF and to deconvolve images. We determined that the most suitable programs to use in a batch processing would be *PSF Generator* [8] and *DeconvolutionLab* (and later *DeconvolutionLab2*, that was applied in the final version of our software) [9] from Biomedical Imaging Group, EPFL. First, both are accessible from a command line (*Fiji* or system), what is essential for scripting. Secondly, they both offer a vast range of algorithms and a user-friendly environment. Although, *DeconvolutionLab* and *DeconvolutionLab2* provide an option of batch image processing, their application is limited. Thus, we decided to develop a separate software that would meet our requirements (see Table 1 for comparison of batch processing algorithms properties between programs).

We implemented both programs into our new bridging *Fiji* plugin we named *BatchDeconvolution*. The graphical user interface was created to mirror most of the options from the base programs (Supplementary Figure 1). We implemented also *BioFormats* repository [18] to enable read-out of most of the popular image formats including their metadata. The access to metadata allowed us to process images of a different voxel and image sizes and number of time points. Therefore, the only common parameter between image files has to be their channel structure which is defined ununiformly between file formats. Because calculations create a high amount of intermediate data (from 2 to 9 times of the size of the original data), we made our plugin to process files in a sequential manner with several check points allowing to delete expendable files (Figure 2, Supplementary Data: Pseudocode). We also implemented option for providing an external PSF (e.g. experimental).

Algorithm testing

We checked our software at all crucial stages of the development for generating results identical to the ones

Table 1: The comparison of batch processing properties of different software.

Property	*DeconvolutionLab*	*DeconvolutionLab2*	*BatchDeconvolution*
Batch image processing	Yes (processing of the whole directory)	Yes (each file has to be scripted separately)	Yes (processing of the whole directory)
Multichannel images processing	No	No	Yes (all files have to have the same channel structure)
Time-lapse images processing	No	No	Yes
Multiposition files processing	No	No	Limited (all positions have to have the same acquisition parameters i.e. number of frames, slices, channel and resolution)
PSF generation	No	Limited (basic algorithms)	Yes (automatic matching parameters with the image)
Image preparation (raw image processing)	Channel, time point and multiposition splitting required	Channel, time point and multiposition splitting required	Not required

PSF, point spread function.

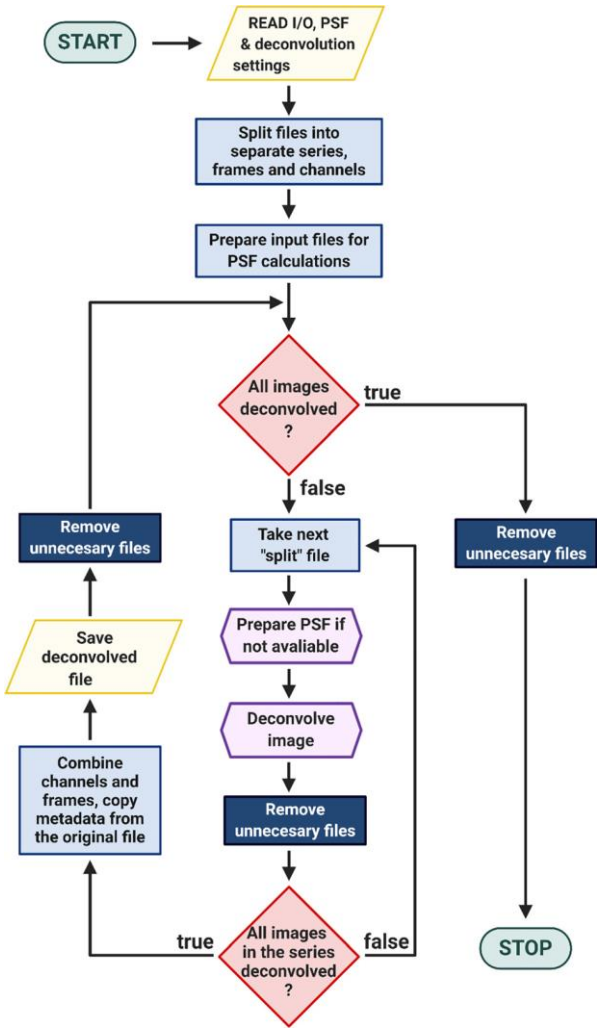

Figure 2: A simplified flowchart of the *BatchDeconvolution*'s algorithm.

generated by the stand-alone base software (*PSF Generator* and *DeconvolutionLab2*). For format compatibility tests, we used all the images available from The Open Microscopy Environment sample images repository [19]. We run the tests on Personal Computers with at least 16 GB of RAM. All the files that met the software requirements (especially: the requirement of an image to have a defined scale; and in case of a multiposition file, the requirement all of images in the file to have the same structure) passed the test. Due to the implementation of *BioFormats* library, we expect that our program will read all the formats covered by the library.

The software has been routinely used (one bachelor thesis, one published article [20], two manuscripts *in review*, two manuscripts *in preparation*) on several different Personal Computers, at different stages of the program's development. Images, that we used, were collected using Nikon wide-field fluorescence microscope or Nikon A1 confocal microscope with NIS Elements Software, Zeiss LSM 710 confocal microscope with ZEN Black software, or Zeiss wide-field fluorescence microscope with ZEN Blue software (.tif, .nd2 and .czi file formats). During our work, we found that only the amount of RAM is crucial for the proper execution of calculations. We were using Personal Computers with the memory of 4–32 GB. In a small number of cases of processing large images on low-memory computers, the software was unable to finalize calculations. Running the software on a higher-RAM computer usually solved the problem. Furthermore, when we had tried to run the stand-alone base software with the same files and parameters, we got the same errors. Thus, we believe that our bridging algorithm has no or a marginal influence on the calculations performance. Other computer components affected calculations only in regard to computing time.

Conclusions

In our work, we bridged *PSF Generator* and *DeconvolutionLab2* programs with a *Fiji* plugin, and we named it *BatchDeconvolution*. We found our solution very useful for processing and analysing large amount of microscopy images. *BatchDeconvolution* provides a user-friendly, intuitive interface, allowing to process a large number of images without a requirement of any additional *Fiji* scripting. Applying *BioFormats* repository allows the software to access metadata of many file formats, that simplifies preparation of program input files and parameters.

Footnotes

Citation

We would like to emphasize that while citing our software, *PSF Generator* [8] and *DeconvolutionLab2* [9] should be cited as well.

Access

The source code and the build version of our software are available to download from https://github.com/Mechanobiology-Lab/BatchDeconvolution.

Troubleshooting

(1) While testing, we found that repetitive calling *DeconvolutionLab2* from *Fiji* command line causes memory build-up within the system. We overcome that by calling *DeconvolutionLab2* externally from the system command line. The drawback of that solution is that Fast Fourier Transform library *JTransforms* [21] that was called by *DeconvolutionLab2* through *Fiji*, is no longer available.
(2) BatchDeconvolution was designed and tested with a fresh installation of *Fiji*. It is incompatible with a clean version of *ImageJ*.

Acknowldgements: The authors would like to thank Olga Adamczyk (Institute of Physics, Jagiellonian University) for providing images for testing the software and Miranda Lin (Markey Cancer Center, University of Kentucky) for insightful comments on the project.
Research funding: This work was supported by the Polish National Science Centre PRELUDIUM grant no. 2018/31/N/NZ3/02031 (to ZB), and the Polish National Science Centre ETIUDA scholarship no. 2019/32/T/NZ3/00444 (to ZB).
Author contributions: Z.B. designed and wrote the software, performed tests, and wrote the manuscript; Z.R. supervised software testing and contributed to the manuscript discussion and writing. All the authors have accepted responsibility for the entire content of this submitted manuscript and approved submission.
Competing interests: The funding organization(s) played no role in the study design; in the collection, analysis, and interpretation of data; in the writing of the report; or in the decision to submit the report for publication.
Ethical approval: The conducted research is not related to either human or animal use.

References

1. Drummen G. Fluorescent probes and fluorescence (microscopy) techniques — illuminating biological and biomedical research. Molecules 2012;17:14067–90.
2. Combs CA, Shroff H. Fluorescence microscopy: a concise guide to current imaging methods. Curr Protoc Neurosci 2017;79. https://doi.org/10.1002/cpns.29.
3. Fischer RS, Wu Y, Kanchanawong P, Shroff H, Waterman CM. Microscopy in 3D: a biologist's toolbox. Trends Cell Biol 2011;21:682–91.
4. Sibarita JB. Deconvolution microscopy. Adv Biochem Eng Biotechnol 2005;95:201–43.
5. McNally JG, Karpova T, Cooper J, Conchello JA. Three-dimensional imaging by deconvolution microscopy. Methods 1999;19:373–85.
6. Lee JS, Wee TLE, Brown CM. Calibration of wide-field deconvolution microscopy for quantitative fluorescence imaging. J Biomol Tech 2014;25:31–40.
7. Cole RW, Jinadasa T, Brown CM. Measuring and interpreting point spread functions to determine confocal microscope resolution and ensure quality control. Nat Protoc 2011;6:1929–41.
8. Kirshner H, Aguet F, Sage D, Unser M. 3-D PSF fitting for fluorescence microscopy: implementation and localization application. J Microsc 2013;249:13–25.
9. Sage D, Donati L, Soulez F, Fortun D, Schmit G, Seitz A, et al. DeconvolutionLab2: an open-source software for deconvolution microscopy. Methods 2017;115:28–41.
10. Swedlow JR. Quantitative fluorescence microscopy and image deconvolution. In: Methods in cell biology. Cambridge, MA: Academic Press; 2013:407–26 pp.
11. Boutet de Monvel J, Le Calvez S, Ulfendahl M. Image restoration for confocal microscopy: improving the limits of deconvolution, with application to the visualization of the mammalian hearing organ. Biophys J 2001;80:2455–70.
12. Day KJ, La Rivière PJ, Chandler T, Bindokas VP, Ferrier NJ, Glick BS. Improved deconvolution of very weak confocal signals. F1000Research 2017;6:787.
13. Dougherty R. Extensions of DAMAS and benefits and limitations of deconvolution in beamforming. In: 11th AIAA/CEAS aeroacoustics conference. Reston, Virigina: American Institute of Aeronautics and Astronautics; 2005.
14. Wendykier P. High performance Java software for image processing. Atlanta: Emory University; 2009.
15. Schindelin J, Arganda-Carreras I, Frise E, Kaynig V, Longair M, Pietzsch T, et al. Fiji: an open-source platform for biological-image analysis. Nat Methods 2012;9:676–82.
16. Schneider CA, Rasband WS, Eliceiri KW. NIH Image to ImageJ: 25 years of image analysis. Nat Methods 2012;9:671–5.
17. Tse JR, Engler AJ. Preparation of hydrogel substrates with tunable mechanical properties. Curr Protoc Cell Biol 2010;47.
18. Linkert M, Rueden CT, Allan C, Burel J-M, Moore W, Patterson A, et al. Metadata matters: access to image data in the real world. J Cell Biol 2010;189:777–82.
19. The open microscopy environment. Image repository. Available from: https://downloads.openmicroscopy.org/images/ [accessed 2020 Apr 3].
20. Baster Z, Li L, Rajfur Z, Huang C. Talin2 mediates secretion and trafficking of matrix metallopeptidase 9 during invadopodium formation. Biochim Biophys Acta Mol Cell Res 2020;1867:118693.
21. Wendykier P, Nagy JG. Large-scale image deblurring in Java. In: Bubak M, van Albada GD, Dongarra J, Sloot PMA, editors Computational science – ICCS 2008, 8th international conference Kraków, Poland, June 23–25, 2008, Proceedings, Part I. Springer, Berlin, Heidelberg; 2008 721–30 pp.
22. Gibson SF, Lanni F. Diffraction by a circular aperture as a model for three-dimensional optical microscopy. J Opt Soc Am A 1989;6:1357. Available from: https://www.osapublishing.org/abstract.cfm?URI=josaa-6-9-1357 [accessed 2017 Jun 29].

Supplementary material: The online version of this article offers supplementary material (https://doi.org/10.1515/bams-2020-0027).

Supplementary Images

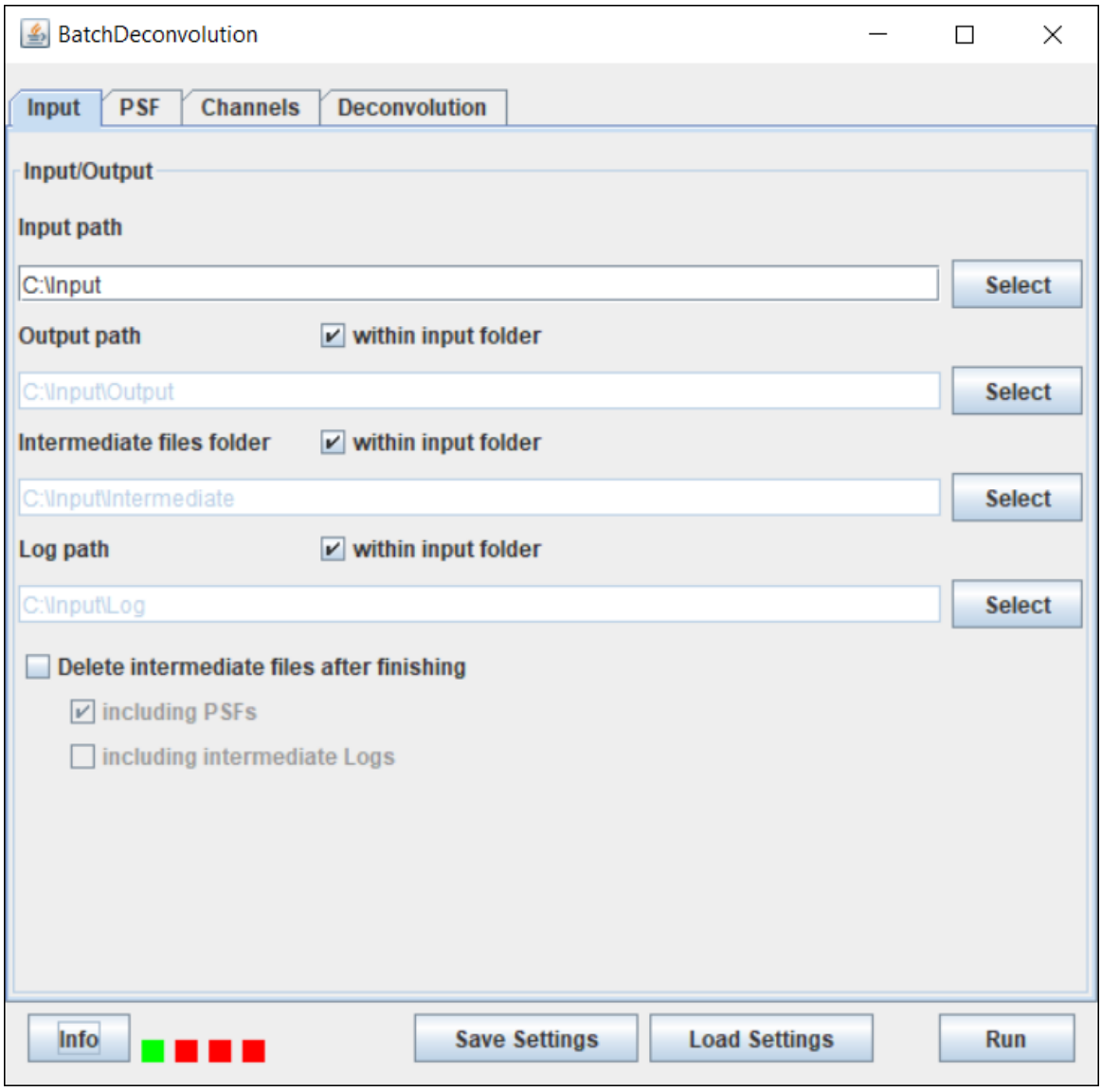

Supplementary Fig. 1. The initial screen of the *Batch Deconvolution* Graphical User Interface.

Supplementary Data

Pseudocode

1. Read parameters.
2. *LOOP* for all files in the input folder:
    A. Read a file.
    B. Split the file into z-stacks of separate positions, frames, and channels.
    C. Collect data of pixel and image sizes for every file for further PSF calculations (if selected).
    D. Save split files.
3. *LOOP* for pixel and image sizes data (if a PSF is not provided):

    Option I: calculate a PSF for every image.

        Prepare a PSF config file (see *PSF Generator instruction*) for every channel (excluding brightfield) of every file.

    Option II: calculate a PSF once for similar images.

        Prepare a PSF config file for every channel of every voxel size, taking the PSF image dimensions from maxima of images of a common voxel size.
4. *IF* a PSF is provided, load it, split into channels, and save as separate files.
5. *LOOP* for all the files in the input folder:
    A. *LOOP* for all the split files from one position:
        a. If the image is of a brightfield channel, copy the image into the intermediate deconvolved images folder.
        b. Calculate a PSF using *PSF Generator* if was not calculated earlier or not provided.

c. Deconvolve the image using *DeconvolutionLab2*. Save the deconvolved image to the intermediate deconvolved images folder.

d. (*IF* option chosen) Delete the split file.

B. Combine all files from the single position (channels, frames), and save it to the output folder.

C. (*IF* option chosen) Delete expendable images from the intermediate deconvolved images folder (single-frame, single-channel images).

D. *IF* a PSF is to be calculated for every file, delete expendable PSFs (*IF* option to delete files chosen).

6. Create the condense Log file
7. (*IF* option chosen)Delete all intermediate files.

Further troubleshooting

1. For parameters optimization we recommend first to work with stand-alone *PSF Generator* and *DeconvolutionLab2* separately and then to input settings into *BatchDeconvolution* for the batch processing.
2. *BatchDeconvolution* reads a voxel size from an image metadata. Such information must be provided for a proper work of the software.
3. Pixel calibration can be set in any units. Their relation to the SI units has to be provided first in *units.dat* file within the *BatchDeconvolution* folder. Some most common units are already provided.
4. If a PSF file is provided, it either has to match the channel structure of the image file (including brightfield channel(s) – though, these channels will not be taken into account) or has to have the same number of fluorescence channels as the image file.

BatchDeconvolution software will account for the different channel structure resulting from missing brightfield channel(s).

5. *Log.dat* file (in *Log* folder) contains condense information about deconvolution process. Check it after processing for eventual errors.
6. The list of file formats supported by *BatchDeconvolution* is included in *extensions.dat* file within the *BatchDeconvolution* folder. We tried to include all the file formats readable by *BioFormats* library. If the library supports an additional file format that is not included in *extensions.dat* file, adding the extension to the data file may allow *BatchDeconvolution* to read the image file.

APPENDIX – PUBLICATION II

Talin2 mediates secretion and trafficking of matrix metallopeptidase 9 during invadopodium formation

Zbigniew Baster, Liqing Li, Zenon Rajfur, Cai Huang

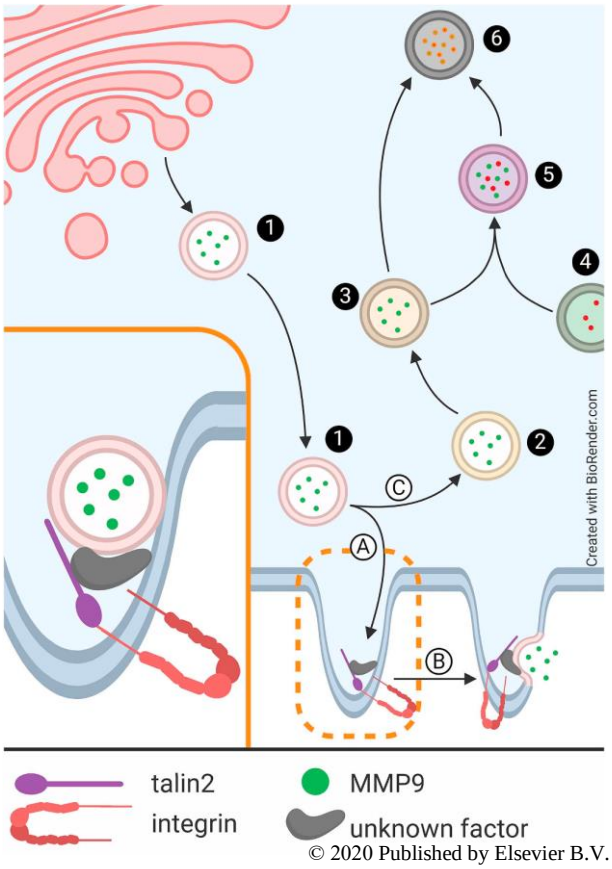

Highlights

- Blocking talin2 expression in breast cancer cells inhibits MMP2 and MMP9 secretion, therefore, inhibits ECM degradation.
- S339C mutation in talin2, that results in reduced affinity towards β1 integrin, also causes MMP9 secretion inhibition.
- Interaction between talin2 and β1 integrin is required for MMP9 vesicle docking.
- Inhibition of MMP9 secretion caused an accumulation of enlarged MMP9-containing vesicles in the lysosomal pathway.
- The accumulation of MMP9 suggests overflow in lysosome degradation process.

BBA - Molecular Cell Research 1867 (2020) 118693

Contents lists available at ScienceDirect

BBA - Molecular Cell Research

journal homepage: www.elsevier.com/locate/bbamcr

Talin2 mediates secretion and trafficking of matrix metallopeptidase 9 during invadopodium formation

Zbigniew Baster[a,b,*], Liqing Li[a], Zenon Rajfur[b], Cai Huang[a,**]

[a] Markey Cancer Center, University of Kentucky, Lexington, KY 40536, United States of America
[b] Institute of Physics, Faculty of Physics, Astronomy and Applied Computer Science, Jagiellonian University, Krakow, Poland

ARTICLE INFO

Keywords:
Matrix metallopeptidase 9
Talin2
β-Integrin
Invadopodia
Metastasis
ECM degradation

ABSTRACT

Talin2 plays an important role in transduction of mechanical signals between extracellular matrix and actin cytoskeleton. Recent studies showed that talin2 is localized to invadopodia and regulates their maturation, subsequently cancer cell invasion and metastasis. However, the molecular mechanism whereby talin2 mediates invadopodium maturation is unknown. Here we show that ablation of talin2 in MDA-MB-231 cells inhibited the secretion of matrix metallopeptidase 9 (MMP9), a proteinase involved in extracellular matrix degradation in invadopodium maturation and metastasis. Furthermore, re-expression of talin2^{WT} in talin2-KO cells rescued MMP9 secretion, but talin2^{S339C}, a mutant with reduced β-integrin binding, did not, indicating that the talin2-β-integrin interaction is involved in the MMP9 secretion. Moreover, ablation of talin2 caused an accumulation of enlarged MMP9 vesicles. These vesicles co-localized with enlarged early, late endosomes and autophagosomes, suggesting talin2 controls MMP9 trafficking process. Therefore, these data suggest that talin2 regulates extracellular matrix degradation and invadopodium maturation by mediating MMP9 secretion.

1. Introduction

Talin is a large focal adhesion protein playing a key role in transmitting mechanical signals from extracellular matrix (ECM) to cells cytoskeleton. It is composed of two distinguished domains [1]: a N-terminal FERM domain responsible for interaction with β-integrin tail [2,3], and a large C-terminal rod domain with 13 subdomains, that has several vinculin- and actin-binding sites [3–5].

In vertebrates, there are two genes responsible for coding two variants of talin: TLN1 and TLN2 encoding talin1 and talin2, respectively [6]. While talin1 is usually associated with cell migration [7], metastasis [8,9], focal adhesion dynamics [7,9–11], and invadopodium formation [12], the biological role of talin2 is less understood. Furthermore, talin2 is localized in invadopodia, a key cellular structure critical for cancer cell invasion and metastasis, and depletion of talin2 in cells severely decreases extracellular matrix degradation [13,14]. However, the molecular mechanism by which talin2 mediates extracellular matrix degradation is unknown. Recent studies show that talin2 has a higher affinity towards β-integrin than talin1, with Ser339 being the key residue responsible for that interaction; Ser339 mutation causes a severe decrease in binding talin2 to β-integrin [14,15].

Matrix metallopeptidase 9 (MMP9) is a member of zinc-metalloproteinases family. It is involved in many physiological and pathophysiological processes, such as embryogenesis [16], synaptic plasticity [17], and metastasis [18]. It has been reported that MMP9 is one of the key proteins required for cancer invasion and invadopodia formation [19–21], but the molecular mechanism that regulates MMP9 secretion during cancer cell invasion still remains to be elucidated.

In the present study, we investigated the role of talin2 in mediating secretion and trafficking of matrix metallopeptidase 9 during invadopodium formation in different tumor cell lines. We show that MMP9 co-localizes with cortactin and talin2 at invadopodia. Although ablation of talin2 did not inhibit MMP9 expression [13], we found that it blocked docking of MMP9 vesicles to ventral membranes and resulted in a significant decrease in secretion of MMP9, which is consistent with the previously reported dependence of MMPs secretion on integrins

Abbreviations: MMP9, matrix metallopeptidase 9; ITGB1, β1-integrin; TLN1/2, talin 1/2; EGF, epidermal growth factor; HGF, hepatocyte growth factor; Baf, bafilomycin; CQ, chloroquine; ECM, extracellular matrix

* Correspondence to: Z. Baster, Institute of Physics, Faculty of Physics, Astronomy and Applied Computer Science, Jagiellonian University, 11 Lojasiewicza Street, 30-348 Krakow, Poland.
** Correspondence to: C. Huang, Markey Cancer Center University of Kentucky, Todd Building, Room 551 789 South Limestone Street, Lexington, KY 40536, United States of America.
E-mail addresses: zbigniew.baster@doctoral.uj.edu.pl (Z. Baster), cai-huang@uky.edu (C. Huang).

https://doi.org/10.1016/j.bbamcr.2020.118693
Received 16 November 2019; Received in revised form 21 February 2020; Accepted 3 March 2020
Available online 18 March 2020

activity [22,23]. We show that re-expression of talin2^{WT} in talin2-KO cells rescued MMP9 docking to ventral membranes, but re-expression of talin2^{S339C}, a mutant with impaired affinity towards β-integrins, did not. Moreover, in talin2-depleted cells unsecreted MMP9 vesicles were rerouted and accumulated in enlarged early, late endosomes and autophagosomes, and subsequently to lysosomes. These results suggest that talin2 mediates MMP9 secretion to modulate invadopodium maturation and cell invasion.

2. Material and methods

2.1. Reagents

Chicken Anti-talin2 polyclonal antibody (GW22654) was from Sigma. Anti-talin2 rabbit polyclonal antibody (PB9961) was from Boster (Pleasanton, CA). Anti-EEA1 rabbit monoclonal antibody (C45B10) and anti-LAMP1 mouse monoclonal antibody (D4O1S) were from Cell Signaling Technology, Inc. (Danvers, MA, USA). Anti-MMP9 rabbit polyclonal antibody (A0289), anti-Rab7A rabbit polyclonal antibody (A12784), anti-GOLGA2 rabbit polyclonal antibody (A5344), and anti-CD63 rabbit polyclonal antibody (A5271) were from ABclonal (Woburn, MA). Anti-LC3β mouse monoclonal antibody was from Santa Cruz Biotechnology (Santa Cruz, CA). Anti-cortactin mouse monoclonal antibody (clone 4F11) was from EMD Millipore. Anti-β1-integrin mouse monoclonal antibody (clone P5D2) was from R&D Systems. OregonGreen488-labeled gelatin was from Thermo Fisher. Dylight 405-labeled goat anti-chicken IgY, DyLight 550- or 633-labeled goat anti-rabbit and anti-mouse IgG (H + L) antibodies were from Immunoreagents (Raleigh, NC). Alexa Fluor 555-labeled goat anti-rabbit IgG (H + L) antibody was from Thermo Fisher. Lipofectamine LTX with PLUS Reagent was from Thermo Fisher. Lafectine RU50 transfection kit was purchased from Syd Labs (Malden, MA). Recombinant human EGF was from Akron Biotech. Recombinant human hepatocyte growth factor (HGF) was from GenScript. Bafilomycin A_1 and chloroquine were from Cayman Chemical.

2.2. Plasmid construction

Human MMP9 cDNA was PCR amplified from the cDNA of MDA-MB-231 cells using primers 5′-ctctgccctcaccatgagcc-3′/5′-tcagggcactg-caggatgtc-3′. MMP9-EGFP was constructed by amplifying the coding sequence of MMP9 using primers 5′-atcaa-gaattcgccaccatgagcctctggcagccc c-3′/5′-aattgctcgagtcctcagggcactgcag-gatgtcatagg-3′, digesting with *Eco*RI/*Xho*I, subcloning into pEGFP-N1 vector via the same sites. MMP9-DsRed was constructed by replacing the EGFP fragment of MMP9-EGFP with DsRed fragment. A pFLAG-AAS1-C1 vector with a modified Kozak sequence was constructed by digesting pEGFP-AAVS1-C1 [14] with *Age*I/*Bgl*II to cleave EGFP, and ligating with annealing oligos 5′-ccggtacgaaaatggactacaaa-gacgatgacgacaaggattacaaggatgacgacgataaga-3′/5′-gatctcttatcgtcgt-catcctt gtaatccttgtcgtcatcgtctttgtagtccattttcgta-3′. The pFLAG-AAVS1-talin2^{WT} and - AAVS1-talin2^{S339C} were constructed using the same 2-step strategy as we made pEGFP-AAVS1-talin2^{WT} and - AAVS1-talin2^{S339C} [14]. All plasmids were sequenced by Eurofins Genomics (Louisville, KY, USA).

2.3. Cell culture and transfection

Talin2-KO MDA-MB-231 cells were described previously in [14]. 4T1 murine breast cancer cells, U2 OS human bone osteosarcoma cells and MDA-MB-231 human breast cancer cells were from American Type Culture Collection and were maintained in Dulbecco's Modified Eagle Medium: Nutrient Mixture F-12 (DMEM/F12; Sigma) for 4T1 cells or Dulbecco's modified Eagle medium (DMEM; Sigma) for U-2 OS and MDA-MB-231 cells, containing 10% fetal bovine serum (FBS; Gibco), penicillin (100 U/ml) and streptomycin (100 μg/ml). MDA-MB-231 cells were transiently transfected using Lipofectamine LTX with PLUS Reagent according to the manufacturer's protocol. U2 OS were transfected using Lafectine RU50 according to the manufacturer's protocol.

2.4. Invadopodium assays

Gelatin-coated glass-bottomed dishes were prepared according to Sharma and collaborators [24]. In brief, dishes were incubated for 10 min at RT with 1 N HCl, then with 50 μg/ml poly-L-lysine for 20 min. In the meantime, Oregon Green 488-labeled gelatin (1 mg/ml) was mixed with 0.2% gelatin at 1:100 ratio, incubated in 60 °C for 20 min. and then left at RT for 5 min to cool down. Dishes were incubated with mixed gelatin in RT for 10 min, then with ice-cold 0.2% glutaraldehyde solution in 4 °C for 15 min, 5 mg/ml borohydride solution at RT for 15 min, 70% ethanol solution at RT for 15 min, and stored in 10× penicillin/streptomycin solution in 4 °C. Before plating, dishes were incubated in culture medium for an hour at RT. All solutions were prepared in PBS. Cells (1×10^5) were plated onto dishes with 0.02 μg/ml Epidermal Growth Factor (EGF) or 0.05 μg/ml HGF and cultured for 10–24 h (depended on cell lines). Cells were fixed with paraformaldehyde and stained for talin2 (or cortactin) and MMP9. Images were acquired using a confocal microscope and analyzed in Fiji ImageJ [25,26] for co-localization.

2.5. MMP secretion assays

Cells were cultured in normal culture media (10% FBS) to 80% confluence. The cells were washed 3 times with PBS and then cultured in serum-free DMEM media including 20 ng/ml HGF for 24 h. The media were collected, concentrated using Spin-X ultrafiltration concentrators (10,000 Da cut-off), and then analyzed for the secretion of MMP2 and MMP9 by Western blotting.

2.6. Real-time Q-PCR assay

Total RNA was extracted from cells with PureLink RNA kit (Ambion). cDNA was synthesized with SuperScript III First Strand Synthesis kit (Invitrogen) from 0.5 to 1.0 μg RNA samples according to the manufacturer's instructions. Quantitative reverse transcriptase PCR (RT-PCR) reactions were carried out using SYBR Green PCR master mix reagents on an ABI Onestep Plus Real-Time PCR System (Applied Biosystems). The relative quantification of gene expression for each sample was analyzed by the ΔC_t method. The following primers were used to amplify MMP2: 5′-CGCCCCCAAAACGGACAAAGA-3′ (forward) and 5′-GCAGTGGGGTCACATCGCTC-3′ (reverse); MMP9: 5′-GGACTCG GTCTTTGAGGAGC-3′ (forward) and 5′-AGCGGTCCTGGCAGAAATAG-3 (reverse); Actin was used as a housekeeping gene to normalize Ct values. Primers for Actin amplification are 5′-CAA CCG CGA GAA GAT GAC-3′ (forward) and 5′-AGG AAG GCT GGA AGA GTG-3′ (reverse). Primers were synthesized by Sigma Life Science.

2.7. Vesicle docking assay

Gelatin-coated glass-bottomed dishes were prepared as stated in invadopodium assay section, with exception of using only 0.2% unlabeled gelatin. MDA-MB-231 cells (2×10^4) were plated onto 35 mm glass-bottom dishes with 0.05 μg/ml HGF, cultured for 36 h, fixed with paraformaldehyde and stained for talin2 (or β1-integrin) and MMP9. Images were acquired using a Nikon Eclipse Ti Total Internal Reflection Fluorescence (TIRF) microscope, equipped with an oil immersion 60 × 1.45 NA objective and CoolSNAP HQ2 CCD camera (Roper Scientific). To calculate the localization of MMP9 at the ventral plasma membrane, cells were outlined, and vesicles were counted and their intensity was analyzed using Find Maxima algorithm in Fiji ImageJ [25,26]. Brightfield images were shade corrected and filtered with 2–40 FFT band bass filter, to reduce noise.

The same samples were used to analyze the co-localization of MMP9 and β1-integrin using confocal microscopy.

2.8. MMP9 – organelle co-localization assay

35-mm fibronectin-coated glass-bottomed dishes were prepared by incubating dishes overnight in 4 °C with 5 μg/ml fibronectin in PBS, and washed with PBS before plating. MMP9-EGFP transfected MDA-MB-231 cells (2×10^4) were plated onto the dishes and cultured for 10–16 h, fixed, permeabilized and stained for MMP9 and EEA1, PSMA2, LC3β, GOLGA2, LAMP1, CD63, or Rab7A. Images were acquired using confocal microscopy.

2.9. Lysosome inhibition assay

35 mm fibronectin-coated glass-bottomed dishes were prepared by incubating dishes overnight in 4 °C with 5 μg/ml fibronectin in PBS, and washed with PBS before plating. MMP9-EGFP transfected MDA-MB-231 cells (2×10^4) were plated onto the dishes, cultured for 10–16 h and treated with lysosome inhibitors: 0.2 μM bafilomycin (Baf) or 200 μM chloroquine (CQ) for 6 h. Then, samples were fixed with paraformaldehyde, stained against LAMP1 and scanned using confocal microscopy.

2.10. Confocal microscopy and data analysis

Confocal imaging was performed using Nikon A1 confocal microscope with an oil immersion 40 × 1.3 NA Plan-Apochromat objective for invadopodium experiments or oil immersion 100 × 1.45 NA Plan-Apochromat objective for other confocal microscopy imaging. Before analysis, z-stack images were deconvolved using BatchDeconvolution Fiji plugin [27–29] with Richardson-Lucy deconvolution algorithm. Point spread function (PSF) was calculated using Gibson-Lanni PSF model with the highest accuracy and parameters matching acquisition. All calculations were made using Fiji ImageJ environment [25,26]. Images were analyzed as 3D z-stacks, but presented as Maximum Intensity Projections.

2.11. Statistical analysis

All distributions were tested for normality using Shapiro-Wilk ($n < 500$) or Kolmogorov-Smirnov ($n \geq 500$) tests. For samples significantly different from normal distribution ($p < 0.05$) Mann-Whitney *U* tests were used to analyze the results. For other samples, two-tailed Student's *t*-tests were used.

3. Results

3.1. MMP9 co-localizes with cortactin and talin2 in invadopodia

To examine whether talin2 co-localizes with MMP9, U2 OS cells were transfected with MMP9-DsRed and plated onto Oregon Green 488-labeled gelatin. Cells were then fixed and stained for talin2. Images were acquired using confocal microscopy. Digestion holes in the substrate are associated with extracellular matrix degradation and invadopodium maturation. Since MMP9 could diffuse quickly together with the fluorophore-free form gelatin after secretion, we found only several locations that MMP9 co-localized with talin2 at digestion spots (Fig. 1A). Similar result was observed in MDA-MB-231 cells plated on gelatin-Cy3 (Fig. 1B). Furthermore, MMP9 co-localized with cortactin at the digestion holes in invadopodia (Supplementary Fig. 1). These results suggest that MMP9 may be involved in talin2-mediated invadopodium maturation.

3.2. Talin2 controls MMP9 vesicles docking to ventral plasma membranes and secretion

To establish the role of talin1 and talin2 in MMP2 and MMP9 secretion, we used CRISPR/Cas9 to ablate talin1 or talin2 in MDA-MB-231 cells [14]. Talin2-null cells were cultured in serum-free DMEM media for 24 h. The media were collected and concentrated using ultrafiltration concentrators, and then analyzed for MMP2 and MMP9 secretion by Western blotting. Talin2-KO significantly inhibited MMP2 and MMP9 secretion (Fig. 2A); ablation of talin1 had similar effect on MMP2 and MMP9 secretion (data not shown). Because MMPs are secreted proteins, which are difficult to detect in cell lysates, we measured mRNA levels in talin2-KO cells. Depletion of talin2 could result in an increase in MMP2 and MMP9 mRNA levels, which are probably caused by a feedback regulation (Fig. 2B), suggesting that the decrease in MMP secretion in talin2-KO cells is not caused by an alteration in MMP expression. We will focus on the role of talin2 in MMP9 secretion in the following studies.

To learn how talin2 mediates MMP9 secretion, control and talin2-KO MDA-MB-231 cells were plated on gelatin, and cultured for 36 h in

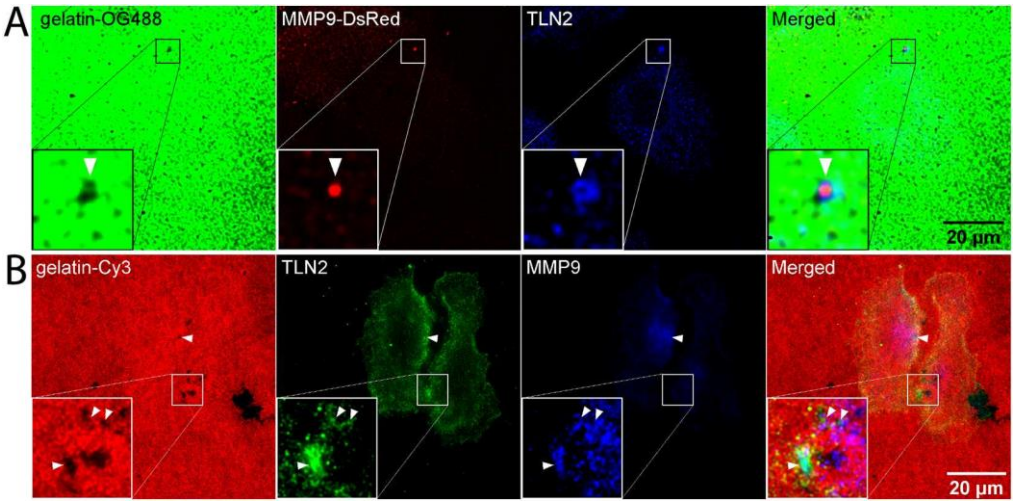

Fig. 1. MMP9 colocalizes with talin2 at digestion spots. (A) U2 OS transfected with MMP9-DsRed plated on gelatin-OregonGreen488 covered bottom-glass dish and stained with anti-talin2 antibody or (B) MDA-MB-231 cells plated on gelatin-Cy3 covered bottom-glass dish and stained with anti-talin2 and anti-MMP9 antibodies were imagined using TIRF microscopy. Arrows point at colocalisation spots between talin2, MMP9 and digested gelatin. Representative images are shown.

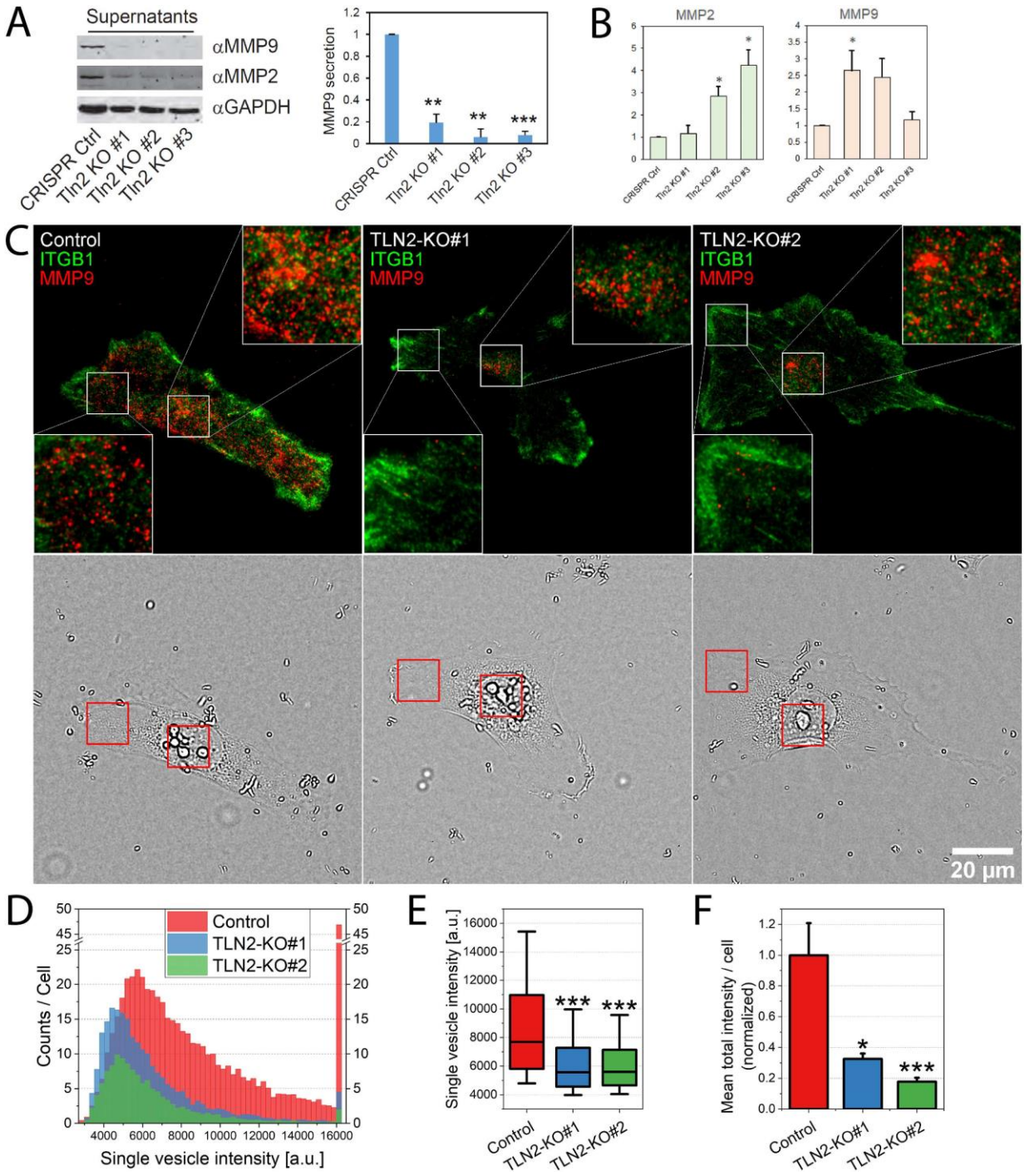

Fig. 2. Ablation of talin2 inhibited MMP2 and MMP9 secretion and caused a reduction in MMP9 vesicles targeting to ventral plasma membrane. A. Secreted MMP2 and MMP9 in talin2-KO MDA-MB-231 cells and CRISPR control cells were collected from serum-free supernatants, concentrated and determined by Western blotting. Data are presented as mean ± SEM of 3 independent experiments. *t*-test, $^{*}P < 0.05$, $^{***}P < 0.01$. B. MMP2 and MMP9 mRNA levels in talin2-KO MDA-MB-231 cells and CRISPR control cells were measured using real-time qPCR. Data are presented as mean ± SEM of 5 independent experiments. *t*-test, $^{*}P < 0.05$. C–F, Talin2-KO MDA-MB-231 cells and CRISPR control cells were plated on gelatin for 36 h with 1% FBS and 0.05 μg/ml HGF. C. Cells were co-stained with anti-β1-integrin and anti-MMP9 antibodies. Representative TIRF and brightfield images are shown. D. Intensities of all vesicles from all imaged cells were measured as their maximum intensity, and presented in form of a histogram normalized for number of cells (Control, $n = 38$; TLN2-KO#1, $n = 44$; TLN2-KO#2, $n = 59$), the peak at the maximum is connected with super-bright vesicles beyond dynamic range of the microscope camera. Data are representative of three independent experiments. E. The same data was presented using box-whisker plot. Data presented as 10-25-50-75-90 percentiles. *U* test, $^{***}P < 0.001$. F. Total intensity of MMP9 fluorescence per cell, measured as a sum of intensity maxima of MMP9 vesicles. Data presented as mean value ± SEM. *U* test, $^{*}P < 0.05$, $^{***}P < 0.001$.

1% FBS medium with HGF. Afterwards, cells were fixed and co-stained against MMP9 and β1-integrin. To analyze the MMP9 secretion, we focused on vesicle docking, the first stage of secretion process [30]. Images were acquired using TIRF microscopy. The vesicles that are associated with the ventral plasma membrane (Fig. 2C) were counted and intensity distributions (Fig. 2D, E) as well as total mean intensity (Fig. 2F) of MMP9 fluorescence staining were compared between talin2-KO and control cells. Ablation of talin2 caused a severe decrease

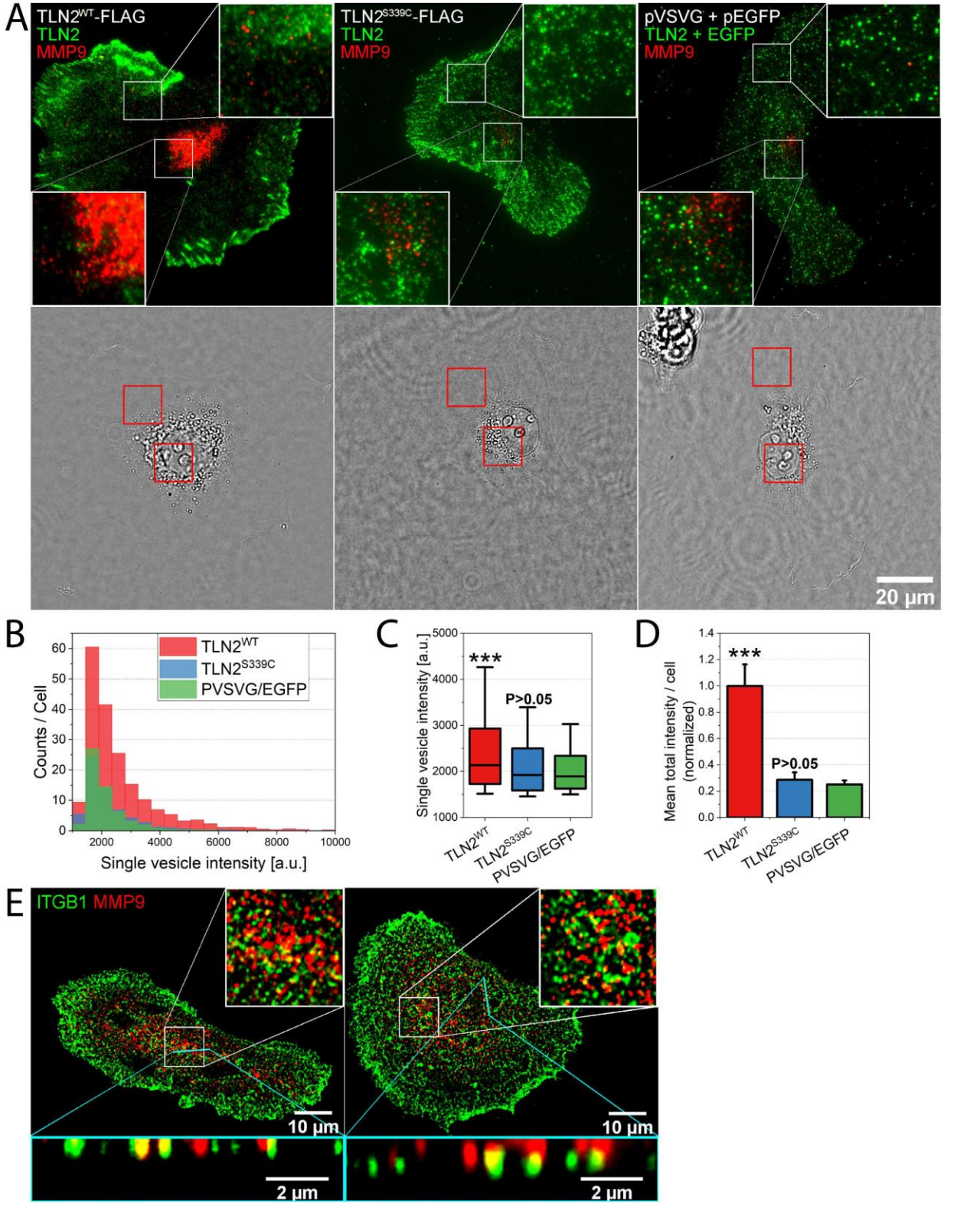

(caption on next page)

Fig. 3. Talin2-β-integrin interaction is essential for MMP9 targeting to the ventral plasma membrane. Talin2-KO MDA-MB-231 cells were transfected with FLAG-talin2^{WT}, -talin2^{S339C} or empty vectors pVSVG/pEGFP-C. After 72 h, cells were plated on gelatin for 36 h with 1% FBS and 0.05 μg/ml HGF. Cells were co-stained with anti-talin2 and anti-MMP9 antibodies. A. Representative TIRF and brightfield images are shown. B. Intensities of all vesicles from all imaged cells were measured as their maximum intensity, and presented in form of a histogram normalized for number of cells (FLAG-talin2^{WT}, n = 22; FLAG-talin2^{S339C}, n = 22; pVSVG + EGFP, n = 26). Data are representative of two independent experiments. C. The same data was presented using box-whisker plot. Data presented as 10-25-50-75-90 percentiles. *U* test, ***P < 0.001. D. Total intensity of MMP9 fluorescence per cell, measured as a sum of intensity maxima of MMP9 vesicles. Data presented as mean value ± SEM. *U* test, ***P < 0.001. E. MMP9 co-localizes with β1-integrin in MDA-MB-231 cells plated on gelatin for 36 h with 1% FBS and 0.05 μg/ml HGF. Cells were co-stained with mouse anti-β-integrin and rabbit anti-MMP9 antibodies. Representative single-plane confocal images of two cells from two separate experiments are shown. Cyan lines show axial projections.

in both number and intensity of MMP9 vesicles associated with the ventral plasma membrane (Fig. 2C–F), suggesting that talin2 plays an important role in MMP9 vesicles trafficking and docking process.

Subsequently, to determine whether the defect in talin2-KO cells can be rescued by re-expression of talin2, talin2-null cells were transiently transfected with FLAG-talin2^{WT} or pEGFP-C1/pVSVG empty vectors, as a control. 72 h after transfection cells were plated and cultured as described before, then fixed, stained against MMP9 and talin2, and images were collected and analyzed in the same way. Transfected cells were recognized with positive talin2 staining or GFP. Re-expression of talin2 significantly rescued the association of MMP9 vesicles to the ventral plasma membrane (Fig. 3A–D).

3.3. Talin2-β-integrin interaction is essential for MMP9 vesicles to attach to the ventral plasma membrane

To examine the importance of β-integrin interaction with talin2 in MMP9 secretion, MDA-MB-231 cells were plated on gelatin, cultured for 36 h in DMEM supplemented with 1% FBS and HGF, fixed, co-stained against MMP9 and β1-integrin, and scanned using confocal microscopy. Images showed co-localization between MMP9 and β-integrin in the ventral plasma membrane (Fig. 3E).

To verify whether the interaction between talin2 and β-integrin is important for MMP9 secretion, talin2-null cells were transiently transfected with FLAG-talin2^{S339C}, a mutant that has reduced affinity towards β-integrin [14]. Samples were prepared and analyzed as described in the rescue experiment in the previous paragraph. The talin2^{S339C} transfection did not significantly rescue the association of MMP9 with the ventral plasma membrane, as compared with the transfection of pEGFP-C1/pVSVG empty vectors (Fig. 3A–D), indicating that interaction between talin2 and β-integrin is essential for MMP9 trafficking and vesicle docking.

3.4. MMP9 is directed towards lysosome degradation in talin2-null cells

Further, we studied the fate of MMP9 vesicles in talin2-depleted cells. Because of its low endogenous concentration, and the high low-signal to noise ratio of confocal microscopy, endogenous MMP9 staining is too week for imaging. Thus, we overexpressed MMP9-EGFP in control and talin2-KO cells through transient transfection. Then, cells were plated on fibronectin, fixed, and stained against GOLGA2 (Golgi marker), EEA1 (early endosome marker), Rab7A (late endosome marker), LAMP1 (lysosome marker), CD63 (exosome and cell surface-derived endosomes), LC3β (autophagosome marker), or PSMA2 (proteasome marker). *Z*-stack images were taken using confocal microscopy.

In control cells, the sizes of MMP9 vesicles were, in general, < 1 μm in diameter. However, talin2-depleted cells generated enlarged (≥ 1 μm in diameter) perinuclear vesicles containing MMP9-EGFP (Fig. 4A, B). All the enlarged vesicles were counted and their diameter was measured. The analysis shows that the median value of the number of enlarged vesicles per cell rises five-fold in talin2-depleted cells in comparison to control cells (Fig. 4A). Furthermore, number of cells having five or more enlarged MMP9 vesicles, or at least one super-enlarged vesicle of > 2 μm in diameter was also around 5 times higher (Fig. 4B).

To examine possible origin and further destination of those vesicles, co-localization analysis was performed. Talin2-KO cells and the control cells were transfected with MMP9-EGFP and stained for GOLGA2 Golgi marker. There was no difference in the co-localization of MMP9 with Golgi apparatus between the talin2-KO and control cells (Supplementary Fig. 2). Cells were also stained against CD63 exosome marker or PSMA2 proteasome marker. There was no significant co-localization of MMP9 with these markers in both control and talin2-KO cells (Supplementary Figs. 3, 4), suggesting no or low participation of exosomes and proteasomes in talin2-mediated MMP9 trafficking, recycling and degradation. However, in talin2-null cells enlarged MMP9 vesicles were co-localized with early endosome marker EEA1 (Fig. 5A), and surrounded by Rab7A late endosome marker (Fig. 5B), suggesting that endosomal transport takes part in MMP9 trafficking. Furthermore, enlarged MMP9 vesicles were surrounded by LC3β autophagosome marker (Fig. 6) and localized to lysosomes (Supplementary Fig. 2) in talin2-KO cells.

In talin2-depleted cells, enlarged MMP9 vesicles were accumulated in endosomes, autophagosomes, and lysosomes in talin2-null cells, suggesting that ablation of talin2 causes lysosomes overload. Lack of enlarged MMP9 vesicles in control cells is not surprising due to ongoing secretion and degradation processes.

In order to examine lysosomes overload hypothesis, MDA-MB-231 control cells expressing MMP9-EGFP were treated with lysosome inhibitors: 0.2 μM bafilomycin (Baf) or 200 μM chloroquine (CQ) for 6 h. Then, samples were fixed, stained against LAMP1 and scanned using confocal microscopy. Both inhibitors caused increase in vesicle size and number of oversized vesicles, comparable to those in talin2-knockout cells (Fig. 4), suggesting that talin2-mediated vesicle docking prevents MMP9 vesicles from being rerouted and degraded.

4. Discussion

Invadopodia degrade extracellular matrix, thus mediating tumor cell invasion, a key step in cancer metastasis. Talin2 binds to β-integrins, localizes to invadopodia, mediates invadopodium formation, and consequently regulates cell invasion [14]. It has been reported that talin2 is essential for podosome- and invadopodium-mediated ECM degradation [13,14], but the molecular mechanism was not established.

It has been demonstrated that MMP9 localizes to invadopodia, and regulates cancer cell invasion and metastasis [20,21,31–33]. In this work, we showed that, even though the intracellular level of MMP9 does not change [13], the ablation of talin2 cause a significant decrease in MMP9 secretion due to an inhibition of docking of secretory vesicles. It also stimulated transcription of MMP9 mRNA probably due to a feedback loop (Fig. 2). The secretion inhibition leads to a decrease in

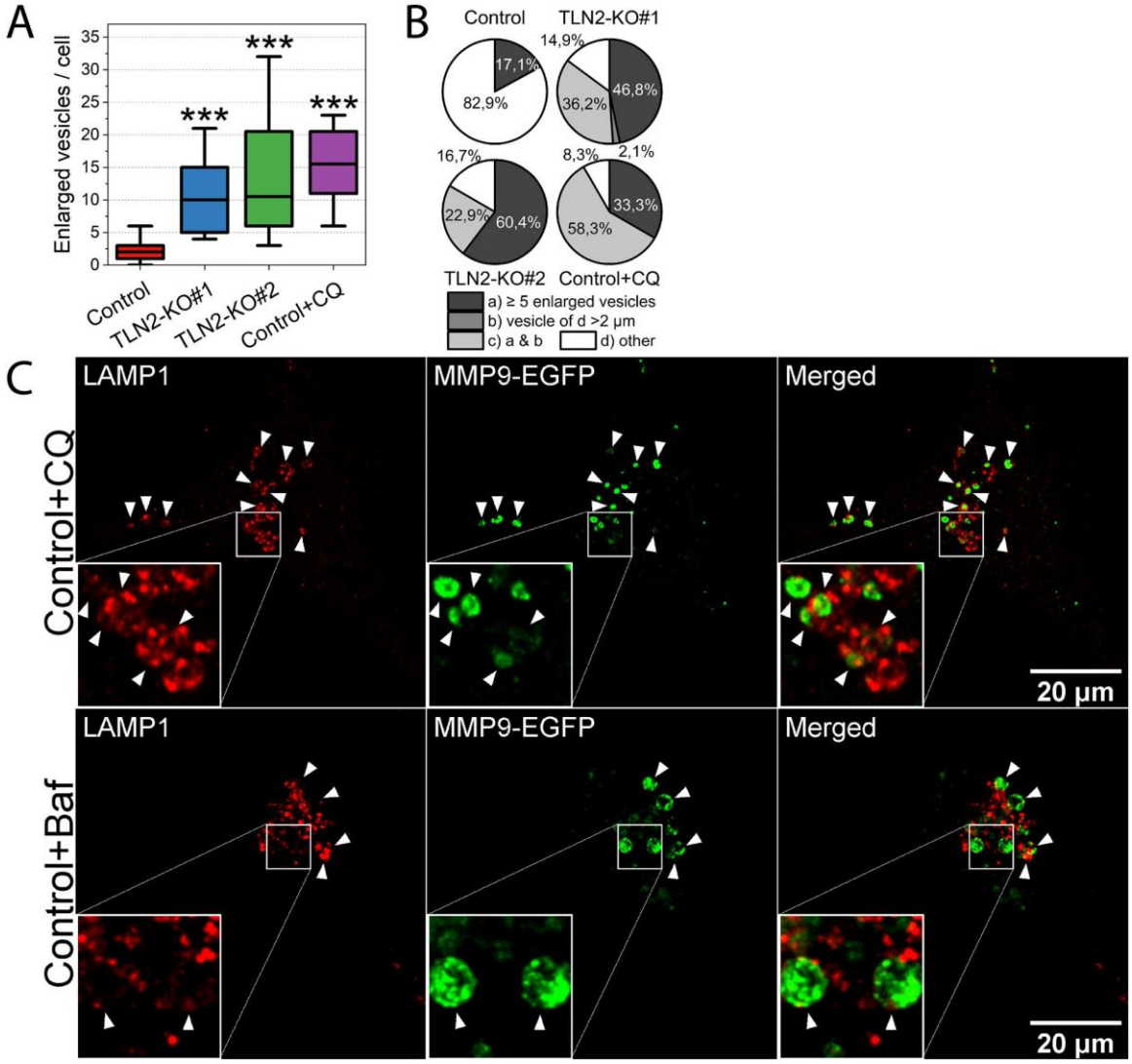

Fig. 4. Talin2-KO caused an accumulation of enlarged MMP9 vesicles. A. Number of enlarged vesicles per cell in talin2-knockout cells, control cells, and control cells treated for 6 h with 200 µM chloroquine (CQ) (Control, $n = 41$; TLN2-KO#1, $n = 47$; TLN2-KO#2, $n = 48$; Control + CQ, $n = 12$). Comparison between cells treated with chloroquine and KO cells shows no statistical difference ($P > 0.05$) U test, ***P < 0.001. B. Pie diagrams showing percentage of cells having a) five or more enlarged vesicles (diameter of 1 µm or more), b) having at least one vesicle with diameter of > 2 µm, c) fulfilling condition a and b, and d) the rest of the cells. C. MMP9 was co-localized with LAMP1 in MDA-MB-231 cells plated on fibronectin after treatment with lysosome inhibitors: 0.2 µM Bafilomycin (Baf) or 200 µM Chloroquine (CQ) for 6 h. In both cases MMP9 was accumulated in multiple enlarged vesicles. Cells were transfected with MMP9-EGFP and stained with anti-LAMP1 antibody. Representative maximum intensity projections (MIP) of confocal images are shown.

ECM degradation [14]. Furthermore, the decrease in MMP9 vesicle docking in talin2-KO cells was restored by re-expressing talin2^{WT}. These results suggest that talin2 regulates invadopodium maturation and invasion by mediating MMP9 secretion (Fig. 3).

We transfected talin2-KO cells with talin2^{WT} and talin2^{S339C}, a mutant with reduced β-integrin binding [14]. The wild-type protein rescued MMP9 secretion, but the mutant did not, indicating that the functional talin2 – β-integrin complex is required for MMP9 secretion (Fig. 3). Previous studies show the importance of several different kind of integrins in MMP9 secretion, including α3β1 in keratinocytes [34,35] and breast cancer cells [36], αvβ3 in breast cancer cells [37] or β1 in neurons [38]. Especially, Redondo-Muñoz and colleagues showed that α4β1 integrin is essential for MMP9 vesicle docking in B cells [39,40]. Our results indicate that MMP9 secretion is dependent specifically on talin2 – β1-integrin interaction. Morini and colleagues demonstrated that selectively blocking α3β1-integrin led to reduction in MMP9 activity in MDA-MB-231 cells [36], while Redondo-Muñoz and colleagues showed direct interaction between MMP9 and α4β1-integrin [39]. These results suggest that the talin2 – β-integrin complex may provide a docking site for MMP9 vesicles, thus controlling MMP9 secretion.

It has been shown that inhibition of MMP9 secretion may lead to lysosomal degradation of MMP9 [20,41] and accumulation of enlarged MMP9 vesicles in the perinuclear area [41]. We examined MMP9 trafficking in talin2-KO cells where MMP9 secretion is impaired, and found the similar phenomena: talin2-KO resulted in a significant perinuclear accumulation of enlarged MMP9 vesicles (Figs. 4–6). These vesicles were co-localized with early endosome marker EEA1, surrounded by late endosome marker Rab7 and autophagosome marker LC3β in talin2-deprived cells (Figs. 5, 6). It has been reported that vesicles that cannot be docked properly to the plasma membrane are directed to early endosomes and ultimately towards lysosomal

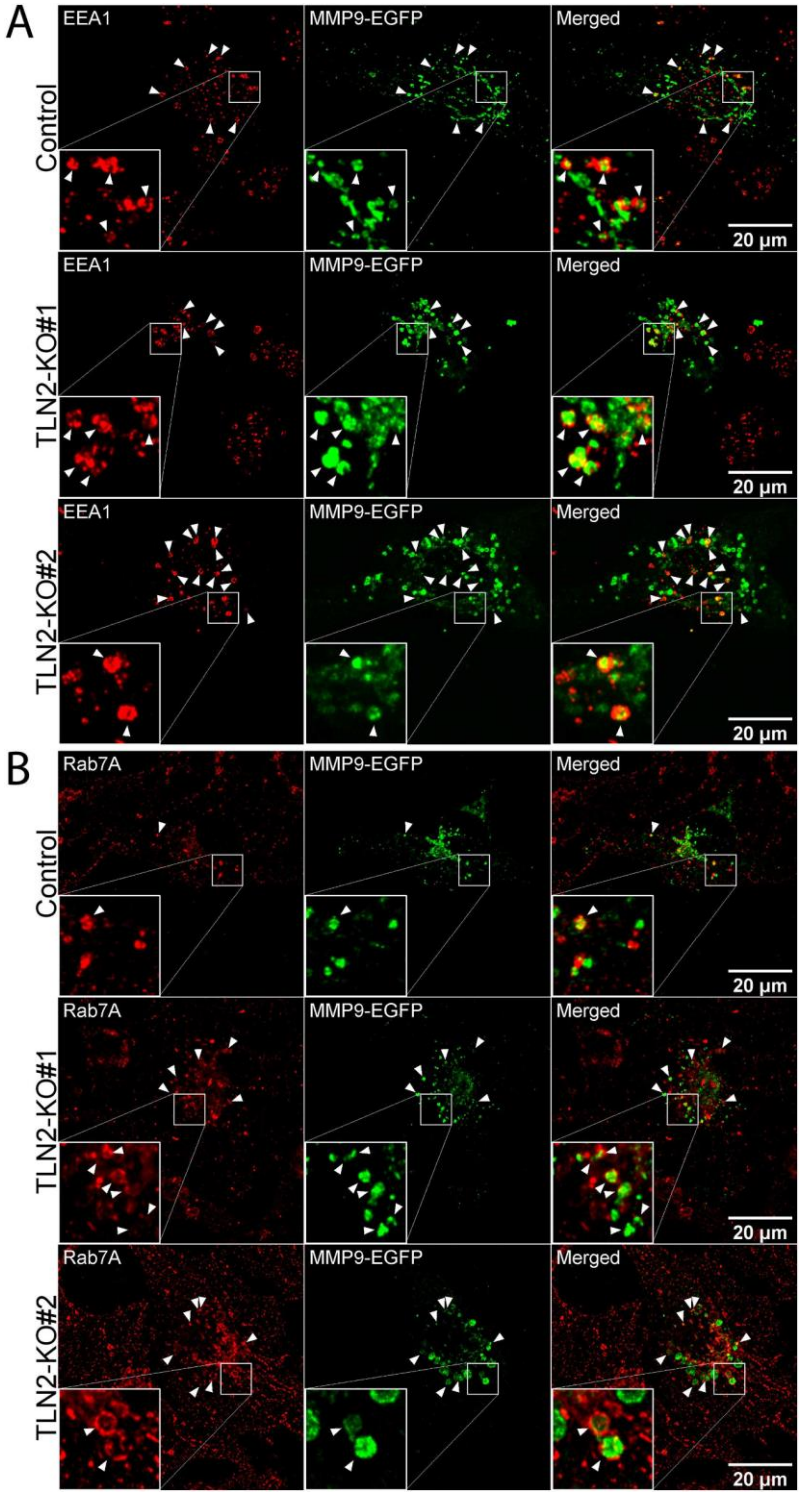

Fig. 5. Enlarged MMP9 vesicles were co-localized with EEA1 early endosome marker and surrounded by late endosome marker Rab7A in talin2-KO cells. Talin2-KO MDA-MB-231 cells and the control cells were transfected with MMP9-EGFP and plated on fibronectin-coated glass-bottom dishes. The cells were fixed and stained with anti-EEA1 (A) or anti-Rab7 (B) antibodies. The co-localization of MMP9 with EEA1 or Rab7A was examined using a Nikon A1 confocal microscope. Representative maximum intensity projections (MIP) of confocal images are shown.

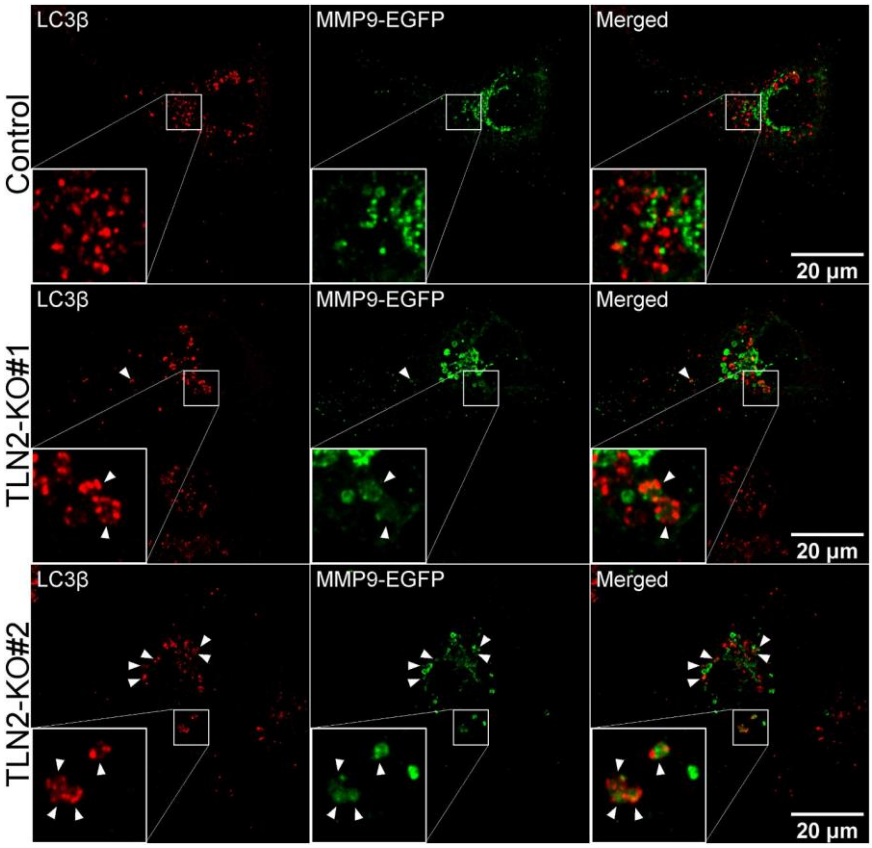

Fig. 6. Enlarged MMP9 vesicles were co-localized with autophagosome marker LC3β in talin2-KO cells. Talin2-KO MDA-MB-231 cells and the control cells were transfected with MMP9-EGFP, plated on fibronectin, and stained with anti-LC3β antibody. Representative maximum intensity projections (MIP) of confocal images are shown.

degradation through late endosomes [42–44]. Furthermore, we believe that MMP9 – LC3β colocalization is not connected with autophagocytosis process directly, but rather as an effect of creation pre-lysosomal amphisomal compartments from MMP9 – late endosomes and autophagosomes [45]. We hypothesize that formation of oversized vesicles is caused by insufficiency in lysosomal degradation process, resulting in temporal storage of MMP9 and other proteins pending for degradation. Additionally, we observed similar vesicles in cells that did not go under transfection (data not shown), suggesting that trafficking pathways of other proteins are impaired, and that higher amount of proteins is directed towards lysosomal degradation. To confirm our hypothesis of lysosomal overflow we inhibited lysosomes with bafilomycin or chloroquine receiving similar results as for talin2-KO cells (Fig. 4). Comparing our results with previous studies, we found that depletion of Rab40B also resulted in MMP9 targeting to lysosomes [20]. These findings suggest that talin2-KO results in defect in MMP9 vesicle docking, consequently causes MMP9 vesicles redirected to endosomes, and lysosomes for degradation.

It was recently shown that MMP9 secretion is affected by extracellular matrix rigidity in hepatic stellate cells [46]. Our results indicate that integrins and both talins: talin1 and talin2 might be involved in mechanosensing pathways of this phenomenon. Moreover, as the ablation of either of talins result in reduction in MMP9 secretion, it indicates different roles of these proteins in the secretion process. Re-expression of S339C talin2 mutant, a protein closely resembling talin1 in terms of talin-integrin interaction [15], in talin2-KO cells did not rescue the secretion, suggesting that Ser339 is specifically involved in this process.

Although talin has not been found to associate directly with protein secretion machinery, it can bind to PIP2, which regulates vesicle trafficking [47,48]. Because the β-integrin-binding site on talin2 is proximal to the PIP2 binding site [15], PIP2 binding may also regulate the interaction of talin2 with β-integrins. Moreover, talin has a moesin binding site in its rod domain [49]. One of possible mechanisms we suspect that may be responsible for talin-mediated MMP secretion is a change in regulation of recruitment of moesin-NHE-1 complex to invadopodia. The complex is responsible for invadopodium stability and matrix degradation [50] and its recruitment is mediated by talin [12]. Moreover, several studies have shown the importance of NHE-1 in MMP2 and MMP9 activity [53,58,59]. Thus, possible differences in interaction between talin1/talin2-moesin may lay behind this interaction. In addition, another hypothesis is that calpain binds to calpain-cleavage/binding site in a talin head-rod linker [54] to modulate MMP secretion. Calpains are intracellular proteases [55], and they are also connected with mediation of protein secretion, including MMPs [51,52]. We hypostatize that the distinct affinities of talin1 and talin2 towards integrins may induce a different conformation of talins, thus changing nature of talin2-calpain interaction. Furthermore, calpain has also an important role in focal adhesion turnover [56], thus inhibition of calpain-mediated cleavage may result in changing focal adhesion organisation; the fact talin2 that creates larger adhesion sites than talin1 [57] supports the talin2-calpain interaction hypothesis (Fig. 7). The connection of talin1 with secretion of MMP9 is still to be determined, as it might be either direct through molecular interactions, as we hypothesize in case of talin2, or indirect through controlling cell adhesion and cell-ECM interaction.

In summary, talin2 interacts with β-integrins and localizes to invadopodia. Thus, talin2-β-integrin complex constitutes a docking site for MMP9 vesicles in invadopodia, mediating MMP9 secretion and trafficking, and cell invasion (Fig. 7).

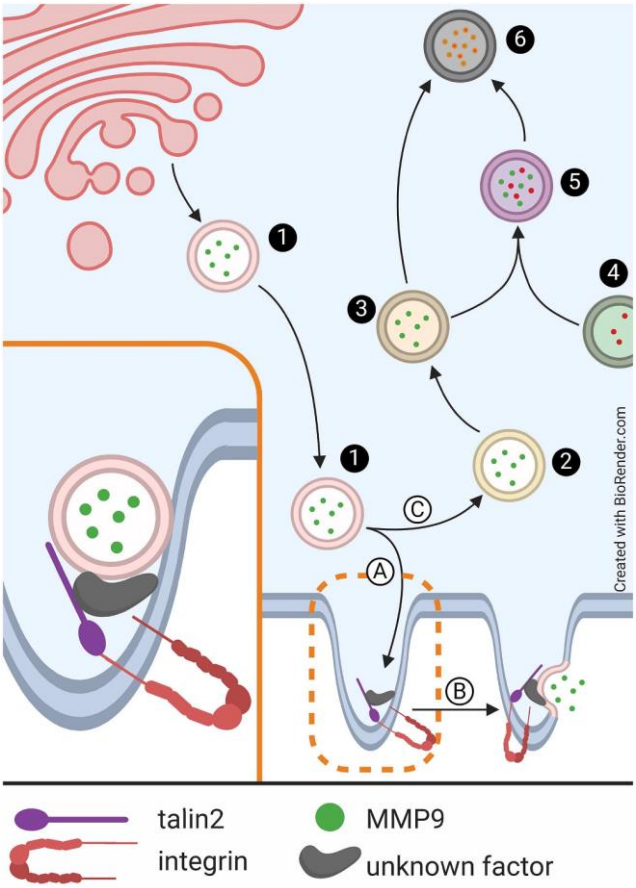

Fig. 7. Scheme of talin2-mediated MMP9 trafficking pathway. MMP9 secretory vesicles (1) released from Golgi apparatus are transported towards ventral membrane where complex of talin2, β1-integrin and unknown factor (either cytoplasmic like moesin-NHE-1 or calpain, or membrane like PIP2) mediate their docking (A) and secretion (B), consequently. In case of absence of the complex, MMP9 vesicles are trafficked towards degradation process (C) in lysosomes (6) through early and late endosomes (2 and 3, respectively), with possible merging with autophagosomes (4) to create amphisome (5).

Author contributions

Z.B. and L.L. performed experiments, analyzed data, and wrote the paper; Z.R. contributed the manuscript discussion and writing; C.H. designed experiments, interpreted results and wrote the paper.

Funding

This work was supported by National Institutes of Health grant R01 GM122994 (to CH), the Polish Ministry of Science and Higher Education through grant no. 7150/E-338/M/2018 (to ZB), and the Polish National Science Center ETIUDA scholarship no. 2019/32/T/NZ3/00444 (to ZB).

Declaration of competing interest

The authors declare no competing or financial interests.

Appendix A. Supplementary data

Supplementary data to this article can be found online at https://doi.org/10.1016/j.bbamcr.2020.118693.

References

[1] D.J.G. Rees, S.E. Ades, S.J. Singer, R.O. Hynes, Sequence and domain structure of talin, Nature. 347 (1990) 685–689, https://doi.org/10.1038/347685a0.
[2] D.A. Calderwood, R. Zent, R. Grant, D.J. Rees, R.O. Hynes, M.H. Ginsberg, The talin head domain binds to integrin beta subunit cytoplasmic tails and regulates integrin activation, J. Biol. Chem. 274 (1999) 28071–28074, https://doi.org/10.1074/JBC.274.40.28071.
[3] D.R. Critchley, Cytoskeletal proteins talin and vinculin in integrin-mediated adhesion, Biochem. Soc. Trans. 32 (2004) 831–836, https://doi.org/10.1042/BST0320831.
[4] M.D. Bass, B.J. Smith, S.A. Prigent, D.R. Critchley, Talin contains three similar vinculin-binding sites predicted to form an amphipathic helix, Biochem. J. 341 (Pt 2) (1999) 257–263, https://doi.org/10.1042/BJ3410257.
[5] L. Hemmings, D.J. Rees, V. Ohanian, S.J. Bolton, A.P. Gilmore, B. Patel, H. Priddle, J.E. Trevithick, R.O. Hynes, D.R. Critchley, Talin contains three actin-binding sites each of which is adjacent to a vinculin-binding site, J. Cell Sci. 109 (Pt 1) (1996) 2715–2726 http://jcs.biologists.org/content/joces/109/11/2715.full.pdf , Accessed date: 18 October 2018.
[6] S.J. Monkley, C.A. Pritchard, D.R. Critchley, Analysis of the mammalian talin2 gene TLN2, Biochem. Biophys. Res. Commun. 286 (2001) 880–885, https://doi.org/10.1006/bbrc.2001.5497.
[7] C. Huang, Z. Rajfur, N. Yousefi, Z. Chen, K. Jacobson, M.H. Ginsberg, Talin phosphorylation by Cdk5 regulates Smurf1-mediated talin head ubiquitylation and cell migration, Nat. Cell Biol. 11 (2009) 624–630, https://doi.org/10.1038/ncb1868.
[8] J.-K. Jin, P.-C. Tien, C.-J. Cheng, J.H. Song, C. Huang, S.-H. Lin, G.E. Gallick, Talin1 phosphorylation activates β1 integrins: a novel mechanism to promote prostate cancer bone metastasis, Oncogene. 34 (2015) 1811–1821, https://doi.org/10.1038/onc.2014.116.
[9] S. Sakamoto, R.O. McCann, R. Dhir, N. Kyprianou, Talin1 promotes tumor invasion and metastasis via focal adhesion signaling and anoikis resistance, Cancer Res. 70 (2010) 1885–1895, https://doi.org/10.1158/0008-5472.CAN-09-2833.
[10] N. Bate, A.R. Gingras, A. Bachir, R. Horwitz, F. Ye, B. Patel, B.T. Goult, D.R. Critchley, Talin contains a C-terminal calpain2 cleavage site important in focal adhesion dynamics, PLoS One 7 (2012) e34461, , https://doi.org/10.1371/journal.pone.0034461.
[11] S.J. Franco, M.A. Rodgers, B.J. Perrin, J. Han, D.A. Bennin, D.R. Critchley, A. Huttenlocher, Calpain-mediated proteolysis of talin regulates adhesion dynamics, Nat. Cell Biol. 6 (2004) 977–983, https://doi.org/10.1038/ncb1175.
[12] B.T. Beaty, Y. Wang, J.J. Bravo-Cordero, V.P. Sharma, V. Miskolci, L. Hodgson, J. Condeelis, Talin regulates moesin–NHE-1 recruitment to invadopodia and promotes mammary tumor metastasis, J. Cell Biol. 205 (2014) 737–751, https://doi.org/10.1083/jcb.201312046.
[13] U. Praekelt, P.M. Kopp, K. Rehm, S. Linder, N. Bate, B. Patel, E. Debrand, A.M. Manso, R.S. Ross, F. Conti, M.-Z. Zhang, R.C. Harris, R. Zent, D.R. Critchley, S.J. Monkley, New isoform-specific monoclonal antibodies reveal different subcellular localisations for talin1 and talin2, Eur. J. Cell Biol. 91 (2012) 180–191, https://doi.org/10.1016/j.ejcb.2011.12.003.
[14] L. Qi, N. Jafari, X. Li, Z. Chen, L. Li, V.P. Hytönen, B.T. Goult, C.-G. Zhan, C. Huang, Talin2-mediated traction force drives matrix degradation and cell invasion, J. Cell Sci. 129 (2016) 3661–3674, https://doi.org/10.1242/jcs.185959.
[15] Y. Yuan, L. Li, Y. Zhu, L. Qi, L. Azizi, V.P. Hytönen, C.-G. Zhan, C. Huang, The molecular basis of talin2's high affinity toward β1-integrin, Sci. Rep. 7 (2017) 41989, https://doi.org/10.1038/srep41989.
[16] R. Cañete-soler, Y.-H. Gui, K.K. Linask, R.J. Muschel, Developmental expression of MMP-9 (gelatinase B) mRNA in mouse embryos, Dev. Dyn. (1995), https://doi.org/10.1002/aja.1002040105.
[17] B. Vafadari, A. Salamian, L. Kaczmarek, MMP-9 in translation: from molecule to brain physiology, pathology, and therapy, J. Neurochem. 139 (2016) 91–114, https://doi.org/10.1111/jnc.13415.
[18] J. Vandooren, P.E. Van den Steen, G. Opdenakker, Biochemistry and molecular biology of gelatinase B or matrix metalloproteinase-9 (MMP-9): the next decade, Crit. Rev. Biochem. Mol. Biol. 48 (2013) 222–272, https://doi.org/10.3109/10409238.2013.770819.
[19] M. Egeblad, Z. Werb, New functions for the matrix metalloproteinases in cancer progression, Nat. Rev. Cancer 2 (2002) 161–174, https://doi.org/10.1038/nrc745.
[20] A. Jacob, J. Jing, J. Lee, P. Schedin, S.M. Gilbert, A.A. Peden, J.R. Junutula, R. Prekeris, Rab40b regulates trafficking of MMP2 and MMP9 during invadopodia formation and invasion of breast cancer cells, J. Cell Sci. 126 (2013) 4647–4658, https://doi.org/10.1242/jcs.126573.
[21] A. Jacob, R. Prekeris, The regulation of MMP targeting to invadopodia during cancer metastasis, Front. Cell Dev. Biol. 3 (2015) 4, https://doi.org/10.3389/fcell.2015.00004.
[22] J. Niu, X. Gu, J. Turton, C. Meldrum, E.W. Howard, M. Agrez, Integrin-mediated signalling of gelatinase B secretion in colon cancer cells, Biochem. Biophys. Res. Commun. 249 (1998) 287–291, https://doi.org/10.1006/bbrc.1998.9128.
[23] J.S. Friedland, J.C. Porter, S. Brilha, R. Wysoczanski, A.M. Whittington, Infection *Mycobacterium tuberculosis* 3 in β V α Regulated by Integrin Extracellular Matrix Breakdown Are Monocyte Adhesion, Migration, and, (2017), https://doi.org/10.4049/jimmunol.1700128.
[24] V.P. Sharma, D. Entenberg, J. Condeelis, High-Resolution Live-Cell Imaging and Time-Lapse Microscopy of Invadopodium Dynamics and Tracking Analysis, Humana Press, Totowa, NJ, 2013, pp. 343–357, https://doi.org/10.1007/978-1-62703-538-5_21.
[25] C.T. Rueden, J. Schindelin, M.C. Hiner, B.E. DeZonia, A.E. Walter, E.T. Arena,

K.W. Eliceiri, ImageJ2: ImageJ for the next generation of scientific image data, BMC Bioinformatics. 18 (2017) 529, https://doi.org/10.1186/s12859-017-1934-z.
[26] J. Schindelin, I. Arganda-Carreras, E. Frise, V. Kaynig, M. Longair, T. Pietzsch, S. Preibisch, C. Rueden, S. Saalfeld, B. Schmid, J.-Y. Tinevez, D.J. White, V. Hartenstein, K. Eliceiri, P. Tomancak, A. Cardona, Fiji: an open-source platform for biological-image analysis, Nat. Methods 9 (2012) 676–682, https://doi.org/10.1038/nmeth.2019.
[27] Z. Baster, Z. Rajfur, BatchDeconvolution: A Fiji Plugin for Icreasing Deconvolution Workflow, Prep. (2020).
[28] D. Sage, L.L. Donati, F.F. Soulez, D. Fortun, G. Schmit, A. Seitz, R. Guiet, C.C. Vonesch, M. Unser, DeconvolutionLab2: an open-source software for deconvolution microscopy, Methods. 115 (2017) 28–41, https://doi.org/10.1016/j.ymeth.2016.12.015.
[29] H. Kirshner, F. Aguet, D. Sage, M. Unser, 3-D PSF fitting for fluorescence microscopy: implementation and localization application, J. Microsc. 249 (2013) 13–25, https://doi.org/10.1111/j.1365-2818.2012.03675.x.
[30] R.F. Toonen, O. Kochubey, H. de Wit, A. Gulyas-Kovacs, B. Konijnenburg, J.B. Sørensen, J. Klingauf, M. Verhage, Dissecting docking and tethering of secretory vesicles at the target membrane, EMBO J. 25 (2006) 3725–3737, https://doi.org/10.1038/sj.emboj.7601256.
[31] Y. Chen, X. Wei, C. Guo, H. Jin, Z. Han, Y. Han, T. Qiao, K. Wu, D. Fan, Runx3 suppresses gastric cancer metastasis through inactivation of MMP9 by upregulation of TIMP-1, Int. J. Cancer 129 (2011) 1586–1598, https://doi.org/10.1002/ijc.25831.
[32] S. Hiratsuka, K. Nakamura, S. Iwai, M. Murakami, T. Itoh, H. Kijima, J.M. Shipley, R.M. Senior, M. Shibuya, MMP9 induction by vascular endothelial growth factor receptor-1 is involved in lung-specific metastasis, Cancer Cell 2 (2002) 289–300 http://www.ncbi.nlm.nih.gov/pubmed/12398893 , Accessed date: 8 November 2018.
[33] L. Qin, L. Liao, A. Redmond, L. Young, Y. Yuan, H. Chen, B.W. O'Malley, J. Xu, The AIB1 oncogene promotes breast cancer metastasis by activation of PEA3-mediated matrix metalloproteinase 2 (MMP2) and MMP9 expression, Mol. Cell. Biol. 28 (2008) 5937–5950, https://doi.org/10.1128/MCB.00579-08.
[34] C.M. DiPersio, M. Shao, L. Di Costanzo, J.A. Kreidberg, R.O. Hynes, Mouse keratinocytes immortalized with large T antigen acquire alpha3beta1 integrin-dependent secretion of MMP-9/gelatinase B, J. Cell Sci. 113 (Pt 1) (2000) 2909–2921, https://doi.org/10.1124/mol.112.084152.
[35] J.M. Lamar, K.M. Pumiglia, C.M. DiPersio, An immortalization-dependent switch in integrin function up-regulates MMP-9 to enhance tumor cell invasion, Cancer Res. 68 (2008) 7371–7379, https://doi.org/10.1158/0008-5472.CAN-08-1080.
[36] M. Morini, M. Mottolese, N. Ferrari, F. Ghiorzo, S. Buglioni, R. Mortarini, D.M. Noonan, P.G. Natali, A. Albini, The α3β1 integrin is associated with mammary carcinoma cell metastasis, invasion, and gelatinase B (mmp-9) activity, Int. J. Cancer 87 (2000) 336–342, https://doi.org/10.1002/1097-0215(20000801)87:3<336::AID-IJC5>3.0.CO;2-3.
[37] M. Rolli, E. Fransvea, J. Pilch, A. Saven, B. Felding-Habermann, Activated integrin alphavbeta3 cooperates with metalloproteinase MMP-9 in regulating migration of metastatic breast cancer cells, Proc. Natl. Acad. Sci. U. S. A. 100 (2003) 9482–9487, https://doi.org/10.1073/pnas.1633689100.
[38] P. Michaluk, L. Mikasova, L. Groc, R. Frischknecht, D. Choquet, L. Kaczmarek, Matrix metalloproteinase-9 controls NMDA receptor surface diffusion through integrin 1 signaling, J. Neurosci. 29 (2009) 6007–6012, https://doi.org/10.1523/JNEUROSCI.5346-08.2009.
[39] J. Redondo-Muñoz, E. Ugarte-Berzal, J.A. García-Marco, M.H. del Cerro, P.E. Van den Steen, G. Opdenakker, M.J. Terol, A. García-Pardo, Alpha4beta1 integrin and 190-kDa CD44v constitute a cell surface docking complex for gelatinase B/MMP-9 in chronic leukemic but not in normal B cells, Blood. 112 (2008) 169–178, https://doi.org/10.1182/blood-2007-08-109249.
[40] J. Redondo-Muñoz, E. Ugarte-Berzal, M.J. Terol, P.E. Van den Steen, M. Hernández del Cerro, M. Roderfeld, E. Roeb, G. Opdenakker, J.A. García-Marco, A. García-Pardo, Matrix Metalloproteinase-9 promotes chronic lymphocytic leukemia B cell survival through its hemopexin domain, Cancer Cell 17 (2010) 160–172, https://doi.org/10.1016/j.ccr.2009.12.044.
[41] D.A. Hickman, G. Syal, M. Fausther, E.G. Lavoie, J.R. Goree, B. Storrie, J.A. Dranoff, C.A. Jonathan Dranoff, MCP-1 downregulates MMP-9 export via vesicular redistribution to lysosomes in rat portal fibroblasts, Physiol Rep. 2 (2014), https://doi.org/10.14814/phy2.12153.
[42] A. Helenius, I. Mellman, D. Wall, A. Hubbard, Endosomes, Trends Biochem. Sci. 8 (1983) 245–250, https://doi.org/10.1016/0968-0004(83)90350-X.
[43] M. Jovic, M. Sharma, J. Rahajeng, S. Caplan, The early endosome: a busy sorting station for proteins at the crossroads, Histol. Histopathol. 25 (2010) 99–112, https://doi.org/10.14670/HH-25.99.
[44] J. Rink, E. Ghigo, Y. Kalaidzidis, M. Zerial, Rab conversion as a mechanism of progression from early to late endosomes, Cell. 122 (2005) 735–749, https://doi.org/10.1016/j.cell.2005.06.043.
[45] J. Xu, R. Camfield, S.M. Gorski, The interplay between exosomes and autophagy - partners in crime, J. Cell Sci. 131 (2018) jcs215210, , https://doi.org/10.1242/jcs.215210.
[46] D. Lachowski, E. Cortes, A. Rice, D. Pinato, K. Rombouts, A. del Rio Hernandez, Matrix stiffness modulates the activity of MMP-9 and TIMP-1 in hepatic stellate cells to perpetuate fibrosis, Sci. Rep. 9 (2019) 7299, https://doi.org/10.1038/s41598-019-43759-6.
[47] N. Thapa, R.A. Anderson, PIP2 signaling, an integrator of cell polarity and vesicle trafficking in directionally migrating cells, Cell Adhes. Migr. 6 (2012) 409–412, https://doi.org/10.4161/cam.21192.
[48] T.F.J. Martin, Role of pi(4,5)p2 in vesicle exocytosis and membrane fusion, Subcell. Biochem. 59 (2015) 111–130, https://doi.org/10.1007/978-94-007-3015-1_4.
[49] R.E. Gough, B.T. Goult, The tale of two talins – two isoforms to fine-tune integrin signalling, FEBS Lett. 592 (2018) 2108–2125, https://doi.org/10.1002/1873-3468.13081.
[50] B.T. Beaty, J. Condeelis, Digging a little deeper: The stages of invadopodium formation and maturation, Eur. J. Cell Biol. 93 (2014) 438–444, https://doi.org/10.1016/j.ejcb.2014.07.003.
[51] L. Jiang, J. Zhang, R.E. Monticone, R. Telljohann, J. Wu, M. Wang, E.G. Lakatta, Calpain-1 regulation of matrix metalloproteinase 2 activity in vascular smooth muscle cells facilitates age-associated aortic wall calcification and fibrosis, Hypertension. 60 (2012) 1192–1199, https://doi.org/10.1161/HYPERTENSIONAHA.112.196840.
[52] B. Chen, J. Tang, Y.-S. Guo, Y. Li, Z.-N. Chen, J.-L. Jiang, Calpains are required for invasive and metastatic potentials of human HCC cells, Cell Biol. Int. 37 (2013) 643–652, https://doi.org/10.1002/cbin.10062.
[53] J. Taves, D. Rastedt, J. Canine, D. Mork, M.A. Wallert, J.J. Provost, Sodium hydrogen exchanger and phospholipase D are required for α_1-adrenergic receptor stimulation of metalloproteinase-9 and cellular invasion in CCL39 fibroblasts, Arch. Biochem. Biophys. 477 (1) (2008) 60–66, https://doi.org/10.1016/j.abb.2008.05.007.
[54] G.H. Nuckolls, C.E. Turner, K. Burridge, Functional studies of the domains of talin, J. Cell Biol. (1990), https://doi.org/10.1083/jcb.110.5.1635.
[55] Y. Ono, H. Sorimachi, Calpains - an elaborate proteolytic system, Biochim. Biophys. Acta - Proteins Proteomics. 1824 (2012) 224–236, https://doi.org/10.1016/j.bbapap.2011.08.005.
[56] S.J. Franco, M.A. Rodgers, B.J. Perrin, J. Han, D.A. Bennin, D.R. Critchley, A. Huttenlocher, Calpain-mediated proteolysis of talin regulates adhesion dynamics, Nat. Cell Biol. (2004), https://doi.org/10.1038/ncb1175.
[57] L. Li, X. Li, L. Qi, P. Rychahou, N. Jafari, C. Huang, The role of talin2 in breast cancer tumorigenesis and metastasis, Oncotarget 8 (2017) 106876–106887, https://doi.org/10.18632/oncotarget.22449.
[58] D. Cong, W. Zhu, Y. Shi, K.B. Pointer, P.A. Clark, H. Shen, J.S. Kuo, S. Hu, D. Sun, Upregulation of NHE1 protein expression enables glioblastoma cells to escape TMZ-mediated toxicity via increased H+ extrusion, cell migration and survival Damin, Carcinogenesis 35 (2014) 2014–2024, https://doi.org/10.1093/carcin/bgu089.
[59] X. Guan, M.N. Hasan, G. Begum, G. Kohanbash, K.E. Carney, V.M. Pigott, A.I. Persson, M.G. Castro, W. Jia, D. Sun, Blockade of Na/H exchanger stimulates glioma tumor immunogenicity and enhances combinatorial TMZ and anti-PD-1 therapy, Cell Death Dis. 9 (2018) 1–16, https://doi.org/10.1038/s41419-018-1062-3.

Baster et al. Supplementary Figure 1

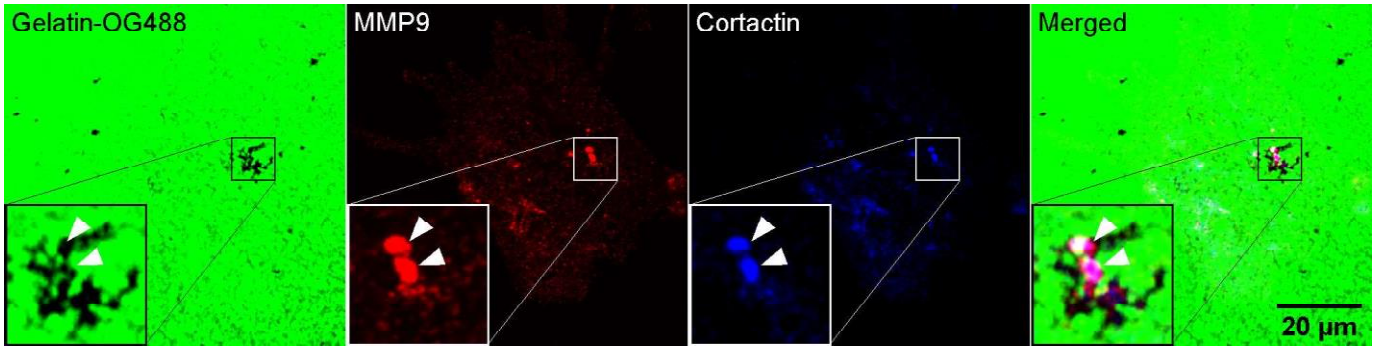

Baster et al. Supplementary Figure 2

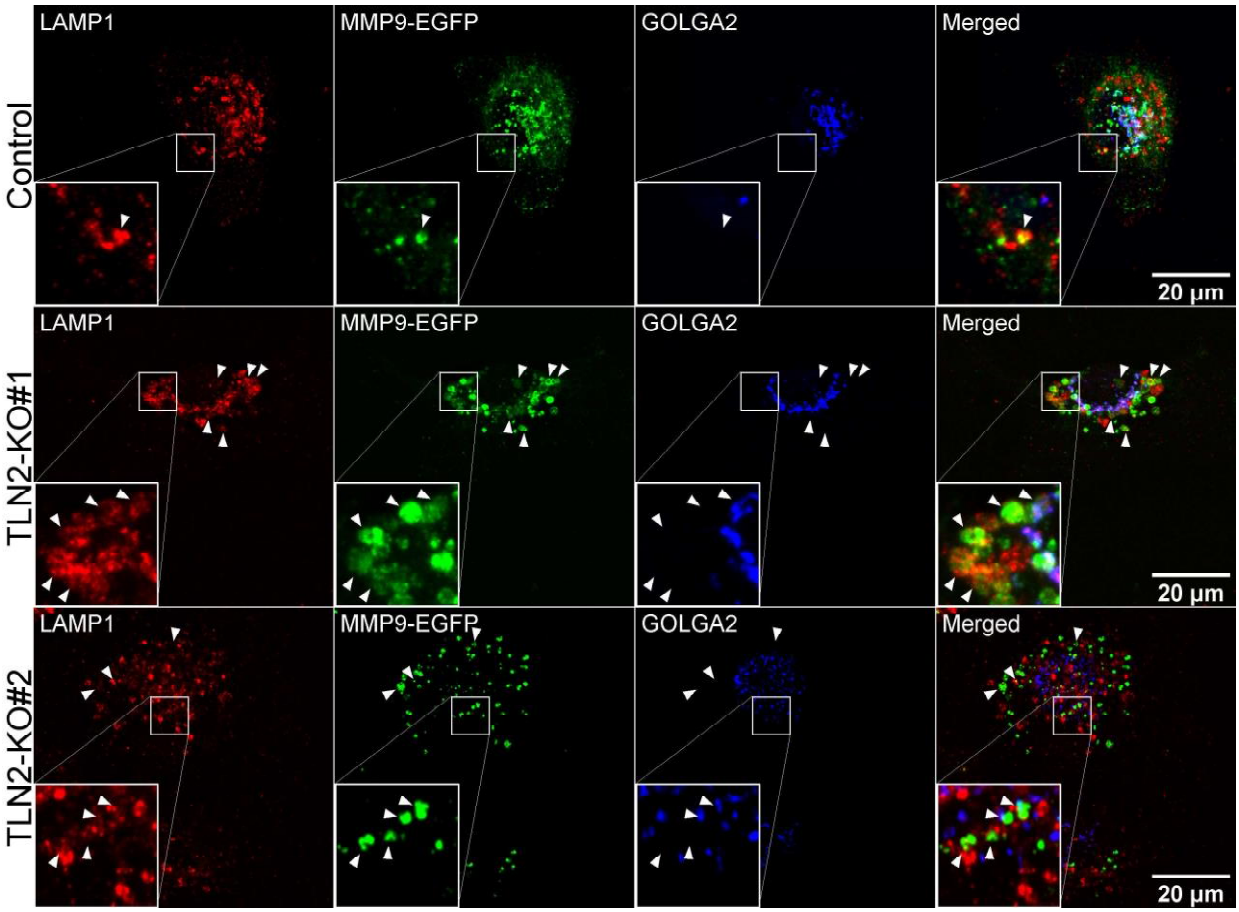

Baster et al. Supplementary Figure 3

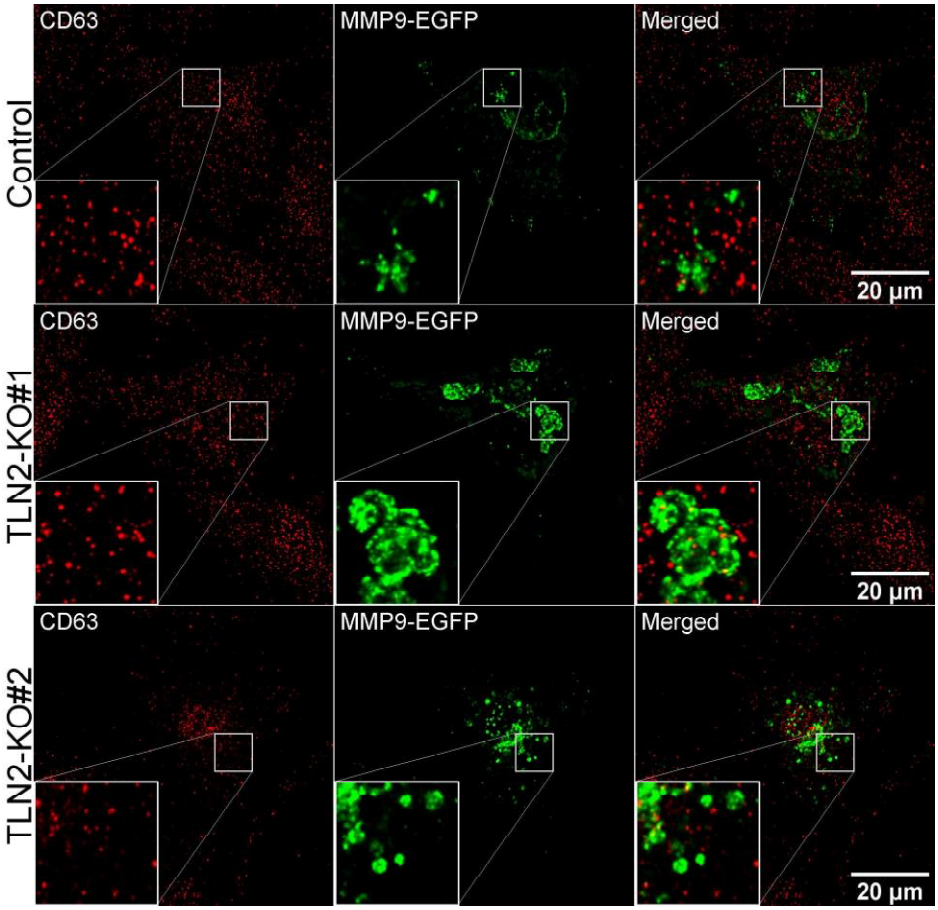

Baster et al. Supplementary Figure 4

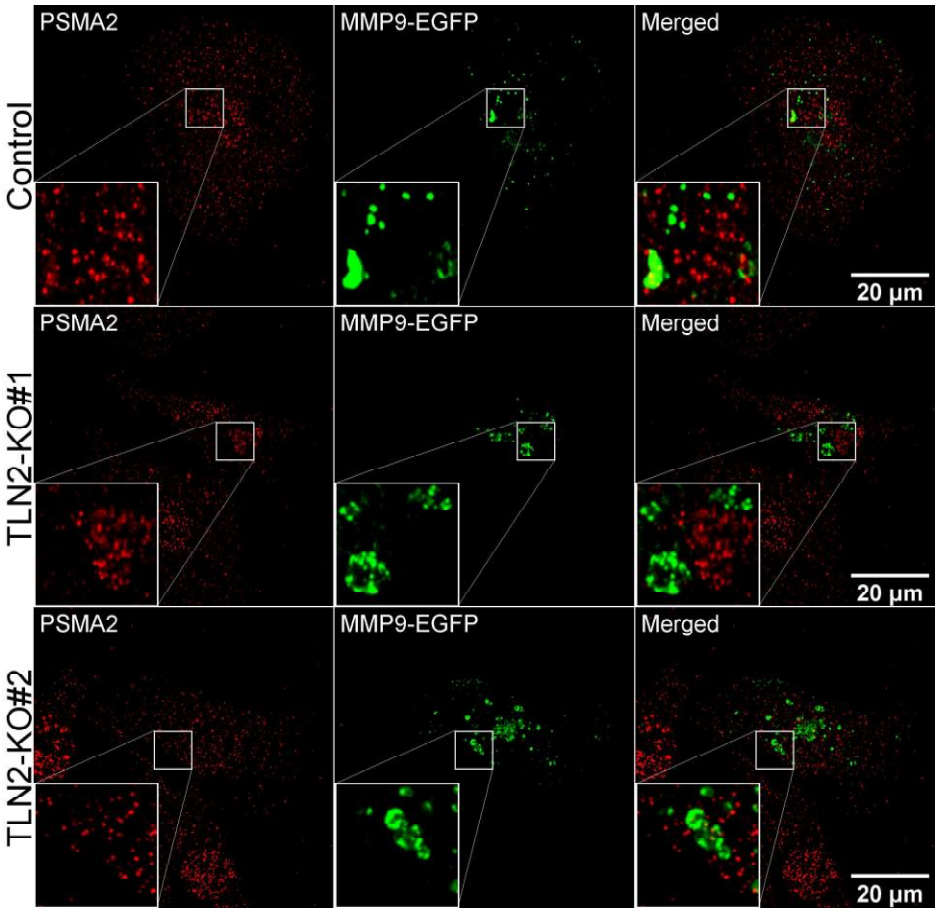

Baster et al. Supplementary Figure Legends

Supplementary Fig. 1. MMP9 colocalizes with cortactin at digestion spots. MDA-MB-231 cells plated on gelatin-Cy3 covered bottom-glass dish and stained with anti-cortactin and anti-MMP9 antiodies were imagined using TIRF microscopy. Arrows point at colocalisation spots between cortactin, MMP9 and digested gelatin. Representative images are shown.

Supplementary. Fig. 2. MMP9 colocalizes with Golgi apparatus and enlarged MMP9 vesicles co-localize with lysosome marker in talin2-KO and control cells. Talin2-KO MDA-MB-231 cells and the control cells were transfected with MMP9-EGFP, plated on fibronectin, and stained with anti-GOLGA2 and anti-LAMP1 antibodies. Representative maximum intensity projections (MIP) of confocal images are shown.

Supplementary. Fig. 3. MMP9 does not colocalize with CD63 exosome marker in MDA-MB-231. Talin2-KO MDA-MB-231 cells and the control cells were transfected with MMP9-EGFP, plated on fibronectin, and stained with anti-CD63 antibodiy. Representative maximum intensity projections (MIP) of confocal images are shown.

Supplementary. Fig. 4. MMP9 does not colocalize with proteasomes marker in MDA-MB-231. Talin2-KO MDA-MB-231 cells and the control cells were transfected with MMP9-EGFP, plated on fibronectin, and stained with anti-PSMA2 antibodiy. Representative maximum intensity projections (MIP) of confocal images are shown.

APPENDIX – PUBLICATION III

Cyanidin-3-glucoside binds to talin and modulates colon cancer cell adhesions and 3D growth

Zbigniew Baster, Liqing Li, Sampo Kukkurainen, Jing Chen, Olli Pentikäinen, Balázs Győrffy, Vesa P. Hytönen, Haining Zhu, Zenon Rajfur, Cai Huang

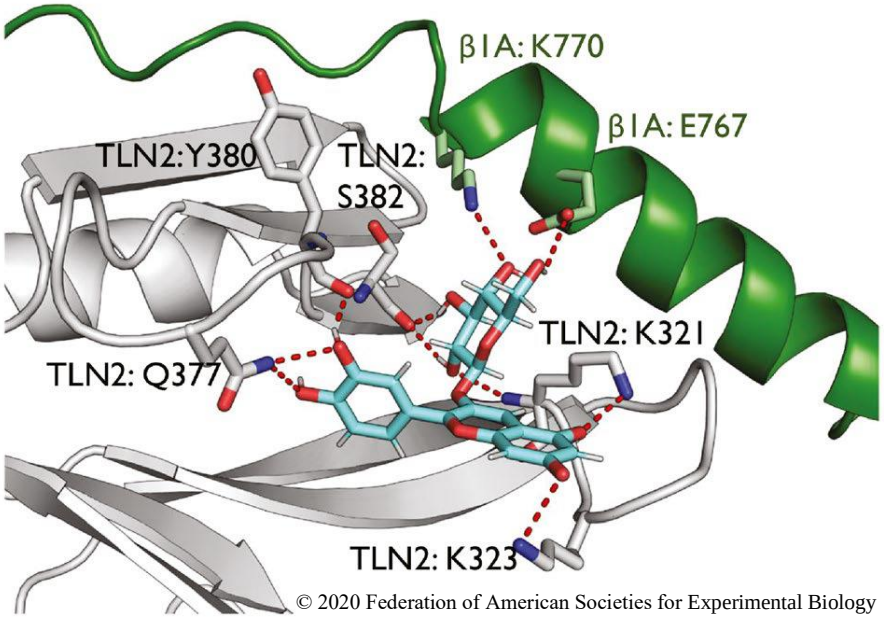

Highlights

- Increased expression of talin1 or β1 integrin correlates negatively with colon cancer patient survival rates.
- Depletion of talin1 inhibits growth of colon cancer mini-tumors (spheroids) in fibrin gels.
- Through binding to talin, cyanidin-3-glucoside (C3G) increases talin's affinity towards β1 integrin.
- C3G locates itself at the talin-integrin interface, influencing the complex's interaction mechanism.
- C3G stimulates adhesion of colon cancer cells plated on a fibronectin substrate but does not influence proliferation.
- C3G inhibits growth of colorectal cancer mini-tumors in fibrin gels.

Received: 11 April 2019 | Revised: 21 May 2019 | Accepted: 25 June 2019

DOI: 10.1096/fj.201900945R

RESEARCH ARTICLE

THE FASEB JOURNAL

Cyanidin-3-glucoside binds to talin and modulates colon cancer cell adhesions and 3D growth

Zbigniew Baster[1,2] | Liqing Li[1] | Sampo Kukkurainen[3] | Jing Chen[4] | Olli Pentikäinen[5] | Balázs Győrffy[6] | Vesa P. Hytönen[3,7] | Haining Zhu[4] | Zenon Rajfur[2] | Cai Huang[1,8]

[1]Markey Cancer Center, Department of Pharmacology and Nutritional Sciences, University of Kentucky, Lexington, KY, USA

[2]Institute of Physics, Faculty of Physics, Astronomy and Applied Computer Science, Jagiellonian University, Krakow, Poland

[3]Faculty of Medicine and Health Technology, Tampere University, Tampere, Finland

[4]Department of Molecular and Cellular Biochemistry, University of Kentucky, Lexington, KY, USA

[5]Institute of Biomedicine, Integrative Physiology and Pharmacology, University of Turku, Turku, Finland

[6]MTA TTK Lendület Cancer Biomarker Research Group, Institute of Enzymology, Hungarian Academy of Sciences, Budapest, Hungary

[7]Fimlab Laboratories, Tampere, Finland

[8]Department of Pharmacology and Nutritional Sciences, University of Kentucky, Lexington, KY, USA

Correspondence
Zenon Rajfur, Institute of Physics, Faculty of Physics, Astronomy and Applied Computer Science, Jagiellonian University, Krakow, Poland.
Email: zenon.rajfur@uj.edu.pl

Cai Huang, Markey Cancer Center, Department of Pharmacology and Nutritional Sciences, University of Kentucky, Todd Building, Room 551, 789 South Limestone St., Lexington, KY 40536, USA.
Email: cai-huang@uky.edu

Funding information
HHS | NIH | National Institute of General Medical Sciences (NIGMS), Grant/Award Number: R01 GM122994; Faculty of Physics, Astronomy, and Applied Computer Science of Jagiellonian University, Grant/Award Number: N17/MNS/000006; BRATNIAK Jagiellonian University Students and Graduates Foundation

[Correction added on February 18, 2020, after first online publication: Country names has been corrected for affiliations 3, 5 & 7.]

Abstract

Cyanidin-3-glucoside (C3G) is a natural pigment, found in many colorful fruits and vegetables. It has many health benefits, including anti-inflammation, cancer prevention, and anti-diabetes. Although C3G is assumed to be an antioxidant, it has been reported to affect cell-matrix adhesions. However, the underlying molecular mechanism is unknown. Here, we show that the expression of talin1, a key regulator of integrins and cell adhesions, negatively correlated with the survival rate of colon cancer patients and that depletion of talin1 inhibited 3D spheroid growth in colon cancer cells. Interestingly, C3G bound to talin and promoted the interaction of talin with β1A-integrin. Molecular docking analysis shows that C3G binds to the interface of the talin-β-integrin complex, acting as an allosteric regulator and altering the interaction between talin and integrin. Moreover, C3G promoted colon cancer cell attachment to fibronectin. While C3G had no significant effect on colon cancer cell proliferation, it significantly inhibited 3D spheroid growth in fibrin gel assays. Since C3G has no or very low toxicity, it could be potentially used for colon cancer prevention or therapy.

KEYWORDS

adhesion, cancer prevention, cyanidin-3-glucoside, drug discovery, molecular docking, talin1, talin2, β-integrin

Abbreviations: 3D, three-dimensional; C3G, cyanidin-3-glucoside; DMSO, dimethyl sulfoxide; EGFP, enhanced green fluorescence protein; ESI, electrospray ionization; FN, fibronectin; GST, glutathione S-transferase; LC-MS, liquid chromatography mass spectrometry; MMP, matrix metalloproteinase; NBT, nitroblue tetrazolium; TBST, tris-buffered saline with Tween-20; WST-8, 2-(2-methoxy-4-nitrophenyl)-3-(4-nitrophenyl)-5-(2,4-disulfophenyl)-2H-tetrazolium.

1 | INTRODUCTION

Cyanidin-3-glucoside (C3G) is a natural dye found in blackberries, bilberries, and several other black-red fruits and vegetables.[1-3] It is the most common member of the anthocyanin family.[4] Many studies describe C3G as an antioxidant[4-7] contributing to anti-inflammation,[7-9] anti-obesity,[10,11] and anti-diabetic[7,11-13] processes, and to the reduction of risk of cardiovascular diseases.[7,14] Furthermore, several reports show the C3G's inhibitory effect on cancer metastasis, tumor progression and cell migration in lung,[15,16] and breast[17,18] cancer cell lines. Chen and colleagues[15] showed that C3G significantly reduces invasiveness, adhesion, and matrix metallopeptidase (MMP) activity in lung cancer cells. Although C3G is thought to be an antioxidant, its effect on cell adhesion suggests that it may regulate integrin activation or integrin signaling pathways.

Talin binding to β-integrin tails is the common step in integrin activation.[19] Talin was first identified in 1983 by Keith Burridge and Laurie Connell[20] as a focal adhesion and ruffling membrane protein. In the following years, the binding of talin toward vinculin[21] and integrin[22] was demonstrated. There are two main domains in talin[23]: an N-terminal head domain responsible for the interaction with β-integrin,[24,25] and a large C-terminal rod domain composed of 13 alpha-helix bundles responsible for the interaction with vinculin and actin.[25-27] There are two different versions of talin protein in human: talin1 (Tln1) and talin2 (Tln2) encoded by *TLN1* and *TLN2* genes, respectively.[28] Talin-integrin affinity differs between two variants of talin. We reported previously that talin2 interacts with β1-integrin stronger than talin1, with Ser-339/Cys-336 (talin2/talin1) disparity in the sequences being the main reason for the difference in affinities.[29,30] The main integrin β1-binding site in both variants of talin is localized in the F3 head domain at the pocket formed by Arg-358/361, Ala-360/363 and Tyr-377/380 (Tln1/Tln2) and at the turn of β1-β2 loop with Asn-326/323 and Lys-327/324 creating hydrogen bonds with the integrin tail.[30,31] Although initially it was hypostatized that talin2 acts redundantly with talin1, latest studies show that the two proteins have distinct functions.[29,32,33] Although both talin1 and talin2 regulate cell migration, invasion, tumor growth, and metastasis, talin1 plays a more prominent role in tumor growth than talin2.[34]

In the present study, we demonstrated the essential role of talin1 in 3D spheroid growth of colon cancer cells in fibrin gel assays and identified C3G as a promoter of the talin-β-integrin interaction. Molecular docking analysis showed that C3G bound to the interface of the talin/β-integrin complex. Furthermore, C3G promoted cell adhesions on fibronectin. Although C3G had little effect on the proliferation of colon cancer cells, it significantly inhibited 3D spheroid growth of colon cancer cells in fibrin gel assays. Therefore, C3G could be a potential therapeutic agent for colon cancers.

2 | MATERIALS AND METHODS

2.1 | Reagents

C3G was a gift from our colleague Dr Jia Lou (University of Kentucky). pLKO1 lentivirus shRNA clones that target talin1 were from Sigma. Talin1 shRNA clones are TRCN0000123105 (#1), TRCN0000299020 (#2), and TRCN0000299022 (#3). Anti-GFP rabbit polyclonal antibody (G1544) and anti-polyhistidine mouse monoclonal antibody (Clone HIS-1) were from Sigma. Anti-talin1 mouse monoclonal antibody (clone 97H6) was from Bio-Rad. Anti-talin2 rabbit polyclonal antibody (PB9961) was from BosterBio (Pleasanton, CA). Anti-tubulin mouse monoclonal antibody (TM4111) was from ECM Bioscience (Versailles, KY). Safectine RU50 transfection kit was purchased from Syd Labs (Malden, MA). Alexa Fluor 700 goat anti-rabbit IgG (H+L) (A21038) and Alexa Fluor 800–conjugated goat anti-mouse IgG (H+L) (A11375) were from Invitrogen. Fibronectin was purified from bovine plasma using gelatin-Sepharose column. Salmon fibrinogen (SEA-133) and Salmon thrombin (SEA-135) were from Searun Holdings (Freeport, ME). N-(1-pyrene)iodoacetamide was from Setareh Biotech (Eugene, OR).

2.2 | Cell culture and transfection

CHO-K1 Chinese hamster ovary cells; human colon cancer cell lines HCT116, Caco2, and SW480; human breast cancer cell lines MDA-MB-231 and BT459; and human melanoma cell line MDA-MB-435S were from the American Type Culture Collection. Human colon cancer cell lines HT-29 and RKO were from Dr Qing-bai She (University of Kentucky). All the cell lines were maintained in DMEM medium (Sigma) containing 10% fetal bovine serum (FBS), penicillin (100 U/mL), and streptomycin (100 μg/mL). CHO-K1 cells were transfected with Safectine RU50.

2.3 | Talin1 knockdown

293FT cells were co-transfected with talin1 shRNA and lentiviral packaging plasmids (pMDLg/pRRE, pRSV-Rev, and CMV-VSVG) using Safectine RU50 transfection reagent according to the manufacturer's protocol. The medium of transfectants was collected at 48 hours and filtered with 0.45-μm filter. The virus particles were applied to overnight cultures of colon cancer cells for infection. Cells stably expressing shRNA control or talin1 shRNAs were obtained by growing infected cells in the presence of 1 μg/mL puromycin for 10 days.

2.4 | Cell proliferation assays

Cells were trypsinized and resuspended in DMEM containing 10% FBS at a density of 5×10^4 cells/mL. Cells were treated with C3G or vehicle (DMSO) where was indicated. One hundred microliters of cells was added to each well of 96-well tissue culture plates. The cells were allowed to grow for 1-4 days (as indicated) in a CO2 incubator and then incubated with 10 μL (per well) of TetraZ (WST-8) cell counting kit. Cell proliferation was determined by measuring absorbance 450 nm using a BioTek plate reader.

2.5 | 3D fibrin gel assays

3D fibrin gel assays were performed as described previously.[35] Briefly, cells were trypsinized and suspended in DMEM containing 10% FBS at a density of 1×10^4 cells/mL. Fibrinogen (2 mg/mL) in T7 buffer (pH 7.4, 50 mM Tris, 150 mM NaCl) was mixed with cell solution (1:1), and 250 μL cell/fibrinogen mixtures were mixed well with pre-added 2 μL thrombin (0.25 U/μL) in each well of 24-well plate. The plate was then incubated in a CO_2 incubator for 10 minutes, and then, 0.5 mL DMEM containing 10% FBS and antibiotics were added. The cells were cultured for 12 days for 3D spheroid formation, with medium/C3G change at 4-day intervals. 3D spheroid tumors were visualized by adding 50 μL of NBT to each well and incubating for 12 hours.

2.6 | Talin-integrin interaction assays

The binding of purified His-tagged proteins to GST-β1-integrin tails was performed in Buffer A (50 mM Tris-HCl, pH 7.4, 0.1% NP-40, 150 mM NaCl, and 1 mM EDTA containing 0.5 mg/mL porcine gelatin unless where specified). Bound protein was eluted with 10 mM glutathione and determined with dot blotting, or separated using SDS-PAGE, stained with Coomassie blue. The gels were scanned with LI-COR Infrared Imager using 700-nm channel. Protein bands were quantified by analyzing inverted images using ImageJ as described previously.[30,36]

For pulldown assays using cell lysates, CHO-K1 cells were transfected with pEGFP-talin$2_{206\text{-}403}$, pEGFP-talin$1_{1\text{-}446}$, or their mutants. At 28 hours post-transfection, the cells were harvested in Buffer A containing 0.5% NP-40 and protease inhibitor cocktail. Cell lysates were cleared by centrifugation and mixed with NP-40-free buffer A (1:4). The cell lysates were mixed with C3G or vehicle and then incubated with glutathione-agarose beads loaded with GST or GST-β1-integrin tails at 4°C for 120 minutes. The beads were washed once with 1 mL of TBST buffer and resuspended in SDS-sample buffer. Samples were analyzed using SDS-PAGE and transferred to nitrocellulose membrane for detecting protein interaction.

2.7 | Interaction of talin with C3G

Recombinant His talin$2_{1\text{-}449}$ was labeled with N-(1-pyrene) iodoacetamide according to the manufacturer's protocol. The unreacted pyrene reagent was removed using a Bio-Gel P-30 gel filtration column. Pyrene-talin$2_{1\text{-}449}$ at 50 μg/mL in Buffer A was mixed with different concentrations of C3G. The fluorescence spectra were determined using Cytation 5 Cell Imaging Reader (BioTek, Winooski, VT), with excitation 344 nm. To determine the affinity of C3G to talin2, fluorescence in presence of different concentrations of C3G (F) and vehicle (F_0) was measured with Excitation 344 nm and Emission 384 nm. $(F_0-F)/F_0$ was plotted against the concentrations of C3G, and the binding constant was determined using SigmaPlot.

2.8 | Analysis of C3G binding using molecular docking

The talin2-β1A-integrin complex structures were constructed based on 3G9W structure[37] by introducing a Q778G point mutation and deleting the C-terminal PIN(N) sequence using PyMOL. Original C3G structure was based on PubChem. Different protonated forms (total 16) of C3G were generated using SPORES software.[38] Molecular docking was carried out with all 16 forms of C3G using PLANTS software.[39]

2.9 | Cell adhesion assays

Non-treated 96-well plates were coated with 5, 10, and 20 μg/mL of FN at 4°C overnight. Cells were trypsinized and suspended in serum-free DMEM at a density of 3×10^5 cells/mL. The cells were treated with C3G or vehicle (DMSO) as indicated. One hundred microliters of cells was added to each well of a FN-coated 96-well plate. The plate was incubated in a CO_2 incubator for 1-4 hours based on the cell lines. Unattached cells were washed away with DPBS, and attached cells were fixed with 4% paraformaldehyde and stained with crystal violet. Stained cells were quantitated with Li-COR Odyssey Imaging System.

2.10 | Liquid chromatography mass spectrometry

Liquid chromatography was performed using a Shimadzu HPLC system consisting of a SIL-20AHT autosampler

and two LC-20 AD pumps (Shimadzu, Canby, OR, USA) with a Kinetex XB-C18 column (100 × 4.6 mm, 2.6 μm, Phenomenex, Torrance, CA, USA) with gradient conditions: mobile phase A: water; B: methanol; and flow rate: 280 μL/min. A TSQ Vantage triple-quadrupole mass spectrometer equipped with an electrospray ionization (ESI) source (Thermo Fisher, Waltham, MA, USA) was used for mass spectrometric detection. Selected reaction monitoring (SRM) of *m/z* 447.4→284.1 for C3G in the negative mode was utilized to conduct quantitative analysis.

3 | RESULTS

To know the correlation between talin1 expression and the survival rate of colon cancer patients, we performed a Cox analysis and generated a Kaplan-Meier plot using a previously established database.[40] Higher talin1 expression negatively correlated with the survival probability of colon cancer patients (Figure 1A). A similar correlation is observed between ITGB1 (β1-integrin) expression and the survival rate of colon cancer patients (Figure 1B). To learn the role of talin1 in the proliferation of colon cancer cells, talin1 in HT-29 cells was depleted and cell proliferation was examined using WST-8 cell proliferation assays. Depletion of talin1 caused a moderate inhibition of HT-29 cell proliferation (Figure 1C). Since 3D spheroid tumor growth in fibrin gel correlates with the tumorigenic capacity of tumor cells in mice,[35] we examined the role of talin1 in mini-tumor (3D spheroid) growth, using 3D fibrin gel assays. Depletion of talin1 in HT-29 and HCT116 colon cancer cells significantly inhibited 3D spheroid growth in fibrin gel assays (Figure 1D,E).

To identify inhibitors or activators that perturb the talin-β-integrin interaction, we examined the effects of more than 180 natural products, including pure compounds and crude extracts, using in vitro GST pulldown assays. Because talin2 has a higher affinity to β-integrin tails than talin1, we used talin2 in the initial screening assays. To this end, recombinant His-tagged talin2$_{1\text{-}449}$ was mixed with different natural products and incubated with recombinant GST-β1A integrin tail preloaded to glutathione beads for 90 minutes at 4°C. Bound proteins were eluted with glutathione and analyzed using dot blotting. During this screen, we did not find any compounds that inhibit talin-β1A-tail interaction. However, we found that C3G and several other fractionated natural products promoted the binding of talin2 to the β1A-integrin tail (Figure 2A). C3G was selected for further examination because C3G is the only pure compound with activity in our screening assays. Further analysis with SDS-PAGE showed that C3G promoted the interaction of β1A-integrin tail with both talin1 and talin2 in a dose-dependent manner (Figure 2B). To determine whether C3G binds to talin, His-tagged talin2 was labeled with N-(1-pyrene) iodoacetamide, and the emission spectrums of pyrene-labeled talin2 were determined in the presence of different concentrations of C3G. As shown in Figure 2C, C3G quenched the fluorescence of pyrene-talin2 in a dose-dependent manner, indicating that C3G binds to talin2. A dissociation constant (K_d) of 26 μM was determined based on the fluorescence quenching assays (Figure 2D).

To identify which domains are responsible for C3G binding, EGFP-talin2$_{206\text{-}403}$ (F2-F3 domains) and EGFP-talin1$_{1\text{-}446}$ were transfected into CHO-K1 cells, respectively. The binding of these proteins to β1A-integrin tails was performed using GST pulldown assays, in the presence of C3G or vehicle (DMSO). The binding of the two proteins to β-integrin tails was promoted by C3G (Figure 3A), suggesting that C3G binds to the F2-F3 domains. To determine the binding site of C3G on talin, molecular docking was performed. The talin2-β1A-integrin complex structure was constructed based on the structure of the talin2-β1D-integrin complex.[30] Molecular docking was carried out with all 16 protonation states of C3G (Figure 3B) using the PLANTS software.[38] The best docking solutions place C3G at the interface of talin2 and integrin (Figure 3C-E) with K323, K321, Q377, S382, and Y380 residues responsible for creating a binding niche in talin2, and E767 and K770 β1A-integrin residues interacting directly with C3G (Figure 3C). To verify this docking model, EGFP-talin1^{WT}, EGFP-talin1^{Y377F,378F} (corresponding to talin2^{Y380F,381F}), and EGFP-talin1^{C336S} were transfected into CHO-K1 cells, respectively. The binding of these proteins to β1A-integrin tails was performed using GST pulldown assays, in the presence of C3G or vehicle. Substitution of Y377 and Y378 with Phe significantly inhibited C3G-induced talin1-β1-integrin interaction, whereas substitution of C336 with Ser had little effect (Figure 3F). Thus, although the molecular docking model remains to be further verified, the current data support the proposed model.

To examine the effect of C3G on cell adhesions, cells were treated with different concentrations of C3G and plated on a fibronectin (FN)-coated 96-well plate. As expected, C3G promoted the attachment of colon cancer cells RKO to low concentrations of FN in a dose-dependent manner, but had no effect at high concentration of FN (Figure 4A,B). Similar results were observed in HT-29, HCT116, and SW480 cancer cell lines (Figure 4C,D). However, C3G had only marginal effect on the attachment of DLD1 cells (Figure 4E). Since DLD1 cells had strong adhesions to FN in the absence of C3G, and C3G had no effect at high concentrations of FN, C3G may be more effective when cells have a loose adhesion.

To determine the bioactivity of C3G, we examined the effect of C3G on cancer cell proliferation, using WST-8 cell proliferation assays. C3G had small effects on the proliferation of HCT116 and SW480 colon cancer cell lines, but had no effects on that of Caco2 and HT-29 (Figure 5A). C3G also had no effects on the proliferation

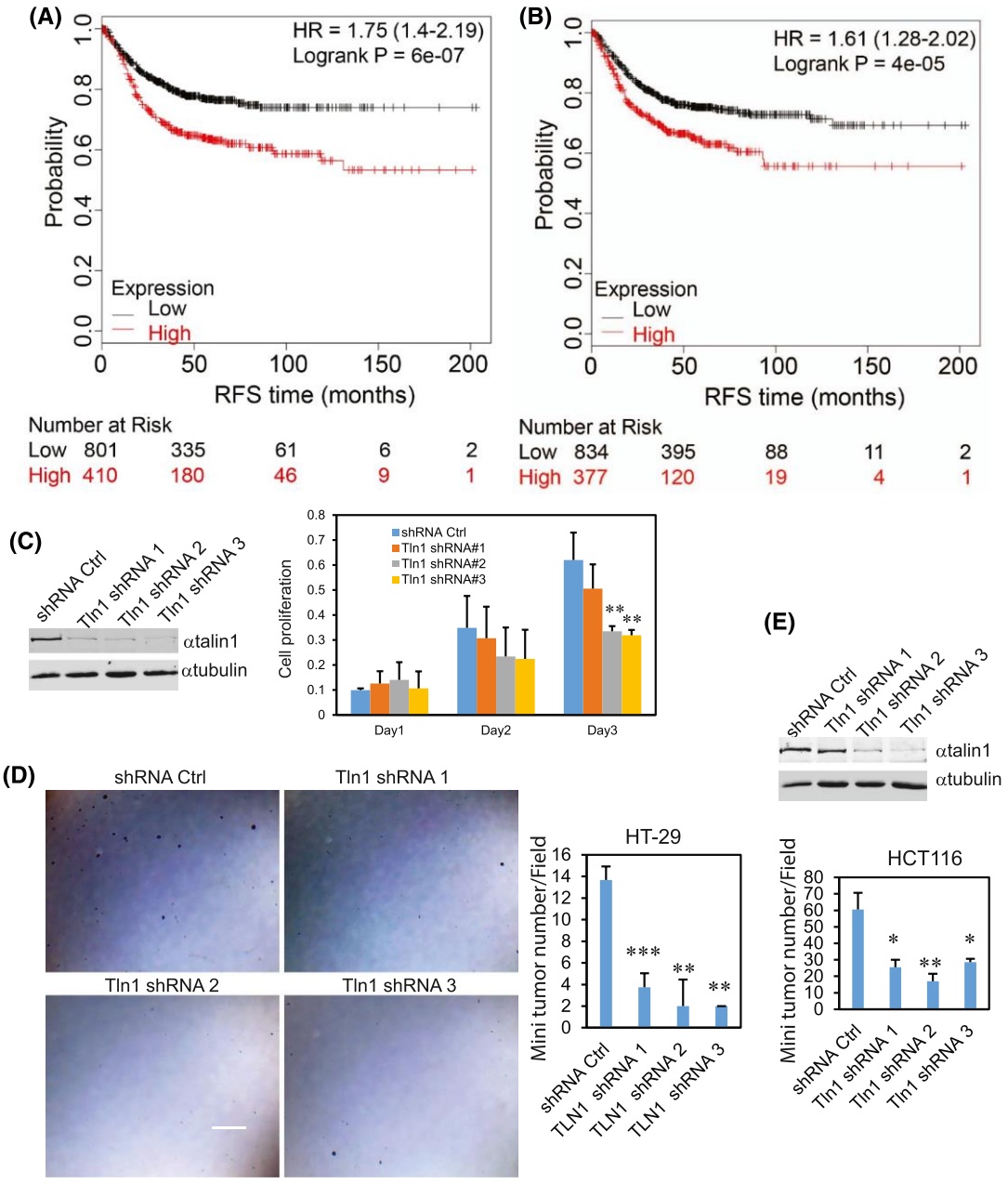

FIGURE 1 Talin1 expression correlates with poor survival rate of colon cancer patients and is essential for 3D mini-tumor growth. A, Kaplan-Meier plot of the correlation between talin1 expression and the survival rate of colon cancer patients. B, Kaplan-Meier plot of the correlation between ITGB1 (β1-integrin) expression and the survival rate of colon cancer patients. C, Depletion of talin1 using shRNA slightly inhibited the proliferation of HT-29 cells. Data = mean ± SD, n = 5, $^{**}P < .01$. D, Depletion of talin1 inhibited the mini-tumor growth of HT-29 cells in fibrin gel assays. Data = mean ± SD, n = 4, $^{**}P < .01$, $^{***}P < .001$. Scale bar, 1 mm. E, Depletion of talin1 using shRNA inhibited the mini-tumor growth of HCT116 cells in fibrin gel. Data = mean ± SD, n = 4, $^{*}P < .05$, $^{**}P < .01$

of BT549, MDA-MB-435S, and MDA-MB-231 cell lines (Figure 5B). However, C3G dramatically inhibited the 3D spheroid tumor growth of HT-29 cells in fibrin gel assays (Figure 5C). It also significantly suppressed the 3D spheroid growth of HCT116 cells (Figure 5D). In addition, it inhibited MMP secretion and the invasion of MDA-MB-231, MDA-MB-468, and MDA-MB-157 cells (data not shown).

Because it has been reported that C3G is thermally unstable,[41] we used LC-MS selected reaction monitoring (SRM) method to examine the stability of C3G in the DMEM media when incubated at 37°C. Approximately 61% and 50% of

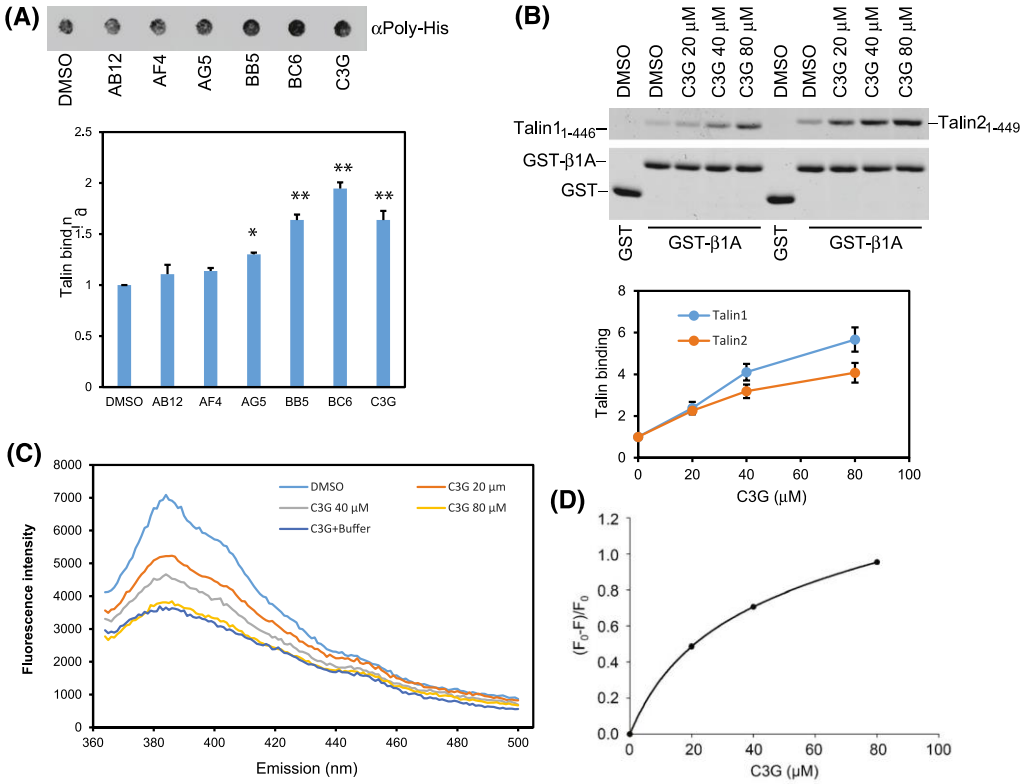

FIGURE 2 C3G bound to talin and promoted talin-b1A-integrin interaction. A, His-tagged talin2$_{1\text{-}449}$ (5 μg) in 100 μL of Buffer A with different natural products or vehicle was incubated with glutathione-agarose beads preloaded with GST or GST-β1A-integrin tails (5 μg). The beads were washed with TBST, and bound proteins were eluted and detected with dot blotting. C3G 20 μM; all other natural products, 100 μg/mL. B, C3G promoted the interaction of His-tagged talin1$_{1\text{-}446}$ and talin2$_{1\text{-}449}$ with GST-β1A-integrin tails in GST pulldown assays. The binding was detected by Coomassie staining. Data = mean ± SD, n = 3. $*P < .05$, $***P < .001$. C, C3G changed the conformation of talin2. His-tagged talin2$_{1\text{-}449}$ was labeled with N-(1-Pyrene)iodoacetamide. Spectrums of pyrene-talin21-449 were determined by excited at 344 nm in the presence of different concentrations of C3G or vehicle (DMSO). As a control, the spectrum of C3G in the assay buffer (C3G + Buffer) was also determined. D, The fluorescence of pyrene-talin2$_{1\text{-}449}$ in different concentrations of C3G (F) or vehicle (DMSO, F_0) was measured with Ex 344 and Em 384 nm. Data were plotted and fitted with SigmaPlot

C3G were retained in the medium after 16 and 30 hours incubation, respectively (Figure 5E), suggesting that C3G was slowly degraded at 37°C.

4 | DISCUSSION

Our previous studies show the importance of talin in tumor growth and tumor metastasis.[29,34,42] Talin binding to β-integrin tails is a common step in integrin activation, a key step for cell-matrix adhesions and focal adhesion formation.[19] In this work, we demonstrated that talin1 is essential for the 3D spheroid tumor growth of colon cancer cells and that C3G bound to the interface of the talin-β-integrin complex, promoted talin binding to β-integrins and cell-matrix adhesions, but unexpectedly inhibited the 3D mini-tumor growth in colon cancer cells.

It has been reported that C3G has a variety of health benefits, including anti-inflammation,[8,9] anti-obesity[10,11] and anti-diabetes,[11,12] and anti-cancer activities. However, its mechanism of action is unclear. Talin binds to β-integrin tails and activates integrins, which regulate many physiological and pathological processes, such as inflammation,[43,44] obesity,[45,46] diabetes,[47-49] and cancer.[50,51] Thus, perturbing the talin-β-integrin interaction could be a potential strategy for intervening these health problems. We found that C3G bound to talin and promoted talin-β-integrin interaction processes (Figure 2). As expected, C3G also promoted the adhesions of multiple colon cancer cell lines on fibronectin (Figure 4), suggesting that C3G can activate integrins or regulate integrin signaling. C3G had distinct effects on the adhesions of different colon cancer cell lines (Figure 4). Even in the same cell line, C3G promoted cell adhesion at low concentrations of FN, but had no effect at high concentrations of FN. In fact, C3G inhibited the cell adhesion of some breast cancer cell lines (unpublished data). Thus, C3G, acting like a double-edge sword, has distinct impacts on cell adhesion under different conditions.

In order to understand how C3G modulates the talin-integrin interaction, we performed molecular docking. The

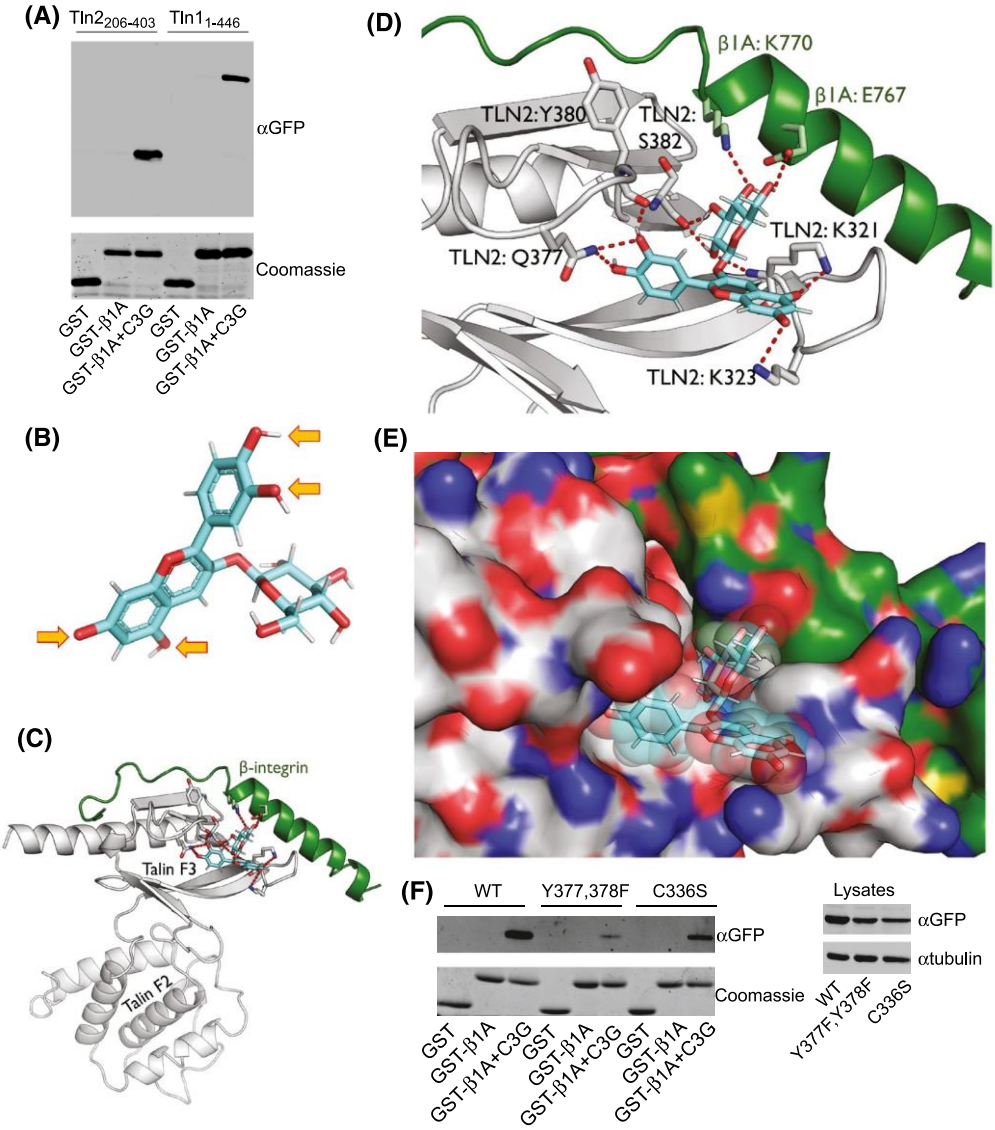

FIGURE 3 Talin2-C3G -β1A-integrin molecular docking simulation. A, EGFP-talin2$_{206-403}$ and EGFP-talin1$_{1-446}$ were transfected into CHO-K1 cells, respectively. The β-integrin binding of these proteins was examined by GST-β1A pulldown assays in the presence of DMSO or C3G (80 μM), using GST as control. B, Structure of C3G, arrows point at potential protonation sites. C, C3G locates at the interface of talin2 and integrin. Talin2 and β1-integrin are represented as gray and green ribbons, respectively. D, C3G docking site with atom-atom interactions is shown. TLN2: K323, K321, Q377, S382, and Y380; and β1A: E767 and K770 residues are shown in a stick model. E, Surface charge map of talin2 and β1-integrin in talin2-C3G-β1A-integrin complex. F, EGFP-talin1$_{1-446}$, EGFP-talin1$_{1-446}^{Y377F,Y378F}$, and EGFP-talin1$_{1-446}^{C336S}$ were transfected into CHO-K1 cells, respectively. The β-integrin binding of these proteins was examined by GST-β1A pulldown assays in the presence of DMSO or C3G (80 μM), using GST as control. The expression of EGFP-talin1$_{1-446}$, EGFP-talin1$_{1-446}^{Y377F,Y378F}$, and EGFP-talin1$_{1-446}^{C336S}$ in cell lysates was shown in the right panel

analysis suggests an interaction mode where C3G binds to the interface of talin2-β1A-integrin complex inside the niche in the F3 domain of talin2 (Figure 3). Within this pocket, C3G interacts with residues Glu767 and Lys770 in β1A-integrin via hydrogen bonds, and with Lys321, Lys323, Gln377, Tyr380, and Ser382 in talin2. It has been reported that β1A-integrin interacts with talin2 F3 domain via Asp759 and Arg760,[30,52] which are two-to-three α-helix turns away from C3G-binding residues and are located on the same side of the helix (Figure 3D). Thus, the macroscopic conformation of talin2-C3G-β1-integrin complex will be similar to the one without C3G. This is consistent with the role of C3G in promoting cell adhesion (Figure 4). On the other hand, C3G interacts with residues Lys323, Lys321 in the β1-β2 loop of talin2 (Figure 3D), which has been shown to highly influence talin-β1-integrin

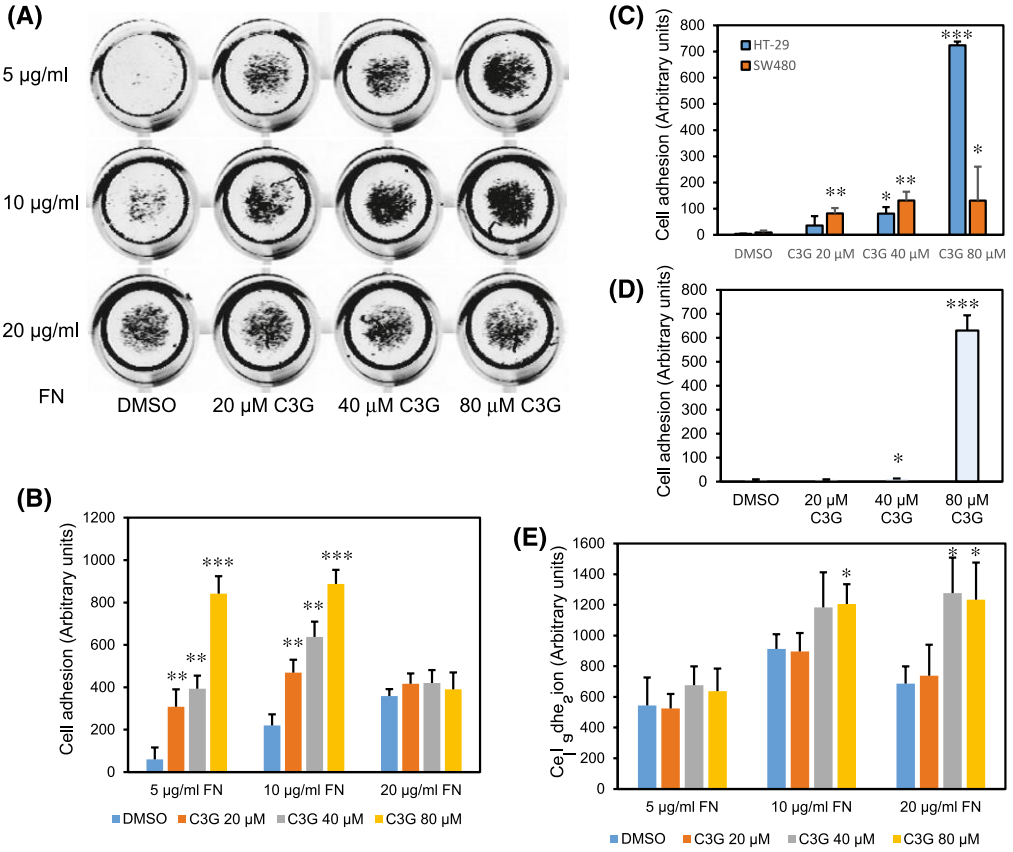

FIGURE 4 C3G promoted colon cancer cell adhesion on FN. A, RKO cells (3×10^4 cells/mL) in 100 μL of serum-free medium were plated on FN-coated 96-well plate in the presence of C3G or vehicle (DMSO), incubated for 1 hour, washed with DPBS, fixed, and stained with crystal violet. B, The 96-well plates were scanned with Li-COR, and the attached cells were quantitated. Data = mean ± SD, n = 5. $^{**}P < .01$, $^{***}P < .001$. C, HT-29 and SW480 cells (3×10^4 cells/mL) in 100 μL of serum-free medium were plated on FN (2.5 μg/mL)-coated 96-well plate with different concentrations of C3G or vehicle (DMSO), incubated for 4 hours, washed with DPBS, fixed, stained with crystal violet, and quantitated with Li-COR. Data = mean ± SD. n = 4. $^{*}P < .05$, $^{**}P < .01$, $^{***}P < .001$. D, HCT116 cells (3×10^4 cells/well) in 100 μL of serum-free medium were plated on FN (2.5 μg/mL)-coated 96-well plates in the presence of C3G or vehicle (DMSO), incubated for 2 hours, fixed, stained with crystal violet, and quantitated. Data = mean ± SD, n = 4. $^{*}P < .05$, $^{***}P < .001$. E, DLD1 cells (3×10^4 cells/well) in 100 μL of serum-free medium were plated on FN-coated 96-well plates with C3G or vehicle (DMSO), incubated for 1 hour, fixed, and stained with crystal violet. Data = mean ± SD, n = 5. $^{*}P < .05$

interaction.[30] Binding of C3G between F3 domain's β1-β2 loop and β-sheet (residues Gln377, Ser382 and Tyr380) may cause a change in native talin2 β1-β2 loop conformation and impair the conformation of talin-β-integrin complex and consequently alter integrin activation. Although, via Glu767 and Lys770 residues, C3G generates separate bonds with integrin thus increasing affinity between both proteins, it is likely that the conformation of talin in the presence of C3G is suboptimal for integrin activation. Thus, we anticipate that C3G would promote cell adhesion when cells have a weak adhesion, while inhibit (or have no effect) when cells are capable of forming strong adhesions, as in the case of some cancer cell lines.

Although C3G has profound effects on the FN adhesions of colon cancer cell lines, it surprisingly did not affect the proliferation of colon cancer cells in 2D (Figure 5). It also had no effect on the proliferation of breast cancer cells. These results indicate that C3G has no or very low toxicity. This can be one of the reasons it has been used as a food additive.[53] Nevertheless, C3G significantly inhibited mini-tumor growth in 3D fibrin gel assays, suggesting that talin-mediated cell adhesions are involved in 3D mini-tumor growth. Because C3G is thermally unstable (Figure 5E) and highly metabolized in vivo,[54,55] the possibility that C3G metabolites, such as protocatechuic acid, inhibit mini-tumor growth has not been ruled out. In addition, it is not clear why C3G promotes cell adhesions while inhibits 3D mini-tumor growth. Since tumor growth is a dynamic process that requires spatiotemporary cell positioning,[56] it is likely that C3G promotes talin-β-integrin interaction and holds integrins in the active state, thus constraining tumor cell positioning and consequently tumor growth (Figure 6).

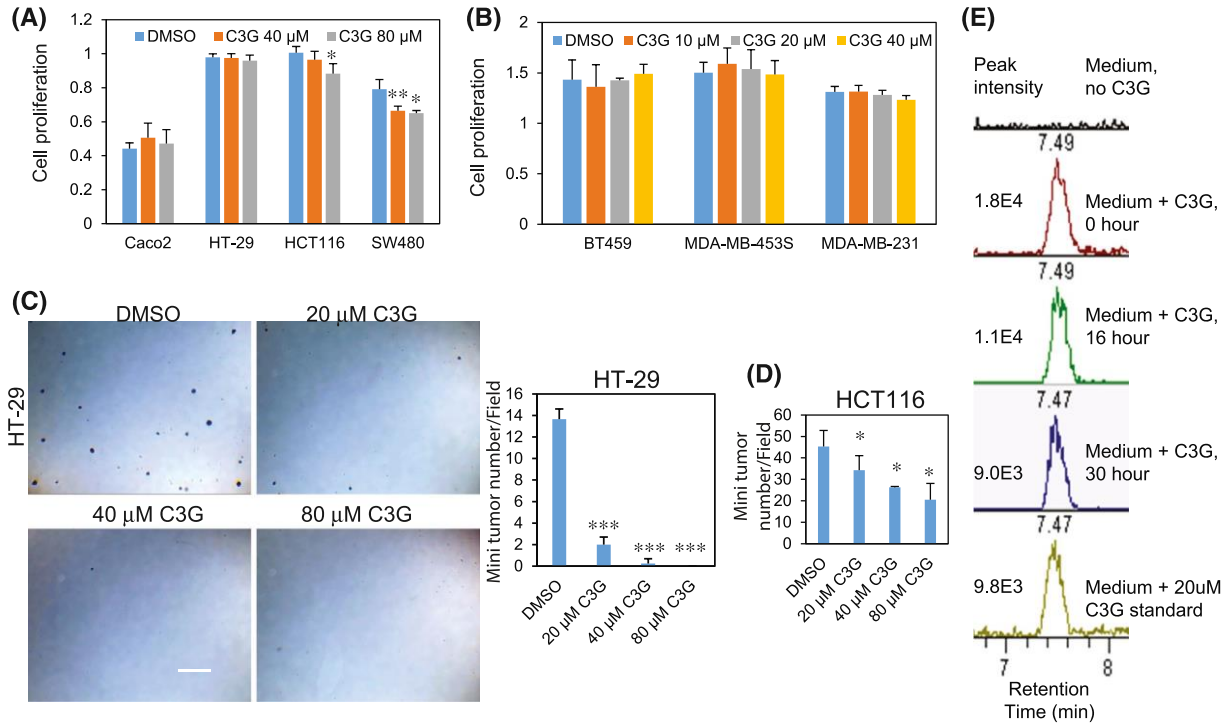

FIGURE 5 C3G had little effect on colon cancer cell proliferation but significantly inhibited 3D mini-tumor growth. A, The proliferation of colon cancer cell lines was determined in the presence of C3G (40, 80 μM) or vehicle (DMSO) using WST-8 cell proliferation kit. Data = mean ± SD, n = 4. *$P < .05$, **$P < .01$. B, The proliferation of breast cancer cell lines was determined in the presence of C3G (10, 20, 40 μM). Data = mean ± SD, n = 4. C, C3G inhibited the mini-tumor growth of HT-29 cells in fibrin gel. Data = mean ± SD, n = 4, ***$P < .001$. Scale bar, 1 mm. D, C3G inhibited the mini-tumor growth of HCT116 cells in fibrin cells. Data = mean ± SD, n = 4. *$P < .05$. E, C3G stability in media analyzed by LC-MS. C3G was added to DMEM, incubated in a CO_2 incubator at 37°C for 0, 16, and 30 hours, respectively, and analyzed with LC-MS SRM method. C3G was quantitated by measuring the intensities of the C3G transition 447.4→284.1 peaks and comparing to those of the standards

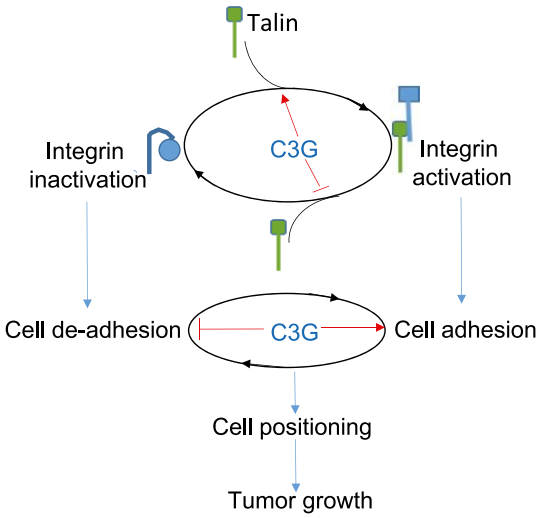

FIGURE 6 A hypothetical model depicting the mechanism whereby C3G inhibits tumor growth

The effective concentration of C3G on 3D spheroid tumor growth was rather high (more than 20 μM). This could be caused by its thermal instability (Figure 5E). However, since C3G had no (or low) cytotoxicity in 2D cell cultures, it could be potentially used to treat certain types of colon cancers. Future studies are needed to define which types of colon cancers are sensitive to C3G and examine the effects in mouse xenograft models.

ACKNOWLEDGMENTS

We thank Dr Jia Lou (University of Kentucky) for C3G compound, and Dr Guojun Wang (Florida Atlantic University) for marine natural products. This work was supported by the National Institutes of Health Grants R01 GM122994 (to CH), by the Faculty of Physics, Astronomy, and Applied Computer Science of Jagiellonian University Grant N17/MNS/000006 for young scientists and PhD students (to Z.B.) and by BRATNIAK Jagiellonian University Students and Graduates Foundation Grant (to Z.B.).

CONFLICT OF INTEREST

The authors declare that there is no conflict of interest.

AUTHOR CONTRIBUTIONS

Z. Baster and L. Li performed experiments and data analysis. S. Kukkurainen and O. Pentikäinen performed molecular docking analysis; J. Chen analyzed the stability of C3G using LC/MS; B. Győrffy developed the KM plot database for cancer survival analysis; Z. Baster, V.P. Hytönen, H. Zhu, and Z. Rajfur contributed to manuscript discussion and writing; and C. Huang directed the research, performed experiments, and wrote the paper.

REFERENCES

1. Lohachoompol V, Srzednicki G, Craske J. The change of total anthocyanins in blueberries and their antioxidant effect after drying and freezing. *J Biomed Biotechnol*. 2004;2004:248-252.
2. Galvano F, La Fauci L, Vitaglione P, Fogliano V, Vanella L, Felgines C. Bioavailability, antioxidant and biological properties of the natural free-radical scavengers cyanidin and related glycosides. *Ann Ist Super Sanita*. 2007;43:382-393.
3. Ding M, Feng R, Wang SY, et al. Cyanidin-3-glucoside, a natural product derived from blackberry, exhibits chemopreventive and chemotherapeutic activity. *J Biol Chem*. 2006;281:17359-17368.
4. Prior RL. Fruits and vegetables in the prevention of cellular oxidative damage. *Am J Clin Nutr*. 2003;78:570s-578s.
5. Guo H, Ling W, Wang Q, Liu C, Hu Y, Xia M. Cyanidin 3-glucoside protects 3T3-L1 adipocytes against H2O2- or TNF-alpha-induced insulin resistance by inhibiting c-Jun NH2-terminal kinase activation. *Biochem Pharmacol*. 2008;75:1393-1401.
6. Lee JS, Kim YR, Song IG, et al. Cyanidin-3-glucoside isolated from mulberry fruit protects pancreatic beta-cells against oxidative stress-induced apoptosis. *Int J Mol Med*. 2015;35:405-412.
7. Rupasinghe HPV, Arumuggam N, Amararathna M, De Silva ABKH. The potential health benefits of haskap (*Lonicera caerulea* L.): role of cyanidin-3-O-glucoside. *J Funct Foods*. 2018;44:24-39.
8. Ferrari D, Cimino F, Fratantonio D, et al. Cyanidin-3-O-glucoside modulates the in vitro inflammatory crosstalk between intestinal epithelial and endothelial cells. *Mediators Inflamm*. 2017;2017:3454023.
9. Pantan R, Tocharus J, Suksamrarn A, Tocharus C. Synergistic effect of atorvastatin and Cyanidin-3-glucoside on angiotensin II-induced inflammation in vascular smooth muscle cells. *Exp Cell Res*. 2016;342:104-112.
10. You Y, Yuan X, Liu X, et al. Cyanidin-3-glucoside increases whole body energy metabolism by upregulating brown adipose tissue mitochondrial function. *Mol Nutr Food Res*. 2017;61:1700261.
11. Tsuda T, Horio F, Uchida K, Aoki H, Osawa T. Dietary cyanidin 3-O-beta-D-glucoside-rich purple corn color prevents obesity and ameliorates hyperglycemia in mice. *J Nutr*. 2003;133:2125-2130.
12. Jayaprakasam B, Vareed SK, Olson LK, Nair MG. Insulin secretion by bioactive anthocyanins and anthocyanidins present in fruits. *J Agric Food Chem*. 2005;53:28-31.
13. Rozanska D, Regulska-Ilow B. The significance of anthocyanins in the prevention and treatment of type 2 diabetes. *Adv Clin Exp Med*. 2018;27:135-142.
14. Reis JF, Monteiro VVS, de Souza Gomes R, et al. Action mechanism and cardiovascular effect of anthocyanins: a systematic review of animal and human studies. *J Transl Med*. 2016;14:315.
15. Chen P-N, Chu S-C, Chiou H-L, Kuo W-H, Chiang C-L, Hsieh Y-S. Mulberry anthocyanins, cyanidin 3-rutinoside and cyanidin 3-glucoside, exhibited an inhibitory effect on the migration and invasion of a human lung cancer cell line. *Cancer Lett*. 2006;235:248-259.
16. Chen P-N, Kuo W-H, Chiang C-L, Chiou H-L, Hsieh Y-S, Chu S-C. Black rice anthocyanins inhibit cancer cells invasion via repressions of MMPs and u-PA expression. *Chem Biol Interact*. 2006;163:218-229.
17. Xu M, Bower KA, Wang S, et al. Cyanidin-3-glucoside inhibits ethanol-induced invasion of breast cancer cells overexpressing ErbB2. *Mol Cancer*. 2010;9:285.
18. Ma X, Ning S. Cyanidin-3-glucoside attenuates the angiogenesis of breast cancer via inhibiting STAT3/VEGF pathway. *Phytother Res*. 2019;33:81-89.
19. Tadokoro S, Shattil SJ, Eto K, et al. Talin binding to integrin ß tails: a final common step in integrin activation. *Science*. 2003;302:103-106.
20. Burridge K, Connell L. Talin: a cytoskeletal component concentrated in adhesion plaques and other sites of actin-membrane interaction. *Cell Motil*. 1983;3:405-417.
21. Burridge K, Mangeat P. An interaction between vinculin and talin. *Nature*. 1984;308:744-746.
22. Horwitz A, Duggan K, Buck C, Beckerle MC, Burridge K. Interaction of plasma membrane fibronectin receptor with talin–a transmembrane linkage. *Nature*. 1986;320:531-533.
23. Rees DJ, Ades SE, Singer SJ, Hynes RO. Sequence and domain structure of talin. *Nature*. 1990;347:685-689.
24. Calderwood DA, Zent R, Grant R, Rees DJG, Hynes RO, Ginsberg MH. The talin head domain binds to integrin β subunit cytoplasmic tails and regulates integrin activation. *J Biol Chem*. 1999;274:28071-28074.
25. Critchley DR. Cytoskeletal proteins talin and vinculin in integrin-mediated adhesion. *Biochem Soc Trans*. 2004;32:831-836.
26. Hemmings L, Rees DJ, Ohanian V, et al. Talin contains three actin-binding sites each of which is adjacent to a vinculin-binding site. *J Cell Sci*. 1996;109:2715-2726.
27. Bass MD, Smith BJ, Prigent SA, Critchley DR. Talin contains three similar vinculin-binding sites predicted to form an amphipathic helix. *Biochem J*. 1999;341(Pt 2):257-263.
28. Monkley SJ, Pritchard CA, Critchley DR. Analysis of the mammalian talin2 gene TLN2. *Biochem Biophys Res Commun*. 2001;286:880-885.
29. Qi L, Jafari N, Li X, et al. Talin2-mediated traction force drives matrix degradation and cell invasion. *J Cell Sci*. 2016;129:3661-3674.
30. Yuan Y, Li L, Zhu Y, et al. The molecular basis of talin2's high affinity toward β1-integrin. *Sci Rep*. 2017;7:41989.
31. García-Alvarez B, de Pereda JM, Calderwood DA, et al. Structural determinants of integrin recognition by talin. *Mol Cell*. 2003;11:49-58.
32. Zhang X, Jiang G, Cai Y, Monkley SJ, Critchley DR, Sheetz MP. Talin depletion reveals independence of initial cell spreading from integrin activation and traction. *Nat Cell Biol*. 2008;10:1062-1068.
33. Jin JK, Tien PC, Cheng CJ, et al. Talin1 phosphorylation activates [beta]1 integrins: a novel mechanism to promote prostate cancer bone metastasis. *Oncogene*. 2015;34:1811-1821.
34. Li L, Li X, Qi L, Rychahou P, Jafari N, Huang C. The role of talin2 in breast cancer tumorigenesis and metastasis. *Oncotarget*. 2017;8:106876-106887.

35. Liu J, Tan Y, Zhang H, et al. Soft fibrin gels promote selection and growth of tumorigenic cells. *Nat Mater*. 2012;11:734-741.
36. Huang C, Rajfur Z, Yousefi N, Chen Z, Jacobson K, Ginsberg MH. Talin phosphorylation by Cdk5 regulates Smurf1-mediated talin head ubiquitylation and cell migration. *Nat Cell Biol*. 2009;11:624-630.
37. Anthis NJ, Wegener KL, Critchley DR, Campbell ID. Structural diversity in integrin/talin interactions. *Structure*. 2010;18:1654-1666.
38. ten Brink T, Exner TE. Influence of protonation, tautomeric, and stereoisomeric states on protein-ligand docking results. *J Chem Inf Model*. 2009;49:1535-1546.
39. Korb O, Stutzle T, Exner TE. Empirical scoring functions for advanced protein-ligand docking with PLANTS. *J Chem Inf Model*. 2009;49:84-96.
40. Sztupinszki Z, Gyorffy B. Colon cancer subtypes: concordance, effect on survival and selection of the most representative preclinical models. *Sci Rep*. 2016;6:37169.
41. Pace E, Jiang Y, Clemens A, Crossman T, Rupasinghe HPV. Impact of thermal degradation of cyanidin-3-O-glucoside of haskap berry on cytotoxicity of hepatocellular carcinoma HepG2 and breast cancer MDA-MB-231 cells. *Antioxidants*. 2018;7:24.
42. Qi L, Kolodziej T, Rajfur Z, Huang C. Roles of Talin2 in traction force generation, tumor metastasis and cardiovascular integrity. *Curr Protein Pept Sci*. 2018;19:1071-1078.
43. Arnaout MA. Biology and structure of leukocyte beta 2 integrins and their role in inflammation. *F1000Research*. 2016;5:2433.
44. Kourtzelis I, Mitroulis I, von Renesse J, Hajishengallis G, Chavakis T. From leukocyte recruitment to resolution of inflammation: the cardinal role of integrins. *J Leukoc Biol*. 2017;102:677-683.
45. Feral CC, Neels JG, Kummer C, Slepak M, Olefsky JM, Ginsberg MH. Blockade of alpha4 integrin signaling ameliorates the metabolic consequences of high-fat diet-induced obesity. *Diabetes*. 2008;57:1842-1851.
46. Heida NM, Leifheit-Nestler M, Schroeter MR, et al. Leptin enhances the potency of circulating angiogenic cells via src kinase and integrin (alpha)vbeta5: implications for angiogenesis in human obesity. *Arterioscler Thromb Vasc Biol*. 2010;30:200-206.
47. Petrovic MG, Hawlina M, Peterlin B, Petrovic D. BglII gene polymorphism of the alpha2beta1 integrin gene is a risk factor for diabetic retinopathy in Caucasians with type 2 diabetes. *J Human Genet*. 2003;48:457-460.
48. Roth T, Podesta F, Stepp MA, Boeri D, Lorenzi M. Integrin overexpression induced by high glucose and by human diabetes: potential pathway to cell dysfunction in diabetic microangiopathy. *Proc Natl Acad Sci USA*. 1993;90:9640-9644.
49. Yang XD, Michie SA, Tisch R, Karin N, Steinman L, McDevitt HO. A predominant role of integrin alpha 4 in the spontaneous development of autoimmune diabetes in nonobese diabetic mice. *Proc Natl Acad Sci USA*. 1994;91:12604-12608.
50. Chung J, Kim TH. Integrin-dependent translational control: implication in cancer progression. *Microsc Res Tech*. 2008;71:380-386.
51. Ruoslahti E. Fibronectin and its integrin receptors in cancer. *Adv Cancer Res*. 1999;76:1-20.
52. Anthis NJ, Wegener KL, Ye F, et al. The structure of an integrin/talin complex reveals the basis of inside-out signal transduction. *EMBO J*. 2009;28:3623-3632.
53. EFSA Panel on Food Additives and Nutrient Sources Added to Food (ANS). Scientific Opinion on the re-evaluation of anthocyanins (E 163) as a food additive. *EFSA J*. 2013;11:3145.
54. Forester SC, Waterhouse AL. Gut metabolites of anthocyanins, gallic acid, 3-O-methylgallic acid, and 2,4,6-trihydroxybenzaldehyde, inhibit cell proliferation of Caco-2 cells. *J Agric Food Chem*. 2010;58:5320-5327.
55. Warner EF, Smith MJ, Zhang Q, et al. Signatures of anthocyanin metabolites identified in humans inhibit biomarkers of vascular inflammation in human endothelial cells. *Mol Nutr Food Res*. 2017;61:1700053.
56. Brú A, Albertos S, Luis Subiza J, García-Asenjo JL, Brú I. The universal dynamics of tumor growth. *Biophys J*. 2003;85:2948-2961.

SUPPORTING INFORMATION

Additional supporting information may be found online in the Supporting Information section.

How to cite this article: Baster Z, Li L, Kukkurainen S, et al. Cyanidin-3-glucoside binds to talin and modulates colon cancer cell adhesions and 3D growth. *The FASEB Journal*. 2020;34:2227–2237. https://doi.org/10.1096/fj.201900945R

APPENDIX – AUTHORS' CONTRIBUTION STATEMENTS

The authors' contribution statements are included within the publications' sections *Author contributions* and were confirmed by every author at the submissions of the manuscripts. Some of the co-authors, including the author of this thesis, have given extended *author's contribution statements* included in the following pages.

List of co-authors contribution forms:

Publication I:

1) Zbigniew Baster, MSE – Jagiellonian University, Kraków, Poland;
2) dr hab. Zenon Rajfur, prof. UJ – Jagiellonian University, Kraków, Poland.

Publication II:

1) Zbigniew Baster, MSE – Jagiellonian University, Kraków, Poland; University of Kentucky, Lexington, KY, USA;
2) Liqing Li – University of Kentucky, Lexington, KY, USA;
3) dr hab. Zenon Rajfur, prof. UJ – Jagiellonian University, Kraków, Poland;
4) prof. Cai Huang, PhD – University of Kentucky, Lexington, KY, USA.

Publication III:

1) Zbigniew Baster, MSE – Jagiellonian University, Kraków, Poland; University of Kentucky, Lexington, KY, USA;
2) Liqing Li – University of Kentucky, Lexington, KY, USA;
3) dr. Jing Chen, PhD – University of Kentucky, Lexington, KY, USA;
4) dr. Balázs Győrffy, MD, PhD, DSc – Hungarian Academy of Science, Budapest, Hungary;
5) dr hab. Zenon Rajfur, prof. UJ – Jagiellonian University, Kraków, Poland;
6) prof. Cai Huang, PhD – University of Kentucky, Lexington, KY, USA.

AUTHOR CONTRIBUTION FORM

Declaration of my personal contribution to the published or accepted scientific paper submitted within the PhD dissertation of Mr. **Zbigniew Baster**, in accordance with Art. 13, par.2 of The Act on Academic Degrees and Academic Title and Degrees and Title in Art (Dz. U. z 2003 nr 65, poz. 595, ze zm.; Dz. U. z 2005 r. nr 164, poz. 136; Dz. U. z 2011 r nr 84, poz. 455; Dz. U. z 2017 r. poz. 859).

Paper: Baster, Z. & Rajfur, Z. BatchDeconvolution: a Fiji plugin for increasing deconvolution workflow. *Bio-Algorithms and Med-Systems* **epub**, (2020). https://doi.org/10.1515/bams-2020-0027.

Name and surname: mgr inż. Zbigniew Baster

Affiliation: Jagiellonian University, Poland

e-mail: zbigniew.baster@doctoral.uj.edu.pl

I. Conceptual development

Formulation of the scientific problem based on research needs and literature studies, design of the software

II. Execution of experimental research

Software development, performance of all the algorithm tests

III. Analysis and interpretation of results

Interpretation and discussion of the results, conclusions formulation

IV. Article preparation and publication

Preparation of the manuscript, graphics design, serving as a corresponding author

V. Other

Funding acquisition

23.09.2020 — Date

Baster Zbigniew — Signature

AUTHOR CONTRIBUTION FORM

Declaration of my personal contribution to the published or accepted scientific paper submitted within the PhD dissertation of Mr. **Zbigniew Baster**, in accordance with Art. 13, par.2 of The Act on Academic Degrees and Academic Title and Degrees and Title in Art (Dz. U. z 2003 nr 65, poz. 595, ze zm.; Dz. U. z 2005 r. nr 164, poz. 136; Dz. U. z 2011 r nr 84, poz. 455; Dz. U. z 2017 r. poz. 859).

Paper: Baster, Z. & Rajfur, Z. BatchDeconvolution: a Fiji plugin for increasing deconvolution workflow. *Bio-Algorithms and Med-Systems* **epub**, (2020). https://doi.org/10.1515/bams-2020-0027.

Name and surname: dr hab. Zenon Rajfur, prof. UJ

Affiliation: Jagiellonian University, Cracow, Poland

e-mail: zenon.rajfur@uj.edu.pl

I. Conceptual development

II. Execution of experimental research

Supervision over testing data acquisition and algorithm testing process

III. Analysis and interpretation of results

Participation in interpretation and discussion of the results

IV. Article preparation and publication

Participation in the manuscript preparation

V. Other

22.09.2020

Date

Signature

AUTHOR CONTRIBUTION FORM

Declaration of my personal contribution to the published or accepted scientific paper submitted within the PhD dissertation of Mr. **Zbigniew Baster**, in accordance with Art. 13, par.2 of The Act on Academic Degrees and Academic Title and Degrees and Title in Art (Dz. U. z 2003 nr 65, poz. 595, ze zm.; Dz. U. z 2005 r. nr 164, poz. 136; Dz. U. z 2011 r nr 84, poz. 455; Dz. U. z 2017 r. poz. 859).

Paper: Baster, Z., Li, L., Rajfur, Z. & Huang, C. Talin2 mediates secretion and trafficking of matrix metallopeptidase 9 during invadopodium formation. *Biochim. Biophys. Acta - Mol. Cell Res.* **1867(7),** 118693 (2020). https://doi.org/10.1016/j.bbamcr.2020.118693.....

Name and surname: mgr inż. Zbigniew Baster .....

Affiliation: Jagiellonian University, Poland; University of Kentucky, USA.....

e-mail: zbigniew.baster@doctoral.uj.edu.pl .....

I. Conceptual development

Development of methodology for vesicle docking analysis, selection of experimental methods

II. Execution of experimental research

Participation in research design, performance of all the microscopy imaging and sample preparation,.....

III. Analysis and interpretation of results

Analysis of microscopy imaging data, development of the molecular model for talin2-mediated MMP9 secretion, interpretation and discussion of the results, conclusions formulation.....

IV. Article preparation and publication

Participation in the manuscript preparation, design of all the figures, serving as a corresponding author.....

V. Other

.....

23.09.2020 ..... Baster Zbigniew .....

Date Signature

AUTHOR CONTRIBUTION FORM

Declaration of my personal contribution to the published or accepted scientific paper submitted within the PhD dissertation of Mr. **Zbigniew Baster**, in accordance with Art. 13, par.2 of The Act on Academic Degrees and Academic Title and Degrees and Title in Art (Dz. U. z 2003 nr 65, poz. 595, ze zm.; Dz. U. z 2005 r. nr 164, poz. 136; Dz. U. z 2011 r nr 84, poz. 455; Dz. U. z 2017 r. poz. 859).

Paper: Baster, Z., Li, L., Rajfur, Z. & Huang, C. Talin2 mediates secretion and trafficking of matrix metallopeptidase 9 during invadopodium formation. *Biochim. Biophys. Acta - Mol. Cell Res.* **1867(7),** 118693 (2020). https://doi.org/10.1016/j.bbamcr.2020.118693. .....
Name and surname: Liqing Li .....
Affiliation: University of Kentucky Markey Cancer Center .....
e-mail: LL48@DUKE.EDU .....

I. Conceptual development

.....

II. Execution of experimental research

Preparation of samples, preparation of bacteria culture substrates, cloning and isolation of DNA plasmids.....

III. Analysis and interpretation of results

.....

IV. Article preparation and publication

.....

V. Other

.....

08/23/2020 ....

Date Signature

AUTHOR CONTRIBUTION FORM

Declaration of my personal contribution to the published or accepted scientific paper submitted within the PhD dissertation of Mr. **Zbigniew Baster**, in accordance with Art. 13, par.2 of The Act on Academic Degrees and Academic Title and Degrees and Title in Art (Dz. U. z 2003 nr 65, poz. 595, ze zm.; Dz. U. z 2005 r. nr 164, poz. 136; Dz. U. z 2011 r nr 84, poz. 455; Dz. U. z 2017 r. poz. 859).

Paper: Baster, Z., Li, L., Rajfur, Z. & Huang, C. Talin2 mediates secretion and trafficking of matrix metallopeptidase 9 during invadopodium formation. *Biochim. Biophys. Acta - Mol. Cell Res.* **1867(7),** 118693 (2020). https://doi.org/10.1016/j.bbamcr.2020.118693.....

Name and surname: dr hab. Zenon Rajfur, prof. UJ.....

Affiliation: Jagiellonian University, Cracow, Poland .....

e-mail: zenon.rajfur@uj.edu.pl.....

I. Conceptual development

.....

II. Execution of experimental research

Supervision over the research done at Jagiellonian University.....

III. Analysis and interpretation of results

Participation in interpretation and discussion of the results.....

IV. Article preparation and publication

Participation in the manuscript preparation .....

V. Other

.....

27.09.2022 .....

Date

.....

Signature

AUTHOR CONTRIBUTION FORM

Declaration of my personal contribution to the published or accepted scientific paper submitted within the PhD dissertation of Mr. **Zbigniew Baster**, in accordance with Art. 13, par.2 of The Act on Academic Degrees and Academic Title and Degrees and Title in Art (Dz. U. z 2003 nr 65, poz. 595, ze zm.; Dz. U. z 2005 r. nr 164, poz. 136; Dz. U. z 2011 r nr 84, poz. 455; Dz. U. z 2017 r. poz. 859).

Paper: Baster, Z., Li, L., Kukkurainen, S., Chen, J., Pentikäinen, O., Győrffy, B., Hytönen, V. P., Zhu, H., Rajfur, Z. & Huang, C. Cyanidin- 3- glucoside binds to talin and modulates colon cancer cell adhesions and 3D growth. *FASEB J.* **34(2),** 2227–2237 (2020). https://doi.org/10.1096/fj.201900945R. .....

Name and surname: Cai Huang, PhD .....

Affiliation: University of Kentucky Markey Cancer Center .....

e-mail: chuang008@hotmail.com.....

I. Conceptual development

Formulation of the scientific problem based on literature research .....

II. Execution of experimental research

Research design, execution of proliferation and adhesion assays, execution of protein-protein interaction kinetics experiments.....

III. Analysis and interpretation of results

Supervision and participation in the analysis and interpretation of experimental results, design of C3G-mediated tumor inhibition model.....

IV. Article preparation and publication

Preparation of the manuscript, literature research, serving as a corresponding author.....

V. Other

Funding acquisition, Principle Investigator of the NIH R01 research project .....

08/21/2020

Date

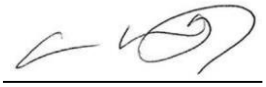

Signature

AUTHOR CONTRIBUTION FORM

Declaration of my personal contribution to the published or accepted scientific paper submitted within the PhD dissertation of Mr. **Zbigniew Baster**, in accordance with Art. 13, par.2 of The Act on Academic Degrees and Academic Title and Degrees and Title in Art (Dz. U. z 2003 nr 65, poz. 595, ze zm.; Dz. U. z 2005 r. nr 164, poz. 136; Dz. U. z 2011 r nr 84, poz. 455; Dz. U. z 2017 r. poz. 859).

Paper: Baster, Z., Li, L., Rajfur, Z. & Huang, C. Talin2 mediates secretion and trafficking of matrix metallopeptidase 9 during invadopodium formation. *Biochim. Biophys. Acta - Mol. Cell Res.* **1867(7),** 118693 (2020). https://doi.org/10.1016/j.bbamcr.2020.118693. .....

Name and surname: Cai Huang, PhD .....

Affiliation: University of Kentucky Markey Cancer Center .....

e-mail: chuang008@hotmail.com.....

I. Conceptual development

Formulation of the scientific problem based on literature research .....

II. Execution of experimental research

Research design, development of knock-out cell lines, development of new DNA plasmids, execution of western-blot and qPCR experiments .....

III. Analysis and interpretation of results

Supervision and participation in the analysis and interpretation of experimental results .....

IV. Article preparation and publication

Participation in the manuscript preparation, acceptance of the final version of the manuscript, literature research, serving as a corresponding author .....

V. Other

Funding acquisition, Principle Investigator of the NIH R01 research project .....

08/21/2020

Date

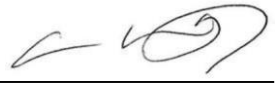

Signature

AUTHOR CONTRIBUTION FORM

Declaration of my personal contribution to the published or accepted scientific paper submitted within the PhD dissertation of Mr. **Zbigniew Baster**, in accordance with Art. 13, par.2 of The Act on Academic Degrees and Academic Title and Degrees and Title in Art (Dz. U. z 2003 nr 65, poz. 595, ze zm.; Dz. U. z 2005 r. nr 164, poz. 136; Dz. U. z 2011 r nr 84, poz. 455; Dz. U. z 2017 r. poz. 859).

Paper: Baster, Z., Li, L., Kukkurainen, S., Chen, J., Pentikäinen, O., Győrffy, B., Hytönen, V. P., Zhu, H., Rajfur, Z. & Huang, C. Cyanidin-3-glucoside binds to talin and modulates colon cancer cell adhesions and 3D growth. *FASEB J.* **34(2),** 2227–2237 (2020). https://doi.org/10.1096/fj.201900945R.

Name and surname: mgr inż. Zbigniew Baster

Affiliation: Jagiellonian University, Poland; University of Kentucky, USA

e-mail: zbigniew.baster@doctoral.uj.edu.pl

I. Conceptual development

Participation in selection of experimental methods

II. Execution of experimental research

Performance of the integrin activation and adhesion studies in breast cancer cells

III. Analysis and interpretation of results

Development of the molecular model for regulation of C3G-mediated talin-integrin interaction regulation, participation in interpretation and discussion of the results

IV. Article preparation and publication

Participation in the manuscript preparation, literature research

V. Other

Funding acquisition

23.09.2020 ..... Baster Zbigniew .....

Date Signature

AUTHOR CONTRIBUTION FORM

Declaration of my personal contribution to the published or accepted scientific paper submitted within the PhD dissertation of Mr. **Zbigniew Baster**, in accordance with Art. 13, par.2 of The Act on Academic Degrees and Academic Title and Degrees and Title in Art (Dz. U. z 2003 nr 65, poz. 595, ze zm.; Dz. U. z 2005 r. nr 164, poz. 136; Dz. U. z 2011 r nr 84, poz. 455; Dz. U. z 2017 r. poz. 859).

Paper: Baster, Z., Li, L., Kukkurainen, S., Chen, J., Pentikäinen, O., Győrffy, B., Hytönen, V. P., Zhu, H., Rajfur, Z. & Huang, C. Cyanidin- 3- glucoside binds to talin and modulates colon cancer cell adhesions and 3D growth. *FASEB J.* **34(2),** 2227–2237 (2020). https://doi.org/10.1096/fj.201900945R. .....

Name and surname: Liqing Li .....

Affiliation: University of Kentucky Markey Cancer Center .....

e-mail: LL48@DUKE.EDU .....

I. Conceptual development

.....

II. Execution of experimental research

Preparation of samples, preparation of bacteria culture substrates, cloning and isolation of DNA plasmids.....

III. Analysis and interpretation of results

.....

IV. Article preparation and publication

.....

V. Other

.....

08/23/2020 .....

Date

Signature

AUTHOR CONTRIBUTION FORM

Declaration of my personal contribution to the published or accepted scientific paper submitted within the PhD dissertation of Mr. **Zbigniew Baster**, in accordance with Art. 13, par.2 of The Act on Academic Degrees and Academic Title and Degrees and Title in Art (Dz. U. z 2003 nr 65, poz. 595, ze zm.; Dz. U. z 2005 r. nr 164, poz. 136; Dz. U. z 2011 r nr 84, poz. 455; Dz. U. z 2017 r. poz. 859).

Paper: Baster, Z., Li, L., Kukkurainen, S., Chen, J., Pentikäinen, O., Györffy, B., Hytönen, V. P., Zhu, H., Rajfur, Z. & Huang, C. Cyanidin-3-glucoside binds to talin and modulates colon cancer cell adhesions and 3D growth. *FASEB J.* **34(2),** 2227–2237 (2020). https://doi.org/10.1096/fj.201900945R

Name and surname: Dr. Jing Chen, PhD

Affiliation: Department of Molecular and Cellular Biochemistry, University of Kentucky, Lexington, KY, USA

e-mail: jchen4@email.uky.edu

I. Conceptual development

II. Execution of experimental research

III. Analysis and interpretation of results

Analysis of the stability of C3G using LC/MS method

IV. Article preparation and publication

V. Other

08/28/2020
Date

Jingchen
Signature

AUTHOR CONTRIBUTION FORM

Declaration of my personal contribution to the published or accepted scientific paper submitted within the PhD dissertation of Mr. **Zbigniew Baster**, in accordance with Art. 13, par.2 of The Act on Academic Degrees and Academic Title and Degrees and Title in Art (Dz. U. z 2003 nr 65, poz. 595, ze zm.; Dz. U. z 2005 r. nr 164, poz. 136; Dz. U. z 2011 r nr 84, poz. 455; Dz. U. z 2017 r. poz. 859).

Paper: .....Baster, Z., Li, L., Kukkurainen, S., Chen, J., Pentikäinen, O. P., Zhu, H., Rajfur, Z. & Huang, C. Cyanidin‐3‐glucoside binds to talin and modulates colon cancer cell adhesions and 3D growth. *FASEB J.* **34(2),** 2227–2237 (2020). https://doi.org/10.1096/fj.201900945R.....

Name and surname: Dr. Balázs Győrffy, MD, PhD, DSc.....

Affiliation: MTA TTK Lendület Cancer Biomarker Research Group, Institute of Enzymology, Hungarian Academy of Sciences, Budapest, Hungary.....

e-mail: gyorffy.balazs@med.semmelweis-univ.hu.....

I. Conceptual development

.....

II. Execution of experimental research

.....

III. Analysis and interpretation of results

Development of the Kaplan-Meier plot database for cancer survival analysis.....

IV. Article preparation and publication

.....

V. Other

.....

....

Date

.....

Signature

AUTHOR CONTRIBUTION FORM

Declaration of my personal contribution to the published or accepted scientific paper submitted within the PhD dissertation of Mr. **Zbigniew Baster**, in accordance with Art. 13, par.2 of The Act on Academic Degrees and Academic Title and Degrees and Title in Art (Dz. U. z 2003 nr 65, poz. 595, ze zm.; Dz. U. z 2005 r. nr 164, poz. 136; Dz. U. z 2011 r nr 84, poz. 455; Dz. U. z 2017 r. poz. 859).

Paper: Baster, Z., Li, L., Kukkurainen, S., Chen, J., Pentikäinen, O., Győrffy, B., Hytönen, V. P., Zhu, H., Rajfur, Z. & Huang, C. Cyanidin-3-glucoside binds to talin and modulates colon cancer cell adhesions and 3D growth. *FASEB J.* **34(2),** 2227–2237 (2020). https://doi.org/10.1096/fj.201900945R.

Name and surname: dr hab. Zenon Rajfur, prof. UJ

Affiliation: Jagiellonian University, Cracow, Poland

e-mail: zenon.rajfur@uj.edu.pl

I. Conceptual development

II. Execution of experimental research

Supervision over the research done at Jagiellonian University

III. Analysis and interpretation of results

Participation in interpretation and discussion of the results

IV. Article preparation and publication

Participation in the manuscript preparation, serving as a corresponding author

V. Other

Funding acquisition

22.01.2020

Date

Signature

AUTHOR CONTRIBUTION FORM

Declaration of my personal contribution to the published or accepted scientific paper submitted within the PhD dissertation of Mr. **Zbigniew Baster**, in accordance with Art. 13, par.2 of The Act on Academic Degrees and Academic Title and Degrees and Title in Art (Dz. U. z 2003 nr 65, poz. 595, ze zm.; Dz. U. z 2005 r. nr 164, poz. 136; Dz. U. z 2011 r nr 84, poz. 455; Dz. U. z 2017 r. poz. 859).

Paper: Baster, Z., Li, L., Kukkurainen, S., Chen, J., Pentikäinen, O., Győrffy, B., Hytönen, V. P., Zhu, H., Rajfur, Z. & Huang, C. Cyanidin- 3- glucoside binds to talin and modulates colon cancer cell adhesions and 3D growth. *FASEB J.* **34(2),** 2227–2237 (2020). https://doi.org/10.1096/fj.201900945R. .....

Name and surname: Cai Huang, PhD .....

Affiliation: University of Kentucky Markey Cancer Center .....

e-mail: chuang008@hotmail.com.....

I. Conceptual development

Formulation of the scientific problem based on literature research .....

II. Execution of experimental research

Research design, execution of proliferation and adhesion assays, execution of protein-protein interaction kinetics experiments.....

III. Analysis and interpretation of results

Supervision and participation in the analysis and interpretation of experimental results, design of C3G-mediated tumor inhibition model.....

IV. Article preparation and publication

Preparation of the manuscript, literature research, serving as a corresponding author.....

V. Other

Funding acquisition, Principle Investigator of the NIH R01 research project .....

08/21/2020

Date

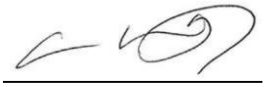

Signature

APPENDIX – COPYRIGHTS LICENSE AGREEMENTS

Some of the materials presented in the thesis were previously published and copyrights to the materials are held by third parties. The following license agreements regulate the reuse of the materials in this work:

1) Fig. 5 – License Agreement between the Author and The Company of Biologists Ltd. provided by The Company of Biologists Ltd. and Copyright Clearance Center no. 1060099-1.
2) Fig. 6A – License Agreement between the Author and Elsevier provided by Elsevier and Copyright Clearance Center.no. 4902800547702.
3) Fig. 7 – License Agreement between the Author and Springer Nature provided by Springer Nature and Copyright Clearance Center no. 4900770040382.
4) Figure on page 96 – License Agreement between the Author and John Wiley and Sons provided by John Wiley and Sons and Copyright Clearance Center no. 4900010880170.
5) Publication III – License Agreement between the Author and John Wiley and Sons provided by John Wiley and Sons and Copyright Clearance Center no. 4900010360092.

ELSEVIER LICENSE
TERMS AND CONDITIONS

Sep 23, 2020

This Agreement between Mr. Zbigniew Baster ("You") and Elsevier ("Elsevier") consists of your license details and the terms and conditions provided by Elsevier and Copyright Clearance Center.

License Number	4902800547702
License date	Sep 05, 2020
Licensed Content Publisher	Elsevier
Licensed Content Publication	Cell
Licensed Content Title	Integrins Bidirectional, Allosteric Signaling Machines
Licensed Content Author	Richard O. Hynes
Licensed Content Date	Sep 20, 2002
Licensed Content Volume	110
Licensed Content Issue	6
Licensed Content Pages	15
Start Page	673
End Page	687
Type of Use	reuse in a thesis/dissertation
Portion	figures/tables/illustrations
Number of figures/tables/illustrations	1
Format	both print and electronic
Are you the author of this Elsevier article?	No
Will you be translating?	No
Title	Interplay between talin and β1-integrin in cancer cells motility
Institution name	Jagiellonian Univeristy
Expected presentation date	Oct 2020
Portions	Fig 1
Requestor Location	Mr. Zbigniew Baster 11 Lojasiewicza Street Cracow, other 30-348 Poland Attn: Mr. Zbigniew Baster
Publisher Tax ID	GB 494 6272 12
Total	**0.00 USD**
Terms and Conditions	

INTRODUCTION

1. The publisher for this copyrighted material is Elsevier. By clicking "accept" in connection with completing this licensing transaction, you agree that the following terms and conditions apply to this transaction (along with the Billing and Payment terms and conditions established by Copyright Clearance Center, Inc. ("CCC"), at the time that you opened your Rightslink account and that are available at any time at http://myaccount.copyright.com).

GENERAL TERMS

2. Elsevier hereby grants you permission to reproduce the aforementioned material subject to the terms and conditions indicated.
3. Acknowledgement: If any part of the material to be used (for example, figures) has appeared in our publication with credit or acknowledgement to another source, permission must also be sought from that source. If such permission is not obtained then that material may not be included in your publication/copies. Suitable acknowledgement to the source must be made, either as a footnote or in a reference list at the end of your publication, as follows:
"Reprinted from Publication title, Vol /edition number, Author(s), Title of article / title of chapter, Pages No., Copyright (Year), with permission from Elsevier [OR APPLICABLE SOCIETY COPYRIGHT OWNER]." Also Lancet special credit - "Reprinted from The Lancet, Vol. number, Author(s), Title of article, Pages No., Copyright (Year), with permission from Elsevier."
4. Reproduction of this material is confined to the purpose and/or media for which permission is hereby given.
5. Altering/Modifying Material: Not Permitted. However figures and illustrations may be altered/adapted minimally to serve your work. Any other abbreviations, additions, deletions and/or any other alterations shall be made only with prior written authorization of Elsevier Ltd. (Please contact Elsevier's permissions helpdesk here). No modifications can be made to any Lancet figures/tables and they must be reproduced in full.
6. If the permission fee for the requested use of our material is waived in this instance, please be advised that your future requests for Elsevier materials may attract a fee.
7. Reservation of Rights: Publisher reserves all rights not specifically granted in the combination of (i) the license details provided by you and accepted in the course of this licensing transaction, (ii) these terms and conditions and (iii) CCC's Billing and Payment terms and conditions.
8. License Contingent Upon Payment: While you may exercise the rights licensed immediately upon issuance of the license at the end of the licensing process for the transaction, provided that you have disclosed complete and accurate details of your proposed use, no license is finally effective unless and until full payment is received from you (either by publisher or by CCC) as provided in CCC's Billing and Payment terms and conditions. If full payment is not received on a timely basis, then any license preliminarily granted shall be deemed automatically revoked and shall be void as if never granted. Further, in the event that you breach any of these terms and conditions or any of CCC's Billing and Payment terms and conditions, the license is automatically revoked and shall be void as if never granted. Use of materials as described in a revoked license, as well as any use of the materials beyond the scope of an unrevoked license, may constitute copyright infringement and publisher reserves the right to take any and all action to protect its copyright in the materials.
9. Warranties: Publisher makes no representations or warranties with respect to the licensed material.
10. Indemnity: You hereby indemnify and agree to hold harmless publisher and CCC, and their respective officers, directors, employees and agents, from and against any and all claims arising out of your use of the licensed material other than as specifically authorized pursuant to this license.
11. No Transfer of License: This license is personal to you and may not be sublicensed, assigned, or transferred by you to any other person without publisher's written permission.
12. No Amendment Except in Writing: This license may not be amended except in a writing signed by both parties (or, in the case of publisher, by CCC on publisher's behalf).
13. Objection to Contrary Terms: Publisher hereby objects to any terms contained in any purchase order, acknowledgment, check endorsement or other writing prepared by you, which terms are inconsistent with these terms and conditions or CCC's Billing and Payment terms and conditions. These terms and conditions, together with CCC's Billing and Payment terms and conditions (which are incorporated herein), comprise the entire agreement between you and publisher (and CCC) concerning this licensing transaction. In the event of any conflict between your obligations established by these terms and conditions and those established by CCC's Billing and Payment terms and conditions, these terms and conditions shall control.

14. Revocation: Elsevier or Copyright Clearance Center may deny the permissions described in this License at their sole discretion, for any reason or no reason, with a full refund payable to you. Notice of such denial will be made using the contact information provided by you. Failure to receive such notice will not alter or invalidate the denial. In no event will Elsevier or Copyright Clearance Center be responsible or liable for any costs, expenses or damage incurred by you as a result of a denial of your permission request, other than a refund of the amount(s) paid by you to Elsevier and/or Copyright Clearance Center for denied permissions.

LIMITED LICENSE

The following terms and conditions apply only to specific license types:

15. **Translation**: This permission is granted for non-exclusive world **English** rights only unless your license was granted for translation rights. If you licensed translation rights you may only translate this content into the languages you requested. A professional translator must perform all translations and reproduce the content word for word preserving the integrity of the article.

16. **Posting licensed content on any Website**: The following terms and conditions apply as follows: Licensing material from an Elsevier journal: All content posted to the web site must maintain the copyright information line on the bottom of each image; A hyper-text must be included to the Homepage of the journal from which you are licensing at http://www.sciencedirect.com/science/journal/xxxxx or the Elsevier homepage for books at http://www.elsevier.com; Central Storage: This license does not include permission for a scanned version of the material to be stored in a central repository such as that provided by Heron/XanEdu.

Licensing material from an Elsevier book: A hyper-text link must be included to the Elsevier homepage at http://www.elsevier.com . All content posted to the web site must maintain the copyright information line on the bottom of each image.

Posting licensed content on Electronic reserve: In addition to the above the following clauses are applicable: The web site must be password-protected and made available only to bona fide students registered on a relevant course. This permission is granted for 1 year only. You may obtain a new license for future website posting.

17. **For journal authors:** the following clauses are applicable in addition to the above:

Preprints:

A preprint is an author's own write-up of research results and analysis, it has not been peer-reviewed, nor has it had any other value added to it by a publisher (such as formatting, copyright, technical enhancement etc.).

Authors can share their preprints anywhere at any time. Preprints should not be added to or enhanced in any way in order to appear more like, or to substitute for, the final versions of articles however authors can update their preprints on arXiv or RePEc with their Accepted Author Manuscript (see below).

If accepted for publication, we encourage authors to link from the preprint to their formal publication via its DOI. Millions of researchers have access to the formal publications on ScienceDirect, and so links will help users to find, access, cite and use the best available version. Please note that Cell Press, The Lancet and some society-owned have different preprint policies. Information on these policies is available on the journal homepage.

Accepted Author Manuscripts: An accepted author manuscript is the manuscript of an article that has been accepted for publication and which typically includes author-incorporated changes suggested during submission, peer review and editor-author communications.

Authors can share their accepted author manuscript:

- immediately
    - via their non-commercial person homepage or blog
    - by updating a preprint in arXiv or RePEc with the accepted manuscript
    - via their research institute or institutional repository for internal institutional uses or as part of an invitation-only research collaboration work-group
    - directly by providing copies to their students or to research collaborators for their personal use
    - for private scholarly sharing as part of an invitation-only work group on commercial sites with which Elsevier has an agreement
- After the embargo period
    - via non-commercial hosting platforms such as their institutional repository

- via commercial sites with which Elsevier has an agreement

In all cases accepted manuscripts should:

- link to the formal publication via its DOI
- bear a CC-BY-NC-ND license - this is easy to do
- if aggregated with other manuscripts, for example in a repository or other site, be shared in alignment with our hosting policy not be added to or enhanced in any way to appear more like, or to substitute for, the published journal article.

Published journal article (JPA): A published journal article (PJA) is the definitive final record of published research that appears or will appear in the journal and embodies all value-adding publishing activities including peer review co-ordination, copy-editing, formatting, (if relevant) pagination and online enrichment.
Policies for sharing publishing journal articles differ for subscription and gold open access articles:
Subscription Articles: If you are an author, please share a link to your article rather than the full-text. Millions of researchers have access to the formal publications on ScienceDirect, and so links will help your users to find, access, cite, and use the best available version.
Theses and dissertations which contain embedded PJAs as part of the formal submission can be posted publicly by the awarding institution with DOI links back to the formal publications on ScienceDirect.
If you are affiliated with a library that subscribes to ScienceDirect you have additional private sharing rights for others' research accessed under that agreement. This includes use for classroom teaching and internal training at the institution (including use in course packs and courseware programs), and inclusion of the article for grant funding purposes.
Gold Open Access Articles: May be shared according to the author-selected end-user license and should contain a CrossMark logo, the end user license, and a DOI link to the formal publication on ScienceDirect.
Please refer to Elsevier's posting policy for further information.
18. **For book authors** the following clauses are applicable in addition to the above: Authors are permitted to place a brief summary of their work online only. You are not allowed to download and post the published electronic version of your chapter, nor may you scan the printed edition to create an electronic version. **Posting to a repository:** Authors are permitted to post a summary of their chapter only in their institution's repository.
19. **Thesis/Dissertation**: If your license is for use in a thesis/dissertation your thesis may be submitted to your institution in either print or electronic form. Should your thesis be published commercially, please reapply for permission. These requirements include permission for the Library and Archives of Canada to supply single copies, on demand, of the complete thesis and include permission for Proquest/UMI to supply single copies, on demand, of the complete thesis. Should your thesis be published commercially, please reapply for permission. Theses and dissertations which contain embedded PJAs as part of the formal submission can be posted publicly by the awarding institution with DOI links back to the formal publications on ScienceDirect.

Elsevier Open Access Terms and Conditions
You can publish open access with Elsevier in hundreds of open access journals or in nearly 2000 established subscription journals that support open access publishing. Permitted third party re-use of these open access articles is defined by the author's choice of Creative Commons user license. See our open access license policy for more information.
Terms & Conditions applicable to all Open Access articles published with Elsevier:
Any reuse of the article must not represent the author as endorsing the adaptation of the article nor should the article be modified in such a way as to damage the author's honour or reputation. If any changes have been made, such changes must be clearly indicated.
The author(s) must be appropriately credited and we ask that you include the end user license and a DOI link to the formal publication on ScienceDirect.
If any part of the material to be used (for example, figures) has appeared in our publication with credit or acknowledgement to another source it is the responsibility of the user to ensure their reuse complies with the terms and conditions determined by the rights holder.
Additional Terms & Conditions applicable to each Creative Commons user license:

Copyright Clearance Center Marketplace™

The Company of Biologists Ltd. - License Terms and Conditions

This is a License Agreement between Zbigniew Baster ("You") and The Company of Biologists Ltd. ("Publisher") provided by Copyright Clearance Center ("CCC"). The license consists of your order details, the terms and conditions provided by The Company of Biologists Ltd., and the CCC terms and conditions.

All payments must be made in full to CCC.

Order Date	02-Sep-2020	**Type of Use**	Republish in a thesis/dissertation
Order license ID	1060099-1		
ISSN	1477-9137	**Publisher**	COMPANY OF BIOLOGISTS LTD.
		Portion	Chart/graph/table/figure

LICENSED CONTENT

Publication Title	Journal of cell science	**Country**	United Kingdom of Great Britain and Northern Ireland
Author/Editor	Company of Biologists.		
Date	01/01/1966	**Rightsholder**	The Company of Biologists Ltd.
Language	English	**Publication Type**	e-Journal
		URL	http://jcs.biologists.org/

REQUEST DETAILS

Portion Type	Chart/graph/table/figure	**Distribution**	Worldwide
Number of charts / graphs / tables / figures requested	1	**Translation**	Original language of publication
		Copies for the disabled?	No
Format (select all that apply)	Print, Electronic	**Minor editing privileges?**	No
Who will republish the content?	Academic institution	**Incidental promotional use?**	No
Duration of Use	Life of current edition	**Currency**	USD
Lifetime Unit Quantity	Up to 250,000		
Rights Requested	Main product		

NEW WORK DETAILS

Title	Interplay between talin and β1-integrin in cancer cells motility	**Institution name**	Jagiellonian University
		Expected presentation date	2020-10-01
Instructor name	Zenon Rajfur		

ADDITIONAL DETAILS

Order reference number	N/A	**The requesting person / organization to appear on the license**	Zbigniew Baster

REUSE CONTENT DETAILS

Title, description or numeric reference of the portion(s)	Talin – the master of integrin adhesions	**Title of the article/chapter the portion is from**	Figure 2A
Editor of portion(s)	Benjamin Klapholz, Nicholas H. Brown	**Author of portion(s)**	Company of Biologists.
		Issue, if republishing an article from a serial	N/A
Volume of serial or monograph	130		

Page or page range of portion	2435-2446	**Publication date of portion**	2017-08-01

PUBLISHER TERMS AND CONDITIONS

The acknowledgement should state "Reproduced / adapted with permission" and give the source journal name. The acknowledgement should either provide full citation details or refer to the relevant citation in the article reference list. The full citation details should include authors, journal, year, volume, issue and page citation. Where appearing online or in other electronic media, a link should be provided to the original article (e.g. via DOI): Development: dev.biologists.org Disease Models & Mechanisms: dmm.biologists.org Journal of Cell Science: jcs.biologists.org The Journal of Experimental Biology: jeb.biologists.org

CCC Republication Terms and Conditions

1. Description of Service; Defined Terms. This Republication License enables the User to obtain licenses for republication of one or more copyrighted works as described in detail on the relevant Order Confirmation (the "Work(s)"). Copyright Clearance Center, Inc. ("CCC") grants licenses through the Service on behalf of the rightsholder identified on the Order Confirmation (the "Rightsholder"). "Republication", as used herein, generally means the inclusion of a Work, in whole or in part, in a new work or works, also as described on the Order Confirmation. "User", as used herein, means the person or entity making such republication.

2. The terms set forth in the relevant Order Confirmation, and any terms set by the Rightsholder with respect to a particular Work, govern the terms of use of Works in connection with the Service. By using the Service, the person transacting for a republication license on behalf of the User represents and warrants that he/she/it (a) has been duly authorized by the User to accept, and hereby does accept, all such terms and conditions on behalf of User, and (b) shall inform User of all such terms and conditions. In the event such person is a "freelancer" or other third party independent of User and CCC, such party shall be deemed jointly a "User" for purposes of these terms and conditions. In any event, User shall be deemed to have accepted and agreed to all such terms and conditions if User republishes the Work in any fashion.

3. Scope of License; Limitations and Obligations.

    3.1. All Works and all rights therein, including copyright rights, remain the sole and exclusive property of the Rightsholder. The license created by the exchange of an Order Confirmation (and/or any invoice) and payment by User of the full amount set forth on that document includes only those rights expressly set forth in the Order Confirmation and in these terms and conditions, and conveys no other rights in the Work(s) to User. All rights not expressly granted are hereby reserved.

    3.2. General Payment Terms: You may pay by credit card or through an account with us payable at the end of the month. If you and we agree that you may establish a standing account with CCC, then the following terms apply: Remit Payment to: Copyright Clearance Center, 29118 Network Place, Chicago, IL 60673-1291. Payments Due: Invoices are payable upon their delivery to you (or upon our notice to you that they are available to you for downloading). After 30 days, outstanding amounts will be subject to a service charge of 1-1/2% per month or, if less, the maximum rate allowed by applicable law. Unless otherwise specifically set forth in the Order Confirmation or in a separate written agreement signed by CCC, invoices are due and payable on "net 30" terms. While User may exercise the rights licensed immediately upon issuance of the Order Confirmation, the license is automatically revoked and is null and void, as if it had never been issued, if complete payment for the license is not received on a timely basis either from User directly or through a payment agent, such as a credit card company.

    3.3. Unless otherwise provided in the Order Confirmation, any grant of rights to User (i) is "one-time" (including the editions and product family specified in the license), (ii) is non-exclusive and non-transferable and (iii) is subject to any and all limitations and restrictions (such as, but not limited to, limitations on duration of use or circulation) included in the Order Confirmation or invoice and/or in these terms and conditions. Upon completion of the licensed use, User shall either secure a new permission for further use of the Work(s) or immediately cease any new use of the Work(s) and shall render inaccessible (such as by deleting or by removing or severing links or other locators) any further copies of the Work (except for copies printed on paper in accordance with this license and still in User's stock at the end of such period).

    3.4. In the event that the material for which a republication license is sought includes third party materials (such as photographs, illustrations, graphs, inserts and similar materials) which are identified in such material as having been used by permission, User is responsible for identifying, and seeking separate licenses (under this Service or otherwise) for, any of such third party materials; without a separate license, such third party materials may not be used.

    3.5. Use of proper copyright notice for a Work is required as a condition of any license granted under the Service. Unless otherwise provided in the Order Confirmation, a proper copyright notice will read substantially as follows: "Republished with permission of [Rightsholder's name], from [Work's title, author, volume, edition number and year of copyright]; permission conveyed through Copyright Clearance Center, Inc. " Such notice must be provided in a reasonably legible font size and must be placed either

immediately adjacent to the Work as used (for example, as part of a by-line or footnote but not as a separate electronic link) or in the place where substantially all other credits or notices for the new work containing the republished Work are located. Failure to include the required notice results in loss to the Rightsholder and CCC, and the User shall be liable to pay liquidated damages for each such failure equal to twice the use fee specified in the Order Confirmation, in addition to the use fee itself and any other fees and charges specified.

3.6. User may only make alterations to the Work if and as expressly set forth in the Order Confirmation. No Work may be used in any way that is defamatory, violates the rights of third parties (including such third parties' rights of copyright, privacy, publicity, or other tangible or intangible property), or is otherwise illegal, sexually explicit or obscene. In addition, User may not conjoin a Work with any other material that may result in damage to the reputation of the Rightsholder. User agrees to inform CCC if it becomes aware of any infringement of any rights in a Work and to cooperate with any reasonable request of CCC or the Rightsholder in connection therewith.

4. Indemnity. User hereby indemnifies and agrees to defend the Rightsholder and CCC, and their respective employees and directors, against all claims, liability, damages, costs and expenses, including legal fees and expenses, arising out of any use of a Work beyond the scope of the rights granted herein, or any use of a Work which has been altered in any unauthorized way by User, including claims of defamation or infringement of rights of copyright, publicity, privacy or other tangible or intangible property.

5. Limitation of Liability. UNDER NO CIRCUMSTANCES WILL CCC OR THE RIGHTSHOLDER BE LIABLE FOR ANY DIRECT, INDIRECT, CONSEQUENTIAL OR INCIDENTAL DAMAGES (INCLUDING WITHOUT LIMITATION DAMAGES FOR LOSS OF BUSINESS PROFITS OR INFORMATION, OR FOR BUSINESS INTERRUPTION) ARISING OUT OF THE USE OR INABILITY TO USE A WORK, EVEN IF ONE OF THEM HAS BEEN ADVISED OF THE POSSIBILITY OF SUCH DAMAGES. In any event, the total liability of the Rightsholder and CCC (including their respective employees and directors) shall not exceed the total amount actually paid by User for this license. User assumes full liability for the actions and omissions of its principals, employees, agents, affiliates, successors and assigns.

6. Limited Warranties. THE WORK(S) AND RIGHT(S) ARE PROVIDED "AS IS". CCC HAS THE RIGHT TO GRANT TO USER THE RIGHTS GRANTED IN THE ORDER CONFIRMATION DOCUMENT. CCC AND THE RIGHTSHOLDER DISCLAIM ALL OTHER WARRANTIES RELATING TO THE WORK(S) AND RIGHT(S), EITHER EXPRESS OR IMPLIED, INCLUDING WITHOUT LIMITATION IMPLIED WARRANTIES OF MERCHANTABILITY OR FITNESS FOR A PARTICULAR PURPOSE. ADDITIONAL RIGHTS MAY BE REQUIRED TO USE ILLUSTRATIONS, GRAPHS, PHOTOGRAPHS, ABSTRACTS, INSERTS OR OTHER PORTIONS OF THE WORK (AS OPPOSED TO THE ENTIRE WORK) IN A MANNER CONTEMPLATED BY USER; USER UNDERSTANDS AND AGREES THAT NEITHER CCC NOR THE RIGHTSHOLDER MAY HAVE SUCH ADDITIONAL RIGHTS TO GRANT.

7. Effect of Breach. Any failure by User to pay any amount when due, or any use by User of a Work beyond the scope of the license set forth in the Order Confirmation and/or these terms and conditions, shall be a material breach of the license created by the Order Confirmation and these terms and conditions. Any breach not cured within 30 days of written notice thereof shall result in immediate termination of such license without further notice. Any unauthorized (but licensable) use of a Work that is terminated immediately upon notice thereof may be liquidated by payment of the Rightsholder's ordinary license price therefor; any unauthorized (and unlicensable) use that is not terminated immediately for any reason (including, for example, because materials containing the Work cannot reasonably be recalled) will be subject to all remedies available at law or in equity, but in no event to a payment of less than three times the Rightsholder's ordinary license price for the most closely analogous licensable use plus Rightsholder's and/or CCC's costs and expenses incurred in collecting such payment.

8. Miscellaneous.

8.1. User acknowledges that CCC may, from time to time, make changes or additions to the Service or to these terms and conditions, and CCC reserves the right to send notice to the User by electronic mail or otherwise for the purposes of notifying User of such changes or additions; provided that any such changes or additions shall not apply to permissions already secured and paid for.

8.2. Use of User-related information collected through the Service is governed by CCC's privacy policy, available online here:https://marketplace.copyright.com/rs-ui-web/mp/privacy-policy

8.3. The licensing transaction described in the Order Confirmation is personal to User. Therefore, User may not assign or transfer to any other person (whether a natural person or an organization of any kind) the license created by the Order Confirmation and these terms and conditions or any rights granted hereunder; provided, however, that User may assign such license in its entirety on written notice to CCC in the event of a transfer of all or substantially all of User's rights in the new material which includes the Work(s) licensed under this Service.

8.4. No amendment or waiver of any terms is binding unless set forth in writing and signed by the parties. The Rightsholder and CCC hereby object to any terms contained in any writing prepared by the User or its principals, employees, agents or affiliates and purporting to govern or otherwise relate to the licensing

transaction described in the Order Confirmation, which terms are in any way inconsistent with any terms set forth in the Order Confirmation and/or in these terms and conditions or CCC's standard operating procedures, whether such writing is prepared prior to, simultaneously with or subsequent to the Order Confirmation, and whether such writing appears on a copy of the Order Confirmation or in a separate instrument.

8.5. The licensing transaction described in the Order Confirmation document shall be governed by and construed under the law of the State of New York, USA, without regard to the principles thereof of conflicts of law. Any case, controversy, suit, action, or proceeding arising out of, in connection with, or related to such licensing transaction shall be brought, at CCC's sole discretion, in any federal or state court located in the County of New York, State of New York, USA, or in any federal or state court whose geographical jurisdiction covers the location of the Rightsholder set forth in the Order Confirmation. The parties expressly submit to the personal jurisdiction and venue of each such federal or state court.If you have any comments or questions about the Service or Copyright Clearance Center, please contact us at 978-750-8400 or send an e-mail to support@copyright.com.

v 1.1

SPRINGER NATURE LICENSE TERMS AND CONDITIONS

Sep 23, 2020

This Agreement between Mr. Zbigniew Baster ("You") and Springer Nature ("Springer Nature") consists of your license details and the terms and conditions provided by Springer Nature and Copyright Clearance Center.

License Number	4900770040382
License date	Sep 02, 2020
Licensed Content Publisher	Springer Nature
Licensed Content Publication	Nature
Licensed Content Title	Nanoscale architecture of integrin-based cell adhesions
Licensed Content Author	Pakorn Kanchanawong et al
Licensed Content Date	Nov 24, 2010
Type of Use	Thesis/Dissertation
Requestor type	academic/university or research institute
Format	print and electronic
Portion	figures/tables/illustrations
Number of figures/tables/illustrations	1
High-res required	no
Will you be translating?	no
Circulation/distribution	50000 or greater
Author of this Springer Nature content	no
Title	Interplay between talin and β1-integrin in cancer cells motility
Institution name	Jagiellonian Univeristy
Expected presentation date	Oct 2020
Portions	Figure 4d
Requestor Location	Mr. Zbigniew Baster 11 Lojasiewicza Street Cracow, other 30-348 Poland Attn: Mr. Zbigniew Baster
Total	**0.00 USD**
Terms and Conditions	

Springer Nature Customer Service Centre GmbH
Terms and Conditions

This agreement sets out the terms and conditions of the licence (the **Licence**) between you and **Springer Nature Customer Service Centre GmbH** (the **Licensor**). By clicking 'accept' and completing the transaction for the material (**Licensed Material**), you also confirm your acceptance of these terms and conditions.

1. Grant of License

1. 1. The Licensor grants you a personal, non-exclusive, non-transferable, world-wide licence to reproduce the Licensed Material for the purpose specified in your order only. Licences are granted for the specific use requested in the order and for no other use, subject to the conditions below.

1. 2. The Licensor warrants that it has, to the best of its knowledge, the rights to license reuse of the Licensed Material. However, you should ensure that the material you are requesting is original to the Licensor and does not carry the copyright of another entity (as credited in the published version).

1. 3. If the credit line on any part of the material you have requested indicates that it was reprinted or adapted with permission from another source, then you should also seek permission from that source to reuse the material.

2. Scope of Licence

2. 1. You may only use the Licensed Content in the manner and to the extent permitted by these Ts&Cs and any applicable laws.

2. 2. A separate licence may be required for any additional use of the Licensed Material, e.g. where a licence has been purchased for print only use, separate permission must be obtained for electronic re-use. Similarly, a licence is only valid in the language selected and does not apply for editions in other languages unless additional translation rights have been granted separately in the licence. Any content owned by third parties are expressly excluded from the licence.

2. 3. Similarly, rights for additional components such as custom editions and derivatives require additional permission and may be subject to an additional fee. Please apply to Journalpermissions@springernature.com/bookpermissions@springernature.com for these rights.

2. 4. Where permission has been granted **free of charge** for material in print, permission may also be granted for any electronic version of that work, provided that the material is incidental to your work as a whole and that the electronic version is essentially equivalent to, or substitutes for, the print version.

2. 5. An alternative scope of licence may apply to signatories of the STM Permissions Guidelines, as amended from time to time.

3. Duration of Licence

3. 1. A licence for is valid from the date of purchase ('Licence Date') at the end of the relevant period in the below table:

Scope of Licence	Duration of Licence
Post on a website	12 months
Presentations	12 months
Books and journals	Lifetime of the edition in the language purchased

4. Acknowledgement

4. 1. The Licensor's permission must be acknowledged next to the Licenced Material in print. In electronic form, this acknowledgement must be visible at the same time as the figures/tables/illustrations or abstract, and must be hyperlinked to the journal/book's homepage. Our required acknowledgement format is in the Appendix below.

5. Restrictions on use

5. 1. Use of the Licensed Material may be permitted for incidental promotional use and minor editing privileges e.g. minor adaptations of single figures, changes of format, colour and/or style where the adaptation is credited as set out in Appendix 1 below. Any other changes including but not limited to, cropping, adapting, omitting material that affect the meaning, intention or moral rights of the author are strictly prohibited.

5. 2. You must not use any Licensed Material as part of any design or trademark.

5. 3. Licensed Material may be used in Open Access Publications (OAP) before publication by Springer Nature, but any Licensed Material must be removed from OAP sites prior to final publication.

6. Ownership of Rights

6. 1. Licensed Material remains the property of either Licensor or the relevant third party and any rights not explicitly granted herein are expressly reserved.

7. Warranty

IN NO EVENT SHALL LICENSOR BE LIABLE TO YOU OR ANY OTHER PARTY OR ANY OTHER PERSON OR FOR ANY SPECIAL, CONSEQUENTIAL, INCIDENTAL OR INDIRECT DAMAGES, HOWEVER CAUSED, ARISING OUT OF OR IN CONNECTION WITH THE DOWNLOADING, VIEWING OR USE OF THE MATERIALS REGARDLESS OF THE FORM OF ACTION, WHETHER FOR BREACH OF CONTRACT, BREACH OF WARRANTY, TORT, NEGLIGENCE, INFRINGEMENT OR OTHERWISE (INCLUDING, WITHOUT LIMITATION, DAMAGES BASED ON LOSS OF PROFITS, DATA, FILES, USE, BUSINESS OPPORTUNITY OR CLAIMS OF THIRD PARTIES), AND
WHETHER OR NOT THE PARTY HAS BEEN ADVISED OF THE POSSIBILITY OF SUCH DAMAGES. THIS LIMITATION SHALL APPLY NOTWITHSTANDING ANY FAILURE OF ESSENTIAL PURPOSE OF ANY LIMITED REMEDY PROVIDED HEREIN.

8. Limitations

8. 1. ***BOOKS ONLY:***Where **'reuse in a dissertation/thesis'** has been selected the following terms apply: Print rights of the final author's accepted manuscript (for clarity, NOT the published version) for up to 100 copies, electronic rights for use only on a personal website or institutional repository as defined by the Sherpa guideline (www.sherpa.ac.uk/romeo/).

9. Termination and Cancellation

9. 1. Licences will expire after the period shown in Clause 3 (above).

9. 2. Licensee reserves the right to terminate the Licence in the event that payment is not received in full or if there has been a breach of this agreement by you.

Appendix 1 — Acknowledgements:

For Journal Content:
Reprinted by permission from [**the Licensor**]: [**Journal Publisher** (e.g. Nature/Springer/Palgrave)] [**JOURNAL NAME**] [**REFERENCE CITATION** (Article name, Author(s) Name), [**COPYRIGHT**] (year of publication)

For **Advance Online Publication papers:**
Reprinted by permission from [**the Licensor**]: [**Journal Publisher** (e.g. Nature/Springer/Palgrave)] [**JOURNAL NAME**] [**REFERENCE CITATION** (Article name, Author(s) Name), [**COPYRIGHT**] (year of publication), advance online publication, day month year (doi: 10.1038/sj.[JOURNAL ACRONYM].)

For Adaptations/Translations:
Adapted/Translated by permission from [**the Licensor**]: [**Journal Publisher** (e.g. Nature/Springer/Palgrave)] [**JOURNAL NAME**] [**REFERENCE CITATION** (Article name, Author(s) Name), [**COPYRIGHT**] (year of publication)

Note: For any republication from the British Journal of Cancer, the following credit line style applies:

Reprinted/adapted/translated by permission from [**the Licensor**]: on behalf of Cancer Research UK: : [**Journal Publisher** (e.g. Nature/Springer/Palgrave)] [**JOURNAL NAME**] [**REFERENCE CITATION** (Article name, Author(s) Name), [**COPYRIGHT]** (year of publication)

For **Advance Online Publication** papers:
Reprinted by permission from The [**the Licensor**]: on behalf of Cancer Research UK: [**Journal Publisher** (e.g. Nature/Springer/Palgrave)] [**JOURNAL NAME**] [**REFERENCE CITATION** (Article name, Author(s) Name), [**COPYRIGHT**] (year of publication), advance online publication, day month year (doi: 10.1038/sj.[JOURNAL ACRONYM])

For Book content:
Reprinted/adapted by permission from [**the Licensor**]: [**Book Publisher** (e.g. Palgrave Macmillan, Springer etc) [**Book Title**] by [**Book author**(s)] [**COPYRIGHT**] (year of publication)

Other Conditions:

Version 1.2

JOHN WILEY AND SONS LICENSE TERMS AND CONDITIONS

Sep 23, 2020

This Agreement between Mr. Zbigniew Baster ("You") and John Wiley and Sons ("John Wiley and Sons") consists of your license details and the terms and conditions provided by John Wiley and Sons and Copyright Clearance Center.

License Number	4900010880170
License date	Sep 01, 2020
Licensed Content Publisher	John Wiley and Sons
Licensed Content Publication	THE FASEB JOURNAL
Licensed Content Title	Cyanidin-3-glucoside binds to talin and modulates colon cancer cell adhesions and 3D growth
Licensed Content Author	Cai Huang, Zenon Rajfur, Haining Zhu, et al
Licensed Content Date	Jan 9, 2020
Licensed Content Volume	34
Licensed Content Issue	2
Licensed Content Pages	11
Type of Use	Dissertation/Thesis
Requestor type	Author of this Wiley article
Format	Print and electronic
Portion	Figure/table
Number of figures/tables	1
Will you be translating?	No
Title	Interplay between talin and β1-integrin in cancer cells motility
Institution name	Jagiellonian Univeristy
Expected presentation date	Oct 2020
Portions	Figure 3(D)
Requestor Location	Mr. Zbigniew Baster 11 Lojasiewicza Street Cracow, other 30-348 Poland Attn: Mr. Zbigniew Baster
Publisher Tax ID	EU826007151
Total	**0.00 USD**

Terms and Conditions

TERMS AND CONDITIONS

This copyrighted material is owned by or exclusively licensed to John Wiley & Sons, Inc. or one of its group companies (each a"Wiley Company") or handled on behalf of a society with which a Wiley Company has exclusive publishing rights in relation to a particular work (collectively "WILEY"). By clicking "accept" in connection with completing this licensing transaction, you agree that the following terms and conditions apply to this transaction (along with the billing and payment terms and conditions established by the Copyright Clearance Center Inc., ("CCC's Billing and Payment terms and conditions"), at the time that you opened your RightsLink account (these are available at any time at http://myaccount.copyright.com).

Terms and Conditions

- The materials you have requested permission to reproduce or reuse (the "Wiley Materials") are protected by copyright.

- You are hereby granted a personal, non-exclusive, non-sub licensable (on a stand-alone basis), non-transferable, worldwide, limited license to reproduce the Wiley Materials for the purpose specified in the licensing process. This license, **and any CONTENT (PDF or image file) purchased as part of your order,** is for a one-time use only and limited to any maximum distribution number specified in the license. The first instance of republication or reuse granted by this license must be completed within two years of the date of the grant of this license (although copies prepared before the end date may be distributed thereafter). The Wiley Materials shall not be used in any other manner or for any other purpose, beyond what is granted in the license. Permission is granted subject to an appropriate acknowledgement given to the author, title of the material/book/journal and the publisher. You shall also duplicate the copyright notice that appears in the Wiley publication in your use of the Wiley Material. Permission is also granted on the understanding that nowhere in the text is a previously published source acknowledged for all or part of this Wiley Material. Any third party content is expressly excluded from this permission.

- With respect to the Wiley Materials, all rights are reserved. Except as expressly granted by the terms of the license, no part of the Wiley Materials may be copied, modified, adapted (except for minor reformatting required by the new Publication), translated, reproduced, transferred or distributed, in any form or by any means, and no derivative works may be made based on the Wiley Materials without the prior permission of the respective copyright owner.**For STM Signatory Publishers clearing permission under the terms of the STM Permissions Guidelines only, the terms of the license are extended to include subsequent editions and for editions in other languages, provided such editions are for the work as a whole in situ and does not involve the separate exploitation of the permitted figures or extracts,** You may not alter, remove or suppress in any manner any copyright, trademark or other notices displayed by the Wiley Materials. You may not license, rent, sell, loan, lease, pledge, offer as security, transfer or assign the Wiley Materials on a stand-alone basis, or any of the rights granted to you hereunder to any other person.

- The Wiley Materials and all of the intellectual property rights therein shall at all times remain the exclusive property of John Wiley & Sons Inc, the Wiley Companies, or their respective licensors, and your interest therein is only that of having possession of and the right to reproduce the Wiley Materials pursuant to Section 2 herein during the continuance of this Agreement. You agree that you own no right, title or interest in or to the Wiley Materials or any of the intellectual property rights therein. You shall have no rights hereunder other than the license as provided for above in Section 2. No right, license or interest to any trademark, trade name, service mark or other branding ("Marks") of WILEY or its licensors is granted hereunder, and you agree that you shall not assert any such right, license or interest with respect thereto

- NEITHER WILEY NOR ITS LICENSORS MAKES ANY WARRANTY OR REPRESENTATION OF ANY KIND TO YOU OR ANY THIRD PARTY, EXPRESS, IMPLIED

OR STATUTORY, WITH RESPECT TO THE MATERIALS OR THE ACCURACY OF ANY INFORMATION CONTAINED IN THE MATERIALS, INCLUDING, WITHOUT LIMITATION, ANY IMPLIED WARRANTY OF MERCHANTABILITY, ACCURACY, SATISFACTORY QUALITY, FITNESS FOR A PARTICULAR PURPOSE, USABILITY, INTEGRATION OR NON-INFRINGEMENT AND ALL SUCH WARRANTIES ARE HEREBY EXCLUDED BY WILEY AND ITS LICENSORS AND WAIVED BY YOU.

- WILEY shall have the right to terminate this Agreement immediately upon breach of this Agreement by you.

- You shall indemnify, defend and hold harmless WILEY, its Licensors and their respective directors, officers, agents and employees, from and against any actual or threatened claims, demands, causes of action or proceedings arising from any breach of this Agreement by you.

- IN NO EVENT SHALL WILEY OR ITS LICENSORS BE LIABLE TO YOU OR ANY OTHER PARTY OR ANY OTHER PERSON OR ENTITY FOR ANY SPECIAL, CONSEQUENTIAL, INCIDENTAL, INDIRECT, EXEMPLARY OR PUNITIVE DAMAGES, HOWEVER CAUSED, ARISING OUT OF OR IN CONNECTION WITH THE DOWNLOADING, PROVISIONING, VIEWING OR USE OF THE MATERIALS REGARDLESS OF THE FORM OF ACTION, WHETHER FOR BREACH OF CONTRACT, BREACH OF WARRANTY, TORT, NEGLIGENCE, INFRINGEMENT OR OTHERWISE (INCLUDING, WITHOUT LIMITATION, DAMAGES BASED ON LOSS OF PROFITS, DATA, FILES, USE, BUSINESS OPPORTUNITY OR CLAIMS OF THIRD PARTIES), AND WHETHER OR NOT THE PARTY HAS BEEN ADVISED OF THE POSSIBILITY OF SUCH DAMAGES. THIS LIMITATION SHALL APPLY NOTWITHSTANDING ANY FAILURE OF ESSENTIAL PURPOSE OF ANY LIMITED REMEDY PROVIDED HEREIN.

- Should any provision of this Agreement be held by a court of competent jurisdiction to be illegal, invalid, or unenforceable, that provision shall be deemed amended to achieve as nearly as possible the same economic effect as the original provision, and the legality, validity and enforceability of the remaining provisions of this Agreement shall not be affected or impaired thereby.

- The failure of either party to enforce any term or condition of this Agreement shall not constitute a waiver of either party's right to enforce each and every term and condition of this Agreement. No breach under this agreement shall be deemed waived or excused by either party unless such waiver or consent is in writing signed by the party granting such waiver or consent. The waiver by or consent of a party to a breach of any provision of this Agreement shall not operate or be construed as a waiver of or consent to any other or subsequent breach by such other party.

- This Agreement may not be assigned (including by operation of law or otherwise) by you without WILEY's prior written consent.

- Any fee required for this permission shall be non-refundable after thirty (30) days from receipt by the CCC.

- These terms and conditions together with CCC's Billing and Payment terms and conditions (which are incorporated herein) form the entire agreement between you and WILEY concerning this licensing transaction and (in the absence of fraud) supersedes all prior agreements and representations of the parties, oral or written. This Agreement may not be amended except in writing signed by both parties. This Agreement shall be binding upon and inure to the benefit of the parties' successors, legal representatives, and authorized assigns.

- In the event of any conflict between your obligations established by these terms and conditions and those established by CCC's Billing and Payment terms and conditions, these terms and conditions shall prevail.

- WILEY expressly reserves all rights not specifically granted in the combination of (i) the license details provided by you and accepted in the course of this licensing transaction, (ii) these terms and conditions and (iii) CCC's Billing and Payment terms and conditions.

- This Agreement will be void if the Type of Use, Format, Circulation, or Requestor Type was misrepresented during the licensing process.

- This Agreement shall be governed by and construed in accordance with the laws of the State of New York, USA, without regards to such state's conflict of law rules. Any legal action, suit or proceeding arising out of or relating to these Terms and Conditions or the breach thereof shall be instituted in a court of competent jurisdiction in New York County in the State of New York in the United States of America and each party hereby consents and submits to the personal jurisdiction of such court, waives any objection to venue in such court and consents to service of process by registered or certified mail, return receipt requested, at the last known address of such party.

WILEY OPEN ACCESS TERMS AND CONDITIONS

Wiley Publishes Open Access Articles in fully Open Access Journals and in Subscription journals offering Online Open. Although most of the fully Open Access journals publish open access articles under the terms of the Creative Commons Attribution (CC BY) License only, the subscription journals and a few of the Open Access Journals offer a choice of Creative Commons Licenses. The license type is clearly identified on the article.

The Creative Commons Attribution License

The Creative Commons Attribution License (CC-BY) allows users to copy, distribute and transmit an article, adapt the article and make commercial use of the article. The CC-BY license permits commercial and non-

Creative Commons Attribution Non-Commercial License

The Creative Commons Attribution Non-Commercial (CC-BY-NC)License permits use, distribution and reproduction in any medium, provided the original work is properly cited and is not used for commercial purposes.(see below)

Creative Commons Attribution-Non-Commercial-NoDerivs License

The Creative Commons Attribution Non-Commercial-NoDerivs License (CC-BY-NC-ND) permits use, distribution and reproduction in any medium, provided the original work is properly cited, is not used for commercial purposes and no modifications or adaptations are made. (see below)

Use by commercial "for-profit" organizations

Use of Wiley Open Access articles for commercial, promotional, or marketing purposes requires further explicit permission from Wiley and will be subject to a fee.

Further details can be found on Wiley Online Library http://olabout.wiley.com/WileyCDA/Section/id-410895.html

Other Terms and Conditions:

v1.10 Last updated September 2015

Questions? customercare@copyright.com or +1-855-239-3415 (toll free in the US) or +1-978-646-2777.

JOHN WILEY AND SONS LICENSE TERMS AND CONDITIONS

Sep 23, 2020

This Agreement between Mr. Zbigniew Baster ("You") and John Wiley and Sons ("John Wiley and Sons") consists of your license details and the terms and conditions provided by John Wiley and Sons and Copyright Clearance Center.

License Number	4900010360092
License date	Sep 01, 2020
Licensed Content Publisher	John Wiley and Sons
Licensed Content Publication	THE FASEB JOURNAL
Licensed Content Title	Cyanidin-3-glucoside binds to talin and modulates colon cancer cell adhesions and 3D growth
Licensed Content Author	Cai Huang, Zenon Rajfur, Haining Zhu, et al
Licensed Content Date	Jan 9, 2020
Licensed Content Volume	34
Licensed Content Issue	2
Licensed Content Pages	11
Type of Use	Dissertation/Thesis
Requestor type	Author of this Wiley article
Format	Print and electronic
Portion	Full article
Will you be translating?	No
Title	Interplay between talin and β1-integrin in cancer cells motility
Institution name	Jagiellonian Univeristy
Expected presentation date	Oct 2020
Requestor Location	Mr. Zbigniew Baster 11 Lojasiewicza Street Cracow, other 30-348 Poland Attn: Mr. Zbigniew Baster
Publisher Tax ID	EU826007151
Total	**0.00 USD**
Terms and Conditions	

TERMS AND CONDITIONS

ANY IMPLIED WARRANTY OF MERCHANTABILITY, ACCURACY, SATISFACTORY QUALITY, FITNESS FOR A PARTICULAR PURPOSE, USABILITY, INTEGRATION OR NON-INFRINGEMENT AND ALL SUCH WARRANTIES ARE HEREBY EXCLUDED BY WILEY AND ITS LICENSORS AND WAIVED BY YOU.

- WILEY shall have the right to terminate this Agreement immediately upon breach of this Agreement by you.
- You shall indemnify, defend and hold harmless WILEY, its Licensors and their respective directors, officers, agents and employees, from and against any actual or threatened claims, demands, causes of action or proceedings arising from any breach of this Agreement by you.
- IN NO EVENT SHALL WILEY OR ITS LICENSORS BE LIABLE TO YOU OR ANY OTHER PARTY OR ANY OTHER PERSON OR ENTITY FOR ANY SPECIAL, CONSEQUENTIAL, INCIDENTAL, INDIRECT, EXEMPLARY OR PUNITIVE DAMAGES, HOWEVER CAUSED, ARISING OUT OF OR IN CONNECTION WITH THE DOWNLOADING, PROVISIONING, VIEWING OR USE OF THE MATERIALS REGARDLESS OF THE FORM OF ACTION, WHETHER FOR BREACH OF CONTRACT, BREACH OF WARRANTY, TORT, NEGLIGENCE, INFRINGEMENT OR OTHERWISE (INCLUDING, WITHOUT LIMITATION, DAMAGES BASED ON LOSS OF PROFITS, DATA, FILES, USE, BUSINESS OPPORTUNITY OR CLAIMS OF THIRD PARTIES), AND WHETHER OR NOT THE PARTY HAS BEEN ADVISED OF THE POSSIBILITY OF SUCH DAMAGES. THIS LIMITATION SHALL APPLY NOTWITHSTANDING ANY FAILURE OF ESSENTIAL PURPOSE OF ANY LIMITED REMEDY PROVIDED HEREIN.
- Should any provision of this Agreement be held by a court of competent jurisdiction to be illegal, invalid, or unenforceable, that provision shall be deemed amended to achieve as nearly as possible the same economic effect as the original provision, and the legality, validity and enforceability of the remaining provisions of this Agreement shall not be affected or impaired thereby.
- The failure of either party to enforce any term or condition of this Agreement shall not constitute a waiver of either party's right to enforce each and every term and condition of this Agreement. No breach under this agreement shall be deemed waived or excused by either party unless such waiver or consent is in writing signed by the party granting such waiver or consent. The waiver by or consent of a party to a breach of any provision of this Agreement shall not operate or be construed as a waiver of or consent to any other or subsequent breach by such other party.
- This Agreement may not be assigned (including by operation of law or otherwise) by you without WILEY's prior written consent.
- Any fee required for this permission shall be non-refundable after thirty (30) days from receipt by the CCC.
- These terms and conditions together with CCC's Billing and Payment terms and conditions (which are incorporated herein) form the entire agreement between you and WILEY concerning this licensing transaction and (in the absence of fraud) supersedes all prior agreements and representations of the parties, oral or written. This Agreement may not be amended except in writing signed by both parties. This Agreement shall be binding upon and inure to the benefit of the parties' successors, legal representatives, and authorized assigns.
- In the event of any conflict between your obligations established by these terms and conditions and those established by CCC's Billing and Payment terms and conditions, these terms and conditions shall prevail.
- WILEY expressly reserves all rights not specifically granted in the combination of (i) the license details provided by you and accepted in the course of this licensing transaction, (ii)

these terms and conditions and (iii) CCC's Billing and Payment terms and conditions.

- This Agreement will be void if the Type of Use, Format, Circulation, or Requestor Type was misrepresented during the licensing process.

- This Agreement shall be governed by and construed in accordance with the laws of the State of New York, USA, without regards to such state's conflict of law rules. Any legal action, suit or proceeding arising out of or relating to these Terms and Conditions or the breach thereof shall be instituted in a court of competent jurisdiction in New York County in the State of New York in the United States of America and each party hereby consents and submits to the personal jurisdiction of such court, waives any objection to venue in such court and consents to service of process by registered or certified mail, return receipt requested, at the last known address of such party.

WILEY OPEN ACCESS TERMS AND CONDITIONS

Wiley Publishes Open Access Articles in fully Open Access Journals and in Subscription journals offering Online Open. Although most of the fully Open Access journals publish open access articles under the terms of the Creative Commons Attribution (CC BY) License only, the subscription journals and a few of the Open Access Journals offer a choice of Creative Commons Licenses. The license type is clearly identified on the article.

The Creative Commons Attribution License

The Creative Commons Attribution License (CC-BY) allows users to copy, distribute and transmit an article, adapt the article and make commercial use of the article. The CC-BY license permits commercial and non-

Creative Commons Attribution Non-Commercial License

The Creative Commons Attribution Non-Commercial (CC-BY-NC)License permits use, distribution and reproduction in any medium, provided the original work is properly cited and is not used for commercial purposes.(see below)

Creative Commons Attribution-Non-Commercial-NoDerivs License

The Creative Commons Attribution Non-Commercial-NoDerivs License (CC-BY-NC-ND) permits use, distribution and reproduction in any medium, provided the original work is properly cited, is not used for commercial purposes and no modifications or adaptations are made. (see below)

Use by commercial "for-profit" organizations

Use of Wiley Open Access articles for commercial, promotional, or marketing purposes requires further explicit permission from Wiley and will be subject to a fee.

Further details can be found on Wiley Online Library http://olabout.wiley.com/WileyCDA/Section/id-410895.html

Other Terms and Conditions:

v1.10 Last updated September 2015

Questions? customercare@copyright.com or +1-855-239-3415 (toll free in the US) or +1-978-646-2777.